2019

Use of soft computing and numerical analysis in design, analysis and management of pavement systems

Orhan Kaya
Iowa State University

Use of soft computing and numerical analysis in design, analysis and management of pavement systems

by

Orhan Kaya

A dissertation submitted to the graduate faculty

in partial fulfillment of the requirements for the degree of

DOCTOR OF PHILOSOPHY

Major: Civil Engineering (Transportation Engineering; Civil Engineering Materials)

Program of Study Committee:
Halil Ceylan, Major Professor
Jing Dong
Sunghwan Kim
Omar G. Smadi
Paul G. Spry
Peter C. Taylor

The student author, whose presentation of the scholarship herein was approved by the program of study committee, is solely responsible for the content of this dissertation. The Graduate College will ensure this dissertation is globally accessible and will not permit alterations after a degree is conferred.

Iowa State University

Ames, Iowa

2019

DEDICATION

To my wife, Eda, for her endless love and patience

TABLE OF CONTENTS

Page

LIST OF FIGURES

Page

LIST OF TABLES

Page

ACKNOWLEDGMENTS

First of all, I would like to thank my major professor, Dr. Halil Ceylan, for his support in this study. I especially admire his technical knowledge, academic dedication and multitasking.

Furthermore, I would like to thank my committee members, Drs. Sunghwan Kim, Jing Dong, Peter C. Taylor, Omar G. Smadi and Paul G. Spry for their guidance and support throughout the course of this research. Special thanks are extended to Dr. Sunghwan Kim who inspired me with his diligence with respect to work discipline, academic dedication and patience.

In addition, I would like to thank the Ministry of National Education of Turkey for providing me with a scholarship and educational opportunity in the U.S.

Last but not least, I would like to thank my beloved parents, Mustafa and Fatma, and siblings, Osman, Okan and Handan, for their endless love and support throughout my life.

ABSTRACT

There are a number of components of pavement engineering, including pavement management, pavement analysis and design, and pavement materials. Historically, the field of pavement management has been interested in monitoring post-construction condition, timing of preventive maintenance and rehabilitation treatments, and economic analysis of alternatives. On the other hand, the field of pavement analysis and design has dealt with optimizing pavement structure; with optimum structure, a pavement system is expected to survive during its service life for given traffic and climate conditions. The performance of pavement materials has been improved to achieve the long-lasting and lower-maintenance pavement systems. A data-driven comprehensive approach considering all aspects of pavement engineering together could be a future direction for advancing pavement engineering practices.

In order to achieve a data-driven comprehensive approach considering all aspects of pavement engineering together as outlined above, a data-driven and efficient pavement design, analysis and management concept has been proposed in this study. To serve as elements of this concept, several models related to pavement structural response models, pavement performance prediction models, and pavement remaining service life (RSL) models have been developed. First, to enable faster three-dimensional finite element (3D-FE) computations of design stresses, artificial neural network (ANN)-based surrogate computational pavement structural response models were developed. These models produce an estimate of the top-down bending stress close to that computed by 3D-FE analysis in rigid airport pavements in a fraction of the time. Second, longitudinal cracking mechanisms of widened jointed plain concrete pavements (JPCP) were demonstrated and

their longitudinal cracking potential was evaluated using numerical analysis. Third, the Federal Aviation Administration's (FAA) current rigid airfield pavement design methodology has been evaluated in great detail to better identify research gaps and remaining needs with respect to cracking failure models so that recommendations could be made as to how current methodology could be improved to accommodate top-down and bottom-up cracking failure modes. Fourth, a detailed step-by-step methodology for the development of a framework for pavement performance and RSL prediction models was explained using real pavement performance data obtained from the Iowa Department of Transportation (DOT)'s Pavement Management Information System (PMIS) database.

CHAPTER 1. GENERAL INTRODUCTION

Pavements are designed to withstand several types of loads, including traffic and environmental loads, and pavements develop structural responses such as stresses, strains, and deflections when they are exposed to such loads. Structural-response models have been developed to estimate structural response of pavements to various load types and magnitudes. State-of-the-art practice in pavement response modeling is to use mechanistic-based models. Mechanistic-empirical pavement design guide (AASHTOWare Pavement ME Design computer program) uses finite-element analysis (FEA) based pavement response models for rigid pavement design and analysis, while it uses two approaches (two-dimensional nonlinear finite-element analysis for the most general case of nonlinear unbound material behavior and multilayer elastic theory (MLET) for the case of purely linear material behavior) for flexible pavement design and analysis (NCHRP 2003). Similarly, with the arrival of New Large Aircraft (NLA) and associated design challenges for pavement designers, including increasing airplane weights and complex gear configurations, the Federal Aviation Administration (FAA) has adopted layered elastic theory for flexible airport pavement design and three-dimensional finite-element (3D-FE) procedures for rigid airport pavement design (FAA 2014). In summary, numerical analysis techniques such as finite-element models comprise state-of-the-art practice for rigid pavement structural response modeling and, along with LEA, they also represent state-of-the art practices for flexible pavement structural response modeling.

Pavement performance models are used to evaluate how pavement performance changes over time. Pavement performance models can be categorized into two groups, deterministic and probabilistic, based on their prediction results (Chen and Mastin 2016;

Sundin and Braban-Lexdoux 2001; Albuquerque and Broten 1997). Deterministic models estimate single condition values at a given time in the design life of pavements, while probabilistic models estimate the probability of each condition value at a given time (Chen and Mastin 2016). Most state highway agencies (SHAs) use deterministic models as part of their pavement management systems for various reasons, including (1) ease of explanation of models to users and (2) ease of incorporating models into their pavement management systems (PMS) (Wolters and Zimmerman 2010).

Mechanistic-empirical pavement design guide (AASHTOWare Pavement ME Design computer program) follows mechanistic-empirical pavement design methodology in which empirical transfer functions relate pavement structural responses to pavement performance estimations (NCHRP 2003). FAA's pavement thickness design computer program FAA Rigid and Flexible Iterative Elastic Layer Design (FAARFIELD) also follows a mechanistic-empirical design methodology in its pavement design computations (FAA 2014).

SHAs are required to develop performance-based approaches in their pavement management decision-making processes based on the Moving Ahead for Progress in the 21st Century (MAP-21) Federal Transportation Legislation (HR 2012). One performance-based approach to facilitating the pavement management decision-making process is to use remaining service life (RSL) models. RSL for pavements can be defined as the time frame between the present time and the time when a significant rehabilitation treatment or reconstruction should occur (FHWA 2018). Although application of a structural overlay or reconstruction would normally be regarded as a sign for termination of pavement service life, minor maintenance treatments or thin overlays are often not considered as such signs

(FHWA 2018). RSL models, developed to predict the remaining life of pavements, are being used as elements of the pavement management process. (Elkins et al. 2013).

Multiple advantages of RSL have been reported in the literature (Mack and Sullivan 2014) and its key positive features include:

- Estimation of the time, expressed in years, before rehabilitation would be required for any given road section
- Ease of understanding (especially for public)
- Can be a multi-conditional measure developed from any type of functional and/or structural data
- Allowing agencies to distinguish between two road sections with the same current condition (i.e., the same current International roughness index (IRI))
- Providing deeper insight by converting "condition measures" into an "operational performance" measure that tells how well or how long the road will continue serving the public
- Providing an ideal tool for addressing the transportation planning and performance management criteria requirements of MAP-21 legislation

Soft computing techniques such as artificial neural networks (ANNs) have been used to model complex pavement engineering problems (Kaya et al. 2017, Kaya et al. 2018). ANN-based models are very effective tools for modeling pavement response and performance, complex problems where various inputs are involved, and by providing complex relationships between inputs and outputs. They have great potential for producing accurate stress predictions in a fraction of the time required by traditional FE-based design programs. ANNs could be practical alternatives to full 3D-FE computation that requires long

computation times. They can also easily and quickly produce pavement performance predictions, especially in network level analysis where thousands of pavement scenarios with various traffic loads, thicknesses, and conditions can be analyzed in seconds.

Motivation

There are a number of components of pavement engineering, including pavement management, pavement analysis and design, and pavement materials. Historically, the field of pavement management has been interested in monitoring post-construction condition, timing of preventive maintenance and rehabilitation treatments, and economic analysis of alternatives. On the other hand, the field of pavement analysis and design has dealt with optimizing pavement structure; with optimum structure, a pavement system is expected to survive during its service life for given traffic and climate conditions. The performance of pavement materials has been improved to achieve the long-lasting and lower-maintenance pavement systems. A data-driven comprehensive approach considering all aspects of pavement engineering together could be a future direction for advancing pavement engineering practices. In such an approach: (1) mechanisms between various pavement materials and structures must be well-understood and well-modeled, (2) for given pavement structures under various traffic and climate conditions, pavement performance must be well-evaluated, (3) remaining service lives based on pavement performance model results must be well-estimated, and (4) to optimize RSL, various pavement preservation or rehabilitation techniques should be considered during the pavement design process. If such a data-driven comprehensive approach could be achieved, pavement structures would be better-optimized and designed during the design stage, potentially avoiding excessive costs because of overdesign or early failure of pavements. Such a system could be efficient, interrelated, data-driven, and based on mechanistic models.

Objectives

To achieve a data-driven comprehensive approach that considers all aspects of pavement engineering together, as outlined above, this study proposes the data-driven and efficient pavement design, analysis, and management concept portrayed in Figure 1.1. In this concept, pavement structural response models relate structural, traffic and climatic inputs to pavement responses, and the pavement responses are related to pavement performance indicators using pavement performance-prediction models. Finally, pavement remaining-service-life models are used to relate pavement performance predictions to remaining service life estimations.

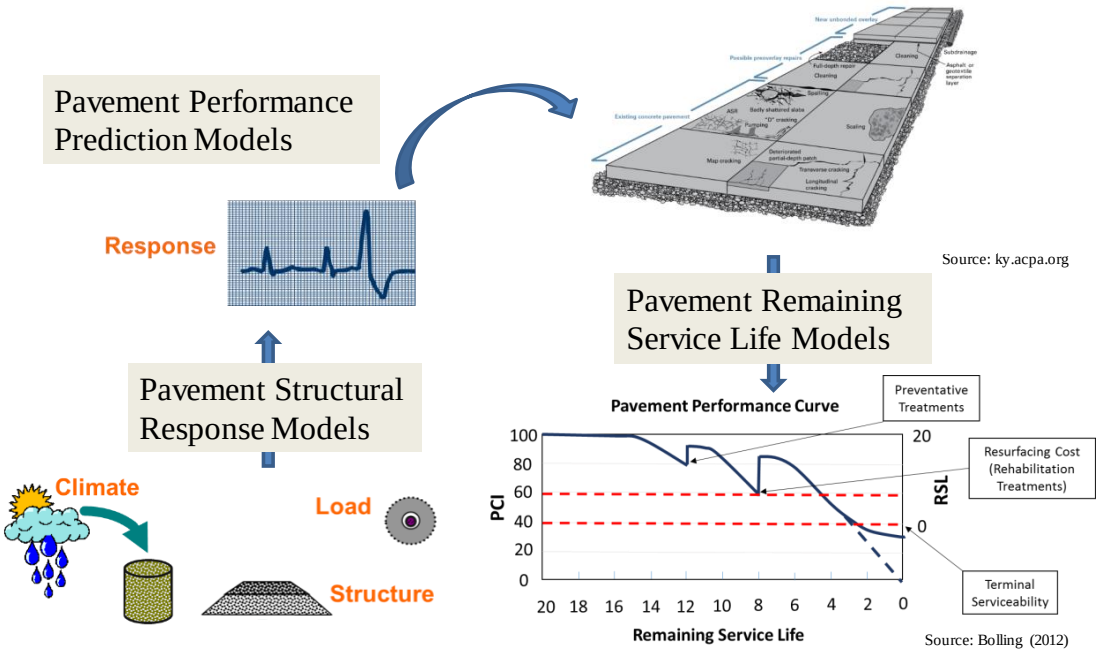

Figure 1.1 A data-driven and efficient pavement design, analysis and management concept

Figure 1.2 shows modeling methods that have been used in the development of models described in Figure 1.1. As part of this study, the following methods have been used in development of pavement structural response models, pavement performance prediction models, and pavement remaining-service-life models: soft computing and numerical analysis

methods were used in the development of pavement structural response models; soft computing and statistical methods were used in the development of pavement performance-prediction models, and soft computing and statistical methods were used in the development of pavement remaining-service-life models.

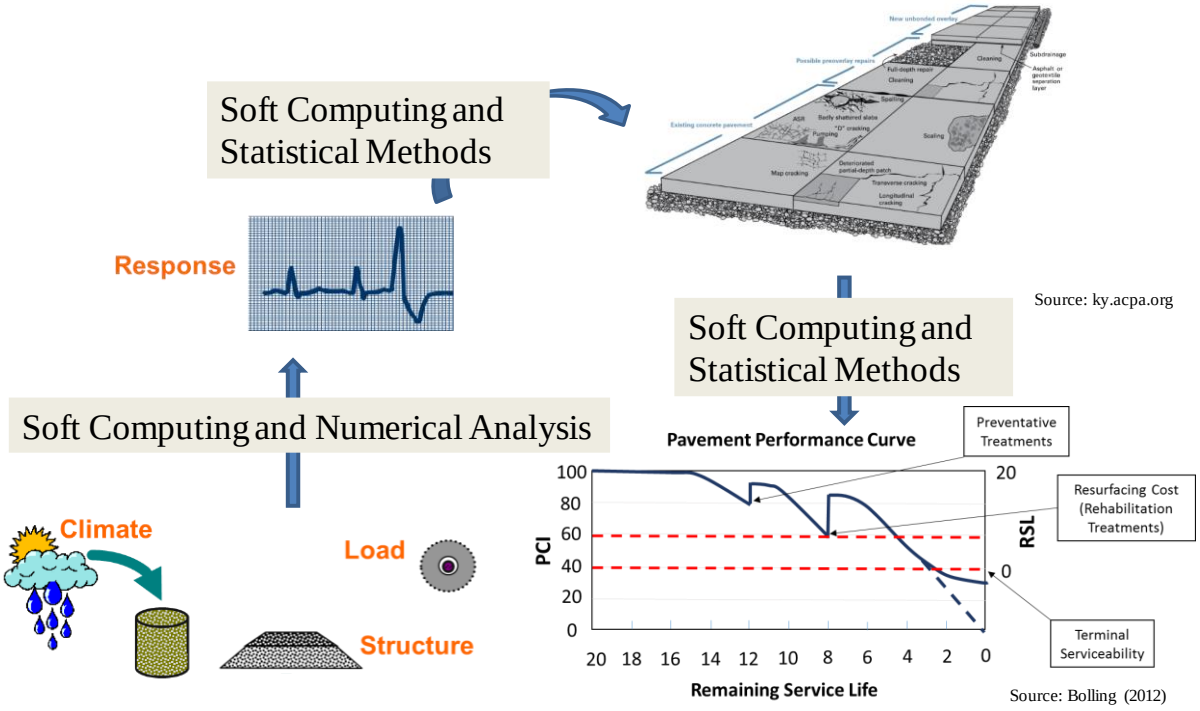

Figure 1.2 Modeling methods used in this study

Dissertation Organization

This dissertation consists of six chapters:

Chapter 1 provides some background about this study, including its motivation and objectives.

Chapter 2 discusses development of ANN-based surrogate computational response models or procedures (suitable for implementation in FAARFIELD 2.0, a research version of the FAARFIELD computer program) that return close estimates of top-down bending stresses in rigid airport pavements normally computed through 3D-FE analysis. The

developed ANN-based surrogate computational response models enable faster 3D-FE computations of design stresses in FAARFIELD 2.0, making it suitable for routine design.

Chapter 3 demonstrates longitudinal cracking mechanisms of widened jointed plain concrete pavements (JPCP) and evaluates their longitudinal cracking potential using numerical analysis. The critical load configuration with the highest longitudinal cracking potential for widened JPCP is identified. Three different shoulder design alternatives are also compared in terms of their contribution to mitigation of longitudinal cracking potential.

Chapter 4 evaluates FAA's current rigid airfield pavement design methodology in great detail to better identify research gaps and needs with respect to cracking-failure models, and provides recommendations for how current methodology could be improved to accommodate both top-down and bottom-up cracking failure modes.

Chapter 5 describes a detailed step-by-step methodology for development of a framework for pavement performance, and RSL prediction models using real pavement performance data obtained from the Iowa DOT PMIS database. To develop RSL models, project and network level pavement performance models are initially developed using two approaches: a statistically (or mathematically) defined approach for project-level model development, and an artificial intelligence (AI) based approach for network-level model development. Using pavement performance models for various pavement performance indicators (IRI for project level models, and rutting, percent cracking, and IRI for network level models) and the Federal Highway Agency (FHWA)-specified threshold limits for these pavement performance indicators, RSL models are then developed for three pavement types: flexible pavements, JPCP, and composite (Asphalt concrete (AC) over JPCP) pavements. These RSL models will significantly assist engineers in their decision-making processes.

Chapter 6 describes and summarizes conclusions, recommendations, and contributions of this study to the literature of the pavement-engineering field.

The research work described in Chapters 2 through 5 can be used as part of the proposed data-driven and efficient pavement design, analysis, and management concept.

References

Albuquerque, N. M., and Broten, M. (1997). "Local agency pavement management application guide." Project 1-37A, Washington State Dept. of Transportation, Olympia, WA.

Bolling, D. (2012). "Pavement preservation: Getting ahead of the curve for locals". Proceedings of the 37th Annual Rocky Mountain Asphalt Conference and Equipment.

Chen, D. and Mastin N. (2016). "Sigmoidal models for predicting pavement performance conditions. ASCE J. Perform. Constr. Facil., 2016, 30(4): 04015078.

FAA. (2014). "Airport design". FAA Advisory Circular (AC) No: 150/5300-13A.

FHWA. (2018). "Pavement health track remaining service life (RSL) forecasting models, Technical Information".

G. E. Elkins, T. M. Thompson, J. L., Groeger, B. Visintine, and G. R. Rada. (2013). "Reformulated pavement remaining service life framework". FHWA.

HR. (2012). "Moving ahead for progress in the 21st century act (MAP–21)". An Act to authorize funds for Federal-aid highways, highway safety programs, and transit programs, and for other purposes, 112 Congress, 2nd Session. Enacted October 1, 2012.

Kaya, O., A. Rezaei-Tarahomi, H. Ceylan, K. Gopalakrishnan, S. Kim, and D.R. Brill. (2018). "Neural network–based multiple-slab response models for top-down cracking mode in airfield pavement design". Journal of Transportation Engineering, Part B: Pavements, 2018. 144 (2).

Kaya, O., A. Rezaei-Tarahomi, H. Ceylan, K. Gopalakrishnan, S. Kim, and D.R. Brill. (2017). "Developing rigid airport pavement multiple-slab response models for top-down cracking mode using artificial neural networks". Presented at 2017 TRB Annual Meeting, Washington D.C.

Mack, J. W. and Sullivan, R. L. (2014). "Using remaining service life as the national performance measure of pavement assets". Proceedings of the 93rd Annual Meeting of the Transportation Research Board (TRB), Washington, DC, January 12–16.

NCHRP (2003). “Guide for mechanistic-empirical design of new and rehabilitated pavement structures”. Champaign, IL.

Sundin, S., and Braban-Lexdoux, C. (2001). “Artificial intelligence-based decision support technologies in pavement management.” Comput. Aided Civ. Infrastruct. Eng., 16(2), 143–157.

Wolters, A. S., and Zimmerman, K. A. (2010). “Current practices in pavement performance modeling, project 08-03 (C07), task 4 report: Final summary of findings.” Penn DOT, Harrisburg, PA.

CHAPTER 2. NEURAL-NETWORK BASED MULTIPLE-SLAB RESPONSE MODELS FOR TOP-DOWN CRACKING MODE IN AIRFIELD PAVEMENT DESIGN

A journal paper published in *Journal of Transportation Engineering: Part B, Pavements*

Orhan Kaya, Adel Rezaei-Tarahomi, Halil Ceylan, Kasthurirangan Gopalakrishnan, Sunghwan Kim and David R. Brill

Abstract

The Federal Aviation Administration (FAA) has recognized for some time that its current rigid pavement design model, involving a single slab loaded at one edge by a single aircraft gear, is inadequate with respect to top-down cracking. Thus, one of the major observed failure modes for rigid pavements is poorly accounted for in the FAA Rigid and Flexible Iterative Elastic Layer Design (FAARFIELD) design software. A research version of the FAARFIELD design software (*Version 2.0*) has been developed, in which the single-slab three-dimensional finite element (3D-FE) response model is replaced by a four-slab 3D-FE model with initial temperature curling to produce reasonable thickness designs accounting for top-down cracking behavior. However, the long and unpredictable run times associated with the four-slab model and curled slabs make routine design with this model impractical. Artificial intelligence (AI) based alternatives such as artificial neural networks (ANNs) have great potential to produce accurate stress predictions in a fraction of the time. ANNs could be practical replacements for a full 3D-FE computation that requires long computation times. In the development of ANN models, both individual input parameters and dimensional analysis have been considered and accuracy of predictions from both methods was compared. ANN models for only mechanical and simultaneous mechanical and thermal loading cases were developed using individual input parameters and dimensional analysis. It

was observed that very high accuracies were achieved in predicting pavement responses for all cases investigated.

Introduction

Airport pavements are designed to withstand repeated loading imposed by aircraft, to resist detrimental effects of traffic, and to endure deterioration induced by adverse weather conditions (e.g., extreme hot or cold weather) and other influences. A typical civil airport is serviced by a fleet of aircraft with different weights and gear configurations and the airport pavement is thus designed to withstand the repeated traffic loading of the entire range of aircraft, not just the heaviest aircraft (FAA 2014), over many years. Historical airport pavement design methodologies were based on simplified formulas (California Bearing Ratio (CBR) and Westergaard equations) combined with observations of field performance. With the arrival of New Large Aircraft (NLA) and the associated design challenges for pavements, including increasing airplane weights and complex gear configurations, the FAA adopted layered elastic theory for flexible airport pavement design and three-dimensional finite element (3D-FE) procedures for rigid airport pavement design. These mechanistic-empirical design methodologies, implemented in the FAA Rigid and Flexible Iterative Elastic Layer Design (FAARFIELD) design software (*Version 1.41*), are robust and can be adapted for addressing future gear configurations without modifying the underlying procedures (FAA 2014).

For rigid pavement design, FAARFIELD uses a 3D-FE computer program called NIKE3D_FAA to compute the maximum horizontal stress at the bottom edge of the Portland Cement Concrete (PCC) slab as the pavement structural life predictor. NIKE3D_FAA is a modification of the NIKE3D program originally developed by the Lawrence Livermore National Laboratory (LLNL) of the U.S. Department of Energy (Brill 1998; Brill 2000). By

limiting horizontal stress at the bottom of the PCC slab, cracking of the surface layer, (the only rigid pavement failure mode considered by FAARFIELD), is controlled. FAARFIELD currently does not consider the failure of subbase and subgrade layers. For a given airplane traffic mix over a particular subgrade/subbase, FAARFIELD provides the required rigid pavement slab thickness (FAA 2009).

The FAA has also developed FEAFAA (Finite Element Analysis – FAA), which makes use of NIKE3D, as a stand-alone tool for 3D-FE analysis of multiple-slab rigid airport pavements and overlays. It computes accurate responses (deflections, stresses and strains) of rigid pavements to individual aircraft landing gear loads. FEAFAA is a research and analysis tool; however, it is not a full-pledged design tool as it lacks the empirical components of FAARFIELD. At the same time, FEAFAA allows more options and greater configurability than the standard 3D-FE mesh implemented in FAARFIELD.

The FAA's current rigid pavement design model, involving a single slab loaded at one edge by a single aircraft gear, is inadequate to account for top-down cracking. Thus, one of the major observed failure modes for rigid pavements is poorly accounted for in the FAARFIELD rigid design procedure. To account for the influence of top-down cracking in thickness design, research version of the FAARFIELD design software has been developed, in which the single-slab three-dimensional finite element (3D-FE) response model is replaced by a four-slab 3D-FE model with initial temperature curling and variable joint spacing (FAARFIELD *Version 2.0*). However, the long and unpredictable run times associated with the four-slab model and curled slabs make routine design with this model impractical. To expand the FAARFIELD design model beyond the current one-slab model, the FAA is seeking practical alternatives to running the 3D-FEM stress computation as client software.

Artificial intelligence (AI) based alternatives such as artificial neural networks (ANNs) have great potential to produce accurate stress predictions in a fraction of the time of traditional FE-based design programs. ANNs could be practical alternatives to replace a full 3D-FE computation that requires long computation times.

The capability of ANN-based surrogate response models to successfully compute all components of tensile stresses as well as deflections at the bottom of jointed concrete airfield pavements has already been illustrated by many studies (Ceylan et al. 1999; Ceylan 2002; Rezaei-Tarahomi et al. 2017a). Some of the input parameters used in these response models were function of type, level, and location of the applied gear load, slab thickness, slab modulus, subgrade support, pavement temperature gradient, and the load transfer efficiencies of the joints.

The objective of this paper is to develop ANN-based surrogate computational response models or procedures (suitable for implementation in FAARFIELD (*Version 2.0*)) that return a close estimate of the top-down bending stress computed by NIKE3D in rigid airport pavements. This will enable faster 3D-FE computations of design stresses in FAARFIELD (*Version 2.0*) making it suitable for routine design. To develop these ANN models, the authors used FEAFAA, the FAA software for stand-alone 3D-FE rigid pavement stress computations. A synthetic database consisting of FEAFAA input parameters and the associated critical pavement responses were created to develop ANN-based surrogate computational response models. This database was developed using the following automated process:

- Step 1: Generate several cases with randomly generated FEAFAA input parameters within specified ranges

- Step 2: Run FEAFAA one case at a time
- Step 3: Extract critical pavement responses from FEAFAA output file
- Step 4: Enter the extracted critical pavement responses into the database
- Step 5: Repeat steps 2-4 for all the cases generated in step 1

In the FEAFAA batch runs, two different load cases were considered and ANN models were developed for these two cases: Case 1: mechanical-load-only, and Case 2: simultaneous mechanical and temperature loading. During the ANN model development for each loading case, two approaches were followed:

- Approach 1: Use all individual input parameters as independent inputs in the development of ANN models
- Approach 2: Use dimensional analysis to reduce the number of inputs in the development of ANN models

The feasibility of dimensional analysis in the ANN model development for the top-down cracking mode was also investigated. The purpose was to evaluate whether ANN models with acceptable prediction accuracies can be obtained with a reduced number of input parameters (Langhaar 1951; Taylor 1974). Dimensional analysis has been successfully used in the past in developing pavement response prediction models (Ceylan 2002; Khazanovich et al. 2001; Ioannides 2005; NCHRP 2003), making it a promising approach.

Synthetic Database Development

To develop an extensive database of input-output records from FEAFAA 2.0, a tool was developed by using the C# programming language together with the AutoIt® scripting tool (Autoit 2017) that minimizes the required time to supply the software with inputs and to post-process, minimizing human involvement in the process. The developed tool can

automatically perform batch runs, obtain the outputs, and then perform the post processing. The post-processing can extract the critical pavement responses along with critical pavement response locations. For each FEAFAA run, critical pavement responses on the top surface of the PCC slab were specified and collected.

A preliminary analysis was carried out to determine the minimum number of samples (i.e., FEAFAA batch runs) to ensure the robustness of the ANN models and to eliminate any possible errors associated with sampling. A set of batch runs were executed for ANN model development using the six-wheel Boeing B777-300ER mechanical-load-only case, $\sigma_{xx,\ max,\ top\text{-}tensile}$ (individual input parameters, mechanical-load-only case), which will be discussed later in this paper. The preliminary analysis used groups of 100, 250, 500 and 939 normally distributed random sampling numbers within the predefined range. Ten consecutive ANN models were developed for each group (100, 250, 500 and 939) to quantify the variance between each ANN model developed, if any. That is, a total of 40 ANN models were developed for this preliminary analysis. Rezaei-Tarahomi et al. (2017b) also evaluated sensitivity of critical pavement responses to each input variation.

The accuracy of ANN models was quantified by statistical indices R^2 (Coefficient of determination) and MSE (Mean squared error) as defined in Equations (2.1) and (2.2). In addition, the standard deviations of statistical indices for ten consecutive ANN models per each group were calculated and presented as error bar along with average of each statistical index in Fig. 2.1.

$$R^2 = \left(\frac{1}{n} \times \sum_{j=1}^{n} \frac{\left[\left(y_j^{solution} - y_{mean}^{solution} \right) \times \left(y_j^{prediction} - y_{mean}^{prediction} \right) \right]}{\sigma_{solution} \times \sigma_{prediction}} \right)^2 \quad (2.1)$$

$$MSE = \frac{1}{n} \times \sum_{j=1}^{n} (y_j^{prediction} - y_j^{solution})^2 \quad (2.2)$$

Where,

$y^{solution}$ = Critical pavement response from FEAFAA

$y^{prediction}$ = Same critical pavement response predicted by ANN models

$\sigma_{solution}$ = Variance of critical pavement response from FEAFAA

$\sigma_{prediction}$ = Variance of same critical pavement response predicted by ANN models

Fig. 2.1 shows the accuracy improvement as the number of samples increases in terms of mean and standard deviation of R^2 and MSE. The mean R^2 increases and the average value of MSE decreases as the number of samples increases. In particular, the variance (standard deviation) of R^2 and MSE within each group decreases as the number of samples increases.

These results indicate that the accuracy of the ANN models increase with the number of samples. Above 500 samples, the accuracy improvement curve started to level off. A model using 500 samples provided comparable accuracy to a model using nearly double the number of samples. Based on this result, the authors decided to use 500 samples for each variable for further development of the ANN models.

Table 2.1 displays the FEAFAA input parameters and their ranges used for the batch runs. Input parameters with only one value indicate those parameters not varied. A Boeing B777-300ER, with a gross weight of 777,000 lbs., was used as the representative aircraft for all cases. Because of symmetry of the problem, only one of the two main aircraft gears was analyzed. Nine slabs with varying slab dimensions (L_x, and L_y), loading angle (θ_g) and gear locations (x_g and y_g) were used in the analysis (Fig. 2.2).

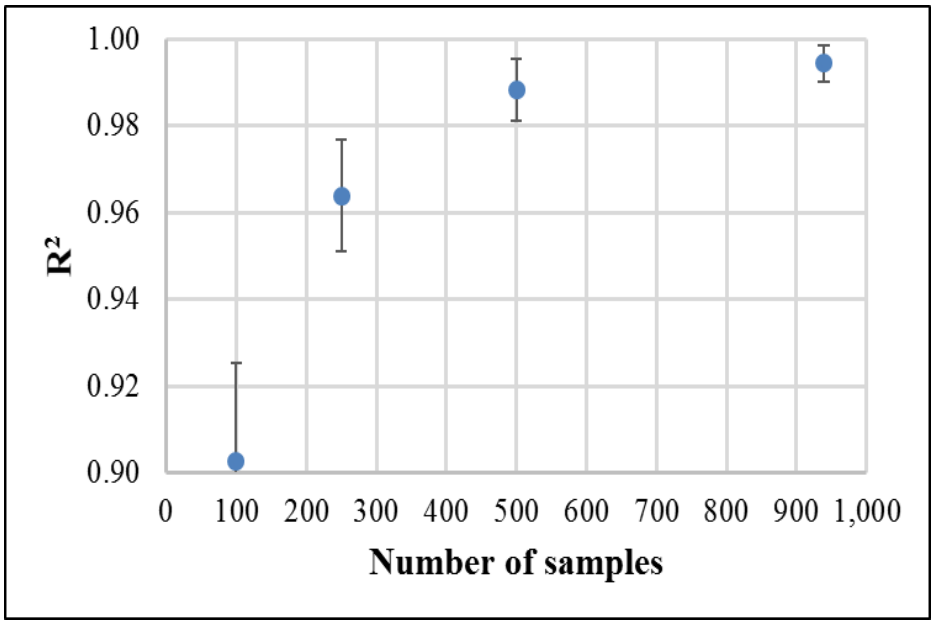

(a)

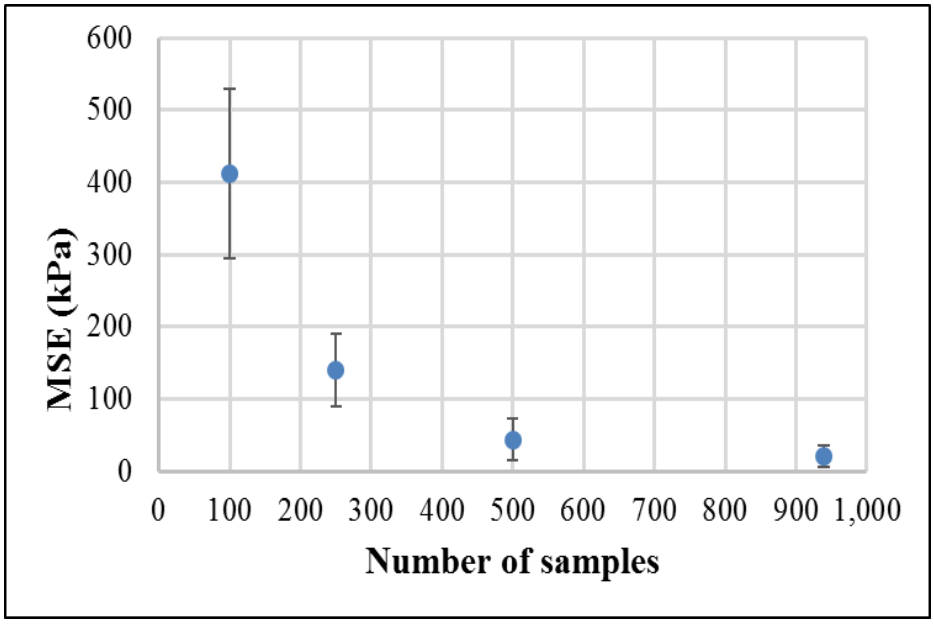

(b)

Figure 2.1 Accuracy improvement using different number of cases in the development of ANN models in terms of (a) R^2 and (b) MSE

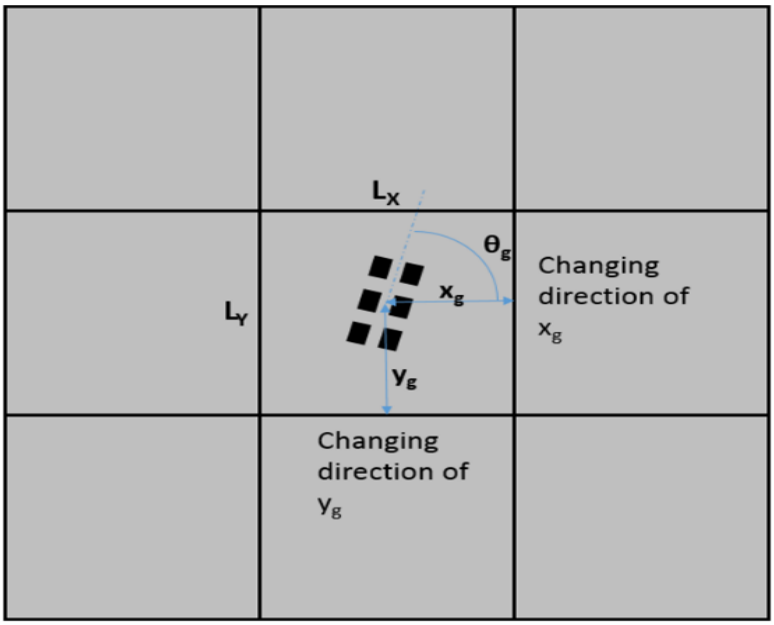

Figure 2.2 Aircraft loading conditions

Table 2.1 Ranges of inputs used for FEAFAA batch runs

Inputs		**Range**	
		Min	**Max**
PCC Slab	Modulus GPa (psi)	20.7 (3×10^6)	48.3 (7×10^6)
	Thickness cm. (in.)	25.4 (10)	61 (24)
	Poisson Ratio	0.15	0.20
Granular Subbase	Modulus GPa (psi)	0.1 (15,000)	0.3 (50,000)
	Thickness cm. (in.)	51 (20)	127 (50)
	Poisson Ratio	0.35	
Subgrade	Modulus GPa (psi)	0.02 (3,000)	(0.21) 30,000
	Poisson Ratio	0.4	
Slab Dimension m. (ft.)		6.1 (20)	9.1 (30)
Slab Number of Elements		30	
Number of Slabs		9	
Foundation Number of Elements		30	
Loading Angle (deg.)		0	90
Temperature Gradient ^oC/cm. (^oF/in.)		2.3	
Thermal Coefficient 1/^oC (1/^oF)		7.4×10^{-6} (4.1×10^{-6})	12.9×10^{-6} (7.2×10^{-6})
Equivalent Joint Stiffness GPa/m. (psi/in.)		20.8 (76,768)	84.5 (311,369)

ANN Model Development

ANN models were developed for both mechanical-load-only and simultaneous mechanical and thermal load cases. For each case, both 'approach 1' and 'approach 2' were followed in the model development. In the ANN model development, a two-layer feed-forward network was trained using a Levenberg-Marquardt algorithm (LMA) in the MATLAB environment (MATLAB 2017).

Mechanical-Load-Only Case

The authors executed a batch run of 439 cases of B777-300ER gear loading (no thermal load), from which they obtained the critical pavement responses required for development of ANN models. The input variables defining the batch run set, with their ranges, are given in Table 2.1.

Use of individual input parameters (approach 1)

As shown in Fig. 2.3, twelve input variables were used in the ANN model development. Among these 12 input parameters, three represent the slab properties, three represent pavement foundation properties, three represent loading location, two represent slab size, and equivalent joint stiffness represents the joint stiffness properties of the pavement system.

For the top-down cracking mode, stresses and deflections at the top of the slab surface are of great interest, so critical pavement stresses and deflections at the top of the slab surface were extracted for each case and used as outputs in the ANN model development. The critical pavement responses used as individual outputs in the ANN model development are as follows:

- $\sigma_{xx,\ max,\ top\text{-}tensile}$
- $\sigma_{yy,\ max,\ top\text{-}tensile}$

- $\tau_{xy,\ max,\ top}$
- δ_{max}

Where,

$\sigma_{xx,\ max,\ top\text{-}tensile}$ = Maximum tensile stress in the x direction on top of the slab surface

$\sigma_{yy,\ max,\ top\text{-}tensile}$ = Maximum tensile stress in the y direction on top of the slab surface

$\tau_{xy,\ max,\ top}$ = Maximum shear stress on top of the slab surface

δ_{max} = Maximum deflection

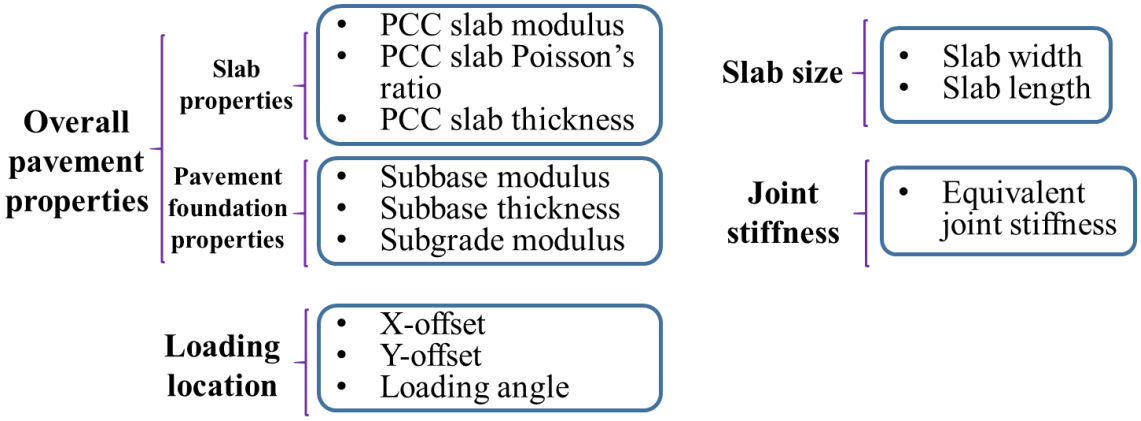

Figure 2.3 Twelve individual input parameters used in the development of ANN models (mechanical-load-only case)

Fig. 2.4 shows the ANN network architecture employed in the model development. The ANN network consists of twelve inputs, one hidden layer with 40 hidden neurons, and one output layer. A separate ANN model was developed to predict each pavement response. Therefore, one output layer showing the related pavement response to be predicted and the ANN model to be developed is shown in the network architecture (Fig. 2.4).

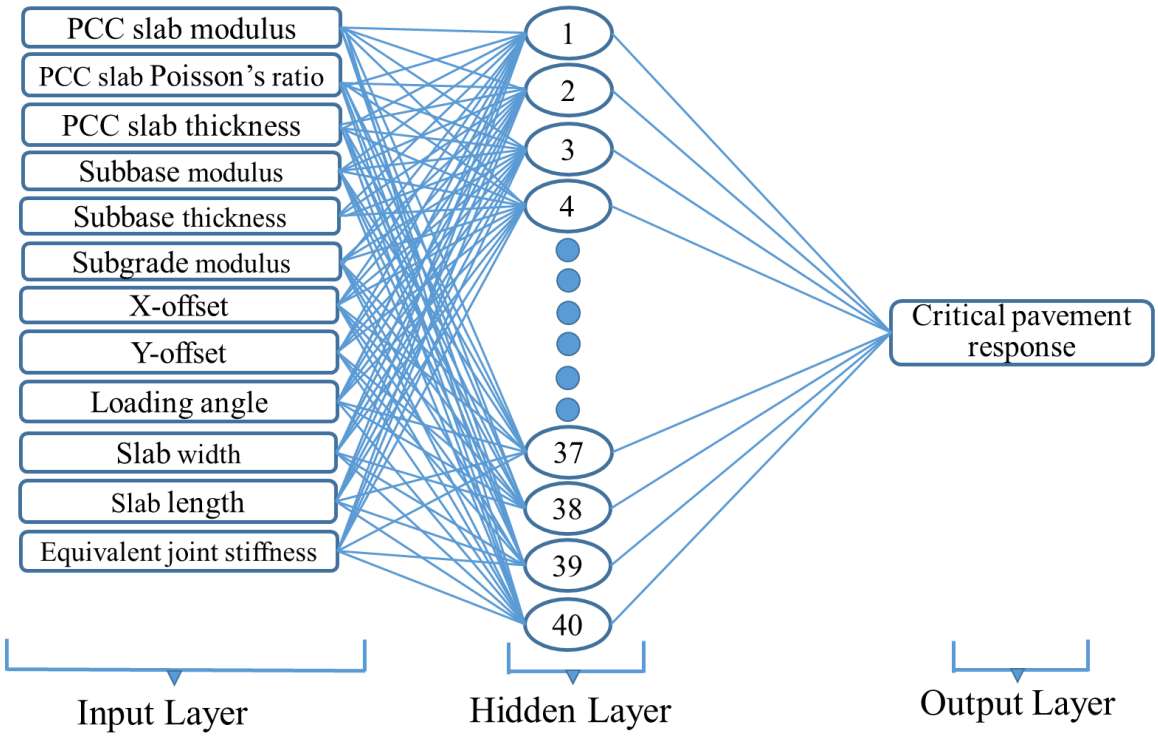

Figure 2.4 ANN network architecture (individual input parameters, mechanical-load-only case)

The choice of forty hidden neurons used in the hidden layer of the ANN network architecture was made as a result of a sensitivity analysis conducted for that study. Using 500 samples for all input variables, ANN models were developed using 10, 20, 40 and 80 hidden neurons. Fig. 2.5 shows the accuracy comparison of ANN models using different numbers of hidden neurons. To eliminate any sampling problems, ten consecutive ANN models were developed for each hidden neuron case. The variation in each case was quantified by the standard deviation (Fig. 2.5). It was determined that 40 hidden neurons produced the highest accuracy. Therefore, this study used 40 hidden neurons for all cases.

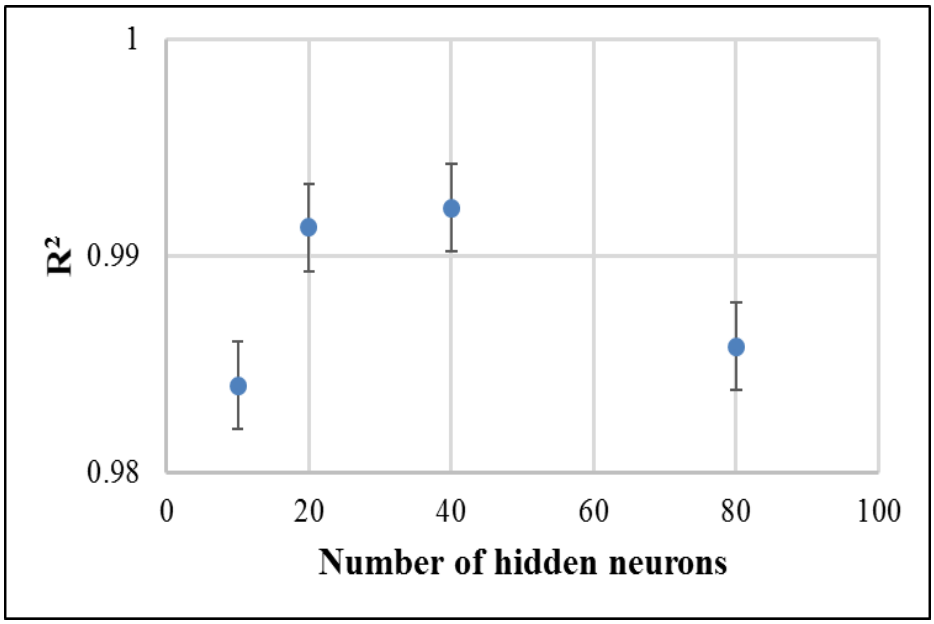

(a)

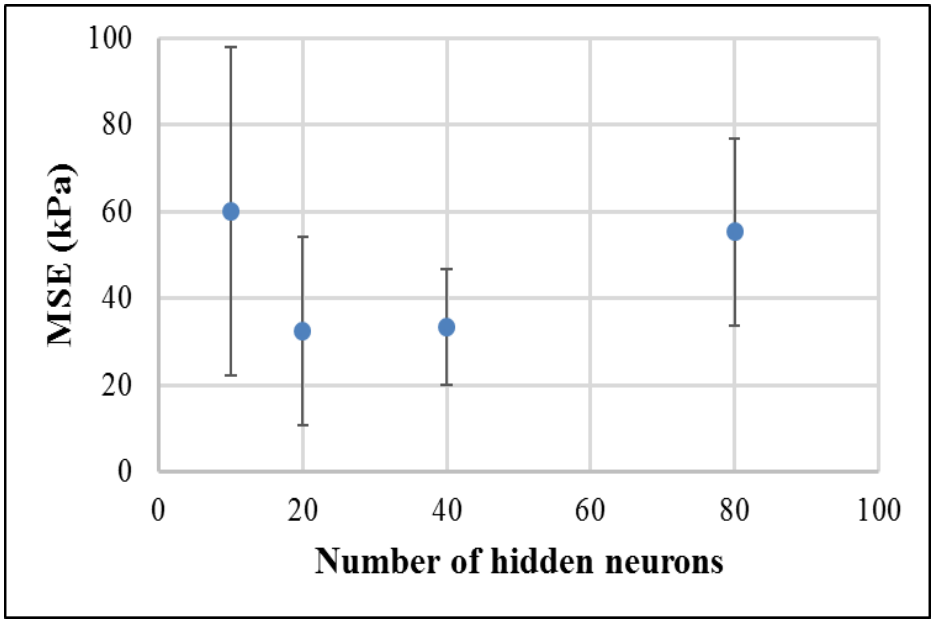

(b)

Figure 2.5 Accuracy comparison using different number of hidden neurons in the development of ANN models in terms of (a) R^2 and (b) MSE

Fig. 2.6 shows pavement response comparisons between the FEAFAA solutions and ANN model solutions for (a) $\sigma_{xx,\ max,\ top\text{-}tensile}$, (b) $\sigma_{yy,\ max,\ top\text{-}tensile}$, (c) $\tau_{xy,\ max,\ top}$ and (d) δ_{max}.

For all pavement response types, in the ANN model development, 307, 66 and 66 cases were used for training, testing and validation, respectively. For all pavement response types, ANN models successfully replicated FEAFAA pavement response solutions. Validation and test sets produced high accuracies comparable to the training set in all pavement response types. This demonstrates the ANN models' success in generalization (i.e., they did not memorize the relationship) and so they are robust and valid.

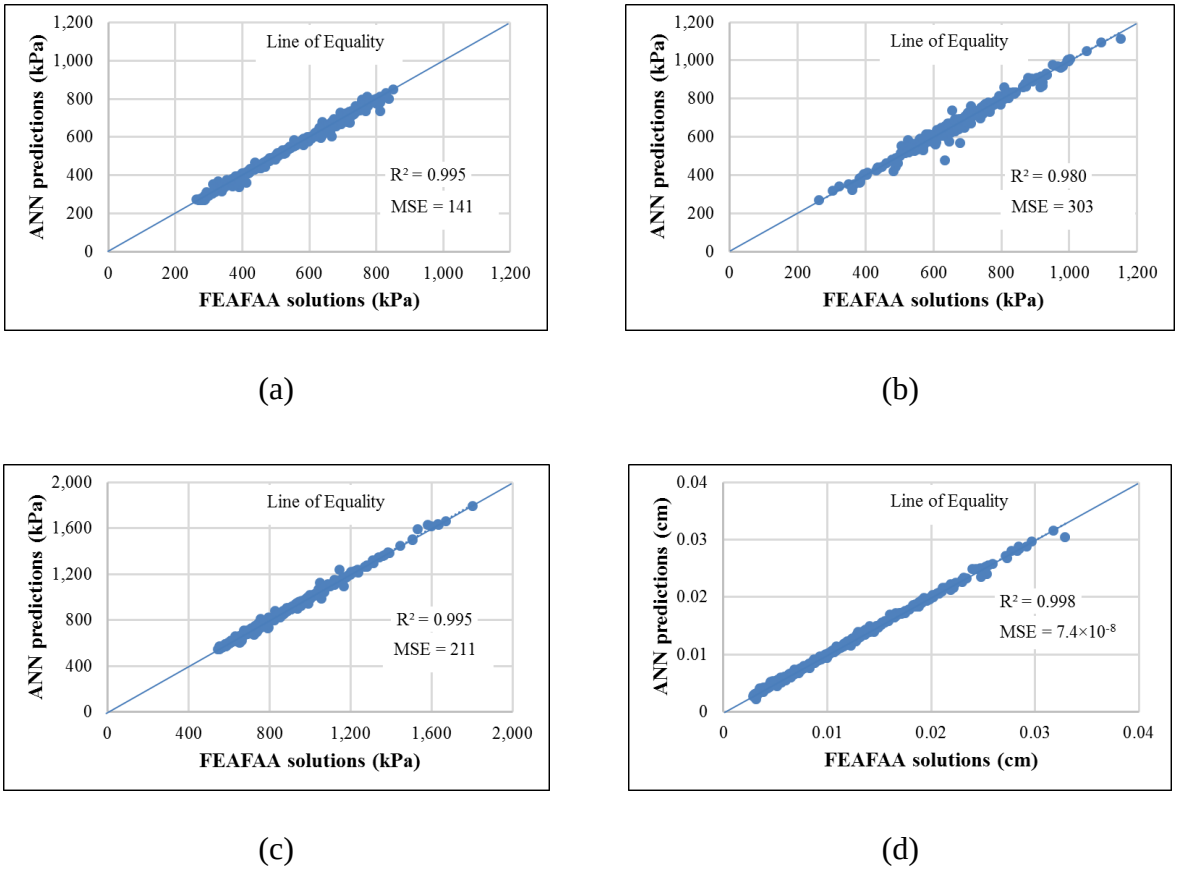

Figure 2.6 FEAFAA solutions vs. ANN predictions for (a) $\sigma_{xx,\ max,\ top\text{-}tensile}$; (b) $\sigma_{yy,\ max,\ top\text{-}tensile}$; (c) $\tau_{xy,\ max,\ top}$; (d) δ_{max} (individual input parameters, mechanical-load-only case)

Use of dimensional analysis (approach 2)

As mentioned previously, dimensional analysis has been used successfully in developing models to predict pavement responses (Ceylan 2002; Khazanovich et al. 2001;

Ioannides 2005; NCHRP 2003). Dimensional analysis has been evaluated in some FE based pavement design and analysis applications such as ISLAB 2000 (Khazanovich 2001). However, FEAFAA has certain unique features that no other available FE based pavement design and analysis applications have. Among these are the use of "infinite" elements to represent subgrades of infinite depth and a unidirectional spring element used for modeling linear elastic joints between adjacent slabs. FEAFAA includes horizontal interfaces in its three-dimensional model that meet the requirements of a full unbonded interface between the slab and base course and a full bond at all other horizontal interfaces (Brill 1998). Most of the available FE based applications have used the simplified Winkler foundation concept to characterize the subgrade and the load transfer efficiency (LTE) concept for joints. These unique features needed to be incorporated in the dimensional analysis.

In FEAFAA, an equivalent shear stiffness k_{joint}, characterizes the joint, in units of force per relative vertical displacement per unit length of the joint. Joints were modeled in such a way that they act as linear elastic springs between adjacent slabs, transmitting vertical loads between adjacent slabs in shear through the joint. The shear force is assumed linearly proportional to the relative vertical displacement between slabs (Hooke's law) (Brill 1998). A value for k_{joint} can be either input to FEAFAA directly or the software can calculate a value from dowel bar diameter, dowel bar spacing and joint opening information. The range of values for k_{joint} used in this study is shown in Table 2.1. In some previous studies, joints have been characterized by the LTE concept and a dimensionless parameter of AGG/kl (explained later in this paper) was used to represent joint behavior of the pavement (Ceylan 2002; Ioannides 2005). However, for FEAFAA, k_{joint} has to be used in joint characterization and a dimensionless parameter including k_{joint} has to be identified to simulate joint behavior.

In FEAFAA, subgrade is modeled as an elastic solid; therefore, it is characterized by elastic properties: the elastic modulus ($E_{subgrade}$) and Poisson's ratio. In addition, the subgrade is assumed to have infinite thickness.

Dimensionless parameters identified in the previous studies were analyzed to find out whether they can also be used in this study. The dimensionless parameters identified in the previous studies (Ceylan 2002; Ioannides 2005; NCHRP 2003) were as follows:

- AGG/k*l*,
- x_g/L_x,
- y_g/L_y,
- a/*l*,
- L_x/l,
- L_y/l,
- *l*

Where,

AGG = Aggregate interlock factor

k = Modulus of subgrade reaction

l = Radius of relative stiffness of the slab-subgrade system

x_g = x-coordinate of applied gear load

y_g = y-coordinate of applied gear load

L_x and L_y = Length and width of the slab

a = Radius of the applied load

Analyzing the parameters above, it was determined that AGG had to be replaced with k_{joint} in the AGG/kl parameter to be used in this study. In addition, $E_{subgrade}$ has to be used in

characterization of the subgrade. Since k cannot be used and k is included in radius of relative stiffness (*l*) equation (Equation 2.3), this equation should be revised for this study.

Original '*l*' equation is shown as l_{ks}, where *ks* stands for *k* value of the subgrade (*s*):

$$l_{ks} = \sqrt[4]{\frac{E\,h^3}{12\,(1-\mu^2)\,k}} \tag{2.3}$$

Where,

h = Slab thickness

E = Modulus of elasticity of PCC

μ = Poisson's ratio for PCC

Based on the previous studies and considering the input parameters used in FEAFAA, the following parameters were determined to be used in dimensional analysis.

- $k_{joint}\, h_{eff}/E_{subgrade}\, l$,
- x_g/L_x,
- y_g/L_y,
- a/l,
- L_x/l,
- L_y/l

Where,

h_{eff} = Effective thickness of two

h_{eff} equation used (Khazanovich et al. 2001),

$$h_{eff} = \sqrt[3]{h_{PCC}^3 + \frac{E_{BASE}}{E_{PCC}}\, h_{BASE}^3} \tag{2.4}$$

Where,

h_{PCC} = Slab thickness

h_{BASE} = Base thickness

E_{PCC} = Modulus of elasticity of PCC

E_{BASE} = Modulus of elasticity of base

Original *l* equation (Equation 2.3) was revised to make all of the parameters dimensionless by taking into account the physical meaning of the original equation. The revised '*l*' equation is shown in Equation 2.5 as 'l_{Es}', where *E* stands for $E_{subgrade}$ and subgrade (*s*), respectively. Note that only difference between l_{Es} and l_{ks} is that *k* and *h* in the l_{ks} equation were replaced by $E_{subgrade}$ and h_{eff}.

'*l*' equation used in dimensional analysis: $l_{Es} = \sqrt[3]{\frac{E\, h_{eff}^3}{12\,(1-\mu^2)\, E_{subgrade}}}$ (2.5)

The critical dimensionless pavement responses used as outputs in the ANN model development are as follows:

- $\sigma_{xx,\ max,\ top\text{-}tensile} \times h^2/P$
- $\sigma_{yy,\ max,\ top\text{-}tensile} \times h^2/P$
- $\tau_{xy,\ max,\ top} \times h^2/P$
- $\delta_{max} \times E_{subgrade} \times l_{Es}{}^2 /P$

Where,

h = Slab thickness

P = Applied load (a combined weight on 6 wheels in one leg of the main gear of Boeing B777-300ER)

Fig. 2.7 shows the ANN network architecture employed in the model development if dimensional analysis is used in the model development. As can be seen in the figure, the ANN network consists of six inputs, one hidden layer with 40 hidden neurons along with one

output layer. The main benefit of using dimensional analysis is that the ANN model is developed with far fewer input parameters: only six input parameters are needed in dimensional analysis (approach 2), compared to fourteen parameters when using individual input parameters (approach 1). Using fewer input parameters can save considerable computational time and other resources.

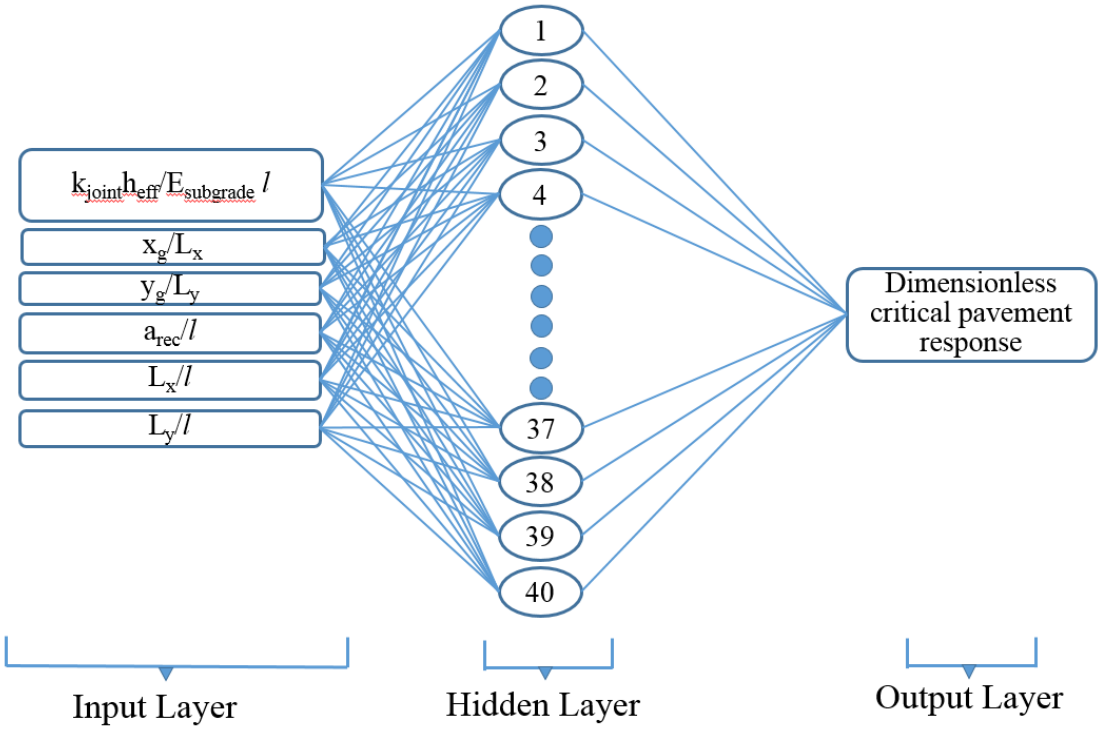

Figure 2.7 ANN network architecture (dimensional analysis, mechanical-load-only case)

Fig. 2.8 shows pavement response comparisons between the FEAFAA solutions and ANN predictions for (a) $\sigma_{xx,\ max,\ top\text{-}tensile}$, (b) $\sigma_{yy,\ max,\ top\text{-}tensile}$, (c) $\tau_{xy,\ max,\ top}$ and (d) δ_{max}, if dimensional analysis is used in the model development. For all pavement response types, in the ANN model development, 307, 66 and 66 cases were used for training, testing and validation, respectively. For all pavement response types, ANN models successfully reproduced FEAFAA pavement response solutions.

Simultaneous Mechanical and Thermal Loading Case

The authors executed a batch run of 500 cases of combined mechanical and thermal loading, from which they obtained the critical pavement responses required for development of ANN models. The input variables defining the batch run set, with their ranges, are given in Table 2.1.

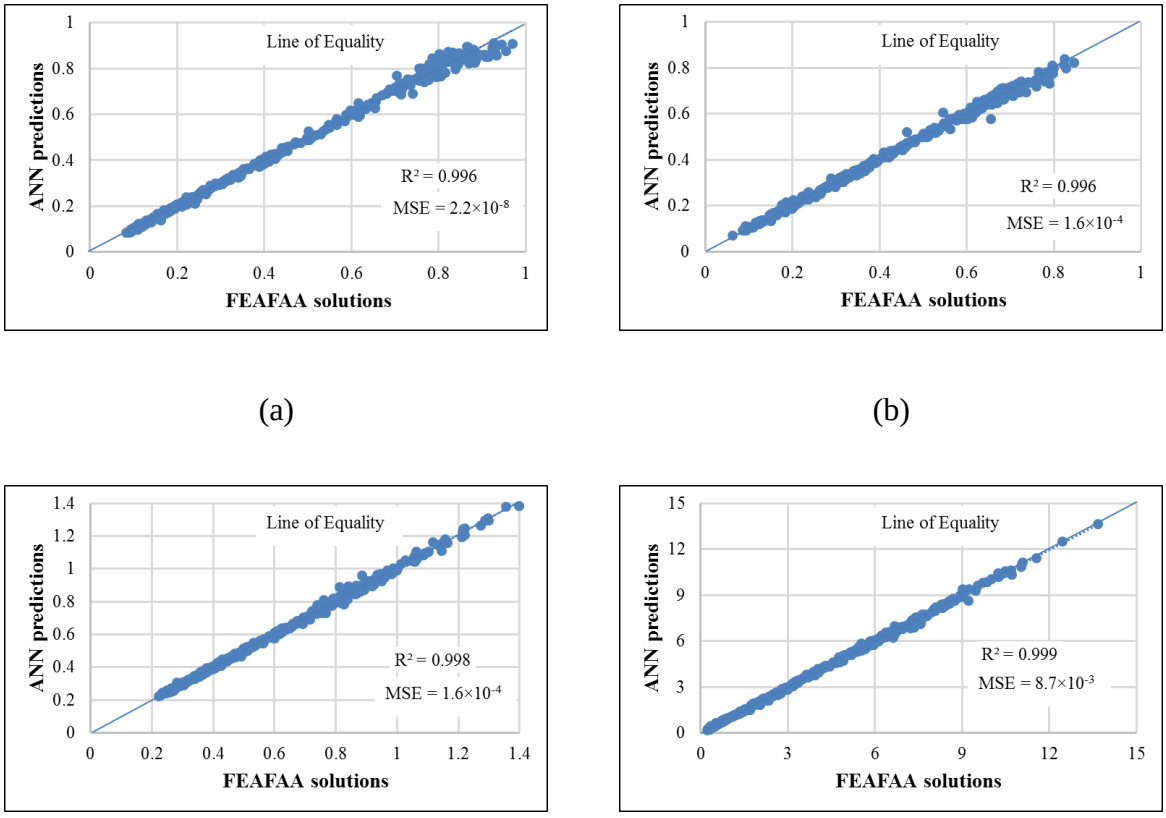

Figure 2.8 FEAFAA solutions vs. ANN predictions for (a) $\sigma_{xx,\,max,\,top\text{-}tensile}$; (b) $\sigma_{yy,\,max,\,top\text{-}tensile}$; (c) $\tau_{xy,\,max,\,top}$; (d) δ_{max} (dimensional analysis, mechanical-load-only case)

Use of individual input parameters (approach 1)

In this approach, all individual varied input parameters were used in ANN models as input parameters. Fig. 2.9 shows the 14 input parameters that must be used in the ANN model development. As can be seen in Fig. 2.9, the only difference between the simultaneous

mechanical and thermal load case and the mechanical-load-only case is the inclusion of two variables to simulate thermal loading. The two additional variables are shown in Fig. 2.9 as slab temperature properties.

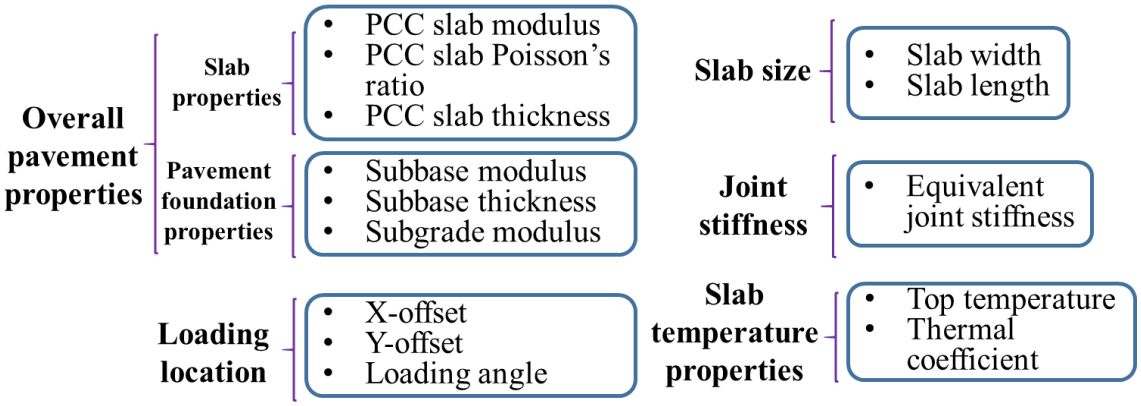

Figure 2.9 Fourteen types of individual input parameters (simultaneous mechanical and thermal loading case)

The ANN network architecture consisted of 14 inputs, one hidden layer with 40 hidden neurons, and one output layer.

Fig. 2.10 shows pavement response comparisons between the FEAFAA solutions and ANN predictions for (a) $\sigma_{xx,\ max,\ top\text{-}tensile}$, (b) $\sigma_{yy,\ max,\ top\text{-}tensile}$, (c) $\tau_{xy,\ max,\ top}$ and (d) δ_{max}. For all response types, 350, 75 and 75 cases were used for training, testing and validation, respectively. Similar to the previous findings, for all pavement response types, ANN models successfully reproduced FEAFAA solutions.

Use of dimensional analysis (approach 2)

The authors executed the feasibility of using dimensional analysis in the ANN model development for the combined mechanical and thermal load case. The only difference compared to the mechanical- load-only case is the inclusion of dimensionless parameter to represent thermal loading.

Korenev's original dimensionless temperature gradient (Equation 2.6) has been successfully used to represent thermal loading (Khazanovich 2001).

$$\Phi = \frac{2\alpha(1+\mu)l^2}{h^2}\frac{k}{\gamma}\Delta T \tag{2.6}$$

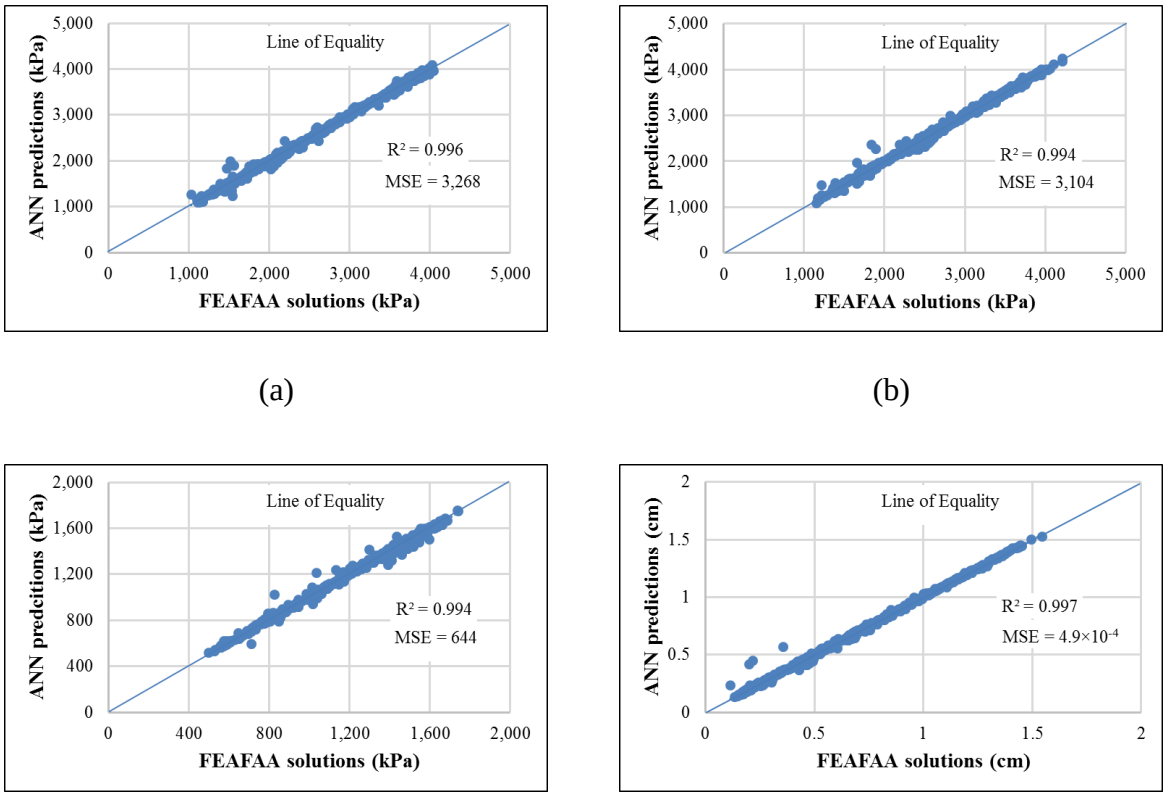

Figure 2.10 FEAFAA solutions vs. ANN predictions for (a) $\sigma_{xx,\ max,\ top\text{-}tensile}$; (b) $\sigma_{yy,\ max,\ top\text{-}tensile}$; (c) $\tau_{xy,\ max,\ top}$; (d) δ_{max} (individual input parameters, simultaneous mechanical and thermal load case)

Equation 2.6 was revised to be applicable to FEAFAA as follows:

$$\Phi_m = \frac{2\alpha(1+\mu)l_m^2}{h^2}\frac{E_{sub}}{\gamma}\Delta T \tag{2.7}$$

Where,

α = Coefficient of thermal expansion

ΔT = Temperature difference through the slab thickness

γ = Unit self-weight of PCC slab

h = Slab thickness

l= Radius of relative stiffness of the plate-subgrade system

μ = Plate Poisson's ratio

k = Modulus of subgrade reaction

E_{sub} = Subgrade elastic modulus

Including the dimensionless thermal gradient obtained through Equation 2.7 and other parameters used for mechanical-load-only case, seven dimensionless parameters were determined to be used as inputs in the ANN model development:

- $k_{joint}/E_{subgrade}\ l$,
- x_g/L_x,
- y_g/L_y,
- a/l,
- L_x/l,
- L_y/l,
- Φ_m

In that case, as the ANN network architecture, sixteen inputs, one hidden layer with 40 hidden neurons along with one output layer was used.

Fig. 2.11 shows pavement response comparisons between the FEAFAA solutions and ANN predictions for (a) $\sigma_{xx,\ max,\ top\text{-}tensile}$, (b) $\sigma_{yy,\ max,\ top\text{-}tensile}$, (c) $\tau_{xy,\ max,\ top}$ and (d) δ_{max}, if

dimensional analysis is used in the model development. For all pavement response types, in the ANN model development, 350, 75 and 75 cases were used for training, testing and validation, respectively. Similar to previous findings, ANN models successfully reproduced FEAFAA solutions for all pavement responses.

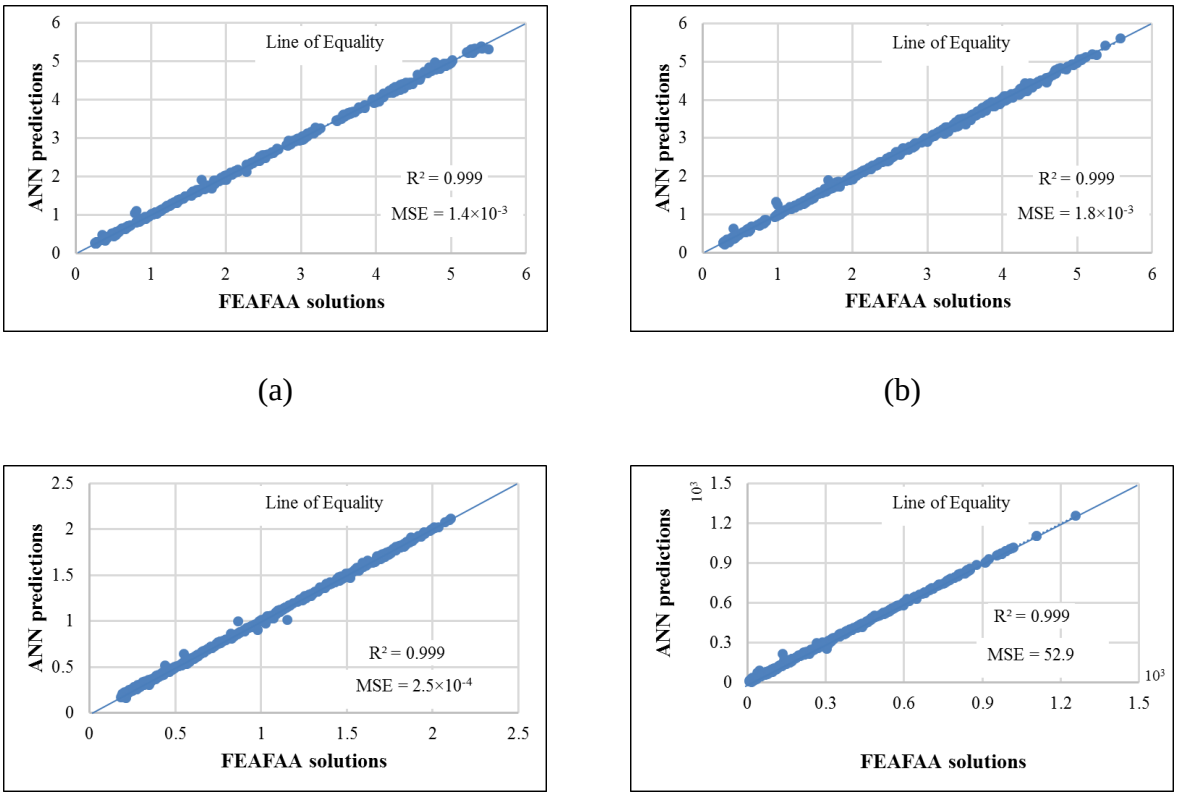

Figure 2.11 FEAFAA solutions vs. ANN predictions for (a) $\sigma_{xx,\,max,\,top\text{-}tensile}$; (b) $\sigma_{yy,\,max,\,top\text{-}tensile}$; (c) $\tau_{xy,\,max,\,top}$; (d) δ_{max} (dimensional analysis, simultaneous mechanical and thermal load case)

Table 2.2 compares accuracy of the ANN models for predicting pavement responses. Accuracy is expressed by the statistics R^2 and MSE. All ANN models successfully predicted pavement responses for both mechanical-load-only and combined mechanical and thermal load cases. Moreover, in both cases, the ANN models developed using dimensional analysis

predicted pavement responses as accurately as those developed using individual input parameters.

Table 2.2 Accuracy comparison of the ANN models in predicting pavement responses for different cases

Loading Case	Method	Accuracy - R^2 (MSE)			
		$\sigma_{xx,\ max,\ top\text{-}tensile}$	$\sigma_{yy,\ max,\ top\text{-}tensile}$	$\tau_{xy,\ max,\ top}$	δ_{max}
Mechanical-load- only case	Individual input parameters	0.995 (141)	0.980 (303)	0.995 (211)	0.998 ($7.4x10^{-8}$)
	Dimensional analysis	0.996 (2.2×10^{-8})	0.996 (1.6×10^{-4})	0.998/ (1.6×10^{-4})	0.999 (8.7×10^{-3})
Simultaneous mechanical and temperature load case	Individual input parameters	0.996 (3,268)	0.994 (3,104)	0.994 (644)	0.997 (4.9×10^{-4})
	Dimensional analysis	0.999 (1.4×10^{-3})	0.999 (1.8×10^{-3})	0.999 (2.5×10^{-4})	0.999 (53)

Summary, Conclusions and Future Work

The FAA is seeking practical alternatives to running the 3D-FEM stress computation that can reduce the time to give accurate stress predictions. Artificial intelligence (AI) based alternatives such as artificial neural networks (ANNs) have great potential and have been successfully used in pavement engineering to solve similar problems for decades.

This paper investigated the feasibility of developing ANN-based surrogate computational response models or procedures (suitable for implementation in FAARFIELD (*Version 2.0*)) that returns a close estimate of the top-down bending stress computed by NIKE3D in rigid airport pavements. These models would enable faster 3D-FE computations of design stresses in FAARFIELD (*Version 2.0*) making it suitable for routine design. To develop these ANN models, FEAFAA, the FAA's computer program for stand-alone 3D-FEM analysis of multi-slab rigid pavements, was used.

To develop ANN-based surrogate computational response models, a synthetic database consisting of FEAFAA input parameters and the associated critical pavement responses was created. In the FEAFAA batch runs, two different loading cases were considered and ANN models for these two cases were developed: mechanical-load-only and simultaneous mechanical and temperature loading. During the ANN model development for each loading case, two approaches were followed:

- Use all individual input parameters as independent inputs in the development of ANN models (approach 1)
- Use dimensional analysis to reduce the number of inputs in the development of ANN models (approach 2)

Specific conclusions of this paper are listed below:

- ANN was found to be a promising alternative in returning very close estimates of the top-down bending stress computed by NIKE3D in rigid airport pavements. By using the ANN models, very accurate stress predictions can be produced in a fraction of time compared to the significant amount of time needed to perform a 3D-FE computation. For instance, stress predictions for thousands of cases can be predicted in seconds using ANN models compared to days, if not months, using 3D-FE computation.
- Dimensional analysis was found to be a promising method to reduce the input feature space in ANN model development. It produced accuracies similar to those produced using individual input parameters in the model development (see Table 2.2).
- An advantage of using dimensional analysis in the development of ANN models is that it significantly reduces the number of required input parameters. For example, six dimensionless input parameters were found to be enough to successfully predict

pavement responses, compared to fourteen individual input parameters needed for mechanical-load-only case.

- Another advantage of using dimensional analysis in the development of ANN models is that the use of these models can be extended for any types of pavements with the same pavement layer configurations and the next generation aircraft with the same gear configurations, if applicable. As long as the dimensionless parameters for the pavements and the next generation aircraft cases are within the ranges that the ANN models were developed, the models can be directly used for these pavements and aircraft without any modification.
- Future studies will focus on creating ANN models for other airplane types.

Acknowledgements

The authors gratefully acknowledge the Federal Aviation Administration (FAA) for supporting this study. The contents of this paper reflect the views of the authors who are responsible for the facts and accuracy of the data presented within. The contents do not necessarily reflect the official views and policies of the FAA and Iowa State University. This paper does not constitute a standard, specification, or regulation.

References

Autoit (2017). <https://www.autoitscript.com/site/autoit/> (Aug. 1, 2017).

Brill, D. R. (1998). *Development of advanced computational models for airport pavement design*. FAA Report DOT/FAA/AR-97/47. Federal Aviation Administration (FAA), Washington, D.C., Available at: http://www.tc.faa.gov/its/worldpac/techrpt/ar97-47.pdf (accessed on May 18, 2015).

Brill, D. R. (2000). *Field verification of a 3D finite element rigid airport pavement model*. FAA Report DOT/FAA/AR-00/33. Federal Aviation Administration (FAA), Washington, D.C.

Ceylan, H., Tutumluer, E., and Barenberg, E. J. (1999). "Artificial neural networks for analyzing concrete airfield pavements serving the Boeing B-777 aircraft." In *Transportation Research Record: Journal of the Transportation Research Board, No. 1684*, Transportation Research Board of the National Academies, Washington, D.C., 1999, pp. 110–117.

Ceylan, H. (2002). *Analysis and design of concrete pavement systems using artificial neural networks*. University of Illinois at Urbana-Champaign, Urbana, IL.

FAA (2014). *Airport design*. FAA Advisory Circular (AC) No: 150/5300-13A. Available at:http://www.faa.gov/documentLibrary/media/Advisory_Circular/150-5300-13A-chg1-interactive.pdf (accessed on May 18, 2015).

FAA (2009). *Airport pavement design and evaluation.* FAA Advisory Circular (AC) No: 150/5320-6E, 2009. Available at: http://www.faa.gov/documentLibrary/media/Advisory_Circular/150_5320_6e.pdf (accessed on May 18, 2015).

FAARFIELD [Computer software]. Federal Aviation Administration Airport Technology R&D Branch, ANG-E262 William J. Hughes Technical Center, Egg Harbor Township, NJ.

FEAFAA version 2.0 [Computer software]. Federal Aviation Administration Airport Technology R&D Branch, ANG-E262 William J. Hughes Technical Center, Egg Harbor Township, NJ.

Ioannides, A. M. (2005). "Stress prediction for cracking of jointed plain concrete pavements, 1925–2000 - An overview". In *Transportation Research Record: Journal of the Transportation Research Board, No. 1919*, Transportation Research Board of the National Academies, Washington, D.C.

ISLAB version 2000 [Computer software]. ERES Consultants, Champaign, IL.

Khazanovich, L., Selezneva O. I., Yu, H. T., and Darter, M. I. (2001). "Development of rapid solutions for prediction of critical continuously reinforced concrete pavement stresses." In *Transportation Research Record: Journal of the Transportation Research Board, No. 0358*, Transportation Research Board of the National Academies, Washington, D.C.

Langhaar, H. L. (1951). *Dimensional analysis and theory of models*. John Wiley and Sons, New York.

MATLAB version 9.0 [Computer software]. MathWorks, Natick, MA

NCHRP (2003). *Guide for mechanistic-empirical design of new and rehabilitated pavement structures, final document, Appendix QQ: Structural response models for rigid pavements*. NCHRP 1-37A Report. Transportation Research Board of the National Academies, Washington, D.C.

NIKE3D_FAA version 1.0 [Computer software]. Federal Aviation Administration Airport Technology R&D Branch, ANG-E262 William J. Hughes Technical Center, Egg Harbor Township, NJ.

Rezaei-Tarahomi, A., Kaya, O., Ceylan, H., Gopalakrishnan, K., Kim, S., and Brill, D. R. (2017a). "Neural networks prediction of critical responses related to top-down and bottom-up cracking in airfield concrete pavement." *Proc., 10th International Conference on the Bearing Capacity of Roads, Railways and Airfields*, June 28-30, Athens, Greece.

Rezaei-Tarahomi, A., Kaya, O., Ceylan, H., Gopalakrishnan, K., Kim, S., and Brill, D. R. (2017b). "Sensitivity quantification of airport concrete pavement stress responses associated with top-down and bottom-up cracking." *International Journal of Pavement Research and Technology*, doi: http://dx.doi.org/10.1016/ j.ijprt.2017.07.001.

Taylor, E. S. (1974). *Dimensional analysis for engineers*. Clarendon Press, Oxford.

CHAPTER 3. NUMERICAL ANALYSIS OF LONGITUDINAL CRACKING IN WIDENED JOINTED PLAIN CONCRETE PAVEMENT SYSTEMS

A journal paper submitted and under review for *International Journal of Pavement Research Technology*

Orhan Kaya, Yang Zhang, Halil Ceylan, Sunghwan Kim, Shuo Yang, Peter C. Taylor and Kasthurirangan Gopalakrishnan

Abstract

While widened slabs have been used to mitigate transverse cracking in jointed plain concrete pavements (JPCP), it is well-known that use of such slabs increases longitudinal cracking potential in JPCP. Field investigations have been conducted in Iowa widened JPCP to seek understanding of mechanisms and causes of observed longitudinal cracks. Based on field investigations it was found that all longitudinal cracks are top-down cracks. Another finding of the field investigations was that longitudinal cracks start mostly from transverse joints about 0.6-1.2 m. (2-4 ft.) away from widened slab edges. Sites with a tied PCC shoulder exhibited fewer longitudinal cracks than sites constructed with hot mix asphalt (HMA) shoulders. In this paper, the longitudinal cracking mechanism of widened JPCP was demonstrated and longitudinal cracking potential was evaluated using numerical analysis. The critical load configuration with the highest longitudinal cracking potential for widened JPCP was identified. Three shoulder design alternatives were also compared in terms of their contributions to mitigation of longitudinal cracking potential. Higher longitudinal cracking potential was identified when widened slabs with partial-depth tied PCC shoulder alternatives were used compared to regular slabs with full-depth tied PCC shoulders. Moreover, a higher top-to-bottom tensile stress ratio value was calculated for regular slabs with an HMA shoulder compared to widened slabs with an HMA shoulder. The findings of

this study provide explanations as to where and how longitudinal cracking is likely to be initiated as well as recommendations as to how longitudinal cracking potential could be mitigated.

Introduction

Widened slabs have been used to mitigate transverse cracking in jointed plain concrete pavements (JPCP) because, since the development of Westergard theory, [1] it has been known that edge load compared to interior or corner loads usually produces the highest stress in JPCP. While widened slabs are usually 4.3 m. (14 ft.) wide and constructed for traffic lanes adjacent to passing lanes (3.7 m. (12 ft.) wide), lane width in widened slabs is still taken to be 3.7 m. (12 ft.) wide, with the extra 0.6 m. (2 ft.) width designated as part of the pavement shoulder. By using widened slabs, load is not applied to slab edges, so transverse cracking potential is significantly diminished, but it has been known that widened slabs increase longitudinal cracking potential in JPCP [2, 3]. It has been also documented that the type of shoulder adjacent to widened slabs might have an effect on longitudinal crack potential in widened slabs [2, 3].

Field investigations have been conducted for widened JPCP in Iowa at 12 identified sites, including 4 control sites and 8 sites suffering from different levels of longitudinal cracking, with the goal of identifying possible reasons for observed longitudinal cracking. Details of these field investigations can be found in another study [4] that revealed that all longitudinal cracks were found to be top-down cracks, initiated at the top surfaces of widened slabs and migrating down to the bottom surfaces of the widened slabs. Another finding of the field investigations was that longitudinal cracks started mostly from transverse joints about 0.6–1.2 m. (2-4 ft.) away from widened slab edges. Field investigations also

revealed that sites with a tied PCC shoulder had fewer longitudinal cracks than sites with hot mix asphalt (HMA) and granular shoulders [4].

While some studies have mentioned that longitudinal cracks might occur in JPCP under certain conditions [5, 6, 7, 8], there has been no previous study focusing solely on modeling longitudinal cracking in widened JPCP.

ISLAB 2005, a numerical analysis software package specifically developed for rigid pavement analysis, has evolved historically, and previous versions have had other names: ILSL2, ILLI-SLAB, and ISLAB2000. The earliest version of ISLAB 2005 was ILSL2 [9], developed through by collaboration of many partners: ERES Consultants in cooperation with Michigan and Minnesota Departments of Transportation, Michigan Technical University, University of Michigan, Michigan State University, and University of Minnesota [2]. ISLAB 2005 has some advanced features that significantly assist in modeling rigid pavement systems as realistically as possible [2, 8, 10]. Among these features are the following capabilities:

- Selection among various subgrade models such as Winkler, elastic solid, Pasternak, Kerr-Vlasov, and Zhemochkin-Sinitsyn-Shtaerman
- Analyze the effects of linear and nonlinear temperature distribution throughout the pavement thickness
- Model interaction between a slab and its base using three models: bonded, unbonded, and Totsky
- Model a portion of a pavement system with different properties and features than the other parts of the pavement system

The objective of this paper is to conduct numerical analysis in order to:

- Seek better understanding of critical loading cases, including both mechanical and temperature loading that increases longitudinal cracking potential in JPCP
- Simulate longitudinal crack initiation on transverse joints
- Examine shoulder design alternatives to compare different shoulder alternatives (paved shoulder (partial-depth tied PCC and HMA), and full-depth tied PCC shoulder) in terms of their contributions to mitigation of longitudinal cracking potential

Numerical Modeling Approach

A typical Iowa widened JPCP was modeled using a six-slab setup (three widened slabs in the traffic direction and three regular slabs adjacent to the widened slabs). Model definitions used throughout this paper are shown in Fig. 3.1, where it can be seen that widened slabs have a width of 4.3 m. (14 ft.) while regular slabs have a width of 3.7 m. (12 ft.). The lane edge shows where the lane marking is located, typically 0.6 m. (2 ft.) away from the widened slab edge.

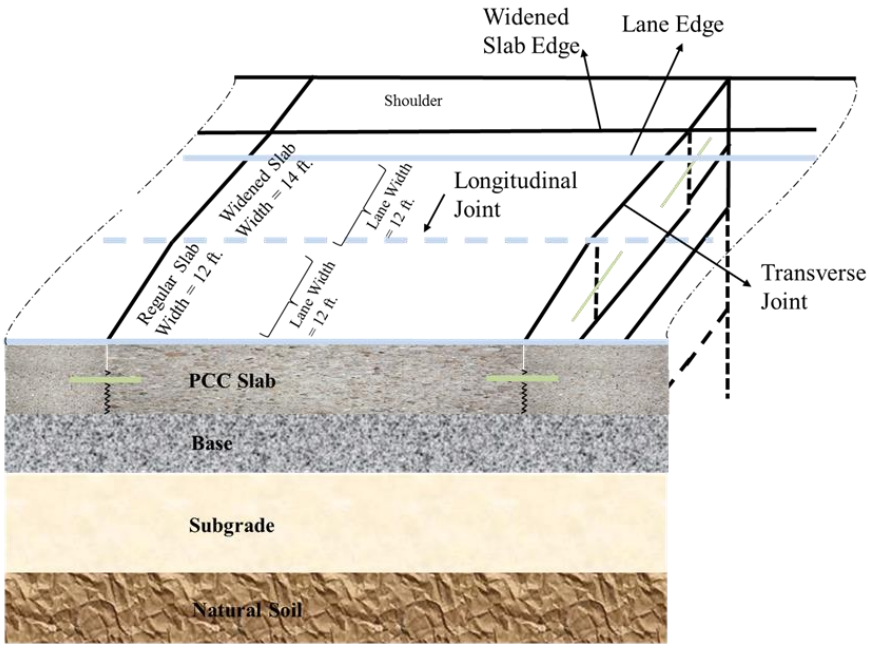

Figure 3.1 FEA model definitions

A pavement configuration with a 25.4 cm. (10 in.) PCC thickness, a 25.4 cm. (10 in.) granular base, and typical Iowa subgrade (A-6) was used. Table 3.1 provides details of the inputs used in the FEA model.

Table 3.1 FEA model inputs

Slab Size and Properties	
Slab Size in Traffic Direction (m.)	6.1
Slab Size in Transverse Direction (m.) - Regular Slab	3.7
Slab Size in Transverse Direction (m.) - Widened Slab	4.3
Finite Element Mesh Size (cm.)	15.2
Slab Thickness (cm.)	25.4
Elastic Modulus (MPa)	27,580
Poisson Ratio	0.2
Coefficient of thermal expansion (CTE) (1/^{o}C)	8.8E-06
Unit weight (kg/m^{3})	2,400
Granular Base Size and Properties	
Base Thickness (cm.)	25.4
Elastic Modulus (MPa)	241
Poisson Ratio	0.35
CTE (1/^{o}C) of granular material	9.0E-06
Unit weight (kg/m^{3})	2,038
Subgrade Properties	
k (MPa/mm)	0.044
Mechanical and Temperature Loading	
Load Level (metric-tons)	9.1 (single axle), 15.4 (tandem axle)
Tire Pressure (kPa)	827
Load Location in Traffic Direction	Every 60 cm. (2 ft.) for single axle load cases
Wander Pattern	0, 30 and 60 cm (0, 1 and 2 ft.) away from lane edge (for single axle load cases) 0, 15, 30, 45 and 60 cm. (0. 0.5, 1, 1.5 and 2 ft.) away from lane edge (for truck load cases)
Long Term Load Transfer Efficiency (LTE) (%)	70
Temperature Gradient ($^{\circ}$C/cm)	-0.3 to 0.3 with an increment of 0.03 (-2 to 2 $^{\circ}$F/in with an increment of 0.2)

ISLAB 2005 FEA software has been used in this study as the main structural model for generating rigid pavement responses of Iowa widened JPCP under mechanical and temperature loading. ISLAB 2005 discretizes modeled slabs into meshes and nodes. FEA uses a fine mesh size (nominal element size of 15.2 cm. (6 in.)). At the completion of FEA, ISLAB produces an output file in "txt" format for each FEA scenario considered (630 txt files in total for the single axle load cases introduced later in this paper), representing stress (in x direction, y direction, principal stress and von mises stress) and deflection results for each nodal value. These output files require post-processing so that critical pavement responses for each FEA scenario can be calculated and extracted.

A post-processing scheme using Microsoft Excel VBA (Visual Basic for Applications) and MATLAB (version 9.3.0.713579 [R2017b]) was developed. It combines all output files, calculates and summarizes critical pavement responses for each FEA scenario, and presents them in a summary worksheet. The post-processing steps are as the following: (1) The output files are initially transferred into a master Excel spreadsheet using Microsoft Excel VBA; (2) Using MATLAB, critical pavement responses are calculated, extracted, and written into a summary Excel spreadsheet. Critical stresses summarized are as follows: maximum top and bottom (top and bottom of slab) tensile stresses in x and y directions, maximum top and bottom principal and von mises stresses and maximum deflections.

Single Axle Load Simulations

Several FEA models were developed for (1) mechanical-load-only cases and (2) combined temperature and mechanical load cases. To simulate mechanical load, a single axle with dual wheels carrying a total load of 9.1 metric-tons (20,000 lbs.) was used. To simulate temperature loads, 21 different temperature cases were used with temperature gradients from

-0.3 to 0.3 (˚C/cm) in increments of 0.03 (˚C/cm) (Table 3.1). A single axle load was placed every 60 cm. (2 ft.) in the traffic direction and three wander distances (0, 30, and 60 cm. (0, 1, and 2 ft. away from lane edge)). A total of 630 FEA scenarios were modeled in ISLAB 2005 for single-axle load simulations (Fig. 3.2)

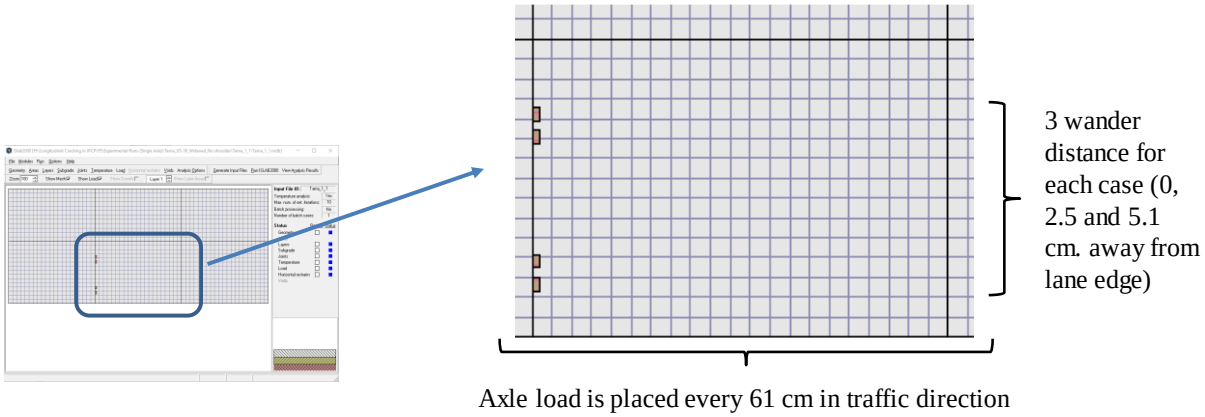

Figure 3.2 Single-axle load cases

ISLAB 2005 produces tensile stress results in the x and y directions (x direction is perpendicular to the traffic direction, y direction is the traffic direction). Tensile stress results on slab surface (top) in the x and y directions as well as deflection results were first analyzed to determine which tensile stress type (in the x or y direction) is the critical tensile stress type for producing longitudinal cracking. Based on analysis results of various mechanical and temperature loading scenarios, tensile stresses in the x direction were found to be the critical stresses for longitudinal cracking because they are tensile stresses perpendicular to the traffic direction. The tensile stresses in the y direction would be critical for transverse cracking because they are tensile stresses parallel to the traffic direction. In this study, tensile stresses in the x direction were used as critical tensile stresses to characterize longitudinal cracking.

Single Axle Load Simulation Results

Fig. 3.3 shows the top-to-bottom tensile stress ratio distribution when single-axle mechanical loads are applied at various locations in both traffic (distance from transverse joints) and wander directions for three different temperature load scenarios; (a) no temperature load (ΔT= 0 ˚C (0 ˚F)), (b) temperature difference between bottom and top of slab of 5.5 ˚C (10 ˚F) (ΔT= top-bottom= -5.5 ˚C (-10 ˚F)), and (c) temperature load with ΔT= -11 ˚C (-20 ˚F). The notation of top-to-bottom tensile stress ratio is used throughout this paper to evaluate for which loading scenarios potential longitudinal cracking might be top-down cracking. Cases where the top-to-bottom ratio is higher than 1 represent those cases where potential longitudinal cracking would be top-down. As discussed earlier, field investigations revealed that all observed longitudinal cracks were top-down cracks. As seen in Fig. 3.3a, higher top-to-bottom tensile stress ratio values were observed when a single-axle mechanical load was applied on transverse joints with no temperature loading. While there was no significant difference in top-to-bottom tensile stress ratio results for different wander distances, a slightly higher top-to-bottom stress ratio was observed when the outer wheel of the single axle was placed 0.3 m. (1 ft.) away from the lane edge, compared to cases when the outer wheel of the single axle was placed on the lane edge and 0.6 m. (2 ft.) away from the lane edge. (Fig. 3.3a). On the other hand, as shown in Fig. 3.3b, a very high top-to-bottom tensile stress ratio (as high as 1.8) was observed when combined mechanical and temperature load (ΔT= -5.5 ˚C (-10 ˚F)) was applied around mid-slab. Although there was no significant difference in the top-to-bottom tensile stress ratio results for different wander distances, when the outer wheel of the single axle was placed on the lane edge, a slightly higher top-to-bottom stress ratio was observed compared to when the outer wheel of the single axle was placed 0.3 m. (1 ft.) and 0.6 m. (2 ft.) away from the lane edge. (Fig. 3.3b).

Similarly, as shown in Fig. 3.3c, a very high top-to-bottom tensile stress ratio (as high as 5.8) was observed when combined mechanical and temperature load (ΔT= -11˚C (-20 ˚F)) was applied around mid-slab.

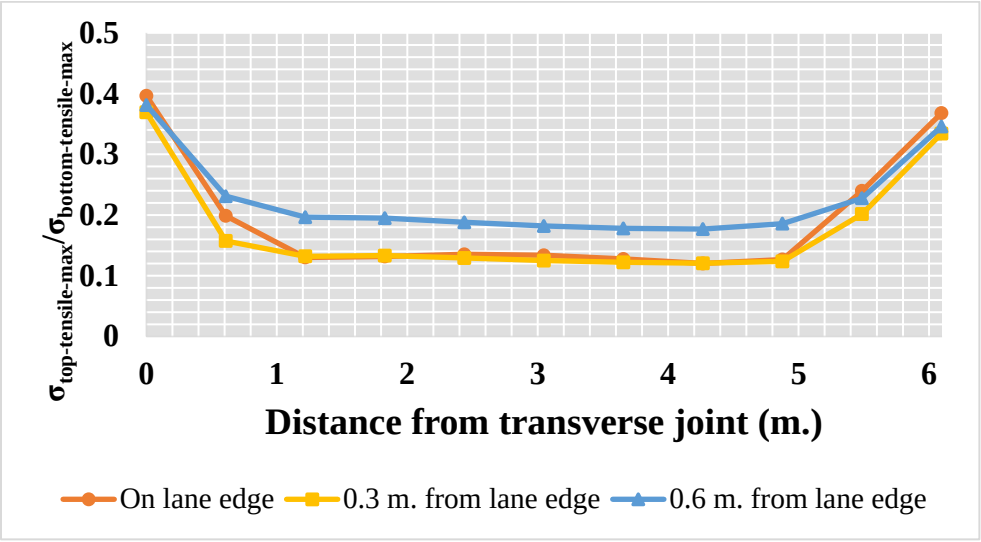

(a)

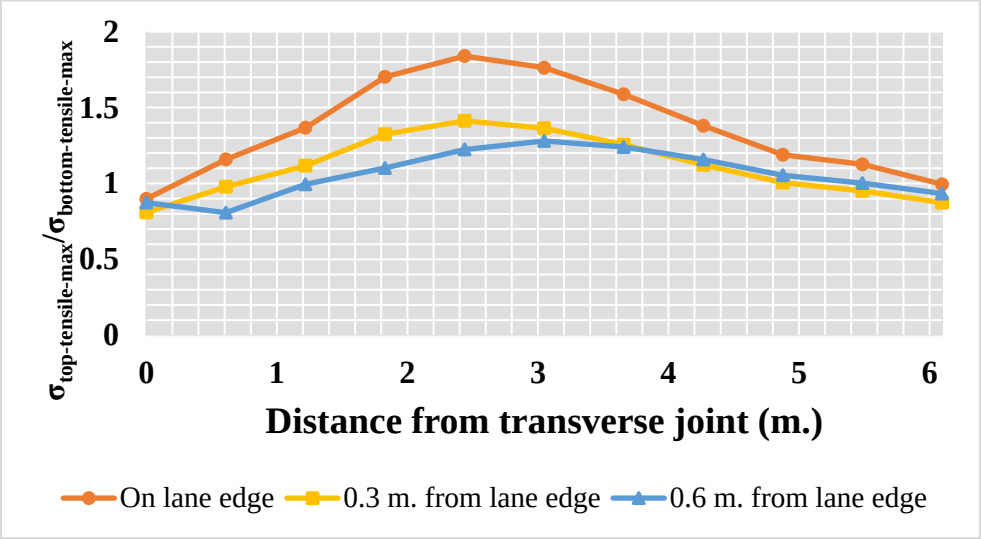

(b)

Figure 3.3 Top and bottom tensile stress ratio distribution for single axle mechanical load combined with three different temperature load scenarios; (a) ΔT= 0 ˚C (0 ˚F), (b) - 5.5 ˚C (-10 ˚F), and (c) ΔT= -11˚C (-20 ˚F) applied on various locations in both traffic and wander directions

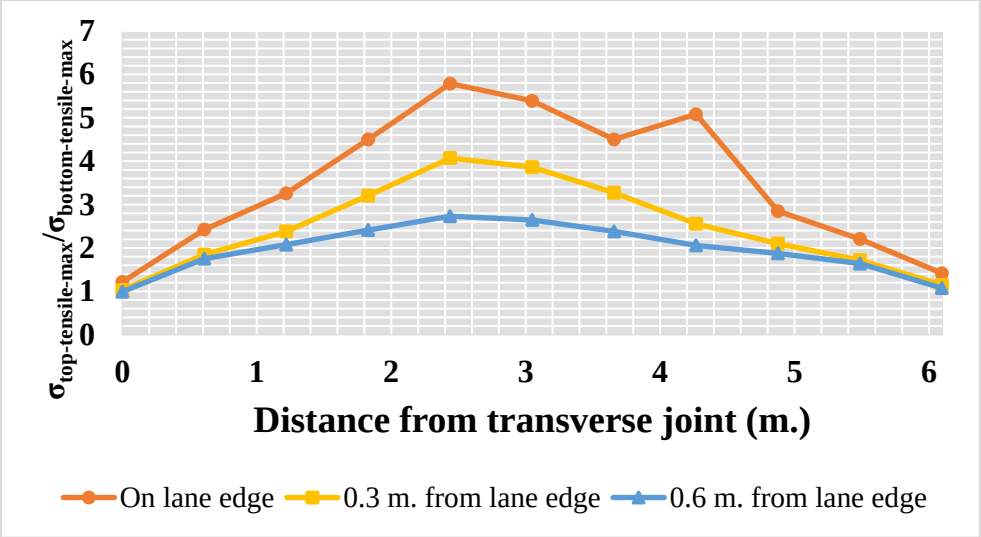

(c)

Figure 3.3 (Continued)

Fig. 3.4 shows the top-to-bottom tensile stress ratio distribution when various combined mechanical and temperature load scenarios are applied at lane edge and various locations in the traffic direction. As can be seen in Fig. 3.4, as the negative temperature gradient increases, higher top-to-bottom tensile stress ratio values are observed around mid-slab.

In summary, various FEA cases using single-axle loads were examined, and the effects of combined mechanical and temperature loads on tensile stress development on slab surfaces were investigated. Effects of load and wander patterns on tensile stress development on slab surfaces also became better understood. It was determined that the critical tensile stress locations are as follows:

- Close to transverse joint for mechanical load only
- Close to mid-slab surface as temperature gradient increases

In combined mechanical and temperature loading cases, as the negative temperature gradient increased, higher top-to-bottom tensile stress ratio values were observed around mid-slab. Further analysis was conducted for applied truck loads.

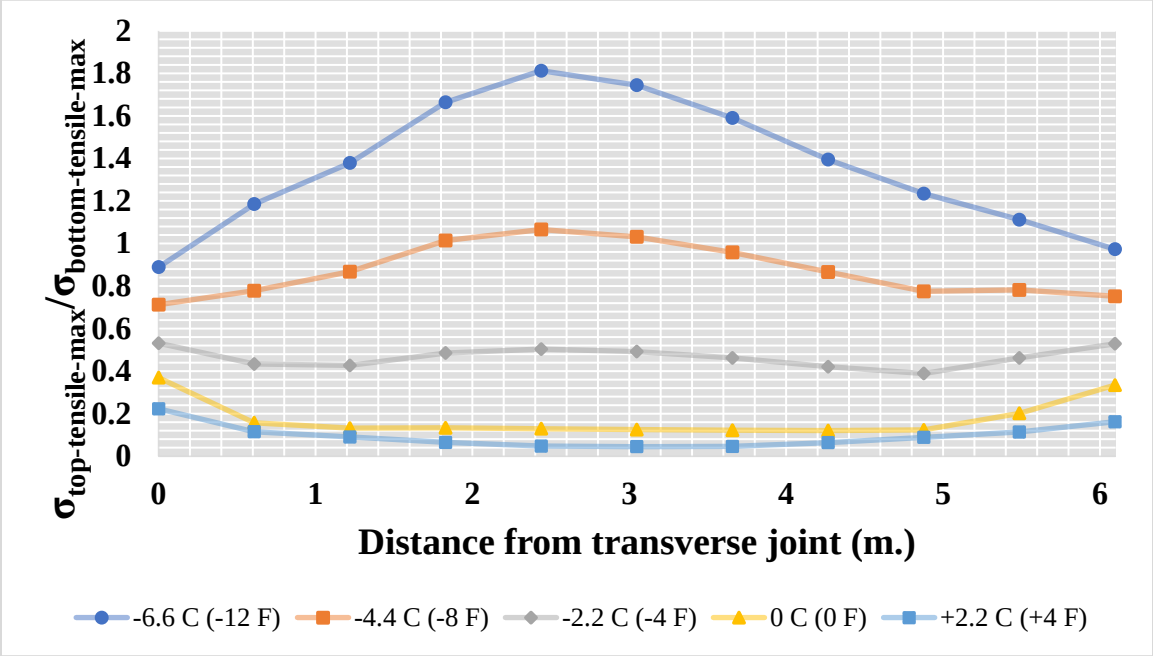

Figure 3.4 Top-to-bottom tensile stress ratio distribution for various combined mechanical and temperature load cases

Truck Load Simulations

Based on the field investigations described in the previous sections of this paper, the failure mechanisms of Iowa JPCP widened slabs with respect to longitudinal cracking include longitudinal cracks initiated from transverse joints as top-down cracking, mainly on the widened traffic lane and about 0.6 to 1.2 m. (2 to 4 ft.) away from the slab edge (Fig 3.5).

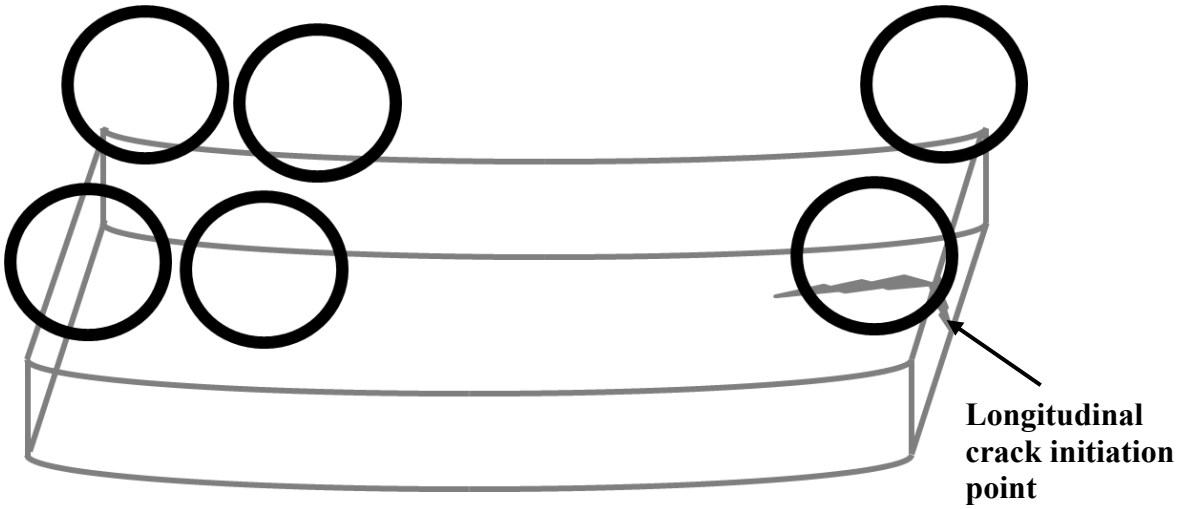

Figure 3.5 Failure mechanism for longitudinal cracking from field investigation

In this section, several truck axle-load and spacing configurations are investigated to evaluate the effects of axle load and spacing configurations on longitudinal cracking, and the critical axle load and spacing configuration resulting in the highest longitudinal cracking potential is also identified.

Mechanical loads for single-axle and tandem axles were applied at levels of 9.1 and 15.4 metric-tons (20 and 34 kips), respectively, based on Federal Highway Administration (FHWA) [11] and Iowa DOT guidelines [12].

Two what-if scenarios including three- and four-axle and spacing configurations were investigated:

- Three-axle truck with 6.1 m (20 ft.) axle spacing placed on a single slab
- Four-axle truck with 7.0 m (23 ft.) axle spacing with both axle groups partially placed on adjacent slabs

Three-Axle Truck with 6.1 m (20 ft.) Axle Spacing Placed on a Single Slab

In this loading scenario, a truck with both a single axle and a tandem axle is used as a truckload (Class 6 based on FHWA truck classification [11] (Fig. 3.6), with single and

tandem axles applying mechanical loads of 9.1 and 15.4 metric-tons (20 and 34 kips), respectively, on the pavement system (Fig. 3.6). The 6.1 m. (20 ft.) figure was selected as the axle spacing, i.e., the distance between the center of the rear axle of the tandem axle and that of the single axle, so that both single and tandem axle loads are placed on two transverse joints of the widened slabs (JPCP has a joint spacing of 6.1 m. (20 ft.)) (Fig. 3.6). Five different wander distances were tested (0, 15, 30, 45, and 60 cm. (0. 0.5, 1, 1.5, and 2 ft.) away from the lane edge (Table 3.1).

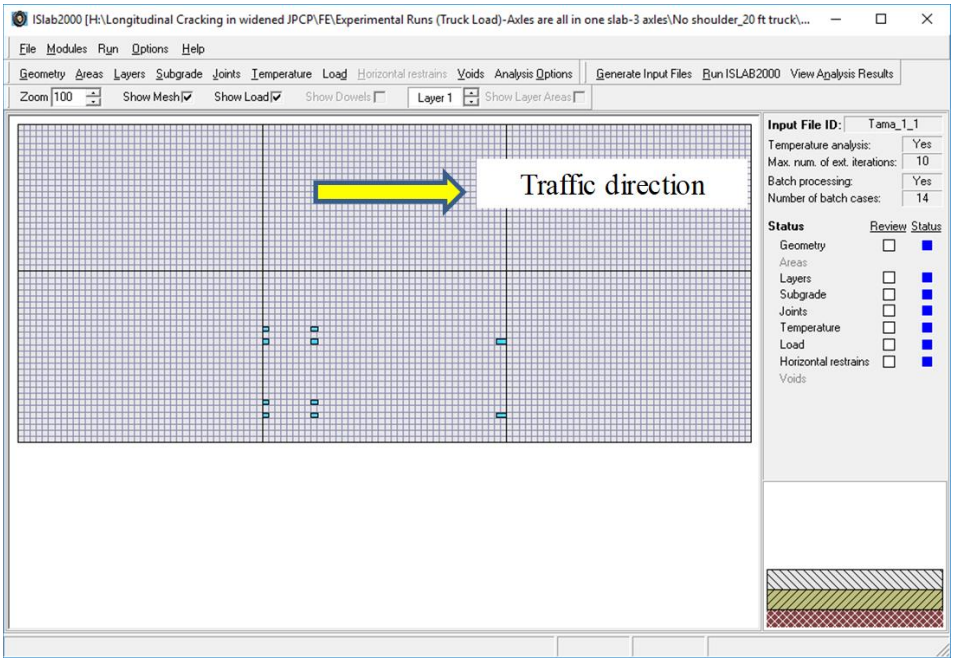

Figure 3.6 Three-axle truck with 6.1 m. (20 ft.) axle spacing – discretized truck load

Fig. 3.7 shows the top tensile stress distribution when a truck load is applied at three wander distances (on lane edge and 0.3 and 0.6 m. (1 and 2 ft.) away from lane edge for two temperature load cases (only mechanical load (ΔT= 0 ˚C) and combined mechanical and temperature load (ΔT= -11 ˚C (-20 ˚F)). As seen in Fig. 3.7, very high top tensile stresses can be observed starting from transverse joints, representing greater potential for longitudinal crack initiation starting from the transverse joint of the slab surface.

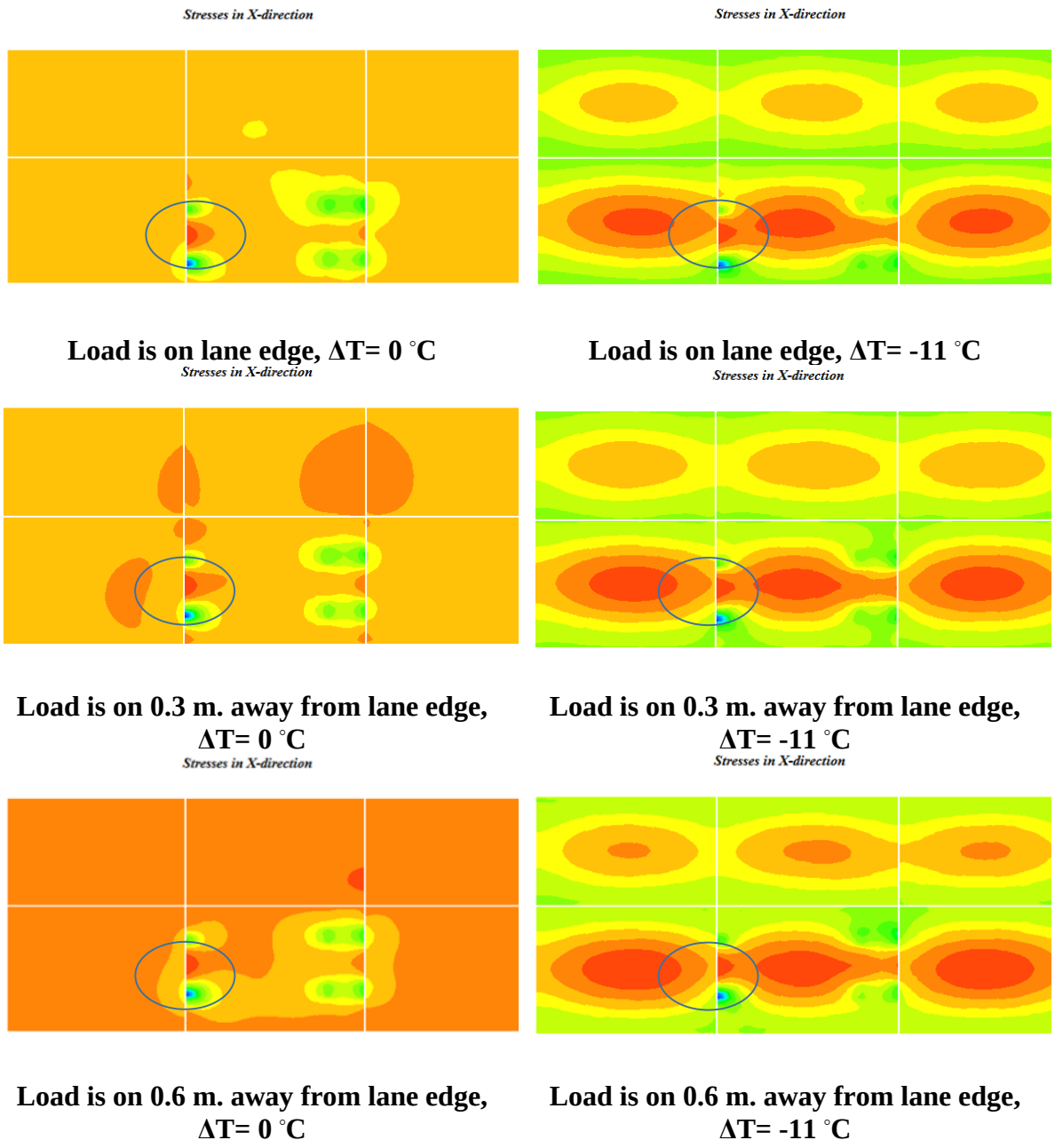

Figure 3.7 Three-axle truck with 6.1 m. (20 ft.) axle spacing – top tensile stress distribution for three wander distances and two temperature load cases

Fig. 3.8 shows the top-to-bottom tensile stress ratio distribution when various combined mechanical and temperature load scenarios are applied at various wander distances (0 to 0.6 m. (0 to 2 ft.)). As can be seen in Fig. 3.8, as the negative temperature gradient increases, the top-to-bottom tensile stress ratios also increase. Moreover, as truck load is

placed closer to the lane edge (wander distance decreases) the top-to-bottom tensile stress ratios increase.

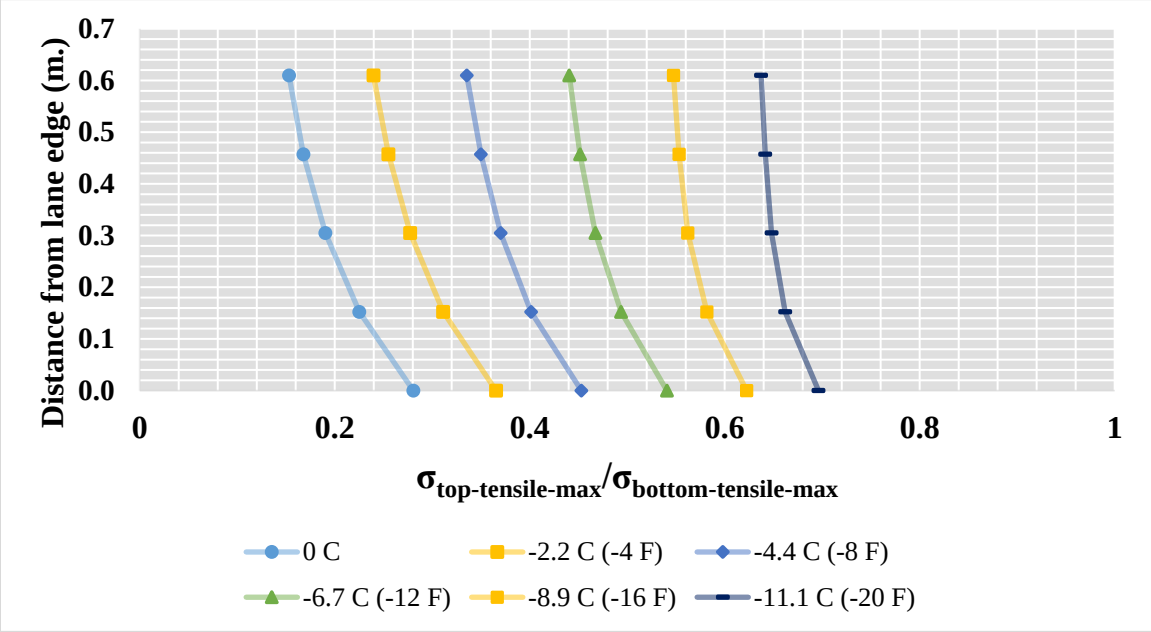

Figure 3.8 Three-axle truck with 6.1 m. (20 ft.) axle spacing – top-to-bottom tensile stress ratio distribution

Fig. 3.9 shows the top tensile stress distribution when various combined mechanical and temperature load scenarios are applied at various wander distances (0 to 0.6 m (0 to 2 ft.)). The top tensile stress distribution exhibits a similar trend as the top-to-bottom tensile stress ratios; as the negative temperature gradient increases, the top tensile stresses also increase; and as the truck load is placed closer to the lane edge, the top tensile stresses also increase.

Results based on this loading scenario can be summarized as follows.

- A higher negative temperature gradient produced higher top-to-bottom tensile stress ratios.

- Higher top and bottom tensile stress ratio values were observed close to the lane edge, (highest right on the lane edge).
- For high temperature load cases, the critical tensile stress location was identified as the transverse slab joint.

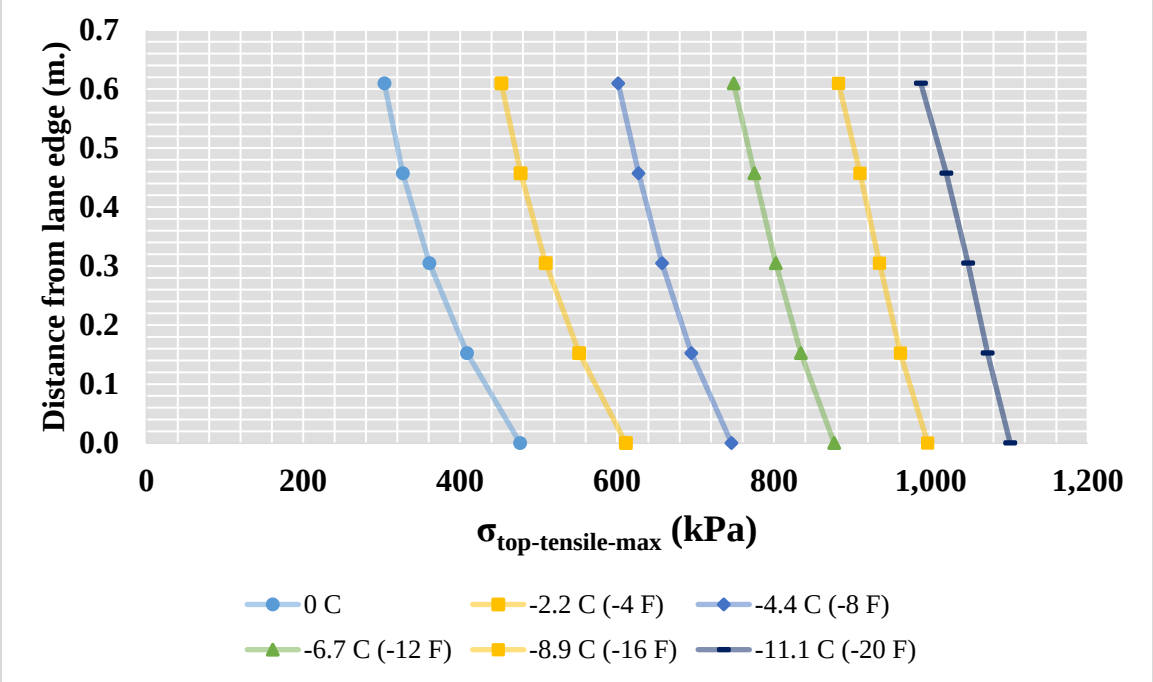

Figure 3.9 Three-axle truck with 6.1 m. (20 ft.) axle spacing – top tensile stress distribution

Four-Axle Truck with 7.0 m (23 ft.) Axle Spacing with both Axle Groups Partially Placed on Adjacent Slabs

It was concluded from the three-axle truck case that when axle loads are placed on adjacent slabs, tensile stresses are transferred to a critical slab (the slab between adjacent slabs), causing very high tensile stress to accumulate around the top surface of the critical slab surface close to the transverse edge. This is especially true for high negative temperature gradient cases (when slabs curl up) where the center of axle loads are placed close to the transverse edges (Fig. 3.10). In that case, the top tensile stresses on the transverse edges of the adjacent slabs are transferred to the critical slabs and very high top tensile stresses are

observed around the transverse joints of the critical slabs (Fig. 3.10). In this loading scenario, a two tandem axles (four-axle) configuration with a 7.0 m. (23 ft.) axle spacing is used, and the centers of the axle loads are placed close to the transverse edges. Each tandem axle applies a total mechanical load of 15.4 metric-tons (34 kips) (Fig. 3.11). Use of two tandem axles as mechanical load simulates the two axles of a Class 9 truck [11] (18-wheeler), the most commonly-used truck type [2]. The objective of this analysis was to determine the critical loading scenario producing the highest top-to-bottom tensile stress ratios.

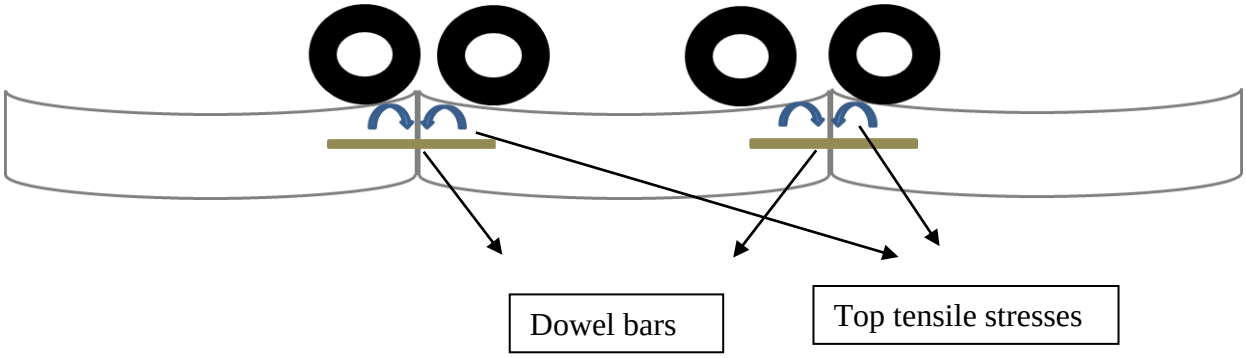

Figure 3.10 Top tensile stress transfer mechanism in four-axle truck

Fig. 3.12 shows the top tensile stress distribution when the truck load is applied on the lane edge for four temperature-load cases, both including mechanical load only and combined mechanical and temperature load (ΔT= -8.9 ˚C (-16 ˚F), -10 ˚C (-18 ˚F) and -11.1 ˚C (-20 ˚F)). As can be seen in Fig. 3.12, very high top-to-bottom tensile stress ratios, as high as 3.2, are observed close to the transverse edge.

Fig. 3.13 shows the top-to-bottom tensile stress ratio distributions when various combined mechanical and temperature load scenarios are applied at various wander distances (0 to 0.6 m (0 to 2 ft.)). As can be seen in Fig. 3.13, as the temperature difference between top and bottom of the slab increases, top-to-bottom tensile stress ratios also increase to as high as 3.2.

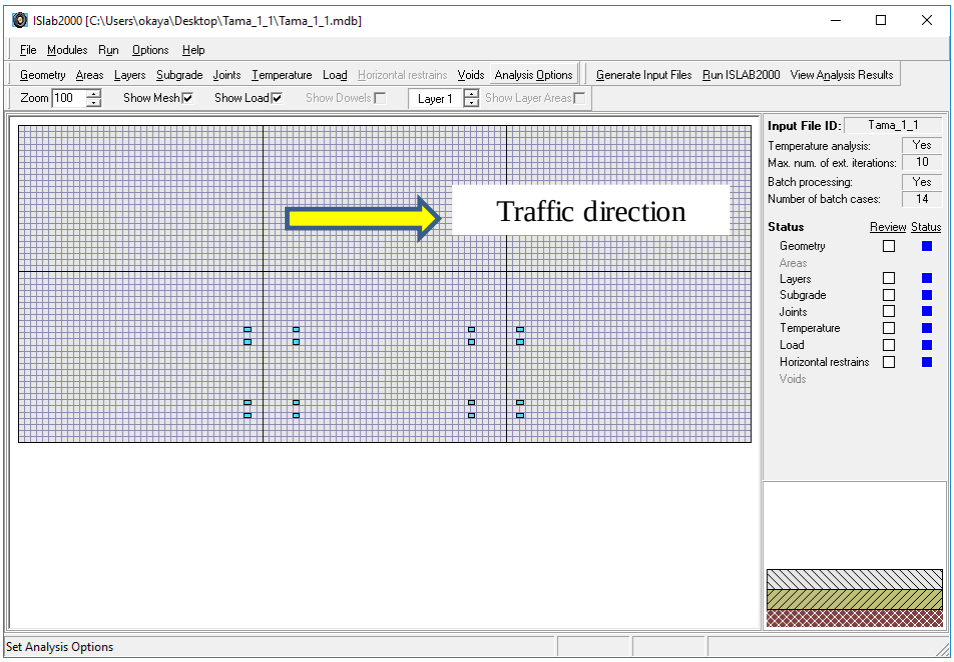

Figure 3.11 Four-axle truck – discretized truck load

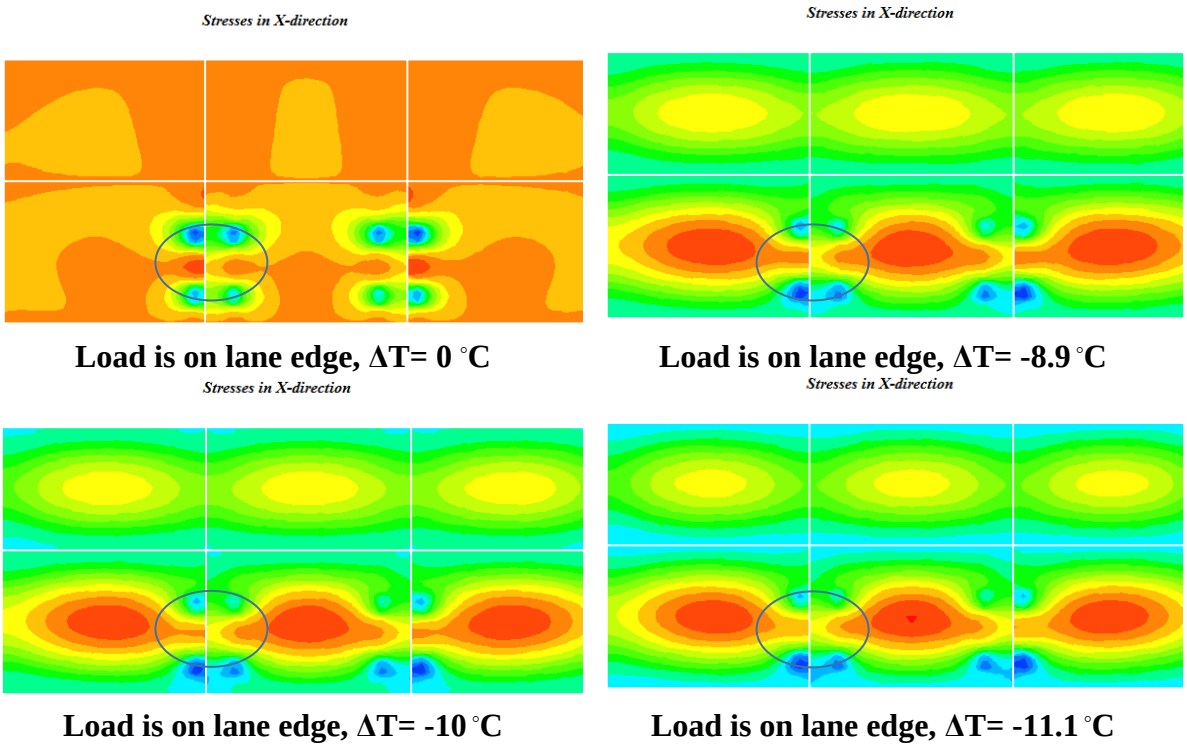

Figure 3.12 Four-axle truck – top tensile stress distribution for four temperature load cases

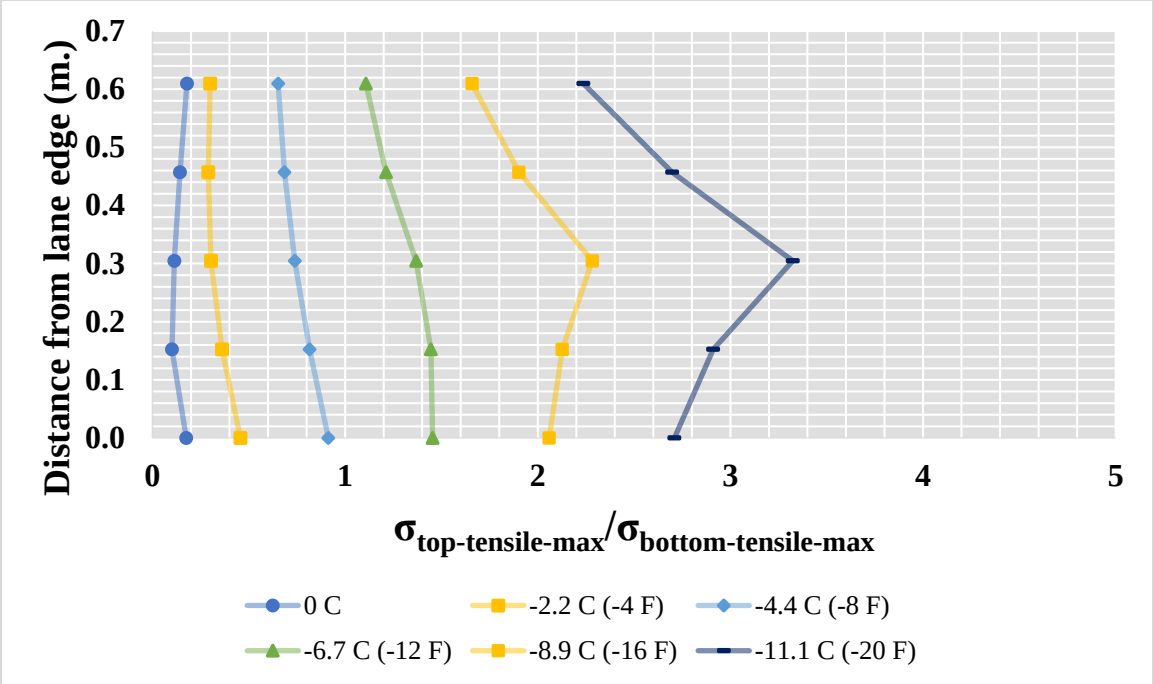

Figure 3.13 Four-axle truck – top-to-bottom tensile stress ratio distribution

Fig. 3.14 shows top tensile stress distributions when various combined mechanical and temperature load scenarios are applied at the lane edge. The top tensile stress distribution shows a similar trend as the top-to-bottom tensile stress ratios, i.e., as the negative temperature gradient increases, the top tensile stresses also increase.

Fig. 3.15 shows comparisons of tensile stress distributions between a three-axle truck and a four-axle tuck for two loading scenarios: mechanical load only and combined mechanical and temperature load (ΔT= -11.1 ˚C (-20 ˚F)). As can be seen in Fig. 3.15, similar top tensile stress results were observed in both cases, except that the truck with a four-axle transfer case produced a significantly higher (as high as 2.7) top-to-bottom tensile stress ratio.

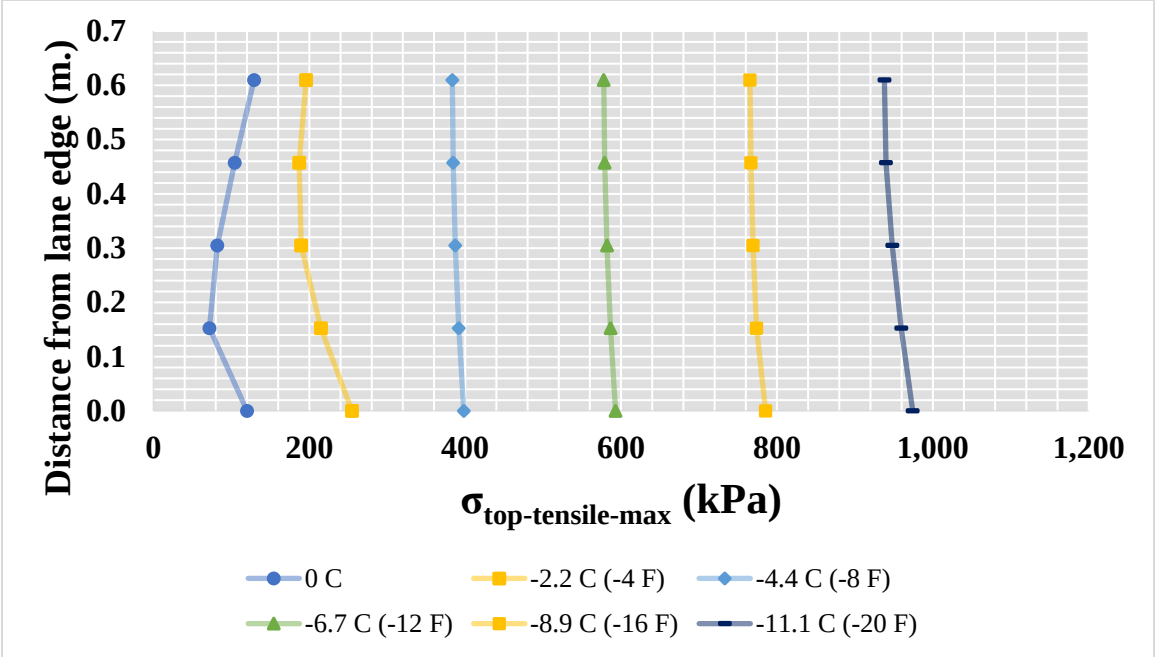

Figure 3.14 Four-axle truck – top tensile stress distribution

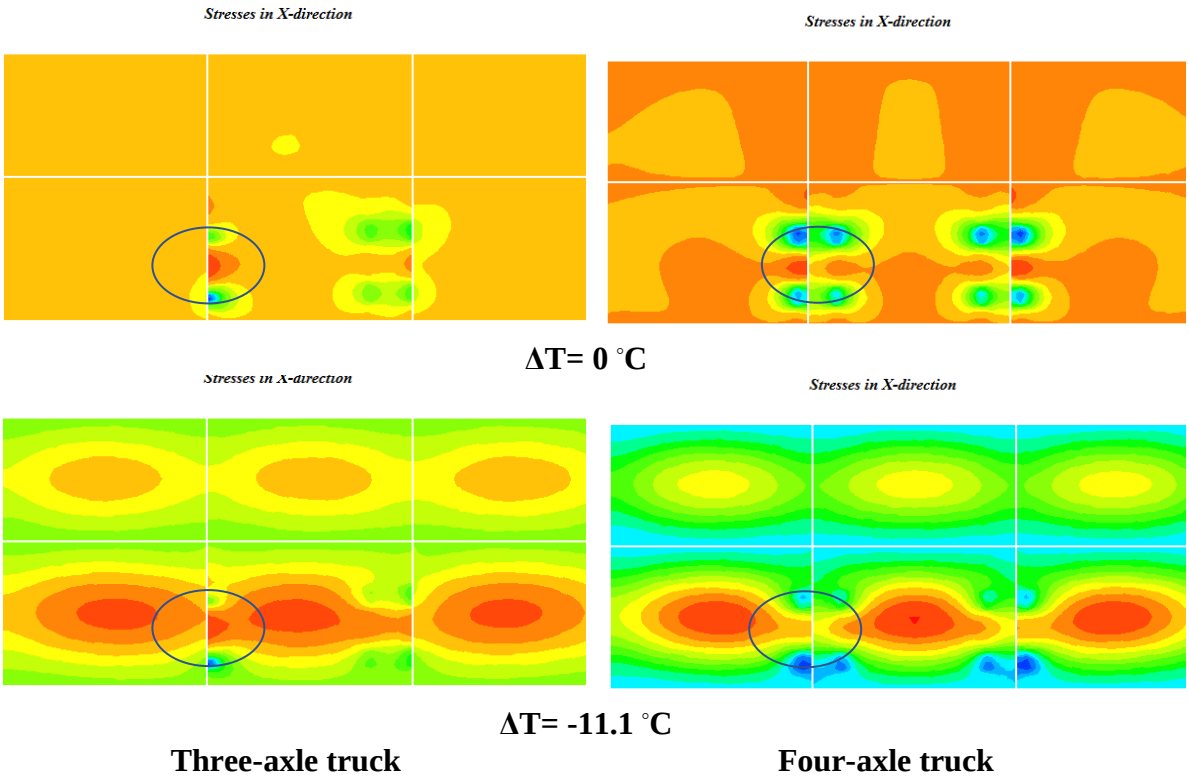

Figure 3.15 Comparisons of tensile stress distributions between a three-axle truck and a four-axle truck

Truck Load Simulations - Summary of Findings

The top-down longitudinal cracking potential for JPCP with widened slabs was satisfactorily demonstrated using several truckload configurations. The key findings were as follows:

- Longitudinal cracking initiates from the transverse joints between the lane edge and wheel path.
- Although both three- and four-axle configurations produced similarly high tensile stresses, a truck with a four-axle case produced significantly higher (as high as 2.7) top-to-bottom tensile stress ratios, so the four-axle truck load configuration was identified as the critical loading scenario.
- A higher negative temperature gradient between the top and bottom of the slab produced higher top-to-bottom tensile stress ratios and, in turn, led to greater longitudinal cracking potential.

Shoulder Design Alternatives Simulations

Three shoulder design alternatives were compared for both widened (4.3 m (14 ft.) wide) and regular size (3.7 m (12 ft.) wide) slabs: Partial-depth tied PCC, HMA (paved shoulder alternates), and full-depth tied PCC shoulder (Fig. 3.16). These shoulder types were modeled based on the Iowa DOT's typical design details [13] (Fig. 3.16).

Shoulder design alternatives were compared for the following cases:

Tied PCC shoulder using:

- Regular slabs (3.7 m. (12 ft.) wide) with a full-depth tied PCC shoulder; shoulder thickness is the same as regular slab thickness (i.e., 25.4 cm. (10 in.))

- Widened slabs (4.3 m. (14 ft.) wide) with a partial-depth tied PCC shoulder alternative; shoulder thickness is less than regular slab thickness (i.e., 17.8 cm. (7 in.))

HMA shoulder using:

- Regular slabs (3.7 m. (12 ft.) wide) with an HMA shoulder alternative; shoulder thickness is less than regular slab thickness (i.e., 20.3 cm. (8 in.))
- Widened slabs (4.3 m. (14 ft.) wide) with an HMA shoulder alternative; shoulder thickness is less than regular slab thickness (i.e., 20.3 cm. (8 in.))

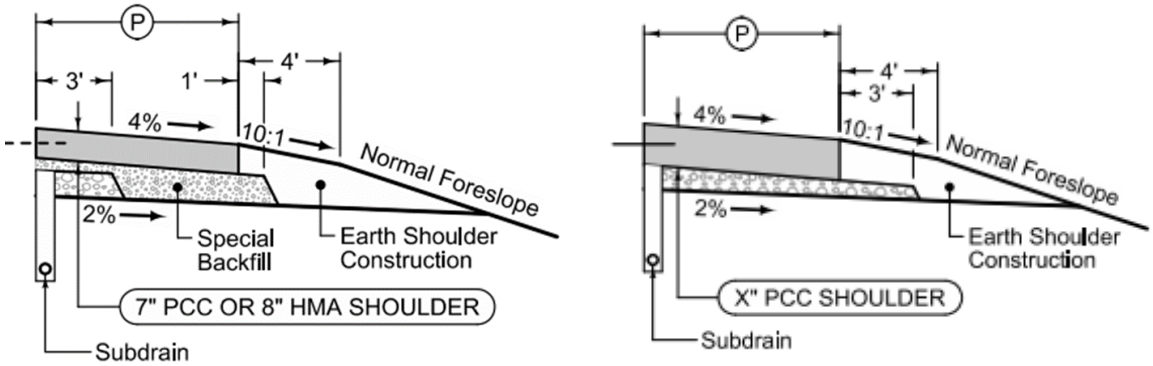

Partial-depth PCC or HMA Shoulder (Paved Shoulder Alternates)

Full-Depth PCC Shoulder

Figure 3.16 Shoulder design alternatives

The critical load configurations found in the truckload simulations were used for mechanical load configurations. Five different wander distances were investigated: 0, 15, 30, 45, and 60 cm. (0. 0.5, 1, 1.5, and 2 ft.), respectively, away from the lane edge for widened slabs, and at the slab edge itself for regular slab sizes. Other model inputs were the same as for the truckload simulations (Table 3.1).

Fig. 3.17 shows the discretized models for the shoulder design alternatives. The widened slab (4.3 m (14 ft.) wide) had a 0.6 m. (2 ft.) extended width compared to a regular slab size (3.7 m. (12 ft.) wide). An alternative shoulder width was selected to ensure that the

total width, including both slab and shoulder, would constitute a 6.1 m (20 ft.) widened slab with a 1.8 m. (6 ft.) shoulder and a regular slab width with a 2.4 m (8 ft.) shoulder.

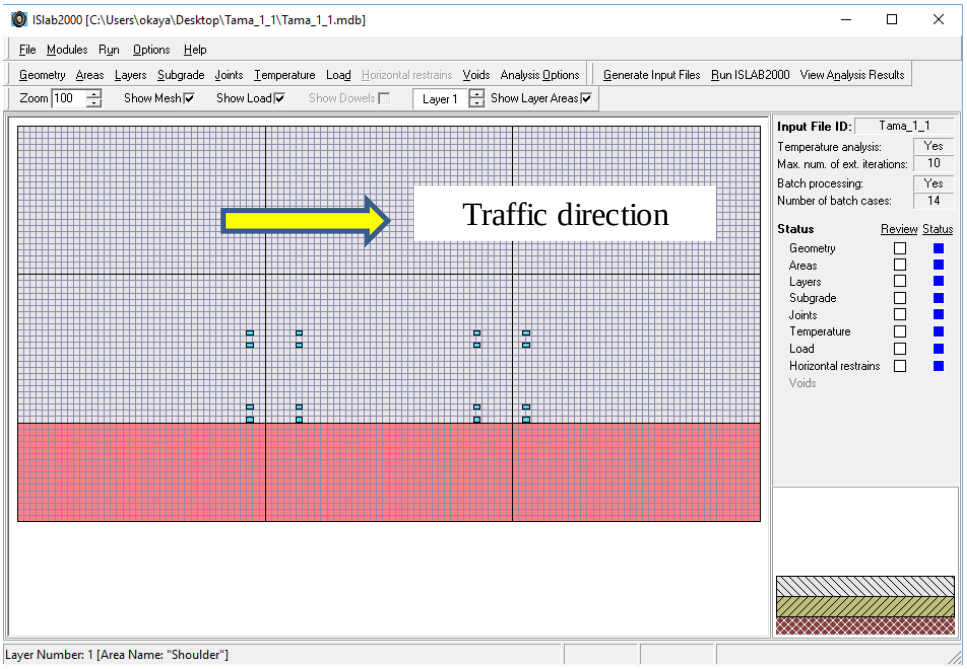

Regular size slabs with shoulder design alternatives

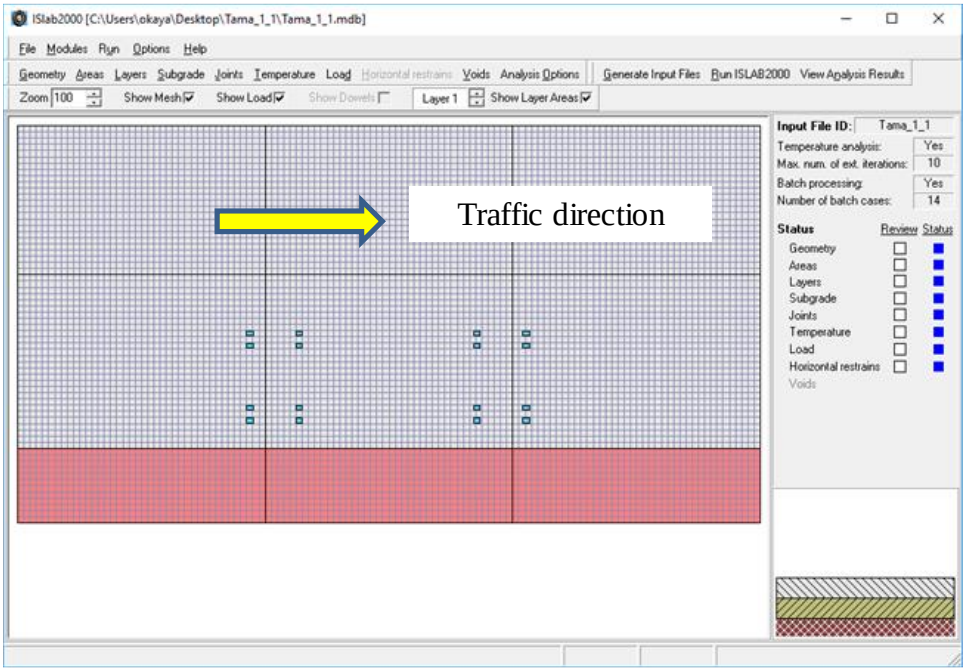

Widened size slabs with shoulder design alternatives

Figure 3.17 Widened and regular size slabs with shoulder design alternatives

Tied PCC Shoulder

In this alternative shoulder scenario, two cases were compared:

- A regular slab (3.7 m. (12 ft.) wide) with a full-depth tied PCC shoulder in which the shoulder thickness has the same thickness as that of regular slab (i.e., 25.4 cm. (10 in.))
- A widened slab (4.3 m. (14 ft.) wide) with a partial-depth tied PCC shoulder alternative in which the shoulder thickness is less than that of a regular slab thickness (i.e., 17.8 cm. (7 in.))

Fig. 3.18 compares the top-to-bottom tensile stress ratios and top tensile stress distributions between a widened slab with a partial-depth tied PCC shoulder and a regular slab with a full-depth tied PCC shoulder. As can be seen in Fig. 3.18, both higher top-to-bottom tensile stress ratios and top tensile stresses were observed for a widened slab with a partial-depth tied PCC shoulder compared to those for a regular slab with a full-depth tied PCC shoulder. In terms of longitudinal cracking potential, the mid-slab edge was found to be critical when regular slabs were used while the transverse joint edge was found to be critical when widened slabs were used.

HMA Shoulder

In this alternative scenario, two cases were compared:

- A regular slab (3.7 m. (12 ft.) wide) with an HMA shoulder alternative in which the shoulder thickness is less than that of a regular slab (i.e., 20.3 cm. (8 in.))
- A widened slab (4.3 m. (14 ft.) wide) with an HMA shoulder alternative in which the shoulder thickness is less than that of a regular slab (i.e., 20.3 cm. (8 in.))

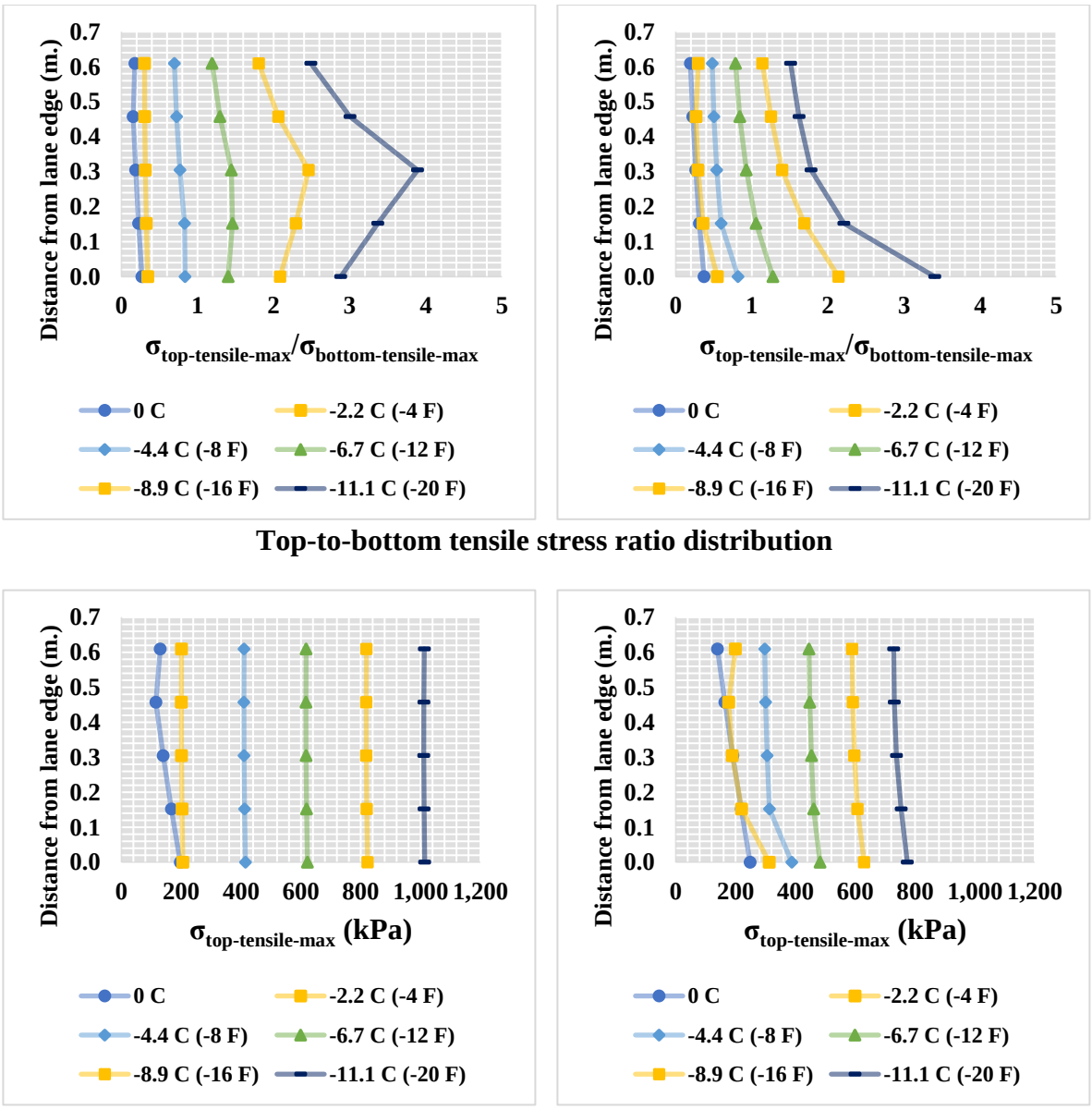

Figure 3.18 Top-to-bottom tensile stress ratio and top tensile stress comparisons between a widened slab with partial-depth tied PCC shoulder and a regular slab with full-depth tied PCC shoulder

Load transfer between a widened or regular slab and an HMA shoulder was modeled in such a way that there is load transfer only between granular bases of the widened or regular size slabs and HMA shoulders. This load transfer is modeled by assigning a load

transfer efficiency (LTE) value of 10% between slabs and HMA shoulders based on a recommendation from an NCHRP report [2].

Fig. 3.19 shows comparisons of tensile stress distributions between widened and regular size slabs with an HMA shoulder for two loading scenarios: combined mechanical and temperature load ((ΔT= -11.1 ˚C (-20 ˚F)) and ((ΔT= -8.9 ˚C (-16 ˚F)). As can be seen in Fig. 3.19, higher top tensile stress results were observed when widened slabs are used with an HMA shoulder compared to when regular slabs are used with an HMA shoulder.

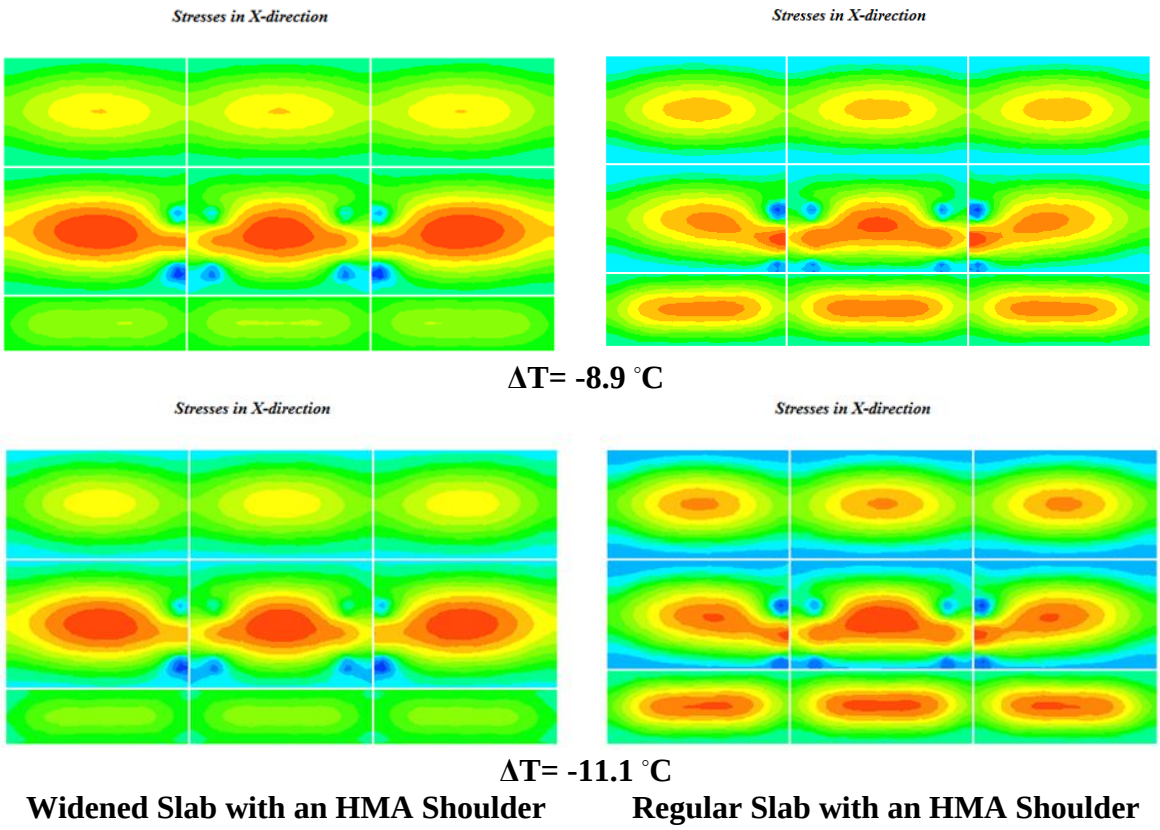

Figure 3.19 Comparisons of tensile stress distributions between widened and regular slabs with an HMA shoulder

Fig. 3.20 compares the top-to-bottom tensile stress ratios between a widened slab with an HMA shoulder, a regular slab with an HMA shoulder, and a regular slab with a full-

depth tied PCC shoulder. As can be seen in Fig. 3.20, among the cases presented the highest top-to-bottom tensile stress ratio was observed for the regular slab with an HMA shoulder.

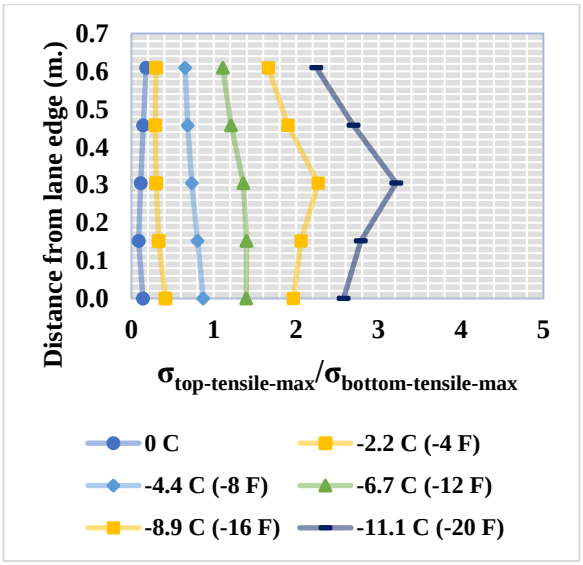

Widened Slab with an HMA Shoulder

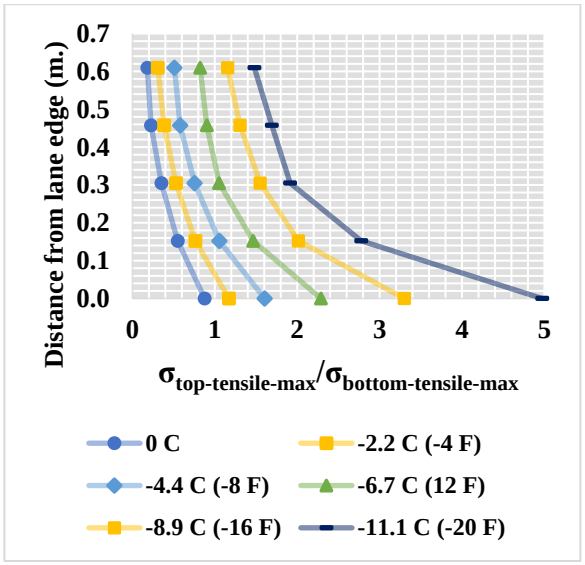

Regular Slab with an HMA Shoulder

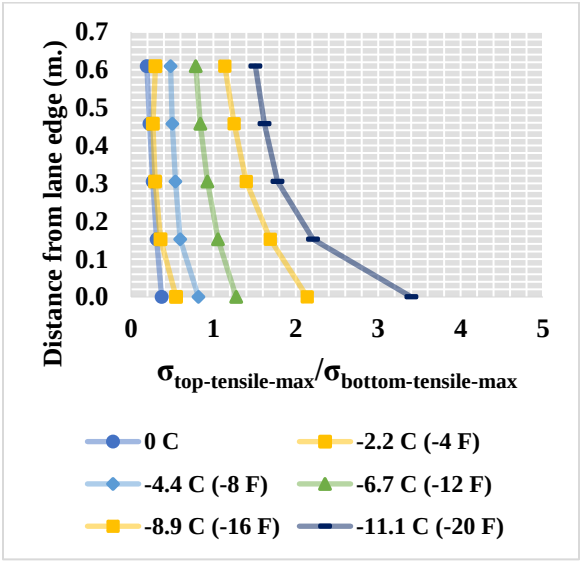

Regular Slab with a Full-Depth Tied Concrete Shoulder

Figure 3.20 Top-to-bottom tensile stress ratio comparisons between widened slab with an HMA shoulder, regular slab an HMA shoulder and regular slab with a full-depth tied PCC shoulder

Shoulder Design Alternatives Simulations - Summary of Findings

A higher (1) top-to-bottom tensile stress ratio and (2) top tensile stress was observed for a widened slab (4.3 m. (14 ft.) wide) with a partial-depth tied PCC shoulder alternative compared to a regular size slab (3.7 m. (12 ft.) wide) with a full-depth tied PCC shoulder. A higher top-to-bottom tensile stress ratio was observed for a regular size slab (3.7 m. (12 ft.) wide) with an HMA shoulder compared to a widened slab (4.3 m. (14 ft.) wide) with an HMA shoulder. On the other hand, higher tensile stresses were observed for a widened slab (4.3 m. (14 ft.) wide) with an HMA shoulder compared those for a regular size slab (3.7 m. (12 ft.) wide) with an HMA shoulder. Compared to the use of a widened slab, the use of a regular size slab was found to be beneficial in mitigating longitudinal cracking at the cost of increasing transverse cracking potential.

Conclusions, Discussions, and Recommendations

One of the objectives of this paper was to understand longitudinal cracking mechanisms and to evaluate longitudinal cracking potential of widened JPCP through numerical analysis. Initially, both tensile stress results on the slab surface (top) in the x and y directions and deflection results were analyzed through single-axle load simulation to determine which tensile stress type (in the x or y direction) is critical in producing longitudinal cracking. Based on the single-axle load simulation results, tensile stresses in the x direction were found to be the critical ones with respect to producing longitudinal cracking. Determining the critical stress type is important because longitudinal crack initiation potential can be evaluated based on the critical stress extent and location. Moreover, based on single-axle load simulation, it was found that as negative temperature gradient increases, critical load location moves closer toward the mid-slab from the transverse edge. This might be because: (1) When only mechanical load without any temperature load applied on the

transverse joints, if restriction of the critical slabs by the adjacent slabs through LTE is considered, top tensile stress accumulation is observed around the transverse joints. (2) Slabs try to curl up when temperature load is applied to them (negative temperature gradient), and because they are restricted by adjacent slabs, they develop top-tensile stresses around their mid-slab. When a combined mechanical and temperature load is applied (negative temperature gradient) around the mid-slab, top-tensile accumulation around the mid-slab further increases.

Although much useful information for characterizing critical load locations for longitudinal cracking can be found through single-axle load simulation, truck load configurations were thought to better simulate the critical loading scenario associated with the highest longitudinal cracking potential, so three and four-axle truck loads were investigated. A truck with a four-axle configuration with the center of its axle loads placed close to transverse edges was identified as the critical loading scenario, because when axle loads were placed on adjacent slabs, tensile stresses were transferred to the critical slab, resulting in very high tensile stress accumulation around the top surface of the critical slab close to the transverse edge. This is especially true for high negative temperature gradient cases (when slabs curl up) where the center of the axle loads is placed close to the transverse edges of an adjacent slab. In that case, the top tensile stresses on the transverse edges of the adjacent slabs are transferred to the critical slabs and extremely high top tensile stresses are observed around the transverse joints of the critical slabs. This finding satisfactorily explains the longitudinal crack initiation at the transverse joints and top slab surface observed in the field investigations.

Another objective of this paper was to compare different shoulder types when used adjacent to either a widened (4.3 m. (14 ft.) wide) or a regular size (3.7 m. (12 ft.) wide) slab in terms of their effects in mitigating longitudinal cracking. Initially, widened slabs with a partial-depth tied PCC shoulder alternative were compared with regular slabs with a full-depth tied PCC shoulder alternative, and it was found that higher (1) top-to-bottom tensile stress ratio and (2) top tensile stress were observed when widened slabs with a partial-depth tied PCC shoulder were used, compared to when regular slabs with a full-depth tied PCC shoulder were used. Higher top-to-bottom tensile stress ratio and top tensile stresses are related to higher longitudinal cracking potential, possibly because even though widened slabs can be used to mitigate transverse cracking, they might increase longitudinal cracking potential. This characteristic of widened slabs does not change much even if when they are used with a partial-depth tied PCC shoulder.

In this paper, widened slabs (4.3 m. (14 ft.) wide) with an HMA shoulder alternative were also compared to regular slabs (3.7 m. (12 ft.) wide) with an HMA shoulder alternative in terms of their effect on mitigating longitudinal cracking. A higher top-to-bottom tensile stress ratio was observed when regular slabs (3.7 m. (12 ft.) wide) with an HMA shoulder were used compared to the situation of widened slabs (4.3 m. (14 ft.) wide) with an HMA shoulder. The difference between an HMA shoulder alternative and a tied PCC shoulder alternative is that the HMA shoulder is not tied to widened or regular slabs so there is no load transfer between a slab and the HMA shoulder, and a LTE of only 10% is defined between the shoulder and slab bases, explaining why the effect of an HMA shoulder on top tensile stress accumulation in widened or regular slabs is minimal. In short, widened slabs or regular

slabs with HMA shoulders demonstrate similar behavior when there is no shoulder used with them in terms of their effect on longitudinal cracking potential.

Recommendations of this study for mitigating longitudinal cracking in widened JPCP can be summarized follows:

- Longitudinal cracks are mainly in the traffic lane and about 0.3-0.6 m. (2~4 ft.) away from slab edge
    - Shorter joint spacing can result in lower curling and warping and also can lead to less chance for longitudinal cracking as well
- Most longitudinal cracks observed start from slab transverse joints
    - Since dowel bars can restrain vertical deflection at joints, so proper dowel bar installation will help mitigate longitudinal cracking
- A tied PCC shoulder design option can perform better than other shoulder design options (HMA and granular) in terms of longitudinal crack potential in widened JPCP.

Acknowledgements

The authors would like to thank the Iowa Department of Transportation (DOT) for sponsoring this research. The project's Technical Advisory Committee (TAC) members, Ben Behnami, Chris Brakke, Vanessa Goetz, Todd Hanson, Kevin Merryman and Jason Omundson of Iowa DOT; Jacob Thorius of Washington County, Iowa; Greg Mulder of Iowa Concrete Paving Association (ICPA); Gordon Smith of ISU CP Tech Center and John Cunningham of Snyder & Associates, Inc. are gratefully acknowledged for their guidance. The contents of this paper reflect the views of the authors who are responsible for the facts and accuracy of the data presented within. The contents do not necessarily reflect the official

views and policies of the Iowa DOT. This paper does not constitute a standard, specification, or regulation.

References

[1] H.M. Westergaard, New Formulas for Stresses in Concrete Pavements of Airfields. Transactions, ASCE, 113 (1948).

[2] NCHRP, Guide for Mechanistic-Empirical Design of New and Rehabilitated Pavement Structures, Champaign, IL, 2003.

[3] R.E. Lederle, Development of a Longitudinal Cracking Fatigue Damage Model for Jointed Plain Concrete Pavements Using the Principles of Similarity, University of Minnesota, MN., 2014.

[4] H. Ceylan, S. Kim, Y. Zhang, S. Yang, O. Kaya, K. Gopalakrishnan and P. Taylor, Prevention of Longitudinal Cracking in Iowa Widened Concrete Pavement, Final Report, IHRB Project TR-700, Iowa State University, 2018.

[5] J.E. Hiller and J.R. Roesler, Determination of Critical Concrete Pavement Fatigue Damage Locations Using Influence Lines, J. Transp. Eng., 131(8) (2005) 599-607.

[6] A.C.Heath, J.R. Roesler and J.T. Harvey, Modeling Longitudinal, Corner and Transverse Cracking in Jointed Concrete Pavements. Int. J. of Pavement Eng., 4 (1) (2003) 51–58.

[7] J.E. Hiller and J.R. Roesler, Transverse Joint Analysis for use in Mechanistic-Empirical Design of Rigid Pavements, Trans. Res. Rec., 1089 (2002) 42–51.

[8] S. Kim, H. Ceylan and K. Gopalakrishnan, Finite Element Modelling of Environmental Effects on Rigid Pavement Deformation, Frontiers of Str. and Civil Eng. J., 8(2) (2014) 101-114.

[9] Khazanovich, Structural Analysis of Multi-Layered Concrete Pavement Systems. Ph.D. Thesis, University of Illinois, Urbana, IL, 1994.

[10] F. Mu and J. Vandenbossche, Evaluation of the Approach used for Modeling the Base under Jointed Plain Concrete Pavements in the AASHTO Pavement ME Design Guide. Int. J. of Pavement Res. and Tec., 9(4) (2016) 264-269.

[11] FHWA, Compilation of Existing State Truck Size and Weight Limit Laws, Washington DC, 2015.

[12] Iowa DOT, Iowa Truck Information Guide, July 2017-July 2018 Edition, 2018.

[13] Iowa DOT, Iowa DOT Office of Design, Road Design Details - Typical Components, 2018.

CHAPTER 4. EVALUATION OF RIGID AIRFIELD PAVEMENT CRACKING FAILURE MODELS

A journal paper to be submitted to *Journal of Transportation Engineering: Part B, Pavements*

Orhan Kaya, Halil Ceylan, Kasthurirangan Gopalakrishnan, Sunghwan Kim, Adel Rezaei-Tarahomi, and David R. Brill

Abstract

The Federal Aviation Administration's (FAA's) pavement thickness design software, FAA Rigid and Flexible Iterative Elastic Layer Design (*FAARFIELD*) uses bottom-up fatigue cracking as the only failure criterion in its rigid pavement design procedure. However, since it has been observed in field studies that, under some circumstances, top-down cracking might also occur in rigid airfield pavement systems, there have been some efforts to include top-down cracking as one of the failure criteria in the analysis and design of rigid airfield pavement systems. In this study, FAA's current rigid airfield pavement design methodology has been reviewed and evaluated in great detail to better identify needs for improvements with respect to cracking failure models and to produce recommendations on how current design methodology could be improved. Critical mechanical loading and pavement response locations for top-down and bottom-up cracking failure modes have also been investigated to seek identification of input scenarios where critical pavement responses at slab-top are higher than those at slab-bottom. The effect of temperature loading in determining which failure mode (top-down or bottom-up cracking) would be dominant in rigid-airfield pavement failure was also studied. Slab thickness calculations were carried out using the same slab thickness determination steps as *FAARFIELD* design software (version 1.42) when top-down cracking and bottom-up cracking failure modes are specified as failure

modes. Recommendations were made with respect to including top-down cracking failure mode in rigid airfield pavement design.

Introduction

The FAA's pavement thickness design software, *FAARFIELD*, uses bottom-up fatigue cracking as the only failure criterion in its rigid pavement design procedure (FAARFIELD version 1.42). Consequently, *FAARFIELD* has been using maximum horizontal stress at the bottom edge of the Portland Cement Concrete (PCC) slab as the critical pavement response related to bottom-up cracking to predict pavement's structural life. (FAA 2016). *FAARFIELD* produces an optimum PCC slab thickness value as a result of its pavement analysis, and a slab designed with this thickness, together with a combination of base, subbase and subgrade, is expected to support a given airplane traffic mix over the course of its structural design life. PCC slab thickness is determined by analyzing cumulative damage caused by the mix of all aircraft expected to use the pavement through the cumulative damage factor (CDF) concept (FAA 2016). Fatigue analysis is carried out using Miner's law, expressed as the ratio of applied load repetitions to allowable load repetitions before failure.

However, since it has been observed in field studies that top-down cracking might also occur in rigid airfield pavement systems under some circumstances (Brill 2010), there have been some efforts to include top-down cracking as one of the failure modes in rigid airfield pavement design (Kaya et al. 2018; Rezaei-Tarahomi et al. 2017).

Objectives

In this study, FAA's current rigid airfield pavement design methodology has been evaluated in great detail to better identify research gaps and needs with respect to the cracking failure models so that recommendations could be made as to how the current

methodology could be improved to accommodate top-down and bottom-up cracking failure modes in its design methodology.

Possible questions that might arise when considering such improvements include:

- What are the critical mechanical loading and pavement response locations for top-down and bottom-up cracking failure modes?
- What is the effect of temperature loading in determining which failure mode (top-down or bottom-up cracking) will be dominant in failure of rigid airfield pavements?
- How will calculation of slab thicknesses be affected and how should failure models be revised if top-down and bottom-up cracking failure modes are included in the design?

In this study, these questions have been addressed and some recommendations with respect to potential inclusion of top-down cracking failure mode in rigid airfield pavement design were made.

Review of Current *FAARFIELD* Rigid Airfield Pavement Design Methodology

The *FAARFIELD* design software (version 1.42) currently carries out rigid airfield design in a step-by-step manner following a mechanistic-empirical pavement design procedure (FAA 2016). Fig. 1 summarizes the steps *FAARFIELD* goes through in determining slab thickness.

Initially, inputs for all pavement layers must be entered into the *FAARFIELD* design software, including modulus and thicknesses (other than slab thickness), aircraft mix, and number of annual departures for each aircraft in the mix. *FAARFIELD* assumes that all standard pavement layers meet FAA's AC 150/5370-10G (FAA 2014) applicable requirements for materials, construction, and quality control.

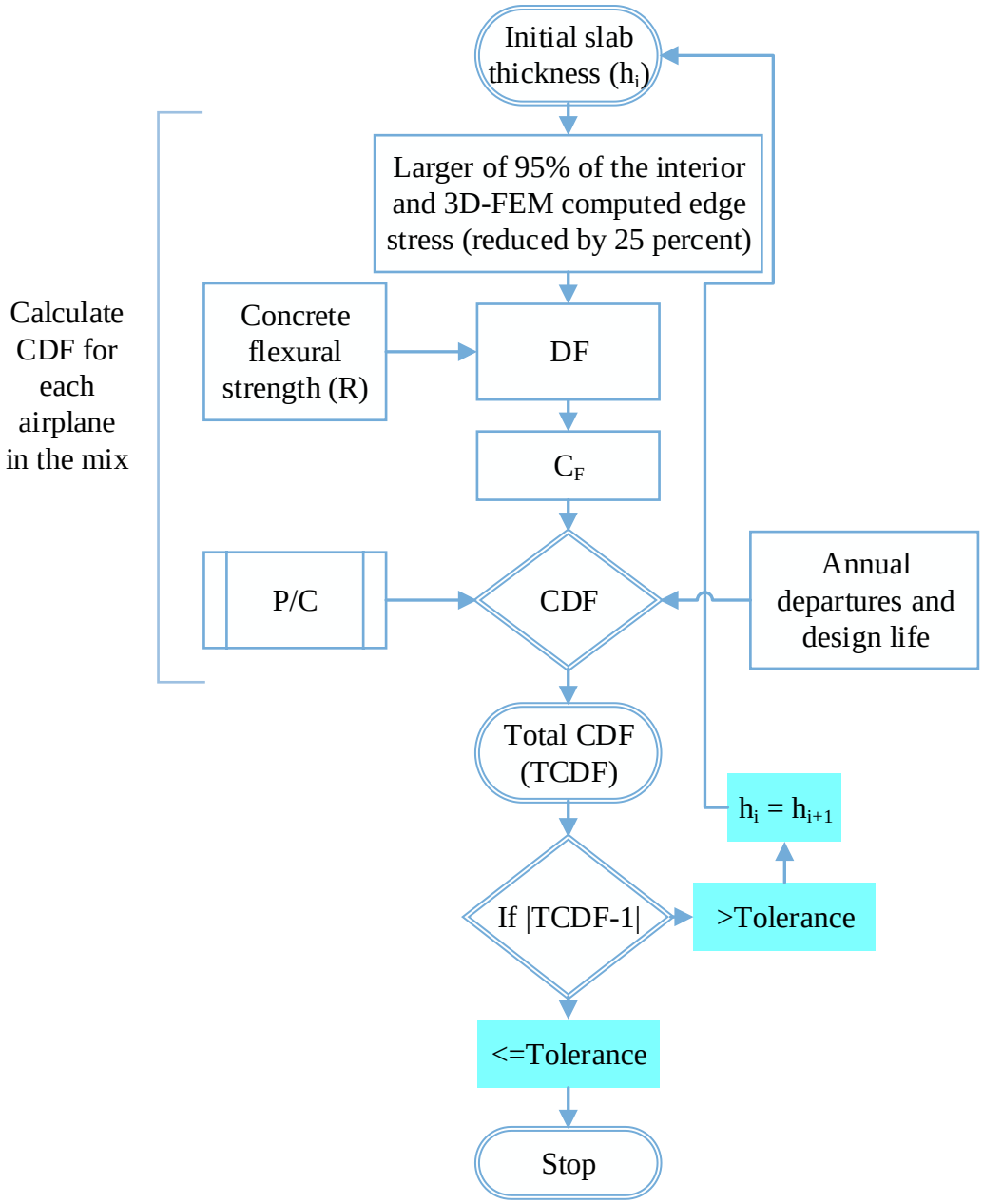

Figure 4.1 Slab thickness determination in FAARFIELD

Step 1: An initial PCC slab thickness is assigned by the program ['Default' assigned PCC slab thickness is 35.6 cm (14 in)]. Slab thickness cannot be less than 15.2 cm (6 in) if a maximum airplane gross weight of 5.7 metric-ton (12,500 lbs) and higher is expected to

operate on a design pavement; if not, minimum slab thickness cannot be less than 12.7 cm (5 in).

Step 2: *FAARFIELD* calculates pavement responses using three-dimensional finite-element models (3D-FEM). It has an internal 3D-FEM engine, called NIKE3D-FAA, that divides slabs into meshes and nodes, then calculates stresses and deflections at each node for a given aircraft load and pavement configuration. FAA also developed a stand-alone pavement response software, finite-element analysis FAA (*FEAFAA*) that also uses NIKE3D-FAA as a 3D-FEM engine. Detailed descriptions and explanations regarding NIKE3D-FAA and *FEAFAA* can be found in other documents (Kaya et al. 2018; Brill 1998; Brill 2000). For a given pavement configuration, a mechanical aircraft load related to the aircraft mix is applied on a slab edge and NIKE3D-FAA calculates edge tensile stress at the bottom-slab edge of the load application location. *FAARFIELD* compares NIKE3D-FAA-computed edge tensile stress (reduced by 25 percent) and 95% of the interior stress computed by a layered elastic computational program [LEAF (Hayhoe 2002)], then takes the higher of these two and calls that value the design stress.

Step 3: The FAA in 2004 calibrated its rigid pavement failure models using data from full-scale tests conducted at the FAA's National Airport Pavement Test Facility (NAPTF) and from previously conducted other tests (Brill 2010) to integrate its new 3D-FEM based response models into its design methodology. 3D-FEM based response models (NIKE3D-FAA) compute edge tensile stresses used in the calculation of design factor (DF), a ratio between tensile strength of a slab and edge tensile stress computed by NIKE3D-FAA calculated using Equation 4.1.

$$DF = \frac{R}{0.75 \times \sigma_e} \tag{4.1}$$

where R is the slab tensile strength and σ_e is the free edge tensile stress computed by the *FAARFIELD* model (3D-FEM), with the 25% reduction in stress accounting for assumed load transfer between slabs.

Step 4: Coverages to failure represents the number of coverages a pavement should serve before it reaches a given failure threshold. The Structural Condition Index (SCI) has been used as part of rigid pavement failure models since it was first introduced by Rollings (Rollings 1988). It counts only load-related distresses, excluding non-material-related distresses. Rollings (Rollings 1988) observed that SCI linearly decreases as number of coverages increases, starting from its initial level of 100, defined as C_0, terminating at the number of coverages before complete failure (C_F), defined as the loss of all slab integrity when SCI = 0. Rollings (Rollings 1988) found that the following distresses contribute to reduction in SCI magnitude: corner break, longitudinal/transverse/diagonal cracking, shattered slab, shrinkage cracks, joint spalling, and corner spalling.

Using the calculated DF value in Step 3, coverages to failure (C_F) value can be calculated using Equation 4.2. It should be noted that Equation 4.2 was developed for bottom-up cracking failure mode:

$$DF = \frac{bd}{\alpha b+(1-\alpha)d} \times log(C_F) + \frac{\alpha bc+(1-\alpha)ad}{\alpha b+(1-\alpha)d} \quad (4.2)$$

Equation 4.2 can be reorganized to yield equation 4.3:

$$C_F = 10^{\left[\frac{DF-\frac{\alpha bc+(1-\alpha)ad}{\alpha b+(1-\alpha)d}}{\frac{bd}{\alpha b+(1-\alpha)d}}\right]} \quad (4.3)$$

In *FAARFIELD* version 1.42, the following α, a, b, c, and d coefficient values were used (Brill 2017):

$\alpha = 0$ (SCI = 0)

$b = d = 0.160$

$$a = 0.760 + 2.543 \times 10^{-5} (E - 4{,}500) \quad (4.4)$$

$$c = 0.857 + 2.314 \times 10^{-5} (E - 4{,}500)$$

where E is the design subgrade modulus in psi. Changes in these parameters were made in *FAARFIELD* version 1.4 because observations in FAA's construction cycle 6 (CC6) tests conducted at FAA's NAPTF (Brill 2014) indicated that a stiffer rigid pavement foundation is more likely to lead to top-down cracking, a failure mode not explicitly considered by the FAARFIELD structural analysis.

Step 5: Total CDF (TCDF) is calculated combining CDF values for all aircraft in the traffic mix. In the design of a new rigid airfield pavement, slab thickness is adjusted until |TCDF – 1| <= tolerance. Otherwise, slab thickness should be increased and another iteration should be performed. Tolerance is a user-defined value - it is set to 0.005 as the default value. If tolerance is increased, a higher or lower slab thickness may result.

The CDF concept can be explained using Equation 4.5. The number of applied load repetitions is calculated by multiplying the designed target annual departures for each aircraft in the traffic mix by the designed life of a pavement (20 years by default). The number of allowable repetitions to failure is calculated by multiplication of an internally program-calculated pass-to-coverage ratio (P/C) and the number of coverages to failure (obtained from Step 4).

$$\text{CDF} = \frac{\text{number of applied load repetitions}}{\text{number of allowable repetitions to failure}} = \frac{(\text{annual departures}) \times (\text{life in years})}{(\text{pass to coverage ratio}) \times (\text{coverages to failure})} \quad (4.5)$$

This equation can be expanded into a generalized Equation (Equation 4.6) relating edge tensile stress calculated by 3D-FEM to CDF:

$$CDF = \frac{(annual\ departures)\times(life\ in\ years)}{(pass\ to\ coverage\ ratio)\times\left(10^{\left[\frac{\frac{R}{0.75\times\sigma_e}-\frac{\alpha bc+(1-\alpha)ad}{\alpha b+(1-\alpha)d}}{\frac{bd}{\alpha b+(1-\alpha)d}}\right]}\right)} \quad (4.6)$$

The P/C ratio is the ratio of number of passes required to apply one full load application to a unit area of the pavement (FAA 2016). Coverage is defined as number of load repetitions required to produce maximum stress at the bottom of the PCC layer. In calculation of P/C, an "effective tire width" concept is used, with the effective tire defined as the nominal tire contact surface width for rigid pavements (FAA 2016). In calculation of CDF, pavement is divided into 25.4-cm (10-inch) wide strips and the P/C value was calculated for each strip, assuming that traffic is normally distributed laterally and that 75 percent of passes fall within a "wander width" of 178 cm (70 inches) (FAA 2016). Design CDF is taken as the maximum CDF among the divided strips. *FAARFIELD* internally performs all CDF computations and generates plots of CDF versus lateral effect for each gear in the design mix, as well as a plot of cumulative CDF for all airplanes in the mix (FAA 2016).

Inclusion of Top-down and Bottom-up Failure Modes in Rigid Airfield Pavement Design

In this section, critical pavement responses at slab-top and slab-bottom were compared to: (1) identify input scenarios where critical pavement responses at slab-tops are higher than at slab-bottoms, (2) evaluate effects of temperature loading with respect to top-down and bottom-up cracking failure modes, and (3) identify critical load and pavement response locations for the cases investigated.

In the second part of this section, design slab thickness calculations are made using the same slab thickness determination steps as *FAARFIELD* (version 1.42) when top-down cracking and bottom-up cracking failure modes are specified as failure modes.

Stress Comparisons

A knowledge database was created that includes inputs required for *FEAFAA* runs and corresponding *FEAFAA* top and bottom-slab critical pavement response outputs, assuming a Boeing B747-8 airplane mechanical load. This airplane has a gross weight of 443.6 metric-ton (978,000 lbs) at take-off, two main landing gears and two other landing gears, each with four wheels with a tire pressure of 1,524 kPa (221 psi). This airplane type was selected for this study because it is the largest 747 version, the largest commercial aircraft built in the United States, and also the longest passenger aircraft in the world.

In the knowledge database development, 2,000 samples were populated using randomly-assigned numbers within the predefined ranges for each input parameter based on a combination of *FEAFAA*'s hard-coded ranges and engineering judgment. The knowledge database was developed to be sufficiently comprehensive to include various scenarios with a wide range of inputs. Detailed discussion related to the actual choice of the number of samples (2,000) in the knowledge database development can be found in another study (Rezaei-Tarahomi et al. 2018). A nine-slab assembly was used in *FEAFAA* analysis, with the center of one of the main landing gears placed at various locations on one quarter of the inner slab, taking advantage of slab symmetry. Types and ranges of input parameters used in *FEAFAA* runs are given in Table 4.1.

Table 4.1 Types and ranges of input parameters used in FEAFAA runs

Inputs		Ranges	
		Minimum	Maximum
PCC Slab	Modulus, GPa (psi)	20.7 (3×10^6)	48.3 (7×10^6)
	Thickness, cm (in)	15.2 (6)	60.9 (24)
	Poisson Ratio	0.10	0.20
Base	Modulus, GPa (psi)	1.4 (2×10^5)	13.8 (2×10^6)
	Thickness, cm (in)	10.0 (4)	76.2 (30)
	Poisson Ratio	0.15	0.25
Granular Subbase	Modulus, GPa (psi)	1×10^{-1} (15,000)	5.2×10^{-1} (75,000)
	Thickness, cm (in)	15.2 (6)	127 (50)
	Poisson Ratio	0.20	0.40
Subgrade	Modulus, GPa (psi)	2.1×10^{-2} (3,000)	3.4×10^{-1} (50,000)
	Poisson Ratio	0.30	0.45
Slab Dimension, m (ft)		4.6 (15)	9.1 (30)
Slab Number of Elements		30	
Number of Slabs		9	
Foundation Number of Elements		30	
Loading Angle		0	90
Temperature Gradient, ^{o}C/cm (^{o}F/in)		-0.3 (-2)	0.3 (2)
Thermal Coefficient, 1/^{o}C (1/^{o}F)		7.4×10^{-6} (4.1×10^{-6})	12.9×10^{-6} (7.2×10^{-6})
Equivalent Joint Stiffness, GPa/m (psi/in)		2.7×10^{-1} (1.0×10^3)	162.6 (6.0×10^5)

FEAFAA produces an output file in txt format containing each node's stress and deflection results for each run. As stated earlier, in the current version of *FAARFIELD* (version 1.42), tensile stresses at the slab bottom edges are used as critical pavement responses, because the main landing gear load is applied on a slab edge without a loading angle, i.e., the gear load is applied parallel to a slab edge. Note that loading angle is the angle at which aircraft wheels are placed on PCC slabs. Critical pavement response location in this loading scenario is assumed to occur at the bottom edge beneath the location of the applied load. The state-of-the-art design methodology for highway pavements, Mechanistic-

Empirical Pavement Design Guide (MEPDG) also uses maximum bending (tensile) stresses as critical pavement responses in the design of rigid pavements (NCHRP 2003).

A postprocessing tool using the C# programming language was developed to extract critical pavement responses at top and bottom surfaces of the slab. Critical pavement responses were then summarized and transferred into a Microsoft excel spreadsheet for each corresponding input record supplied to *FEAFAA*. The postprocessing tool can extract and transmit maximum tensile stresses at the top and bottom surface of slabs into the knowledge database. *FEAFAA* produces tensile stress results in x and y directions. The critical tensile stress at slab-top and slab-bottom was determined by taking the higher of maximum tensile stress values in x and y directions. The postprocessing tool can also internally calculate principal stresses (σ_1 and σ_2) at each nodal point of the finite-element model and transmit the maximum values of such stresses at slab-top and slab-bottom into the knowledge database.

The principal stress hypothesis predominantly serves to describe failure of brittle materials that occurs either when the maximum principal stress reaches the tensile strength (σ_t) or when the minimum principal stress reaches the compressive strength ($-\sigma_p$) of a material. (Gould 1993; Gross and Seelig 2011). Concrete material exhibits brittle material behavior, with failure occurring when principal stress reaches the tensile strength of concrete. In this study, since gear load is applied at various locations with various loading angles, the combined effect of tensile stresses in both x and y directions can be evaluated using maximum principal stresses. Principal stress angles (Θ_p) can also represent potential crack propagation angles.

In this study, two critical pavement response types were considered for various input scenarios:

- Maximum tensile stresses at the bottom and top slab surfaces
- Maximum principal stresses at the bottom and top slab surfaces

Fig. 4.2 shows maximum (a) tensile and (b) principal stress distributions for 2,000 input scenarios. As can be seen in Fig. 4.2, while bottom stresses in most cases were higher than top stresses for both tensile and principal stress cases, in a significant number of cases, top stresses were higher than bottom stresses. It can also be observed that absolute maximum principal stress values were higher to some extent than absolute maximum tensile stress values for all cases evaluated.

Fig. 4.3 shows top-to-bottom (a) tensile and (b) principal stress ratio distributions for 2,000 input scenarios. As can be seen in Fig. 4.3, in about 35% of cases, top stresses were higher than bottom stresses and in about 6% of cases, top stresses were significantly higher than bottom stresses (top-to-bottom ratio was higher than 2) for both tensile and principal stress cases. Conversely, in about 65% of the cases, bottom stresses were higher than top stresses for both tensile and principal stress cases. More cases where bottom stresses were higher than top stresses was to be expected because bottom-up cracking is the most common failure mode in rigid airfield pavements. Understanding distribution of top-to-bottom stress ratio is important because it reveals whether the mode of fatigue cracking, if any, is top-down or bottom-up cracking. If the top-to-bottom stress ratio is greater than 1.0, a possible fatigue crack is likely to occur top-down, otherwise it is likely to appear as a bottom-up crack.

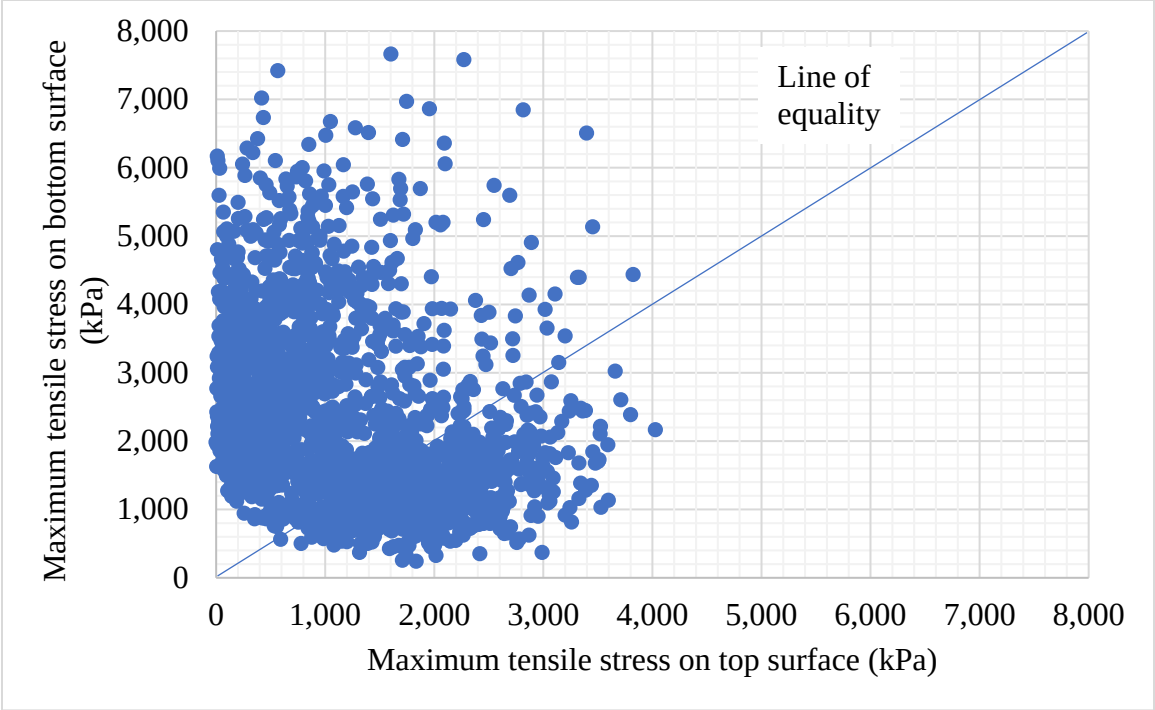

(a)

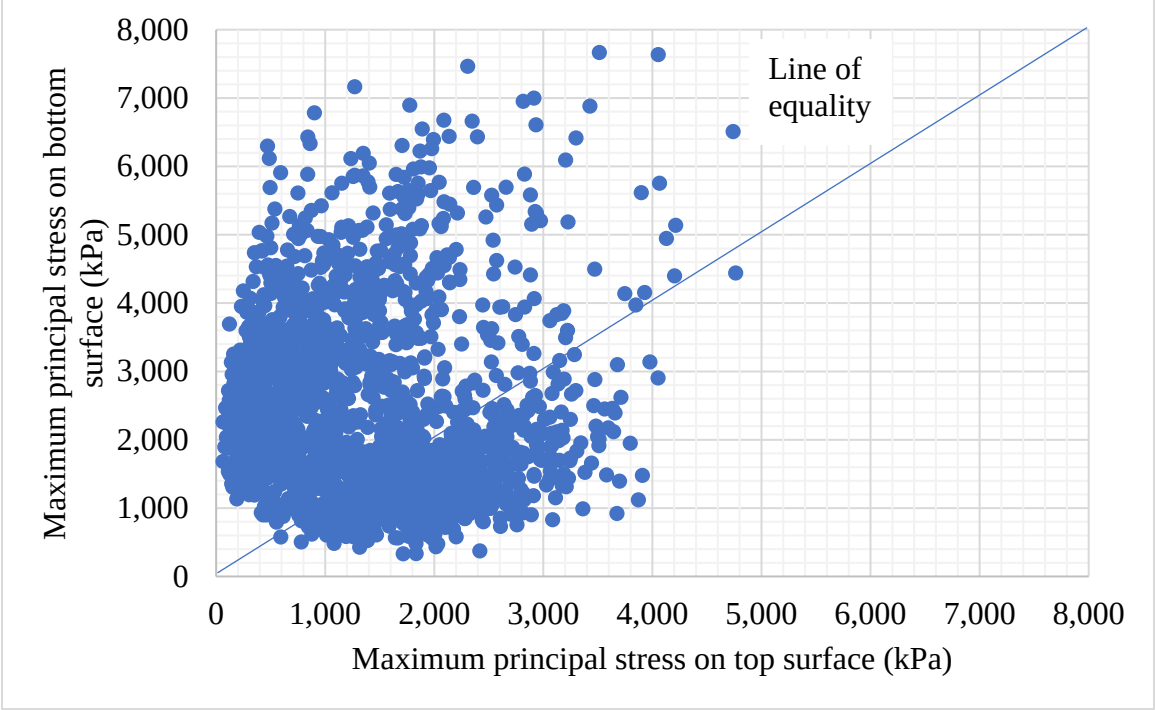

(b)

Figure 4.2 Maximum (a) tensile and (b) principal stress distribution at the bottom and top slab surfaces for 2,000 cases

Fig. 4.4 shows top-to-bottom tensile and principal stress ratio distributions for input cases with various temperature gradient values. As can be seen in Fig. 4.4, as a temperature gradient increases negatively, the average top-to-bottom tensile and principal stress ratios increase. Since top-to-bottom stress ratios were as high as 10 for tensile stress cases and as high as 8 for principal stress cases, is clear that input cases with negative gradients were the ones producing higher top-to-bottom stress ratios and, in turn, higher top-down cracking potential.

In this study, mechanical load locations were distributed in such a way that more load locations were around slab edges and corners. This was because slab edges were critical load locations for bottom-up cracking and it was found in this study that higher top-to-bottom ratio values were observed for cases where mechanical load locations were closer to slab corners. Fig. 4.5 shows a distribution of center locations of a main B747-8 landing gear for 2,000 input scenarios. In cases where this center is closer to slab edges and corners, gear loads were partially placed on adjacent slabs. It is important to note that slab aspect ratios (ratios between slab dimensions) varied in each input case. In Fig. 4.5, load locations were normalized to slab dimensions (load locations in x and y coordinates (Xg, Yg), and divided by slab sizes in x and y directions (Lx and Ly) as Xg/Lx, Yg/Ly) to seek understanding of effects of relative mechanical load locations to slab edges and corners. Each unit in Fig. 4.5 represents a single slab, and a nine-slab assembly was used in this study.

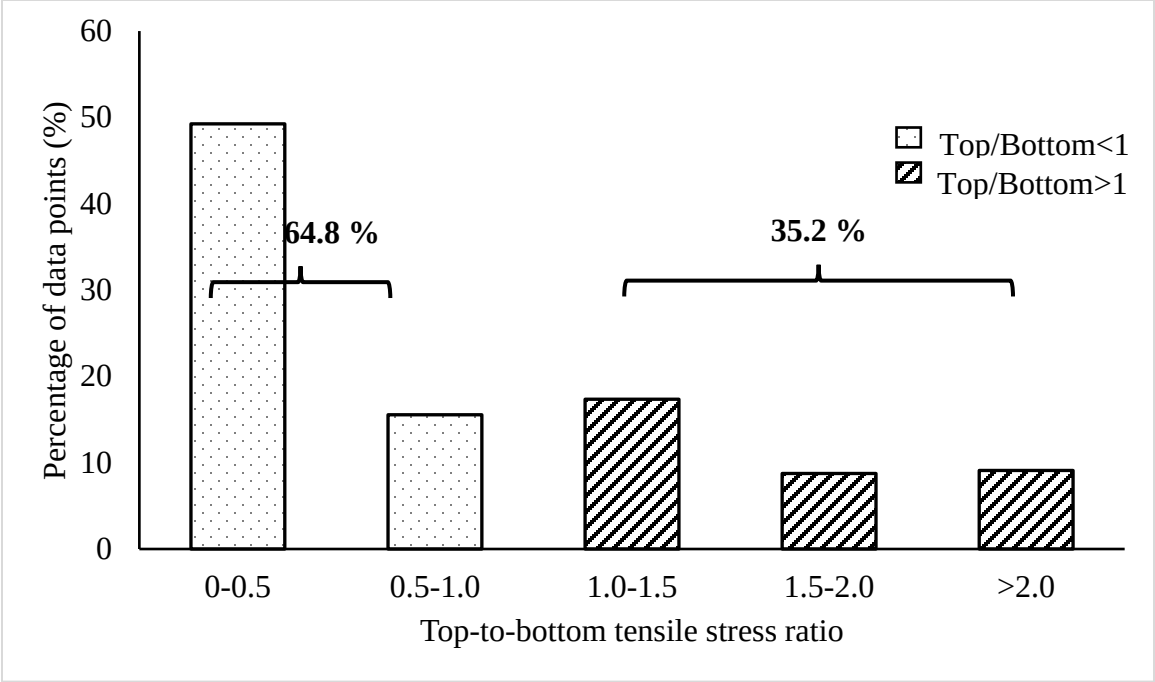

(a)

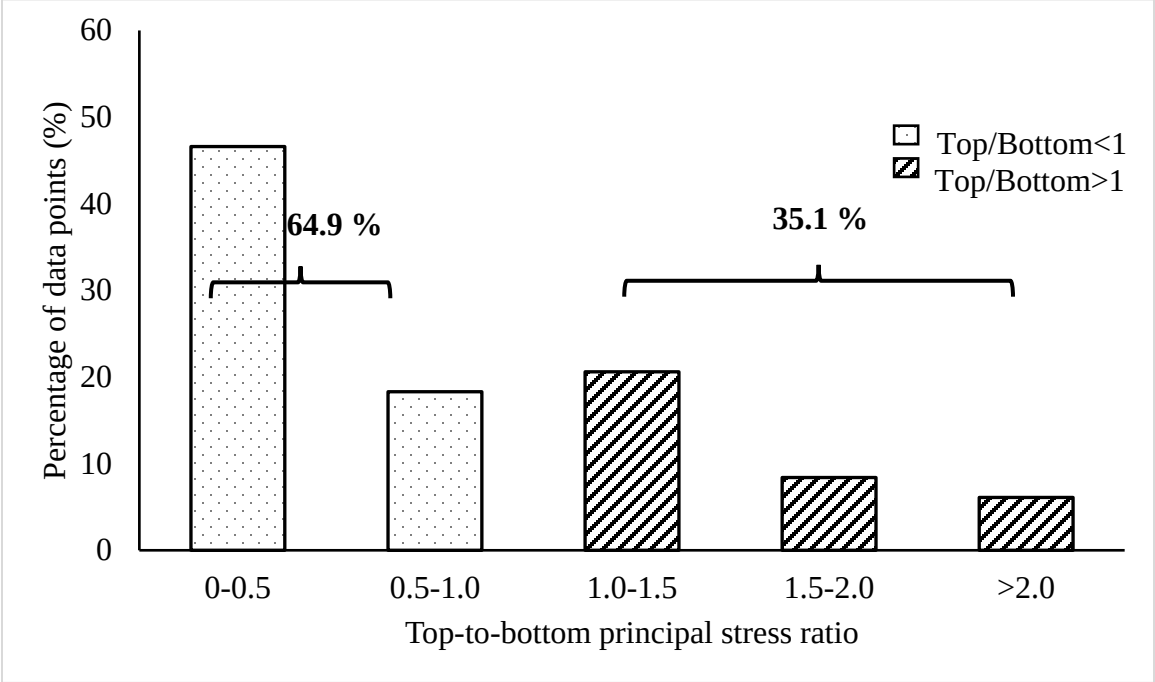

(b)

Figure 4.3 Top-to-bottom (a) tensile and (b) principal stress ratio distribution for 2,000 cases

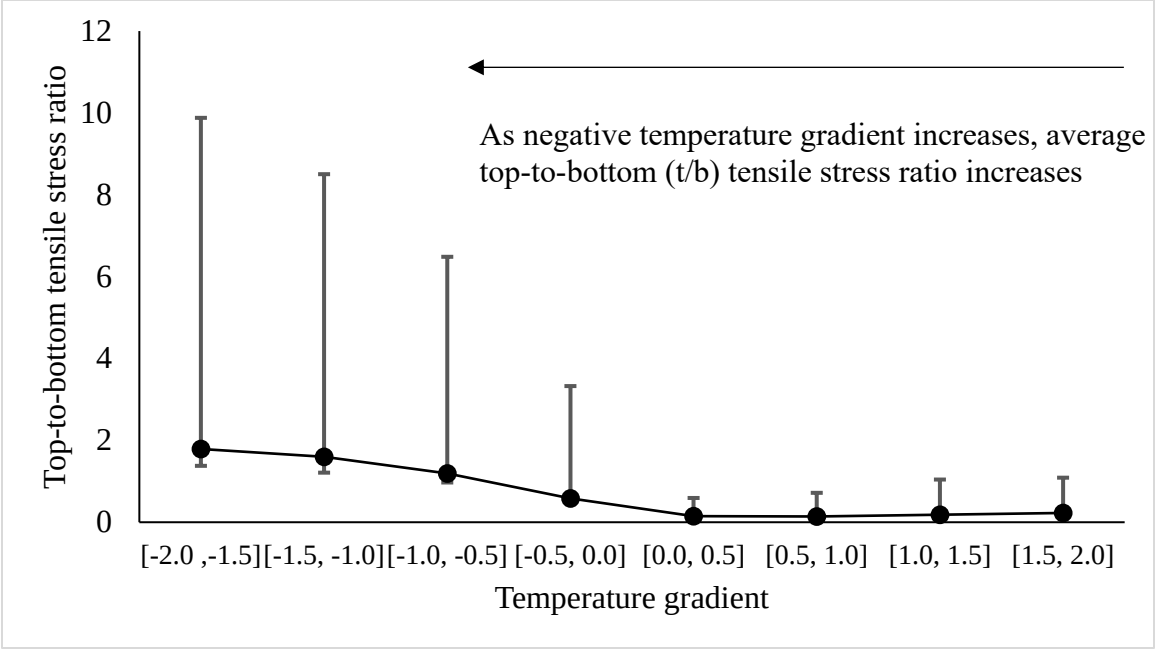

(a)

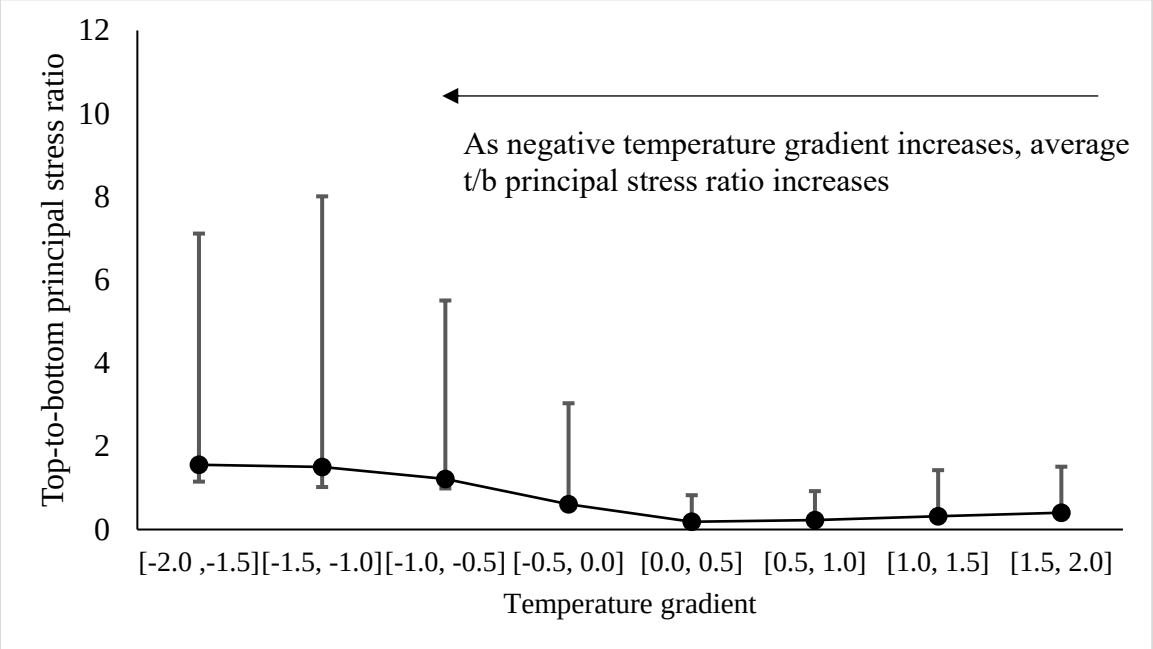

(b)

Figure 4.4 Top-to-bottom (a) tensile and (b) principal stress ratio distribution for various temperature gradient cases

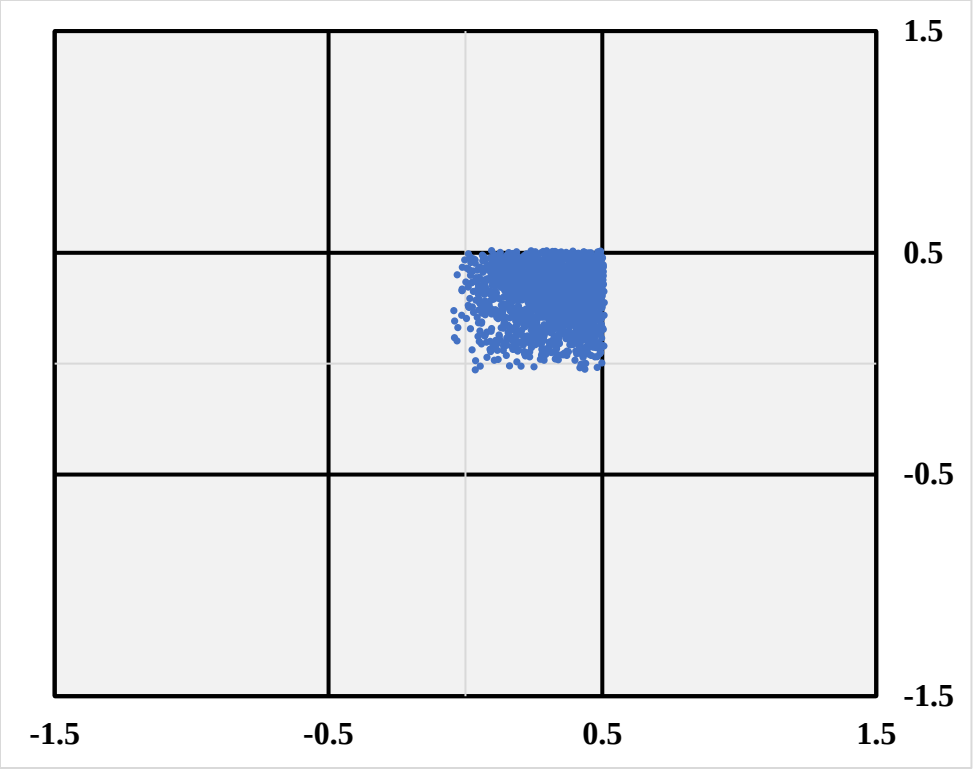

Figure 4.5 Distribution of applied mechanical load

Figs. 4.6a and 4.6b shows critical pavement response locations where maximum top tensile and principal stresses, respectively, were observed. As can be seen in the figures, critical response locations mostly accumulated around joints of adjacent slabs rather than within the slabs where mechanical load was applied. This effect was more pronounced in maximum principal stress cases than in maximum tensile stress cases. This finding generally supports field observations where top-down cracks have been found to occur near joints (Hayhoe 2004).

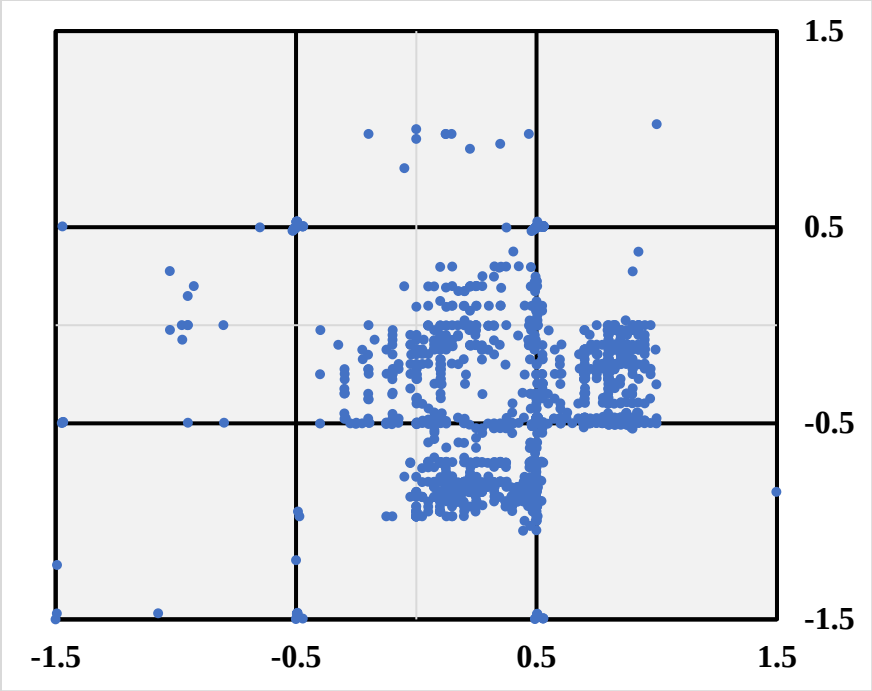

(a)

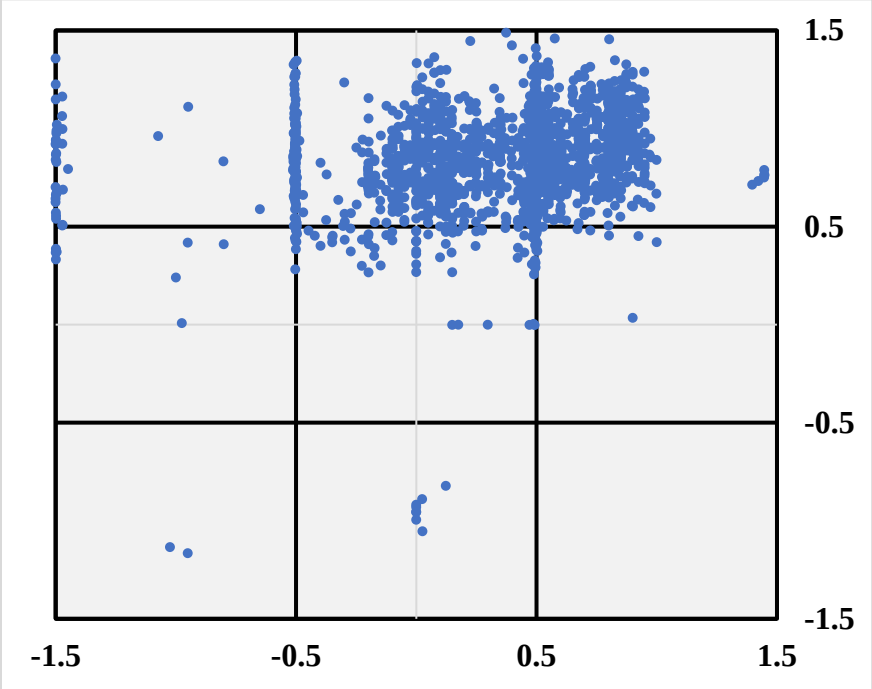

(b)

Figure 4.6 Distribution of critical pavement response locations where maximum top (a) tensile and (b) principal stresses were observed

Design Slab Thickness Calculations

This section describes additional *FEAFAA* runs in which maximum top and bottom stresses were extracted to be used in the calculation of slab thicknesses. In the first part of this paper, slab thickness determination steps used in the *FAARFIELD* design software (version 1.42) were described in great detail. As stated earlier, at the time of writing this paper, *FAARFIELD* design software (version 1.42) used bottom-edge tensile stresses only for determining design stress. In this study, maximum top and bottom tensile and principal stresses that *FEAFAA* outputted were used as design stresses for various slab thickness scenarios. Then, using these design stresses (four design stresses: top-tensile, bottom-tensile, top-principal and bottom-principal), coverages to failures (Equation 4.3) were calculated. All coverages to failure and CDF calculations were carried out outside the *FAARFIELD* design software.

In *FEAFAA* runs, a four-layer rigid airfield pavement configuration has been used (Table 4.2). All materials and corresponding material properties follow the FAA's allowable values (FAA 2016). Slab thickness was varied from 20.3 cm to 40.6 cm (8 in. to 16 in.) and all other thickness and material properties were kept the same for all *FEAFAA* runs (Table 4.2).

Table 4.2 Types of input parameters used in FEAFAA runs for thickness calculations

Layers	E Modulus, GPa (psi)	Poisson's Ratio	Thickness
P-501 Slab	27.6 (4,000,000)	0.15	Various 20.3 - 40.6 cm (8 - 16 in)
P-306 Lean Concrete	4.8 (700,000)	0.20	15.2 cm (6 in)
P-209 Crushed Aggregate	0.5 (75,000)	0.35	15.2 cm (6 in)
Subgrade	0.1 (15,000)	0.40	Infinite

The same mechanical load was used as in a previous section of this paper, i.e., a main landing gear of a Boeing B747-8. Two critical mechanical load locations were considered: corner load for top-down cracking (maximum top stresses used as critical pavement responses) and edge load for bottom-up cracking (maximum bottom stresses used as critical pavement responses) (Fig. 4.7).

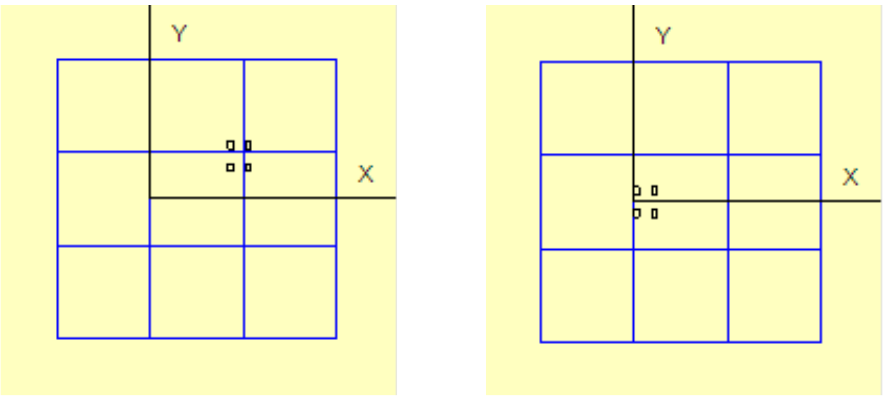

(a) (b)

Figure 4.7 Mechanical load locations: (a) corner load and (b) edge load

As temperature load, a temperature gradient of -0.3 ^{o}C/cm (-2 ^{o}F/in.) was applied to all cases investigated. For each critical mechanical load location and slab thickness, top and bottom critical pavement responses were extracted, and CDF values for these cases were calculated to determine the optimum slab thickness.

Other inputs required to calculate CDF were as follows:

- Assumed tensile strength of slab: 4.5 MPa (650 psi)
- Annual departures: 4,000
- Calculated P/C: 3.55
- Design life: 20 years

In the calculation of design factor "DF" (Equation 4.1), the 25% reduction in stress used to account for assumed load transfer between slabs, this reduction was because the model in *FAARFIELD* (version 1.42) uses single-slab, was not applied to slab thickness calculations in this study since a nine-slab assembly was used in *FEAFAA* runs, load transfer between slabs had already been considered in the runs. The following "DF" equation was used in this study:

$$DF = \frac{R}{\sigma_{design}} \tag{4.9}$$

where R is slab tensile strength and σ_{design} is the design stress computed by *FEAFAA* for each case.

Table 4.3 shows slab thickness comparisons when maximum (a) top-tensile, (b) bottom-tensile, (c) top-principal and (d) bottom-principal stresses are used as design stresses using *FAARFIELD* version 1.42 design methodology. The CDF values were calculated using these stresses for various slab thicknesses to determine the optimum slab thickness where |CDF – 1| <= 0.005 as a tolerance (i.e., 0.995 <= CDF <= 1.005). For cases where CDF values were relatively higher than 1.005 and lower than 0.995, the corresponding larger thickness was conservatively chosen. For example, as can be seen in Table 4.3a, CDF values were calculated as 1.03 and 0.57 for the slab thicknesses of 27.9 and 30.5 cm (11 and 12 in), respectively. None of these two slab thicknesses satisfy optimum slab thickness criterion where the optimum slab thickness should produce a CDF value of |CDF – 1| <= 0.005. However, it is obvious that the optimum thickness should be between 27.9 and 30.5 cm (11 and 12 in) since 27.9 cm (11 in) slab thickness produces slightly higher CDF value and 30.5 cm (12 in) slab thickness produces slightly lower CDF value compared to when |CDF – 1| <=

0.005. For this case, the larger of these slab thicknesses is determined as optimum slab thickness [i.e., 30.5 cm (12 in)].

Rows in bold show optimum slab thickness values for each design stress scenario (Table 4.3). Table 4.3 also shows all parameters used in CDF calculation for each design stress scenario. All calculations for slab thickness determination were carried out using the steps described earlier in this paper. Coverage to failure (Equation 4.3) was calculated for each slab thickness using the coefficients given in Equation 4.4. As can be seen in Table 4.3, slab thicknesses calculated using principal stresses were higher than those calculated using tensile stresses because, as shown in the previous section of this paper, absolute principal stress values were found to be higher than absolute tensile stresses for the same input scenarios. Table 4.3 also shows that slab thicknesses calculated using top stresses were higher than those calculated using bottom stresses, because a negative temperature gradient [-0.3 ^{o}C/cm (-2 ^{o}F/in.)] was applied to all cases investigated, so slightly higher top stresses than bottom stresses were observed.

Table 4.4 summarizes optimum slab thickness results using maximum top and bottom tensile and principal stresses as design stresses in *FAARFIELD* version 1.42 design methodology. There was a general trend in optimum slab thickness results that optimum slab thicknesses were higher when (1) maximum top stresses (as opposed to maximum bottom stresses) and (2) maximum principal stresses (as opposed to maximum tensile stresses) were considered as design stresses. That the optimum slab thicknesses were higher when maximum top stresses (as opposed to maximum bottom stresses) were considered as design stresses could be explained by the fact that coverage to failure (C_F) values for both cases were calculated using Equation 4.3, which only considers bottom-up cracking mode. This

equation is recommended to be revised and calibrated for top-down cracking failure mode. That way, more realistic slab thicknesses for top-down cracking failure mode can be calculated.

Table 4.3 Slab Thickness comparisons using FAARFIELD Version 1.42 design methodology

(a) Maximum top tensile stress is used as design stress

Slab Thickness, cm (in)	Top Tensile Stress, MPa (psi)	Esubgrade, MPa (psi)	Assumed Slab Tensile Strength, MPa (psi)	DF	CF	Annual Departures	P/C	CDF	Life for Failure (years)
20.3 (8)	2.63 (381)	103 (15,000)	4.48 (650)	1.71	17,462	4,000	3.55	1.29	15
22.9 (9)	2.67 (387)	103 (15,000)	4.48 (650)	1.68	11,452	4,000	3.55	1.97	10
25.4 (10)	2.65 (384)	103 (15,000)	4.48 (650)	1.69	14,354	4,000	3.55	1.57	13
27.9 (11)	2.60 (377)	103 (15,000)	4.48 (650)	1.72	21,936	4,000	3.55	1.03	19
30.5 (12)	**2.53 (368)**	**103 (15,000)**	**4.48 (650)**	**1.76**	**39,518**	**4,000**	**3.55**	**0.57**	**35**
33.0 (13)	2.55 (370)	103 (15,000)	4.48 (650)	1.76	35,789	4,000	3.55	0.63	32
35.6 (14)	2.47 (358)	103 (15,000)	4.48 (650)	1.81	82,735	4,000	3.55	0.27	73
38.1 (15)	2.36 (343)	103 (15,000)	4.48 (650)	1.89	265,520	4,000	3.55	0.08	236
40.6 (16)	2.30 (333)	103 (15,000)	4.48 (650)	1.95	592,162	4,000	3.55	0.04	526

(b) Maximum bottom tensile stress is used as design stress

Slab Thickness, cm (in)	Bottom Tensile Stress, MPa (psi)	Esubgrade, MPa (psi)	Assumed Slab Tensile Strength, MPa (psi)	DF	CF	Annual Departures	P/C	CDF	Life for Failure (years)
20.3 (8)	**2.56 (371)**	**103 (15,000)**	**4.48 (650)**	**1.75**	**32,406**	**4,000**	**3.55**	**0.70**	**29**
22.9 (9)	2.28 (331)	103 (15,000)	4.48 (650)	1.96	691,426	4,000	3.55	0.03	614
25.4 (10)	2.16 (313)	103 (15,000)	4.48 (650)	2.08	-	4,000	3.55	0.01	-
27.9 (11)	2.09 (303)	103 (15,000)	4.48 (650)	2.14	-	4,000	3.55	0.00	-
30.5 (12)	1.90 (276)	103 (15,000)	4.48 (650)	2.35	-	4,000	3.55	0.00	-
33.0 (13)	1.83 (265)	103 (15,000)	4.48 (650)	2.45	-	4,000	3.55	0.00	-
35.6 (14)	1.69 (245)	103 (15,000)	4.48 (650)	2.64	-	4,000	3.55	0.00	-
38.1 (15)	1.65 (239)	103 (15,000)	4.48 (650)	2.71	-	4,000	3.55	0.00	-
40.6 (16)	1.50 (217)	103 (15,000)	4.48 (650)	2.99	-	4,000	3.55	0.00	-

Table 4.3 (Continued)

(c) Maximum top principal stress is used as design stress

Slab Thickness, cm (in)	Top Principal Stress, MPa (psi)	Esubgrade, MPa (psi)	Assumed Slab Tensile Strength, MPa (psi)	DF	CF	Annual Departures	P/C	CDF	Life for Failure (years)
20.3 (8)	2.81 (407)	103 (15,000)	4.48 (650)	1.60	3,592	4,000	3.55	6.27	3
22.9 (9)	2.84 (412)	103 (15,000)	4.48 (650)	1.58	2,751	4,000	3.55	8.19	2
25.4 (10)	2.85 (413)	103 (15,000)	4.48 (650)	1.57	2,554	4,000	3.55	8.82	2
27.9 (11)	2.81 (407)	103 (15,000)	4.48 (650)	1.60	3,556	4,000	3.55	6.34	3
30.5 (12)	2.79 (404)	103 (15,000)	4.48 (650)	1.61	4,164	4,000	3.55	5.41	4
33.0 (13)	2.74 (397)	103 (15,000)	4.48 (650)	1.64	6,367	4,000	3.55	3.54	6
35.6 (14)	2.67 (387)	103 (15,000)	4.48 (650)	1.68	11,703	4,000	3.55	1.93	10
38.1 (15)	**2.54 (368)**	**103 (15,000)**	**4.48 (650)**	**1.76**	**40,653**	**4,000**	**3.55**	**0.55**	**36**
40.6 (16)	2.44 (353)	103 (15,000)	4.48 (650)	1.84	114,275	4,000	3.55	0.20	101

(d) Maximum bottom principal stress is used as design stress

Slab Thickness, cm (in.)	Bottom Principal Stress, MPa (psi)	Esubgrade, MPa (psi)	Assumed Slab Tensile Strength, MPa (psi)	DF	CF	Annual Departures	P/C	CDF	Life for Failure (years)
20.3 (8)	2.89 (419)	103 (15,000)	4.48 (650)	1.55	1,827	4,000	3.55	12.33	2
22.9 (9)	**2.52 (365)**	**103 (15,000)**	**4.48 (650)**	**1.78**	**51,338**	**4,000**	**3.55**	**0.44**	**46**
25.4 (10)	2.23 (324)	103 (15,000)	4.48 (650)	2.00	1,230,534	4,000	3.55	0.02	1,092
27.9 (11)	2.09 (303)	103 (15,000)	4.48 (650)	2.14	-	4,000	3.55	0.00	-
30.5 (12)	1.91 (277)	103 (15,000)	4.48 (650)	2.34	-	4,000	3.55	0.00	-
33.0 (13)	1.88 (272)	103 (15,000)	4.48 (650)	2.38	-	4,000	3.55	0.00	-
35.6 (14)	1.76 (255)	103 (15,000)	4.48 (650)	2.55	-	4,000	3.55	0.00	-
38.1 (15)	1.71 (248)	103 (15,000)	4.48 (650)	2.62	-	4,000	3.55	0.00	-
40.6 (16)	1.74 (253)	103 (15,000)	4.48 (650)	2.57	-	4,000	3.55	0.00	-

Table 4.4 Summary of slab thickness comparisons

FAARFIELD Version	Version 1.42	
Stress Type	Tensile Stress	Principal Stress
Top Stress Based Optimum Thickness, cm (in)	30.5 (12)	38.1 (15)
Bottom Stress Based Optimum Thickness, cm (in)	20.3 (8)	22.9 (9)

Conclusions

In this study, FAA's current rigid airfield pavement design methodology has been evaluated in great detail to seek better understanding with respect to research gaps and needs

in cracking failure models to provide recommendations on how the current methodology could be improved to accommodate top-down and bottom-up cracking failure modes in its design methodology.

The conclusions from this study can be summarized by answering the three fundamental questions raised in the introduction:

- "*What are the critical mechanical loading and pavement response locations for top-down and bottom-up cracking failure modes?*" In this study, two critical pavement response types were considered: maximum tensile and principal stresses at the bottom and top surfaces of the slab. In about 35% of all cases, top stresses were higher than bottom stresses, while in about 65% of cases, bottom stresses were higher than top stresses for both tensile and principal stress cases. This result was expected because bottom-up cracking failure mode is the most common failure mode in rigid airfield pavements. Understanding distribution of top-to-bottom stress ratio is important because it reveals the mode of fatigue cracking, top-down or bottom-up, if any. If top-to-bottom stress ratio is greater than 1.0, a possible top-down fatigue crack is likely to occur; if not, it is likely to appear as a bottom-up crack. It was also observed that absolute maximum principal stress values were to some extent higher than absolute maximum tensile stress values for all cases evaluated. For cases where mechanical loading was closer to slab corners, since higher top-to-bottom ratio values were observed, slab corners were found to be critical mechanical load locations for top-down cracking failure mode. Critical response locations mostly accumulated around joints of adjacent slabs rather than within the slabs where mechanical load was applied. This was more pronounced in maximum principal

stress cases than maximum tensile stress cases. This finding closely supports field observations where top-down cracks have been found to occur close to joints.

- "*What is the effect of temperature loading in determining which failure mode (top-down or bottom-up cracking) will be dominant in the failure of rigid airfield pavements?*" As negative temperature gradient increased, average top-to-bottom tensile and principal stress ratios also increased. It is clear that input cases with negative temperature gradients were the ones producing higher top-to-bottom stress ratios and resulting higher top-down cracking potential.
- "*How will calculated slab thicknesses be affected and how should the failure model will be revised if top-down and bottom-up cracking failure modes are included in the design?*" There was a general trend in optimum slab thickness results that optimum slab thicknesses were higher when (1) maximum top stresses (as opposed to maximum bottom stresses) and (2) maximum principal stresses (as opposed to maximum tensile stresses) were considered as design stresses. This was because (1) absolute principal stress values were higher than absolute tensile stresses for the same input scenarios, and since a negative temperature gradient [-0.3 ^{o}C/cm (-2 ^{o}F/in)] was applied to all cases investigated, slightly higher top stresses were observed compared to bottom stresses. That the optimum slab thicknesses were higher when maximum top stresses (as opposed to maximum bottom stresses) were considered as design stresses could be explained by the fact that coverage to failure (C_F) values for both cases were calculated using Equation 4.3, which only considers bottom-up cracking mode.

Recommendations

Based on the study findings, the following recommendations on potential inclusion of both top-down and bottom-up cracking failure modes in rigid airfield pavement design can be made:

- This study showed that top and bottom stresses should be considered in rigid airfield pavement design. The coverages-to-failure equation (Equation 4.3) is recommended to be revised and calibrated to accommodate top-down cracking failure mode as well. That way, more realistic slab thicknesses for top-down cracking failure mode can be calculated. Moreover, a set of protocol/framework steps should be established in determining the final slab thickness.
- Use of maximum principal stress for design stress can be considered as an alternative to maximum tensile stress. In this way, mechanical loading at an angle can be better represented and potential crack propagation direction could be identified. Rather than using pre-determined load locations (as done in the current design methodology) and calculating design stress based on them, a mechanical load can at each time be placed at several load locations and maximum stresses on slab top and bottom of can be automatically calculated. Calculated maximum stresses can then be used as design stresses.
- In the calculation of design factor (DF), two different tensile strength values can be considered (one for top and the other for bottom of the slab) because the slab top is exposed to the sun and wind so higher evaporation occurs on that surface. This might reduce slab tensile strength close to the top surface, especially for projects constructed on hot and windy days.

- In this study, while a theoretical temperature gradient [-0.3 °C/cm (-2 °F/in)] was used in slab thickness determination cases, each construction site should be individually evaluated so that curling and warping of slabs can be better predicted and more realistic temperature gradients can be used in design.

Acknowledgements

The authors gratefully acknowledge the Federal Aviation Administration (FAA) for supporting this study. The contents of this paper reflect the views of the authors who are responsible for the facts and accuracy of the data presented within. The contents do not necessarily reflect the official views and policies of the FAA and Iowa State University. This paper does not constitute a standard, specification, or regulation.

References

Brill, D. R. (1998). "Development of advanced computational models for airport pavement design." *FAA Rep. DOT/FAA/AR-97/47*, Federal Aviation Administration, Washington, D.C.

Brill, D. R. (2000). "Field verification of a 3D finite element rigid airport pavement model." *FAA Rep. DOT/FAA/AR-00/33*, Federal Aviation Administration, Washington, D.C.

Brill, D. R. (2010). "Calibration of FAARFIELD rigid pavement design procedure." *FAA Rep. DOT/FAA/AR-09/57*, Federal Aviation Administration, Washington, D.C.

Brill, D. R. and I. Kawa. (2014). "Relative Performance of CC6 concrete pavement test items at the FAA National Airport Pavement Test Facility". *Proc., 2014 FAA Worldwide Airport Technology Transfer Conference*, Galloway Township, NJ.

Brill, D. R. and I. Kawa (2017). "Advances in FAA pavement thickness design software: FAARFIELD 1.41". *Proc., 2017 Airfield and Highway Pavements Conferenc*e, Philadelphia, PA.

FAA (2014). "Standards for specifying construction of airports." *FAA Advisory Circular (AC) No: 150/5370-10G*, Federal Aviation Administration, Washington, D.C.

FAA (2016). "Airport pavement design and evaluation." *FAA Advisory Circular (AC) No: 150/5320-6F*, Federal Aviation Administration, Washington, D.C.

FAARFIELD [Computer software]. Federal Aviation Administration Airport Technology R&D Branch, ANG-E262 William J. Hughes Technical Center, Egg Harbor Township, NJ.

FEAFAA version 2.0 [Computer software]. Federal Aviation Administration Airport Technology R&D Branch, ANG-E262 William J. Hughes Technical Center, Egg Harbor Township, NJ.

Gould, P.L. (1993). *Introduction to linear elasticity*. Springer, New York.

Gross, D and Seelig. T. (2011). *Fracture Mechanics with an Introduction to Micromechanics*. Springer, Berlin Heidelberg.

Hayhoe, G. F. (2002). "LEAF – A new layered elastic computational program for FAA pavement design and evaluation procedures." *Proc., 2002 Federal Aviation Administration Airport Technology Transfer Conference*. Galloway Township, NJ.

Hayhoe, G. F. (2004). "Traffic testing results from the FAA's National Airport Pavement Test Facility". *Proc., 2nd International Conference on Accelerated Pavement Testing*, University of Minnesota, Minneapolis, MN.

Kaya, O., Rezaei-Tarahomi, A., Ceylan, H., Gopalakrishnan, K., Kim, S., and Brill, D. R. (2018). "Neural network–based multiple-slab response models for top-down cracking mode in airfield pavement design". *J. Transp. Eng., Part B: Pavements, 144(2): 04018009.*

NCHRP (National Cooperative Highway Research Program). (2003). "Guide for mechanistic-empirical design of new and rehabilitated pavement structures, final document, Appendix QQ: Structural response models for rigid pavements." *NCHRP 1-37A Rep.*, Transportation Research Board of the National Academies, Washington, DC.

Rezaei-Tarahomi, A., Kaya, O., Ceylan, H., Gopalakrishnan, K., Kim, S., and Brill, D. R. (2017). "Sensitivity quantification of airport concrete pavement stress responses associated with top-down and bottom-up cracking." *International Journal of Pavement Research and Technology*, doi: http://dx.doi.org/10.1016/ j.ijprt.2017.07.001.

Rezaei-Tarahomi, A., Kaya, O., Ceylan, H., Gopalakrishnan, K., Kim, S., and Brill, D. R. (2018). "Evaluation of neural network algorithms for rigid airfield pavements." *Proc., International Conference on Advances in Materials and Pavement Performance Prediction (AM3P)*, April 16-18, 2018, Doha, Qatar.

Rollings, R. S (1988). "Design of overlays for rigid airport pavements." *FAA Report DOT/FAA/PM-87/19.*, Federal Aviation Administration, Washington, D.C.

CHAPTER 5. DEVELOPMENT OF A FRAMEWORK FOR PROJECT AND NETWORK LEVEL PAVEMENT PERFORMANCE AND REMAINING SERVICE LIFE PREDICTION MODELS FOR IOWA PAVEMENT SYSTEMS

Abstract

In their pavement management decision-making processes, state highway agencies (SHAs) are required to develop performance-based approaches based on The Moving Ahead for Progress in the 21st Century (MAP-21) Federal Transportation Legislation. One of the performance-based approaches to facilitate pavement management decision-making process is use of remaining service life (RSL) models. In this study, a detailed step-by-step methodology for the development of pavement performance and RSL prediction models for Iowa pavement systems is described. To develop such RSL models, pavement performance models for both project and network-level analysis were initially developed. While statistically (or mathematically) defined pavement performance models were found to be accurate in predicting pavement performance at project level, artificial intelligence (AI) based pavement performance models were found to be successful in predicting pavement performance in network level analysis. Network level pavement performance models using both statistical and AI based approaches were also developed to evaluate the relative success of these two models for network-level pavement-performance modeling. As part of this study, in development of pavement RSL prediction models for three pavement types, automation tools for future pavement performance predictions were developed and used along with Federal Highway Agency (FHWA)-specified threshold limits for various pavement performance indicators. These RSL models will help engineers in both network and project level decision-making processes and for different types of pavement-management business decisions.

Introduction

State highway agencies (SHAs) are required to develop performance-based approaches in their pavement management decision-making processes based on the Moving Ahead for Progress in the 21st Century (MAP-21) Federal Transportation Legislation (*1*). One such performance-based approach to facilitate the pavement management decision-making process is to use a remaining-service-life (RSL) model. A RSL for pavements can be defined as the time span between the present time and the time when a significant rehabilitation treatment or reconstruction should occur (*2*). Although application of a structural overlay or reconstruction would normally be regarded as a sign for termination of pavement service life, minor maintenance treatments or thin overlays are often not considered as such signs (*2*). RSL models for predicting the remaining life of pavements have been developed and are being used as part of the pavement management process. (*3*).

Multiple advantages of RSL have been reported in the literature (*4*), with key positive RSL features that include the following:

- Provides the time, expressed in years, before rehabilitation is required for any given road section
- Easy to understand (especially for public)
- Can be a multi-conditional measure developed from any type of functional and/or structural data
- Allows agencies to distinguish between two road sections with the same current condition (i.e., the same current International roughness index (IRI))

- Provides deeper insight by converting “condition measures” into an “operational performance” measure that tells how well or long the road will continue serving the public
- Can be an ideal tool to address the transportation planning and performance management criteria requirements of the MAP-21 legislation

Performance curves or pavement performance models are used to evaluate how pavement’s performance changes over the time. They could be developed using various pavement performance indicators (International roughness index (IRI), distresses, etc.). Pavement performance models can be categorized into two groups, deterministic and probabilistic, based on their prediction results: (*5-8*). Deterministic models estimate a single condition value for a given time during a pavement’s design life, while probabilistic models estimate the probability of a condition value for a given time (*5*). Most SHAs use deterministic models as part of their pavement management systems for various reasons: (1) ease in explaining such models to users and (2) ease in incorporating such models into pavement management systems (PMS) (*9*).

Threshold limits are determined performance indicator values at which a significant rehabilitation treatment or reconstruction is needed (*3*). Performance indicators and threshold limits are agency-specific parameters used for rehabilitation decision-making processes. Both performance models and threshold limits are components used in the development of RSL models.

Objectives

In this study, a detailed step-by-step methodology in the development of a framework for project and network level pavement performance and RSL prediction models is explained

using real pavement performance data obtained from the Iowa Department of Transportation (DOT) pavement management information system (PMIS) database. Project and network level pavement performance models are developed using two approaches, a statistically (or mathematically) defined approach for project level model development and artificial intelligence (AI) based approach for network level model development.

Network level pavement performance models are also developed using statistical and AI based approaches, with the same input parameters used in both approaches to evaluate their relative success in network-level pavement-performance modeling.

Microsoft Excel based automation tools have been developed for both project and network level pavement performance modeling and analysis to facilitate pavement-performance and RSL model development, to make future pavement performance predictions, and to estimate RSL for any given road section. These tools, that make use of real pavement performance data to produce realistic future condition predictions, can be easily incorporated into pavement management processes and help engineers make better-informed performance-based pavement infrastructure planning decisions and optimize agency resource expenditures.

Descriptions of Overall Approaches and Data Preparation

Figure 5.1 depicts the pavement performance and RSL model development stages followed in this study. Initially, project and network level pavement performance models were developed using two approaches: a statistically (or mathematically) defined approach for project level model development and an artificial intelligence (AI) based approach for network-level model development. Both project and network-level pavement performance models were developed for three pavement types: flexible, JPCP, and composite (AC over JPCP). Project-level pavement performance models were developed for each pavement

section in each pavement type, while network-level pavement performance models were developed for each pavement performance indicator, or a condition matrix (i.e. distresses and IRI) for each pavement type.

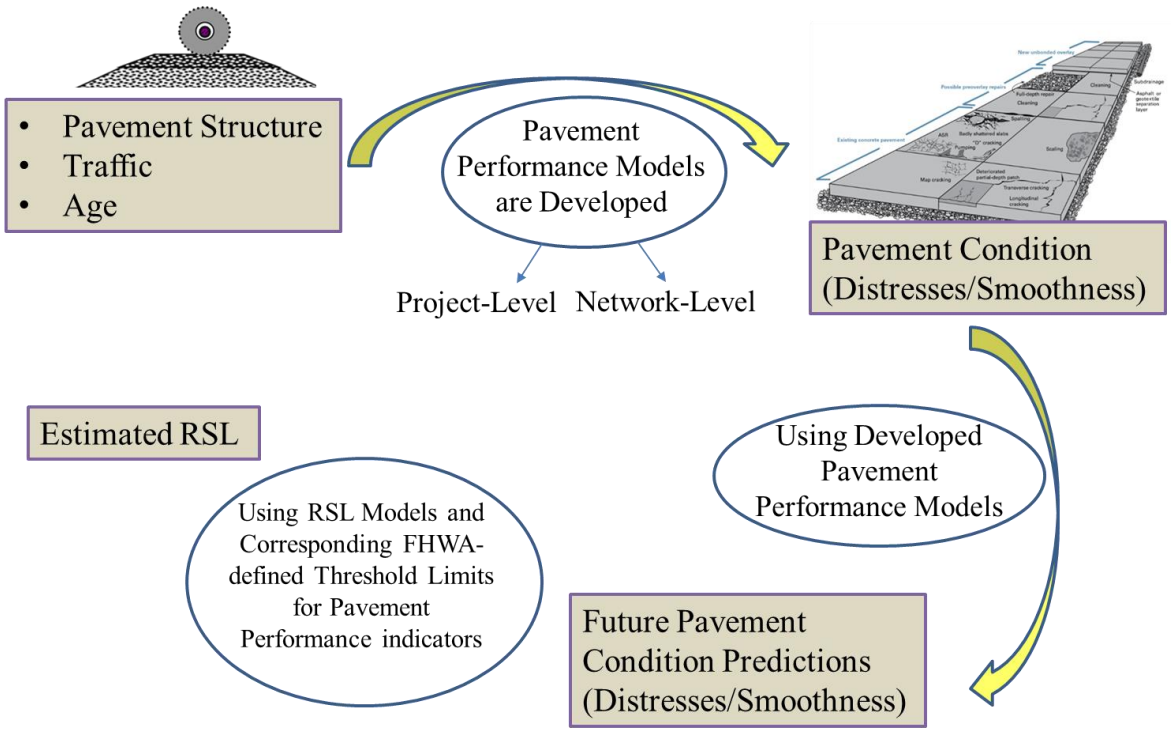

Figure 5.1 Pavement performance and RSL model development stages

Success of the pavement performance prediction models in mimicking measured pavement performance indicators was quantified using a line-of-equality coefficient of correlation (R^2) (Equation 5.1) and an absolute average error (AAE) (Equation 5.2). Higher R^2 and lower AAE values are signs of accurate model prediction.

$$R^2 = 1 - \frac{\Sigma_{j=1}^{n}\left(y_j^{measured} - y_j^{predicted}\right)^2}{\Sigma_{j=1}^{n}\left(y_j^{measured} - y_{mean}^{measured}\right)^2} \quad (5.1)$$

$$AAE = \frac{\sum_{j=1}^{n} \left| y_j^{measured} - y_j^{predicted} \right|}{n} \quad (5.2)$$

Where,

- n = Data set size
- j = Case number in the data set
- $y^{measured}$ = Measured IRI or calculated PCI value
- $y^{prediction}$ = Model predictions for IRI and PCI

Once pavement performance models were developed for the three pavement types, remaining service lives for the pavement sections were calculated using threshold limits for various performance indicators. Based on the Federal Highway Administration (FHWA)'s Final Rule (effective February 17, 2017) regarding implementation of the performance management requirements of MAP-21 and the Fixing America's Surface Transportation Act (*1*, *10*), condition of the pavements is required to be determined based on the following metrics: IRI, percent cracking, rutting, and faulting (Table 5.1). IRI was used as a construction trigger for the rehabilitation decision-making process in project level RSL calculations. Rutting, percent cracking, and IRI were used as construction triggers for rehabilitation decision-making process in network level RSL calculations. RSL is determined based on the year when future performance predictions reach the "poor" condition threshold for the corresponding condition metric (these thresholds and corresponding condition metrics are highlighted in Table 5.1).

Table 5.1 Pavement condition rating thresholds determined by FHWA (*10*)

Condition Metric	Performance Level	Threshold
IRI (in/mile), AC and JPCP	Good	<95
	Fair	95-170
	Poor	>170
Percent cracking, AC	Good	<5%
	Fair	5-20%
	Poor	>20%
Percent cracking, CRCP	Good	<5%
	Fair	5-10%
	Poor	>10%
Percent cracking, JPCP	Good	<5%
	Fair	5-15%
	Poor	>15%
Rutting (in), AC	Good	<0.20
	Fair	0.20-0.40
	Poor	>0.40
Faulting (in)	Good	<0.10
	Fair	0.10-0.15
	Poor	>0.15

The Iowa DOT has been collecting pavement condition data and storing them in its PMIS, and pavement structural design features and traffic volume information are also available as part of the PMIS. Iowa DOT's PMIS database has been used as data source in this study. This database includes all information related to traffic, distress, and construction information related to the pavement sections.

The number of pavement sections and the total number of data points for each pavement type used in this study are as follows:

- 35 sections for flexible pavements (430 data points)
- 34 sections for rigid pavements (483 data points)
- 60 sections for composite pavements (644 data points)

The pavement sections used in this study represent a variety of geographical locations across Iowa with various traffic levels, thicknesses, and ages. Distributions of locations, traffic levels, thicknesses, and ages for these pavement sections and other detailed information can be found in another study (*11*).

While analyzing pavement condition data points for each pavement section in PMIS database, it was realized that in some pavement sections, measured pavement condition values for some pavement performance indicators remained the same over some number of years, after which an increase in those pavement condition values was observed. This might have been because a pavement condition data was not collected or recorded every year, but rather that the pavement condition measurements reported for previous years had been recorded as pavement condition measurements for upcoming years. In such cases, a systematic data preparation methodology similar to one described in the literature for previous studies was developed (*5*, *12*): A linear increase was achieved between the first year when pavement condition data points started to be the same over a number of years and the year when an increase in those pavement condition values was observed. Figure 5.2 provides a comparison before and after this data preparation methodology was applied in a flexible pavement section as an example based on three pavement performance indicators: IRI, longitudinal cracking, and transverse cracking. Applying this data preparation methodology, more realistic pavement condition records can be obtained, and in turn, more accurate pavement performance models can be developed.

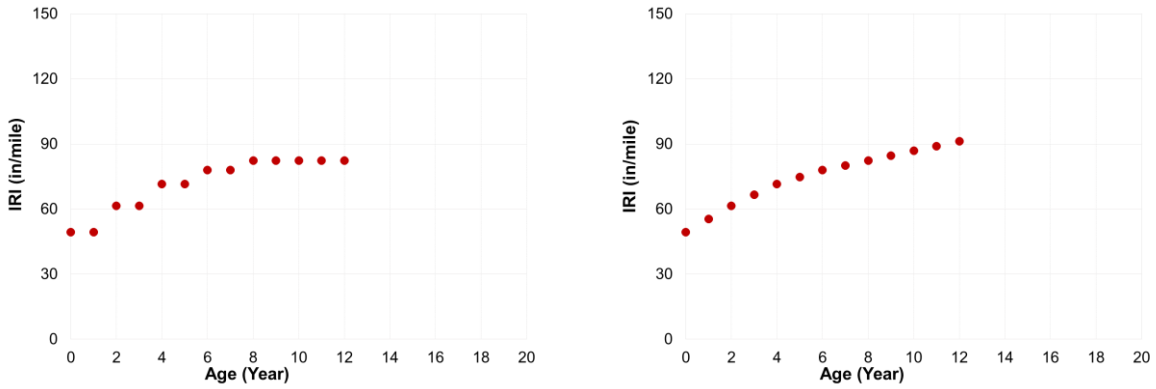

a) IRI (in/mile)

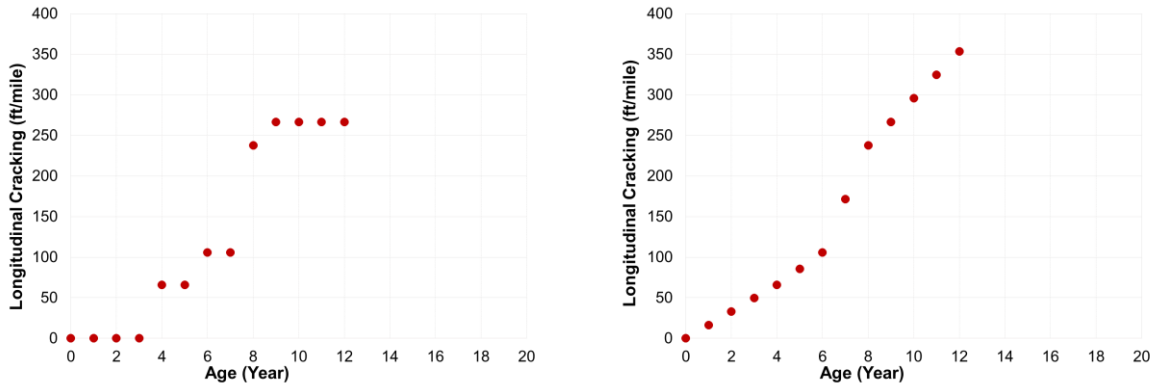

b) Longitudinal cracking (ft/mile)

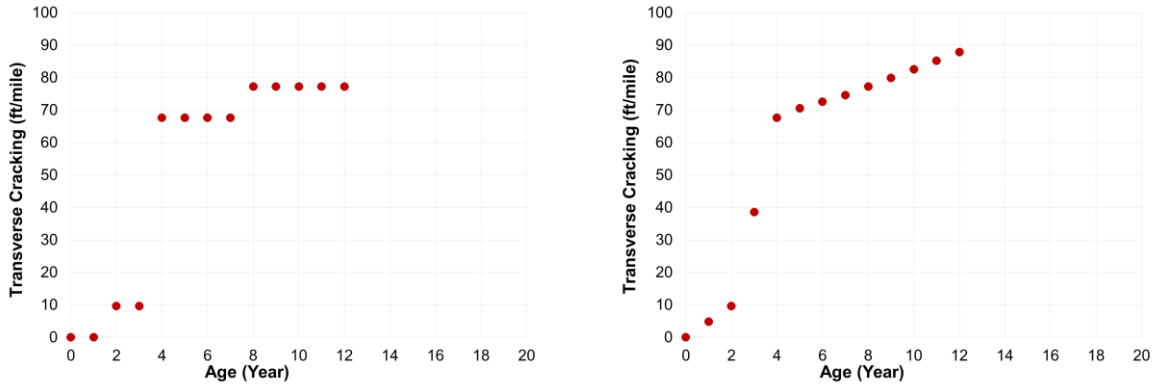

c) Transverse cracking (ft/mile)

Before data preparation **After data preparation**

Figure 5.2 Comparisons between before and after data preparation methodology was applied in a flexible pavement section based on three pavement performance indicators: a) IRI, b) longitudinal cracking and c) transverse cracking (US 18, MP 212.74 to 214.39, E, Traffic (AADTT): 1,885, Construction year: 2000)

Project Level Pavement Performance Model Development and Accuracy Evaluations

A statistically (or mathematically) defined sigmoid pavement-deterioration curve-based approach was used for project level pavement performance model development in this study. Sigmoidal equations have been particularly used in statistical model development because: (1) they have a low initial slope and an increasing slope with time and (2) they follow a trend in which pavement condition always gets worse and damage is irreversible, and both these features of sigmoidal models cause these models to mimic pavement deterioration behavior observed in field studies (*5, 13, 14*). Since sigmoidal equations have been found to successfully model pavement deterioration when there is single pavement deterioration trend (project-level), a sigmoidal equation for each pavement section in each pavement type was optimized, with each equation having different coefficients. IRI was used as a performance indicator in project-level pavement performance models.

Equation 5.3 is the generalized sigmoidal equation used for IRI calculation.

$$IRI = C_1 + \frac{C_2}{1+e^{(C_3+C_4\times age)}} \tag{5.3}$$

where C_1, C_2, C_3 and C_4 are coefficients that represent contributions of different input parameters.

Sigmoidal curves were fitted to measured IRI values by minimizing the square of differences value between measured and predicted IRI values. The fitting process was carried out by manipulating prediction coefficients (Equation 5.3) to produce minimum error.

Figure 5.3 shows examples of IRI prediction models for JPCP, flexible, and composite (AC over JPCP) pavement types. Using these models, future IRI predictions can be calculated for these pavement types.

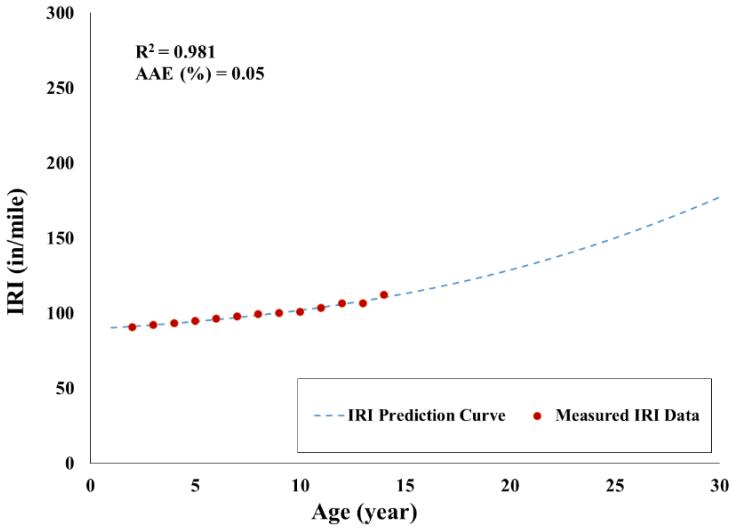

$$IRI = 80.30 + \frac{307.34}{1 + e^{(3.48 - 0.09 \times age)}}$$

a. JPCP (US 18, MP 208.94 to 211.75, W, Traffic (AADTT): 2,104, Construction year: 2000

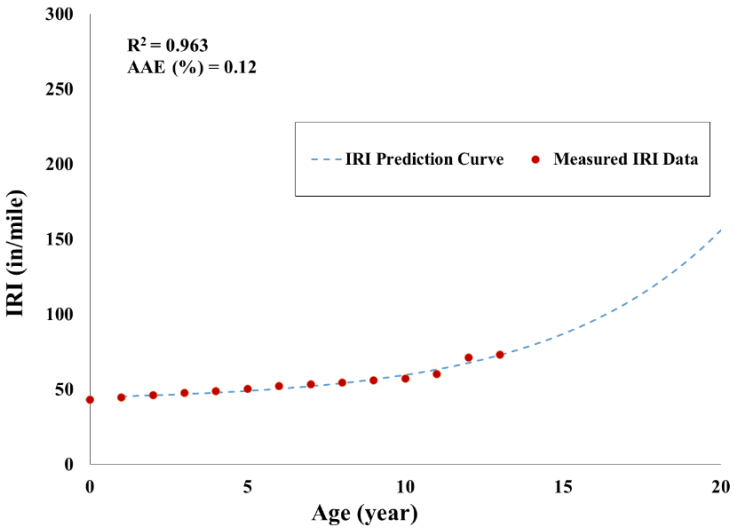

$$IRI = 42.24 + \frac{4335.36}{1 + e^{(7.42 - 0.19 \times age)}}$$

b. Flexible (US 61, MP 167.95 to 174.74, N, Traffic (AADTT): 1,154, Construction year: 1999)

Figure 5.3 IRI prediction model results and equations for a new JPCP, new flexible and composite (AC over JPCP) pavement sections as examples

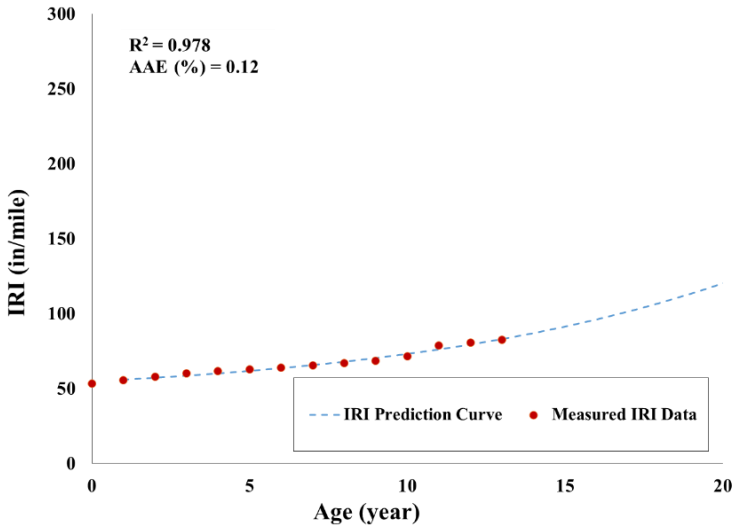

$$IRI = 44.07 + \frac{1197.96}{1 + e^{(4.70 - 0.10 \times age)}}$$

c. Composite (AC over JPCP) (US 30, MP 310.08 to 318.84, W, Traffic (AADTT): 1,264, Restoration year: 2000

Figure 5.3 (Continued)

As part of this study, a Microsoft Excel Macro-based automation tool was developed, automatically updating and improving pavement performance prediction models as more data were added into the model development dataset. Figure 5.4 presents the calculation steps and capabilities of this automation tool. The benefit of this tool is that, as engineers add more data into the model development dataset, they will be able to automatically refine performance prediction models and make decisions using the most recent and more accurate pavement performance models. Another benefit of using this tool is that pavement performance prediction models can be developed using very few data points.

Figure 5.5 shows an example of IRI prediction model changes as more measured IRI data points are used in model development for a flexible pavement section. As can be seen in this figure, as more data are added to the model development dataset, prediction equations slightly change and model accuracy increases.

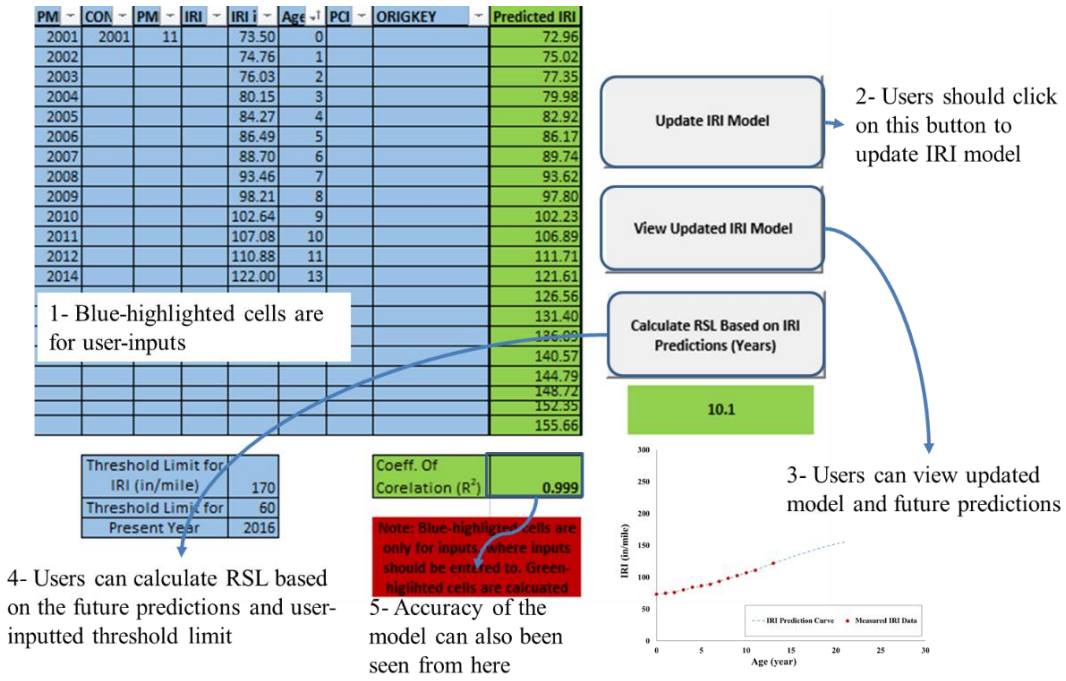

PM	CON	PM	IRI	IRI i	Age	PCI	ORIGKEY	Predicted IRI
2001	2001	11		73.50	0			72.96
2002				74.76	1			75.02
2003				76.03	2			77.35
2004				80.15	3			79.98
2005				84.27	4			82.92
2006				86.49	5			86.17
2007				88.70	6			89.74
2008				93.46	7			93.62
2009				98.21	8			97.80
2010				102.64	9			102.23
2011				107.08	10			106.89
2012				110.88	11			111.71
2014				122.00	13			121.61
								126.56
								131.40
								136.09
								140.57
								144.79
								148.72
								152.35
								155.66

Figure 5.4 Project level "tunable" pavement performance prediction automation tool

Project Level Pavement RSL Model Development and Results

Once pavement performance models have been developed for pavement sections, as explained in the previous section, the remaining service lives for these pavement sections can be calculated using threshold limits for the pavement performance indicators. In this study, IRI was used as a performance indicator for project level RSL calculations because: (1) it quantifies functional performance of pavement systems, the aspect most road users care about, as well as giving some indirect idea of structural performance of a pavement systems, (2) it has also been adopted as a standard for the Federal Highway Performance Monitoring System (*16*), and (3) it is also one of the condition metrics identified for use by FHWA (*10*). The same threshold level recommended by FHWA for poor pavement condition (an IRI value of 170 in/mile) was selected as the threshold value in this study for project-level RSL calculations (*10*).

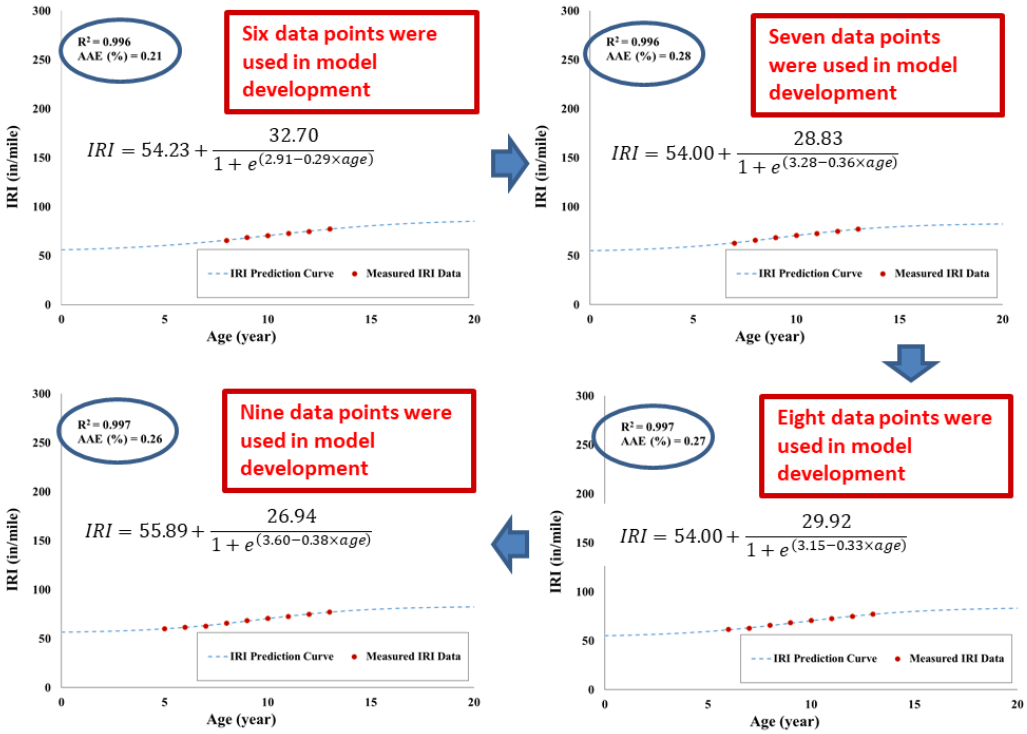

Figure 5.5 IRI model changes as more data points are added into the model development dataset as an example for a flexible pavement section (IA 3, MP 039.09 to 044.12, E, Traffic (AADTT): 500, Construction year: 1999)

The RSL for each pavement section was calculated by the following steps (Figure 5.6):

1. Statistically (or mathematically) defined pavement performance models were developed for each pavement section in each pavement type.
2. Using the developed pavement performance models, future IRI predictions were calculated for each pavement section.
3. Whether future IRI predictions reached the threshold limit (170 in/mi) was checked.
    a. If yes, the RSL value for each pavement section was calculated by subtracting the present year from the year when IRI predictions first reached the threshold limit.
    b. If no, meaning that, based on available measured IRI data, future IRI predictions had not reached 170 in/mile over a long period of analysis time (i.e. 50 years). In

other words, these pavement sections performed very well in terms of smoothness criteria. Adding more data points (i.e., future performance measurements) would change the model and increase its accuracy.

Figures 5.7, 5.8 and 5.9 show the distribution of RSL for JPCP, flexible and composite (AC over JPCP) pavement sections investigated in this study, respectively. Average RSL for JPCP, flexible and composite (AC over JPCP) pavement sections were found to be 7.2, 9.3 and 4.4 years, respectively.

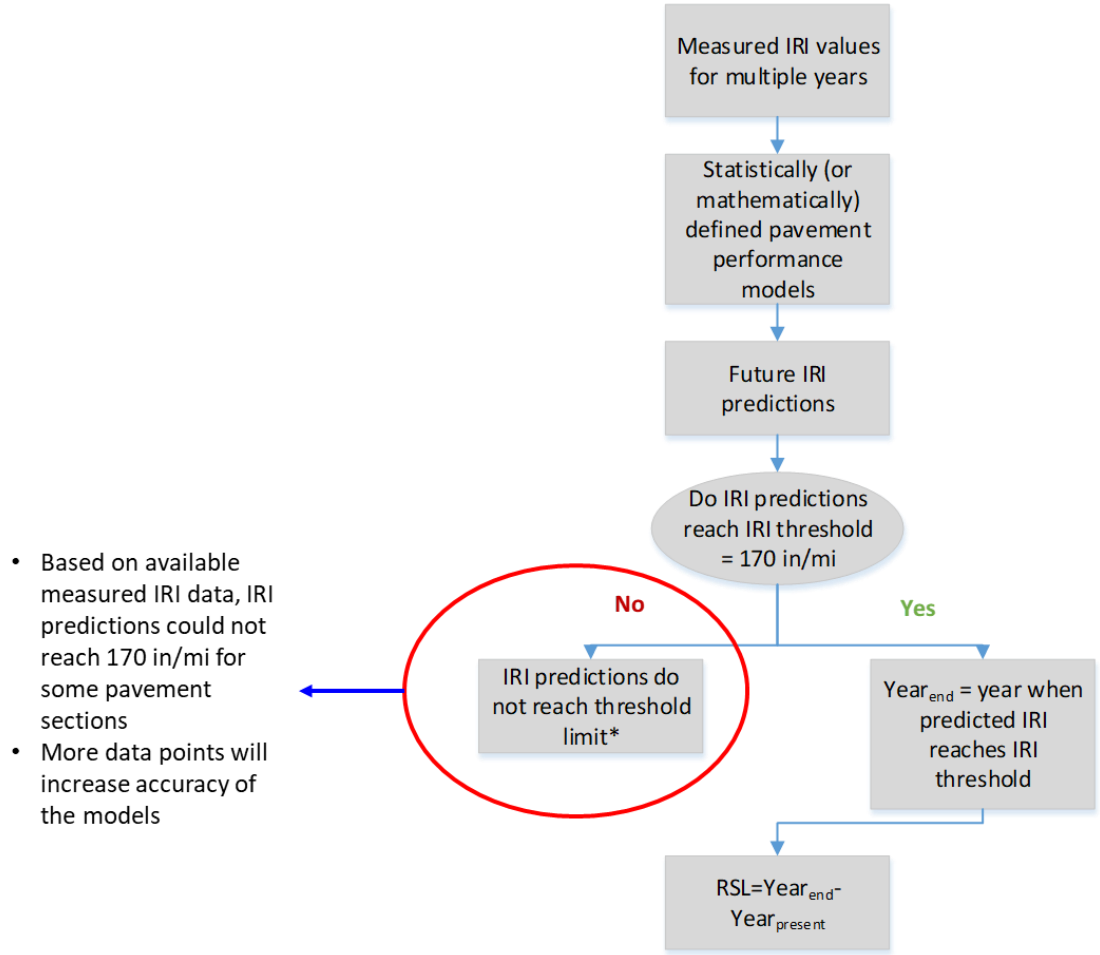

Figure 5.6 Project-level RSL calculation steps

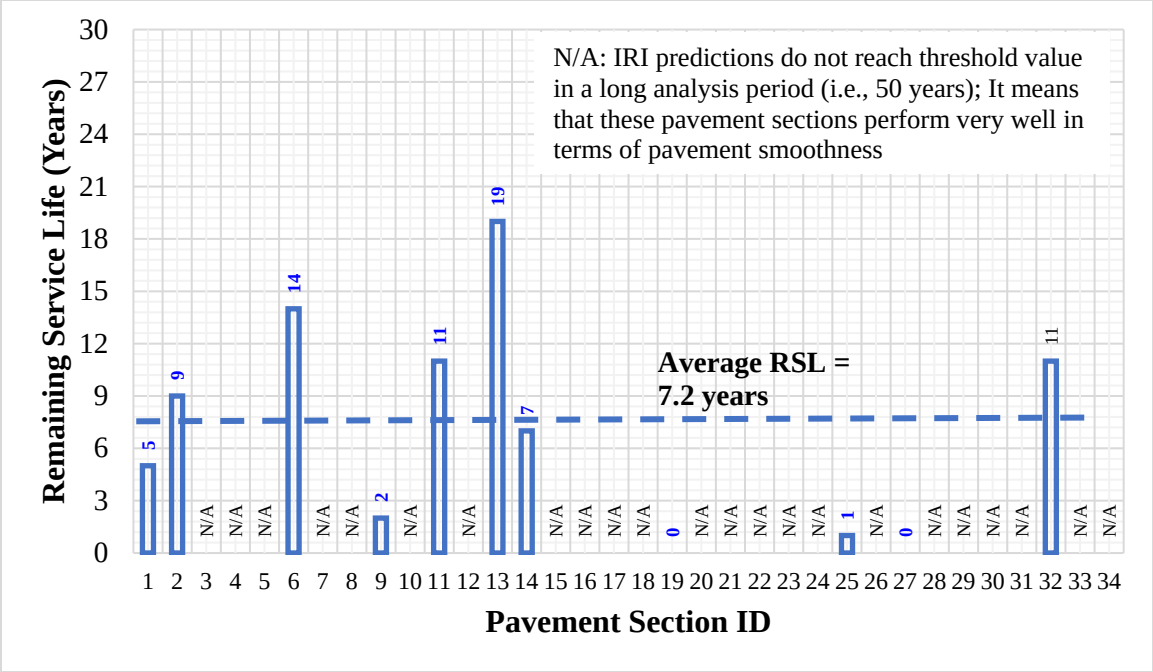

(a)

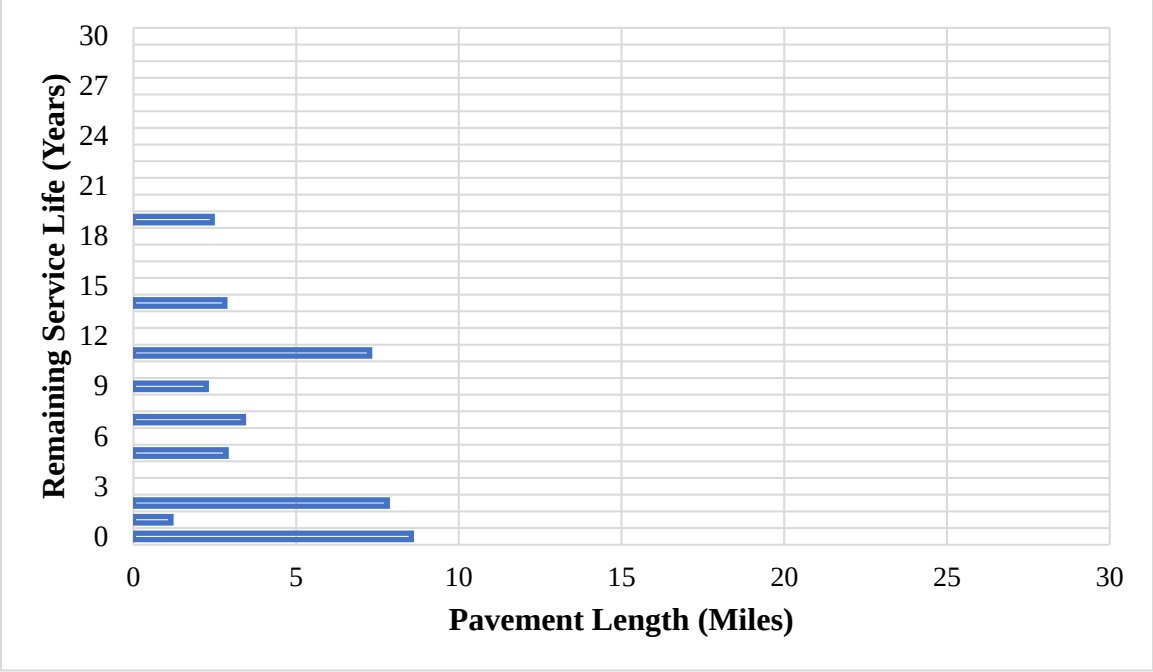

(b)

Figure 5.7 RSL distribution for JPCP pavement sections (a) based on pavement section ID and (b) based on pavement length

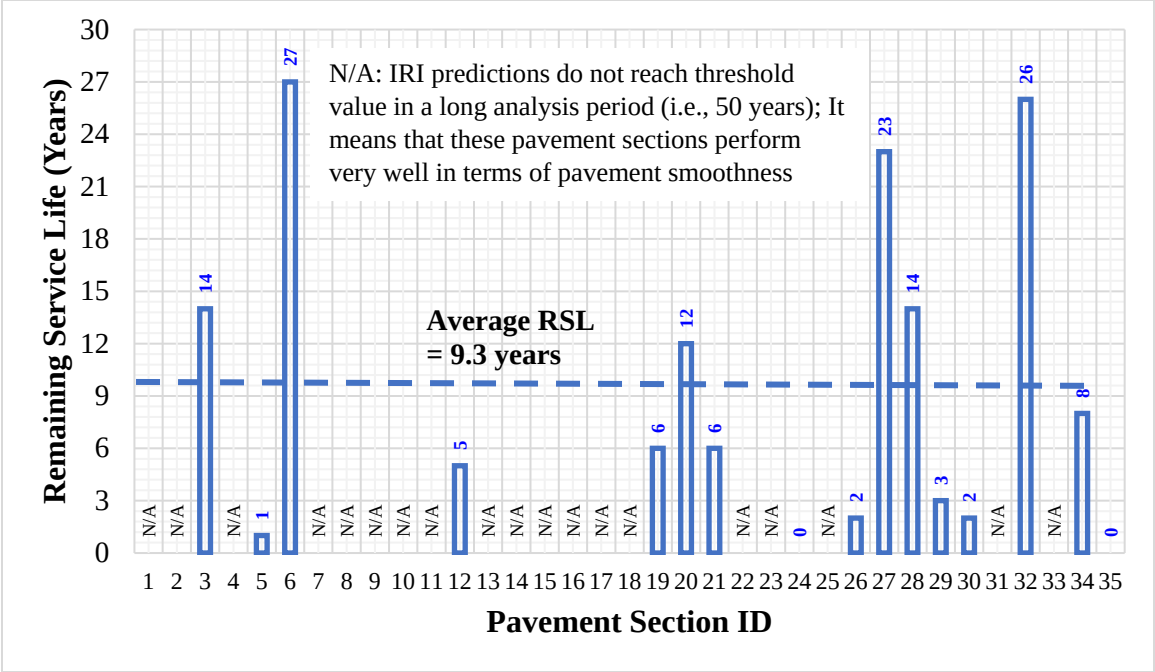

(a)

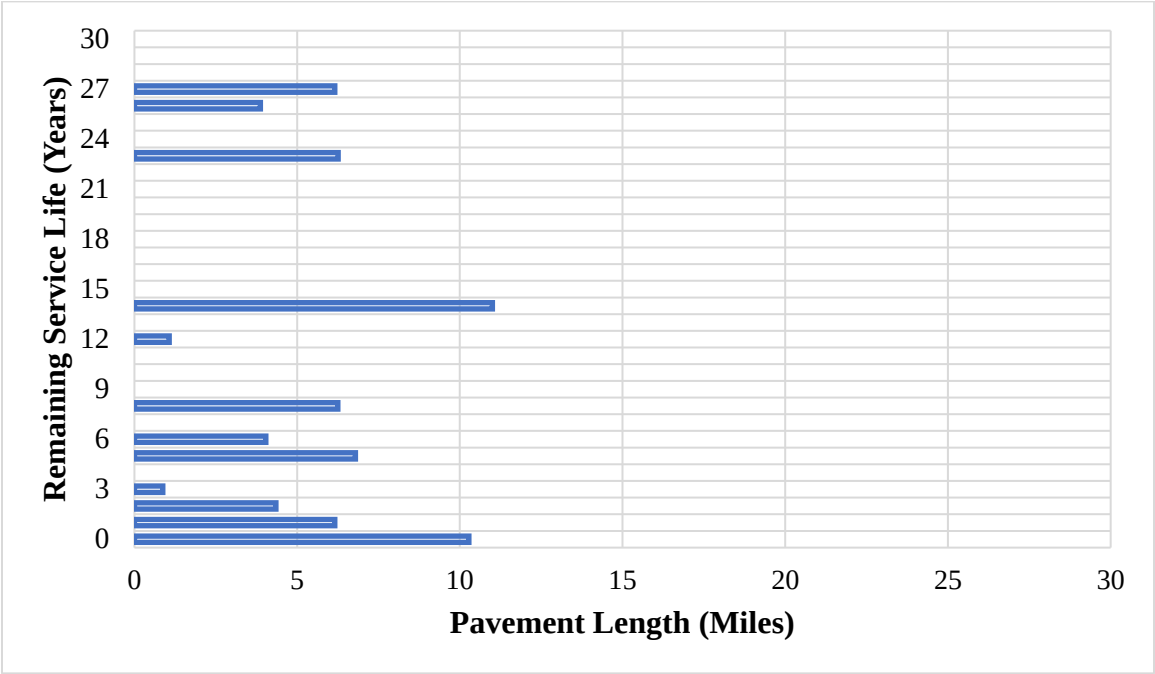

(b)

Figure 5.8 RSL distribution for flexible pavement sections (a) based on pavement section ID and (b) based on pavement length

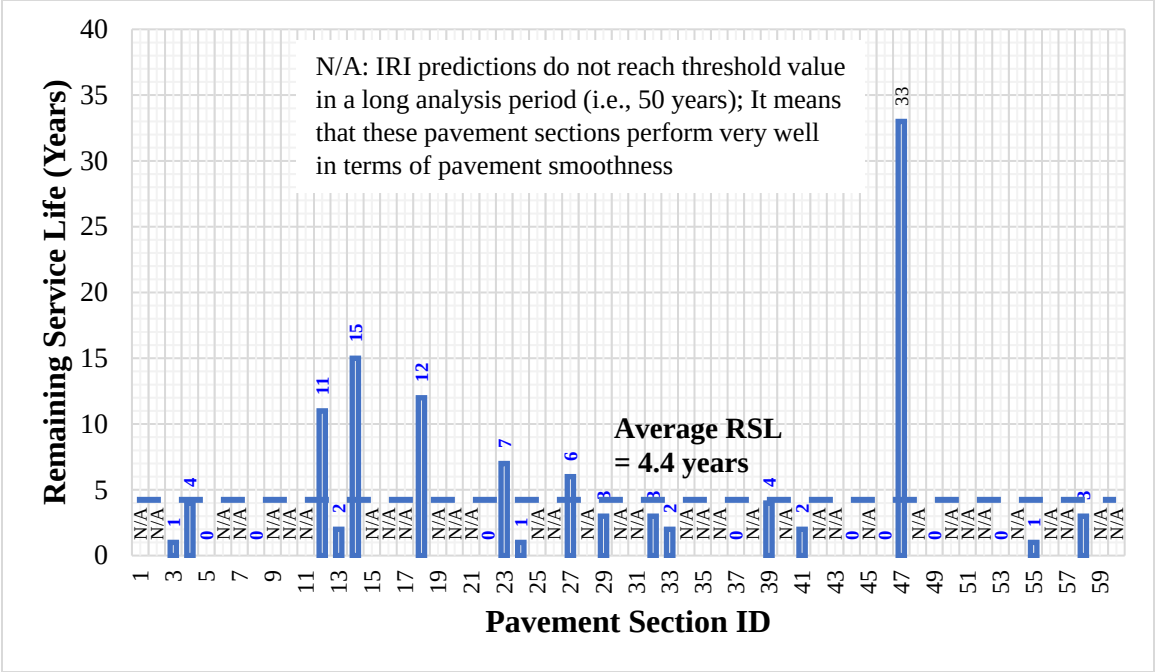

(a)

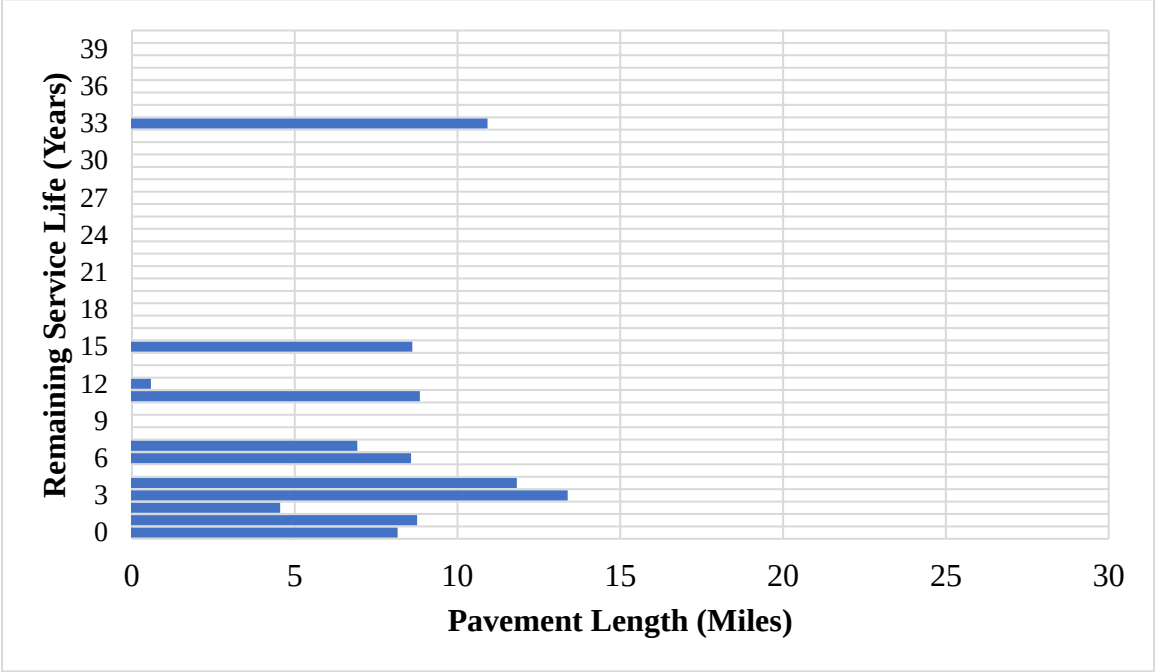

(b)

Figure 5.9 RSL distribution for composite (AC over JPCP) pavement sections (a) based on pavement section ID and (b) based on pavement length

Network Level Pavement Performance Model Development and Accuracy Evaluations

Artificial intelligence (AI) based pavement performance models were used for network level pavement performance model development in this study. Artificial intelligence (AI) techniques, such as artificial neural networks (ANNs), have been widely used to model complex pavement engineering problems (*17*, *18*). ANN-based models are very useful tools for modeling pavement deterioration when considering many pavement sections with various traffic, thickness (network-level) or deterioration trends. They are also very fast tools with which thousands of pavement scenarios for which various traffic, thickness, and conditions can be solved in seconds. Both these features of ANN models make them useful tools to be used in the development of network-level pavement-performance modeling. In this study, an ANN-based pavement-performance model was developed for each pavement-performance indicator (i.e. distress, IRI) and for each pavement type: JPCP, flexible, and composite (AC over JPCP). 80% of all data points in each pavement type was used in the model development, and out of this set of data points, 48%, 8% and 24%, respectively, were used as training, testing, and validation datasets. The remaining 20% of all data points were not used in model development but rather were used as an independent testing dataset.

ANN models must have the following capabilities:

- High accuracy: they must successfully produce results very similar to those from measured distresses
- Physically meaningful future distress predictions: distress predictions must increase in the future unless a maintenance or repair activity occurs

A Microsoft Excel Macro based network-level pavement performance prediction automation tool was developed that predicts future pavement performance using developed

ANN models (Figure 5.10). This tool calculates future pavement performance predictions for any pavement performance indicator.

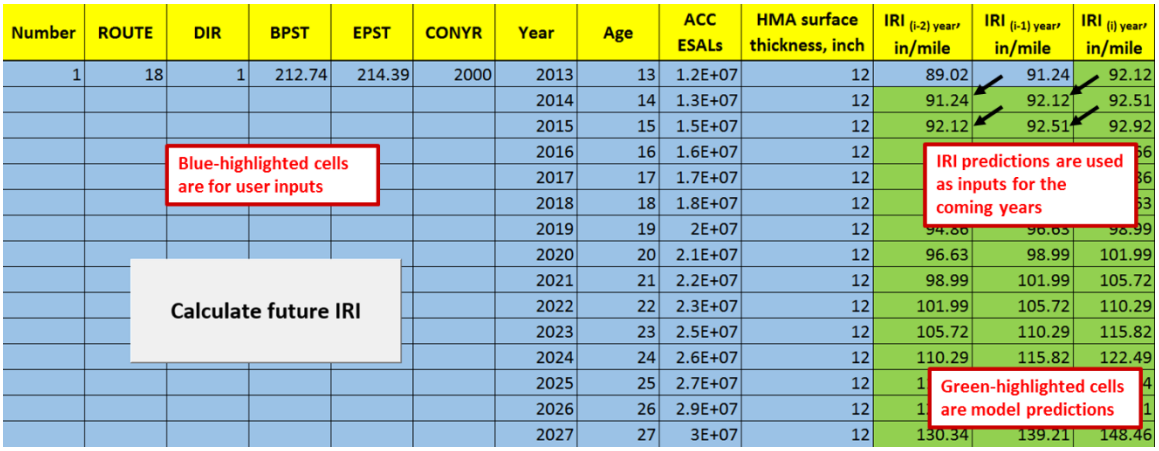

Figure 5.10 Network level pavement performance prediction automation tool

The following steps were used in the development of this tool:

1. ANN models were developed in the MATLAB® environment using six training algorithms and a variable number of hidden neurons (from 5 to 60).
2. The ANN model producing highest accuracy was selected as the final model for the given pavement performance indicator.
3. Weights and biases for the final ANN model were extracted into the automation tool.
4. Using these extracted weights and biases, through matrix multiplications, future distress predictions were calculated for the given thickness, accumulated equivalent single axle load (ESAL) traffic, age, and previous two years' pavement performance records for any pavement performance indicator. 1% compound truck traffic growth was assumed in calculating future traffic.

As part of this study, an ANN model for each pavement type was developed for the following pavement performance indicators:

- JPCP pavements: transverse cracking and IRI

- Flexible and composite (AC over JPCP) pavements: rutting, longitudinal cracking, transverse cracking, and IRI

Input parameters used in the ANN model development along with ANN model results for each pavement performance indicator in each pavement type are presented below.

JPCP Pavement Performance Models for Network Level

Three pavement performance ANN models were developed for JPCP pavements: Transverse cracking, IRI (approach 1), and IRI (approach 2). 34 JPCP pavement sections with 396 data points were used in model development and independent testing. 190, 32, 95 and 79 data points, respectively, were used as training, testing, validation, and independent testing datasets. Table 5.2 summarizes input and output parameters used in the three ANN models developed for JPCP pavements. As can be seen in Table 5.2, PCC slab thickness, traffic (accumulated ESALs), age, and previous two years' pavement performance records were used in transverse cracking and IRI (approach 1) model development. On the other hand, in approach 2, an IRI model was developed using age, measured distress values (transverse cracking in this case), and previous two years' measured IRI data. In approach 2, ANN-model-predicted transverse cracking values along with other input parameters were used as inputs to predict future IRI values.

Figure 5.11 compares measured pavement condition records and ANN model predictions using a) transverse cracking, b) IRI (approach 1), and c) IRI (approach 2) ANN models, respectively, for JPCP pavements. While developed ANN models accurately predicted corresponding pavement performance indicators, IRI models produced more accurate predictions than the transverse cracking model because of their higher R^2 and lower AAE values. IRI models developed using approach 1 and approach 2 produced similar

accuracies. In all cases, high R^2 and low AAE values were obtained for all training, testing, validation, and independent testing datasets.

Table 5.2 Summary of input and output parameters used in three ANN Models development for JPCP pavements

Model Name	Input Parameters	Output Parameter
Transverse Cracking	PCC thickness, traffic (accumulated ESALs), age, transverse cracking $_{(i-2)\ year}$, transverse cracking $_{(i-1)\ year}$	Transverse cracking $_{(i)\ year}$
IRI (Approach 1)	PCC thickness, traffic (accumulated ESALs), age, IRI $_{(i-2)\ year}$, IRI $_{(i-1)\ year}$	IRI $_{(i)\ year}$
IRI (Approach 2)	Age, transverse cracking $_{(i)\ year}$, IRI $_{(i-2)\ year}$, IRI $_{(i-1)\ year}$	IRI $_{(i)\ year}$

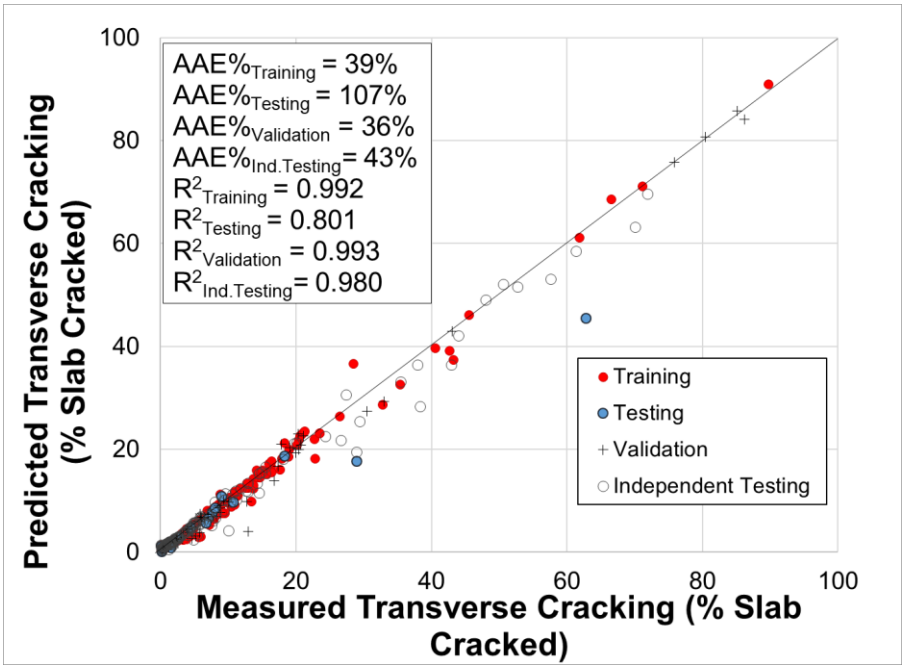

(a)

Figure 5.11 Comparisons between measured pavement condition records and ANN model predictions using a) transverse cracking, b) IRI (approach 1) and c) IRI (approach 2) ANN models for JPCP pavements

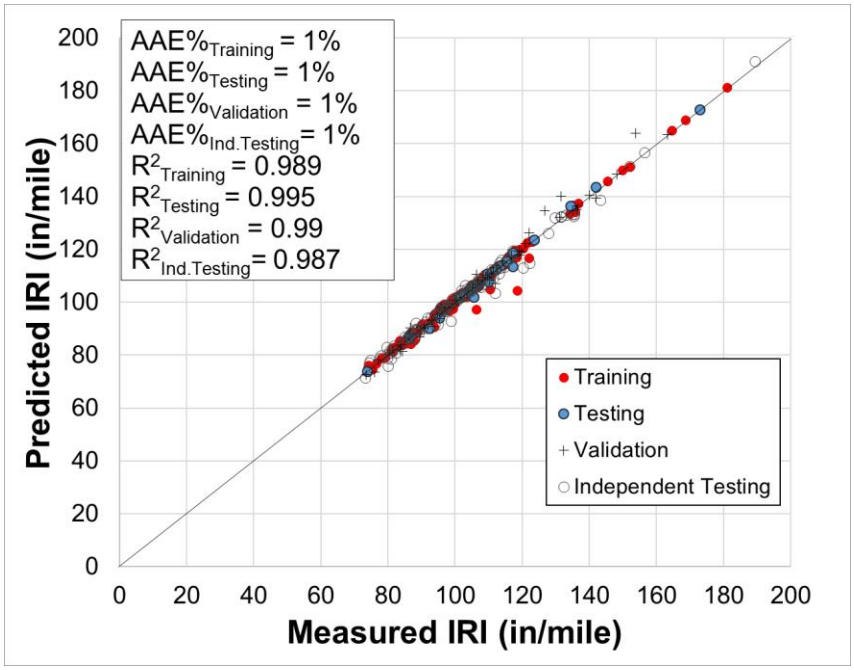

(b)

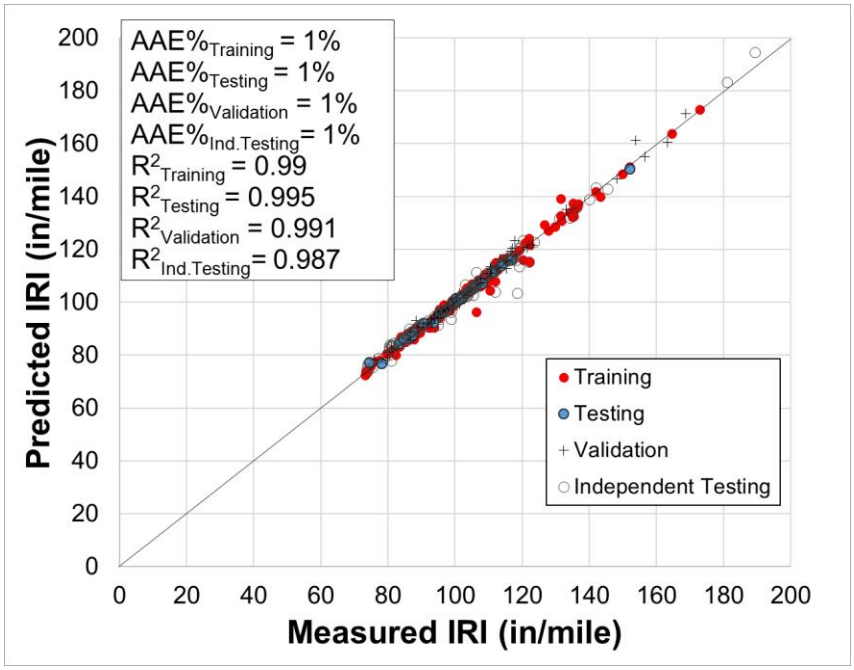

(c)

Figure 5.11 (Continued)

Figure 5.12 compares measured pavement condition records and ANN model predictions using a) transverse cracking, b) IRI (approach 1), and c) IRI (approach 2) ANN models, respectively, using a JPCP pavement section as an example. As can be seen in Figure 5.12, developed ANN models not only produced very similar results to measured pavement condition records, but also produced physically meaningful future pavement condition predictions. Moreover, IRI models developed using approach 1 and approach 2 produced very similar IRI predictions.

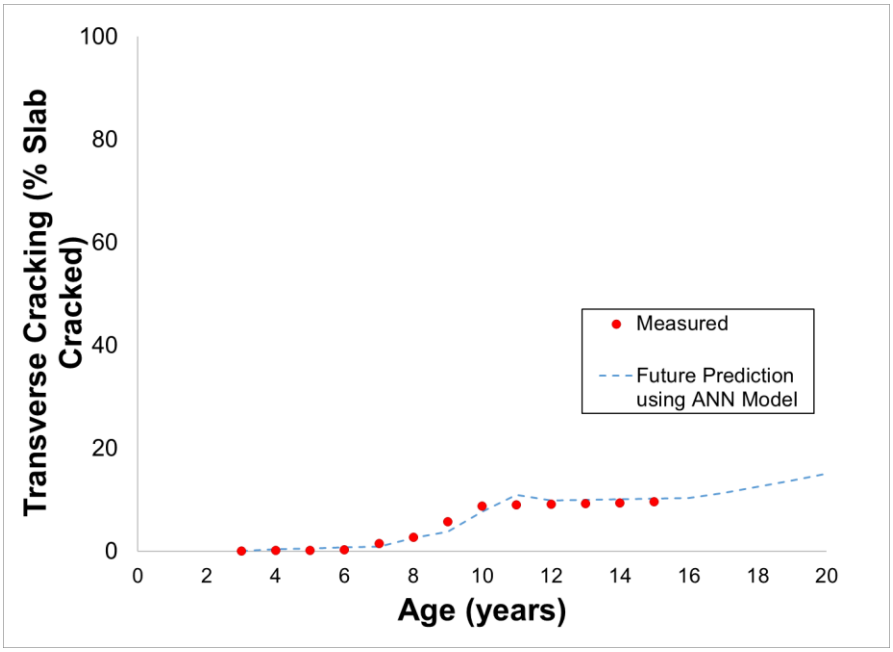

(a)

Figure 5.12 Comparisons between measured pavement condition records and ANN model predictions using a) transverse cracking, b) IRI (approach 1) and c) IRI (approach 2) ANN models, respectively, for a JPCP pavement section as an example (IA 5, MP 85.24 to 88.06, N, Traffic (AADTT): 799, Construction year: 1999)

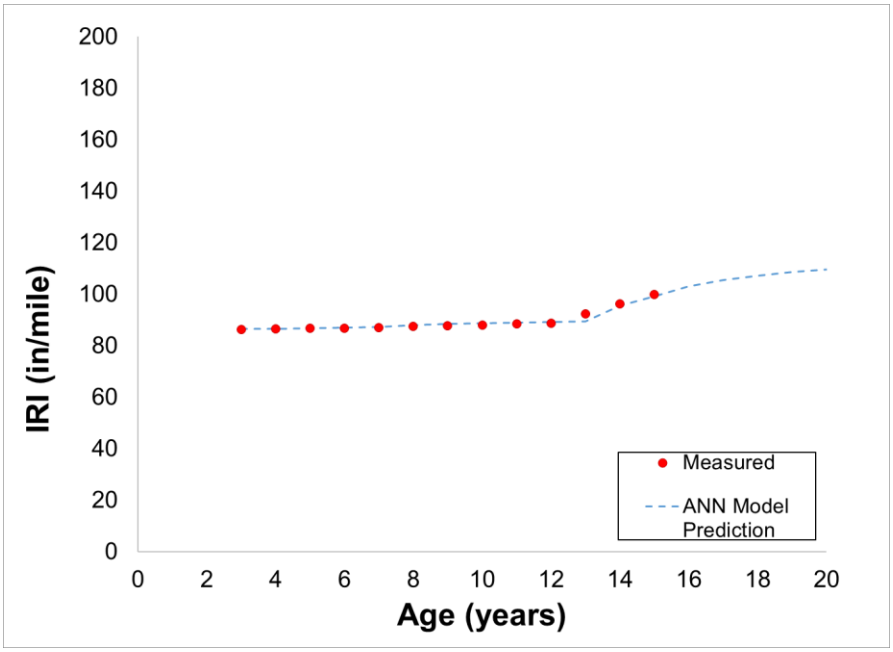

(b)

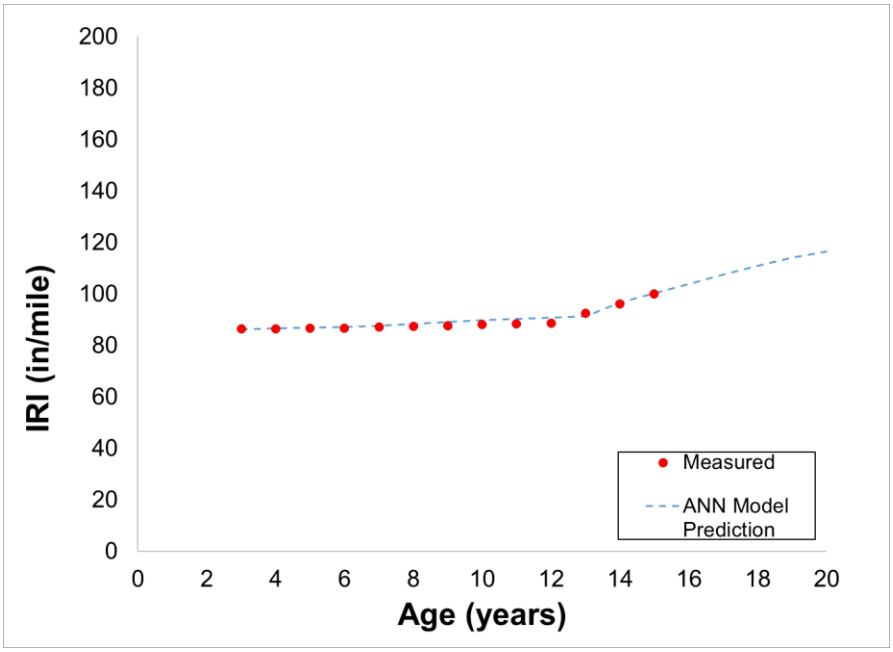

(c)

Figure 5.12 (Continued)

Flexible Pavement Performance Models for Network Level

Five pavement performance ANN models have been developed for flexible pavements: Rutting, longitudinal cracking, transverse cracking, IRI (approach 1), and IRI (approach 2). 35 flexible pavement sections with 360 data points were used in model development and independent testing. 172, 30, 86 and 72 data points, respectively, were used as training, testing, validation, and independent testing datasets. Table 5.3 summarizes input and output parameters used in the five ANN models developed for flexible pavements. As can be seen in Table 5.3, asphalt concrete (AC) thickness, traffic (accumulated ESALs), age, and previous two years' pavement performance records were used in rutting, longitudinal cracking, transverse cracking, and IRI (approach 1) model development. On the other hand, in approach 2, IRI model was developed using age, measured distress values (rutting, longitudinal cracking and transverse cracking in this case), and previous two years' measured IRI data. In approach 2, ANN-model-predicted rutting and longitudinal and transverse cracking values, along with other input parameters, were used as inputs to predict future IRI.

Figure 5.13 compares measured pavement condition records and ANN model predictions using a) rutting, b) longitudinal cracking, c) transverse cracking, d) IRI (approach 1), and e) IRI (approach 2) ANN models, respectively. While the ANN models accurately predicted corresponding pavement performance indicators, the IRI models produced more accurate predictions compared to the rutting, longitudinal cracking, and transverse cracking models because of their higher R^2 and lower AAE values. The IRI models developed using approach 1 and approach 2 produced similar accuracies. In all cases investigated, high R^2 and low AAE values were obtained for all training, testing, validation and independent testing datasets.

Table 5.3 Summary of input and output parameters used in five ANN models development for flexible pavements

Model Name	Input Parameters	Output Parameter
Rutting	AC thickness, traffic (accumulated ESALs), age, rut $_{(i-2)\ year}$, rut $_{(i-1)\ year}$	Rut $_{(i)\ year}$
Longitudinal Cracking	AC thickness, traffic (accumulated ESALs), age, longitudinal cracking $_{(i-2)\ year}$, longitudinal cracking $_{(i-1)\ year}$	Longitudinal cracking $_{(i)\ year}$
Transverse Cracking	AC thickness, traffic (accumulated ESALs), age, transverse cracking $_{(i-2)\ year}$, transverse cracking $_{(i-1)\ year}$	Transverse cracking $_{(i)\ year}$
IRI (Approach 1)	AC thickness, traffic (accumulated ESALs), age, IRI $_{(i-2)\ year}$, IRI $_{(i-1)\ year}$	IRI $_{(i)\ year}$
IRI (Approach 2)	Age, rut $_{(i)\ year}$, longitudinal cracking $_{(i)\ year}$, transverse cracking $_{(i)\ year}$, IRI $_{(i-2)\ year}$, IRI $_{(i-1)\ year}$	IRI $_{(i)\ year}$

Figure 5.14 compares measured pavement condition records and ANN model predictions using a) rutting, b) longitudinal cracking, c) transverse cracking, d) IRI (approach 1), and e) IRI (approach 2) ANN models, respectively, for a flexible pavement section as an example. As can be seen in the figure, the ANN models not only produced very similar results to those from measured pavement condition records, but also produced physically meaningful future pavement condition predictions. Moreover, IRI models developed using approach 1 and approach 2 produced very similar IRI predictions.

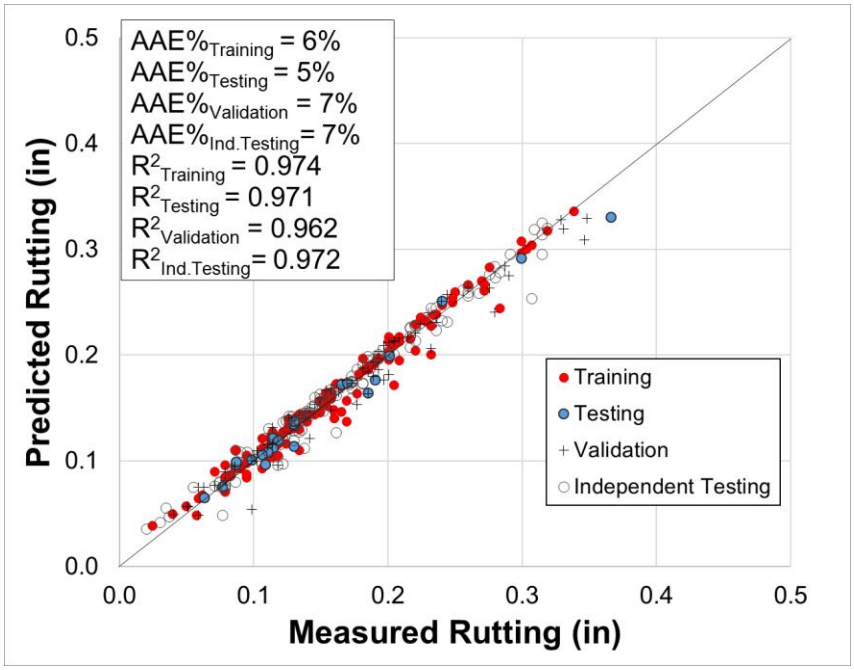

(a)

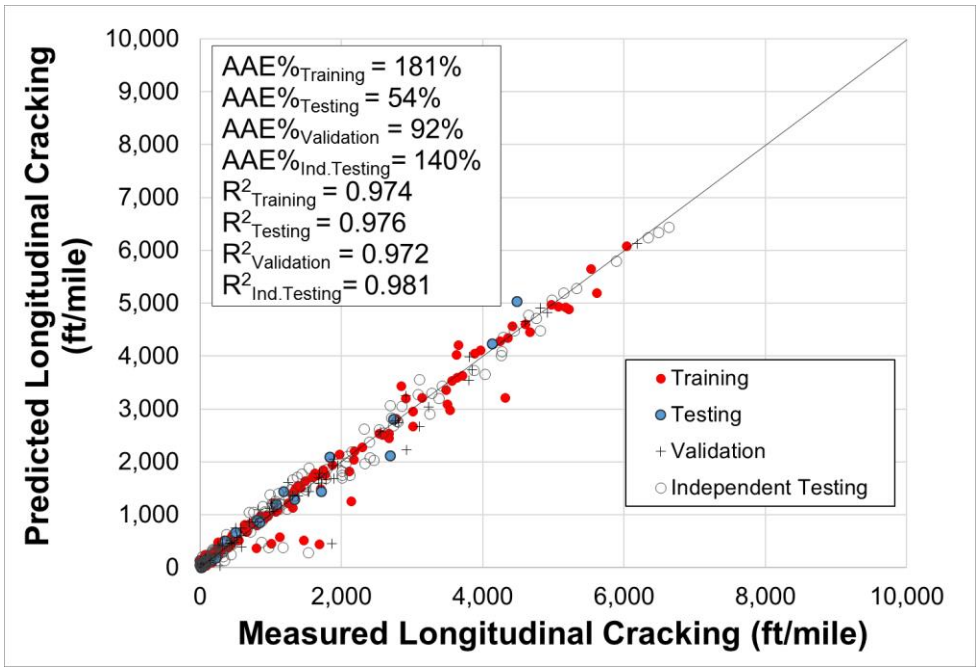

(b)

Figure 5.13 Comparisons between measured pavement condition records and ANN model predictions using a) rutting, b) longitudinal cracking, c) transverse cracking, d) IRI (approach 1) and e) IRI (approach 2) ANN models for flexible pavements

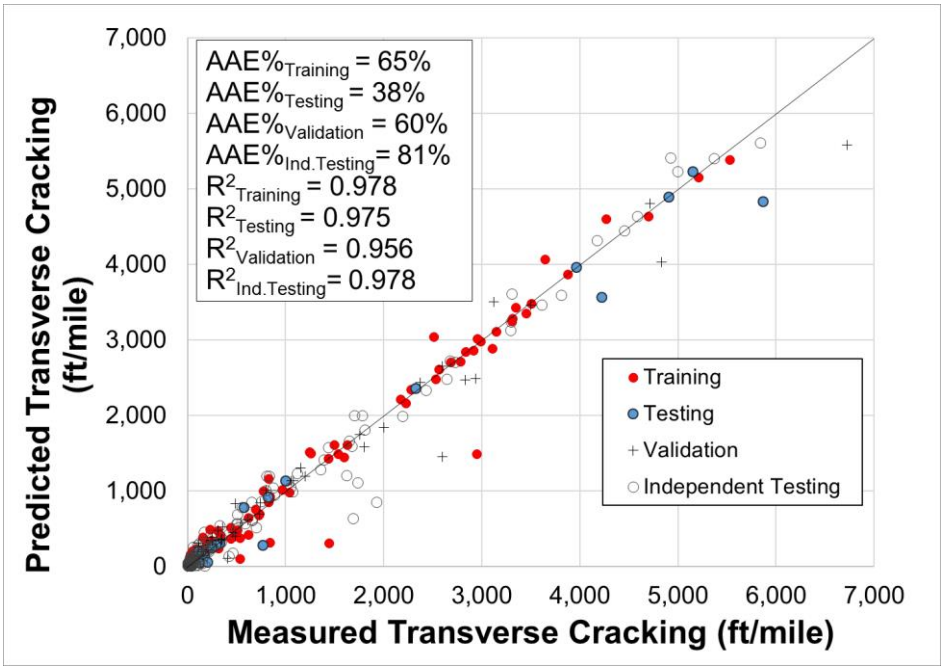

(c)

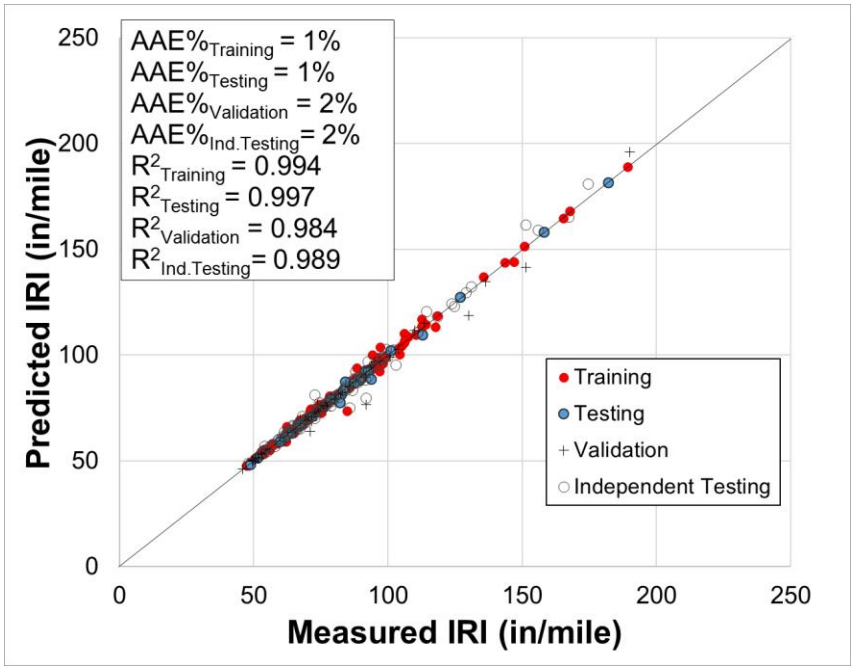

(d)

Figure 5.13 (Continued)

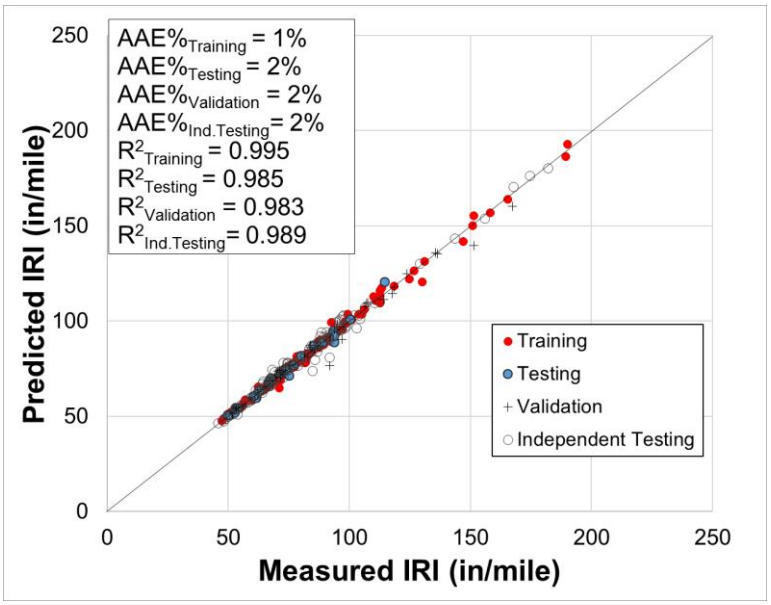

(e)

Figure 5.13 (Continued)

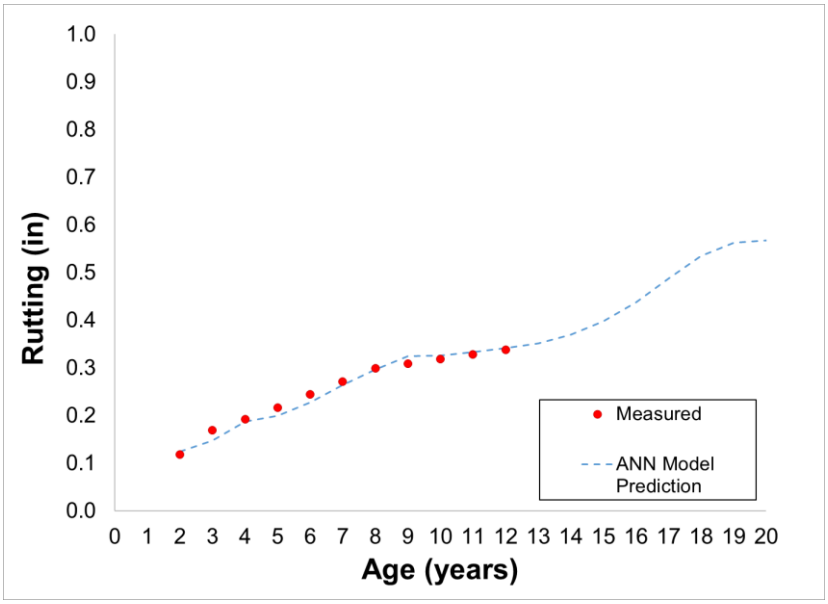

(a)

Figure 5.14 Comparisons between measured pavement condition records and ANN model predictions using a) rutting, b) longitudinal cracking, c) transverse cracking, d) IRI (approach 1) and e) IRI (approach 2) ANN models, respectively, for a flexible pavement section as an example (US 18, MP 212.74 to 214.39, E, Traffic (AADTT): 1,885, Construction year: 2000)

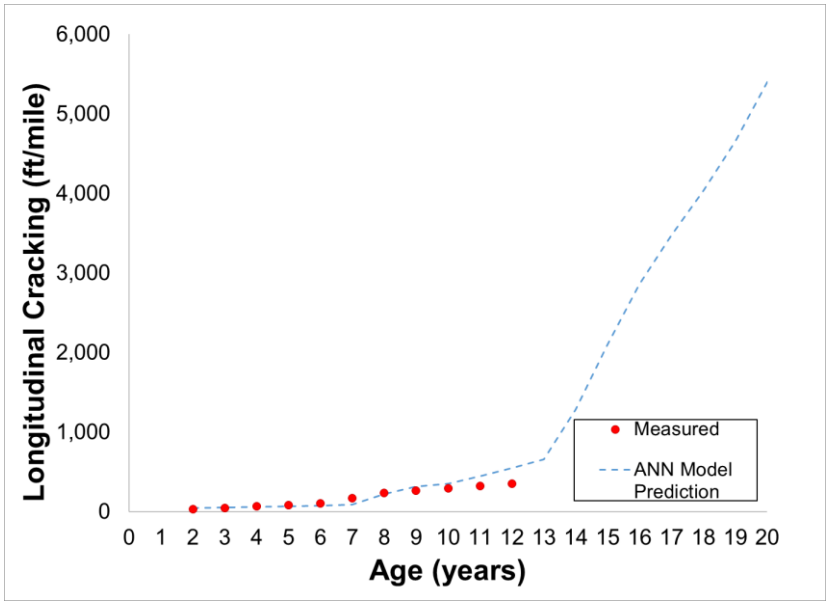

(b)

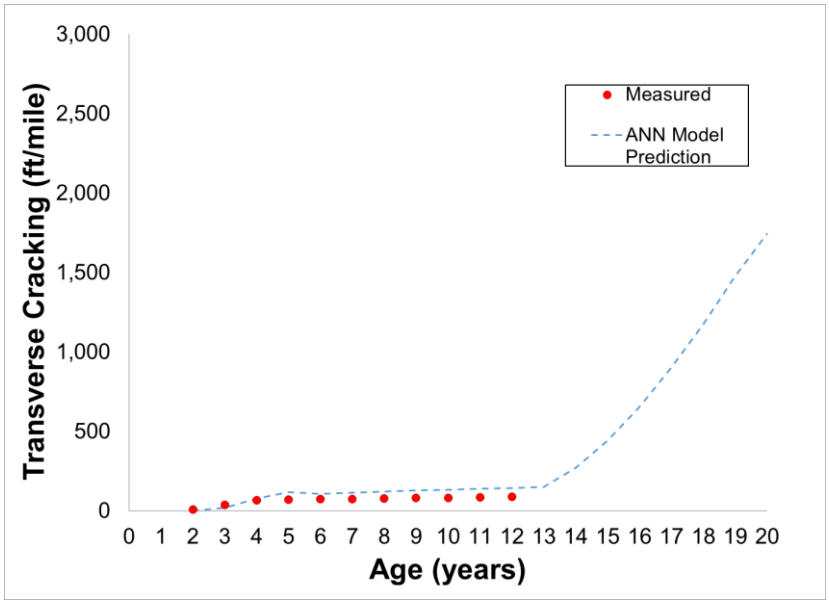

(c)

Figure 5.14 (Continued)

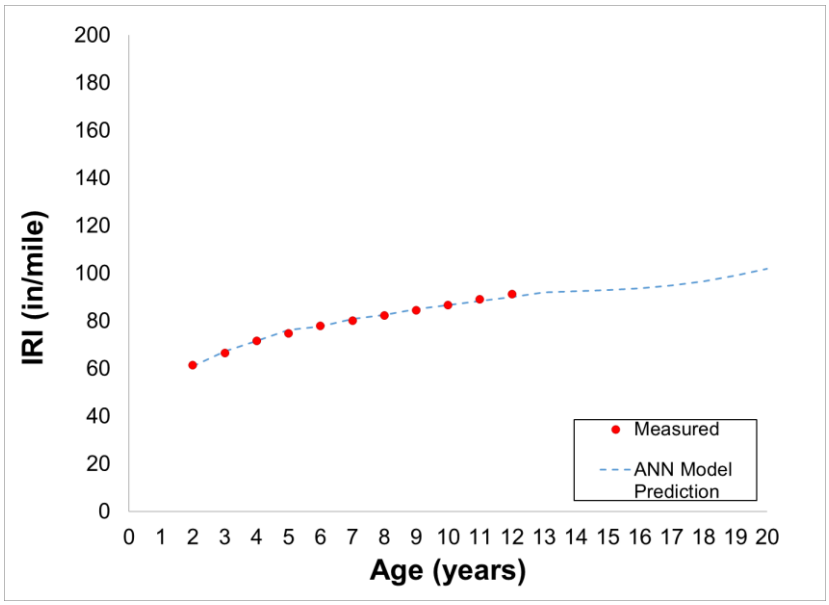

(d)

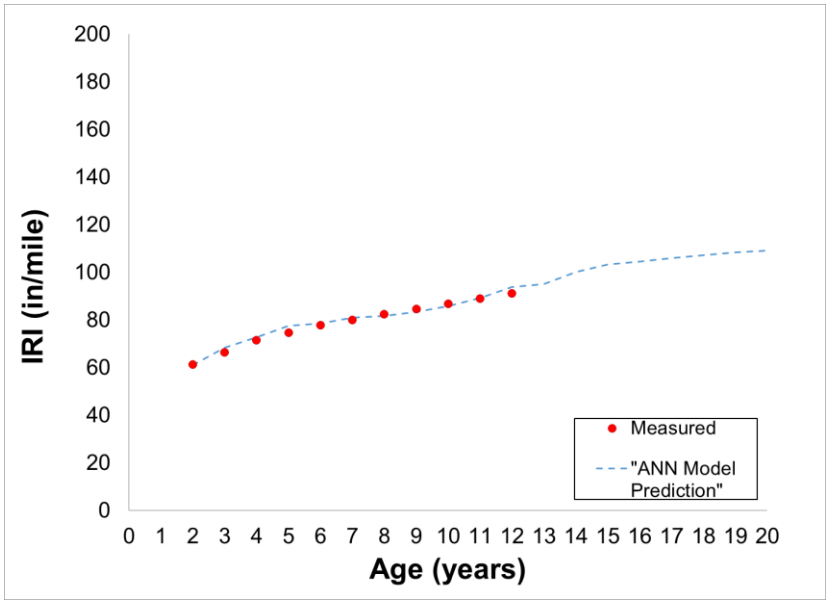

(e)

Figure 5.14 (Continued)

Composite (AC over JPCP) Pavement Performance Models for Network Level

Five pavement-performance ANN models were developed for composite pavements: rutting, longitudinal cracking, transverse cracking, IRI (approach 1) and IRI (approach 2). 60 composite pavement sections with 524 data points were used in model development and independent testing. 251, 42, 126 and 105 data points, respectively, were used as training, testing, validation, and independent testing datasets. Table 5.4 summarizes input and output parameters used in the five ANN models developed for composite pavements. As can be seen in Table 5.4, AC thickness, traffic (accumulated ESALs), age, and previous two years' pavement performance records were used in rutting, longitudinal cracking, transverse cracking, and IRI (approach 1) model development. On the other hand, in approach 2, an IRI model was developed using age, measured distress values (rutting, longitudinal cracking, and transverse cracking in this case), and previous two years' measured IRI data. In approach 2, ANN-model-predicted rutting, longitudinal and transverse cracking values along with other input parameters were used as inputs for predicting future IRI.

Figure 5.15 compares measured pavement condition records and ANN model predictions using a) rutting, b) longitudinal cracking, c) transverse cracking, d) IRI (approach 1), and e) IRI (approach 2) ANN models, respectively. While the ANN models accurately predicted corresponding pavement performance indicators, the IRI models produced more accurate predictions compared to the rutting, longitudinal cracking, and transverse cracking models because of their higher R^2 and lower AAE values. IRI models developed using approach 1 and approach 2 produced similar accuracies. In all cases investigated, high R^2 and low AAE values were obtained for all training, testing, validation, and independent testing datasets.

Table 5.4 Summary of Input and output parameters used in five ANN models development for composite pavements

Model Name	Input Parameters	Output Parameter
Rutting	AC thickness, traffic (accumulated ESALs), age, rut $_{(i-2)\ year}$, rut $_{(i-1)\ year}$	Rut $_{(i)\ year}$
Longitudinal Cracking	AC thickness, traffic (accumulated ESALs), age, longitudinal cracking $_{(i-2)\ year}$, longitudinal cracking $_{(i-1)\ year}$	Longitudinal cracking $_{(i)\ year}$
Transverse Cracking	AC thickness, traffic (accumulated ESALs), age, transverse cracking $_{(i-2)\ year}$, transverse cracking $_{(i-1)\ year}$	Transverse cracking $_{(i)\ year}$
IRI (Approach 1)	AC thickness, traffic (accumulated ESALs), age, IRI $_{(i-2)\ year}$, IRI $_{(i-1)\ year}$	IRI $_{(i)\ year}$
IRI (Approach 2)	Age, rut $_{(i)\ year}$, longitudinal cracking $_{(i)\ year}$, transverse cracking $_{(i)\ year}$, IRI $_{(i-2)\ year}$, IRI $_{(i-1)\ year}$	IRI $_{(i)\ year}$

Figure 5.16 compares measured pavement condition records and ANN model predictions using a) rutting, b) longitudinal cracking, c) transverse cracking, d) IRI (approach 1), and e) IRI (approach 2) ANN models, respectively, using a composite pavement section as an example. As can be seen in the figure, the ANN models not only produced results very similar to measured pavement condition records, but also produced physically meaningful future pavement condition predictions. Moreover, IRI models developed using approach 1 and approach 2 produced very similar IRI predictions.

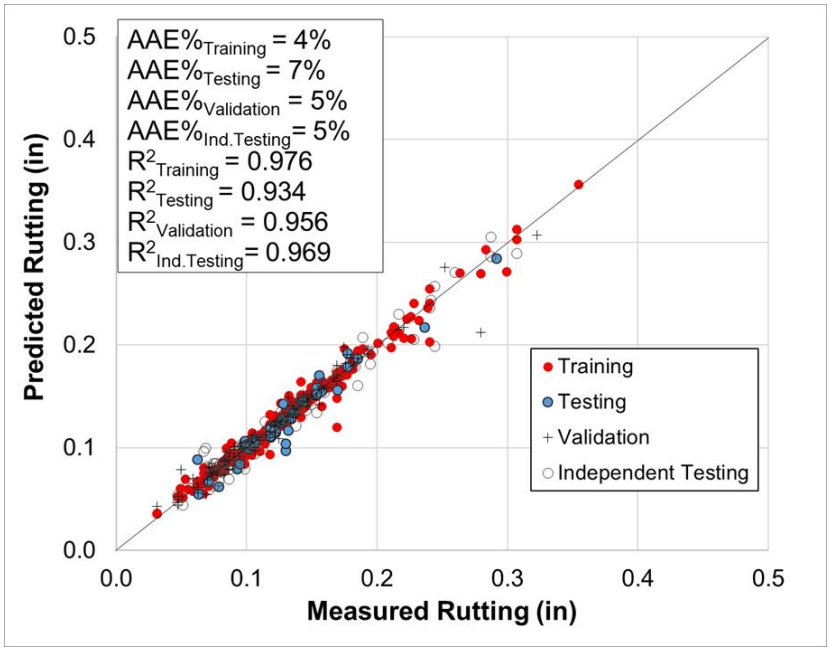

(a)

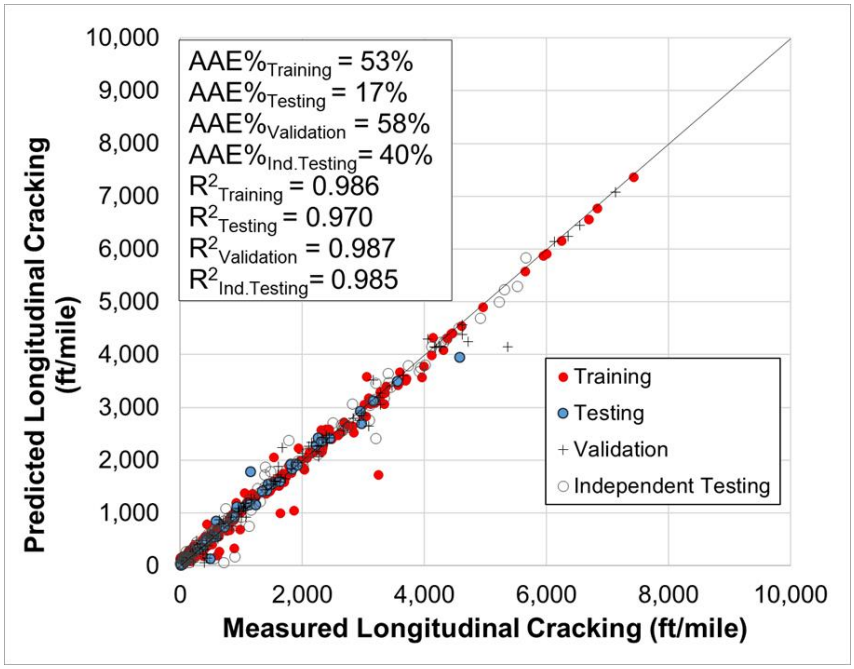

(b)

Figure 5.15 Comparisons between measured pavement condition records and ANN model predictions using a) rutting, b) longitudinal cracking, c) transverse cracking, d) IRI (approach 1) and e) IRI (approach 2) ANN models for composite pavements

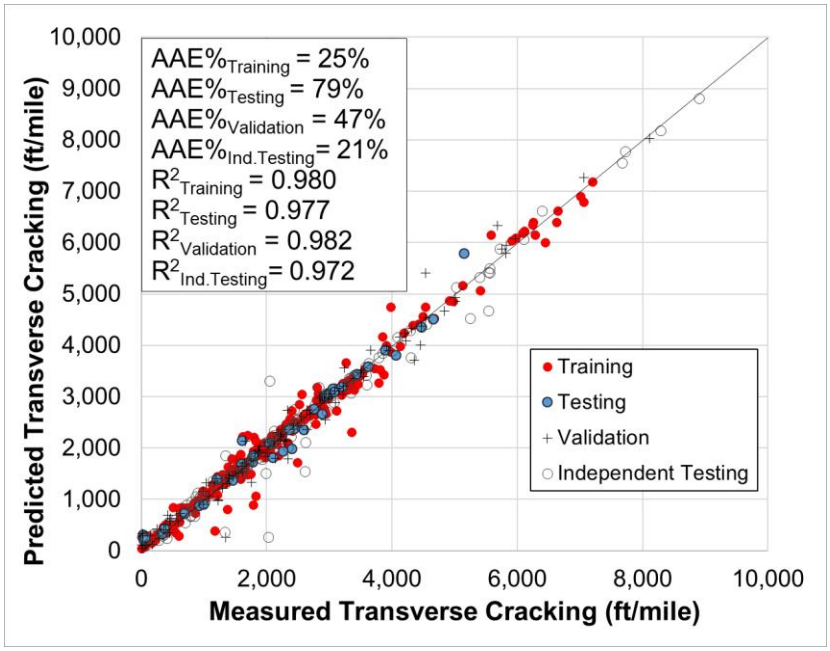

(c)

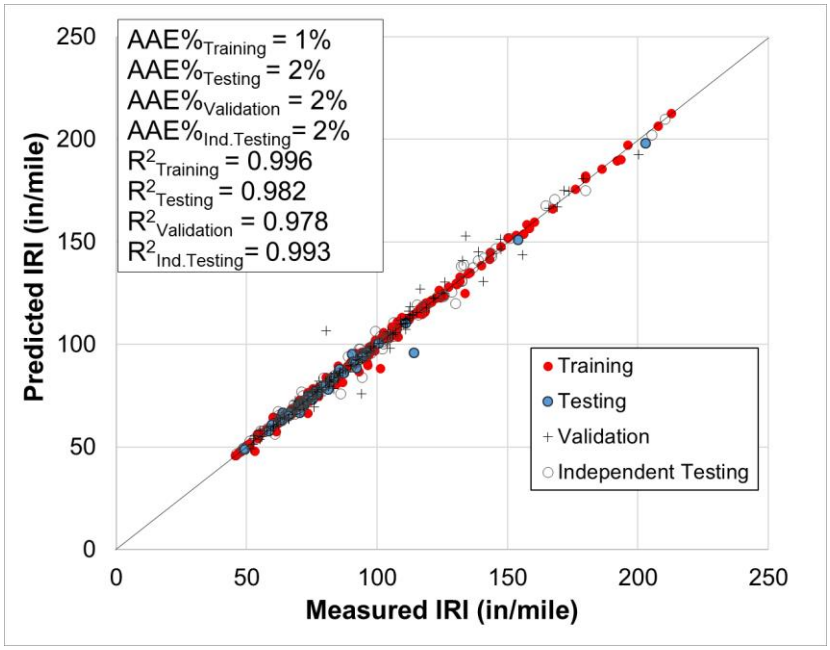

(d)

Figure 5.15 (Continued)

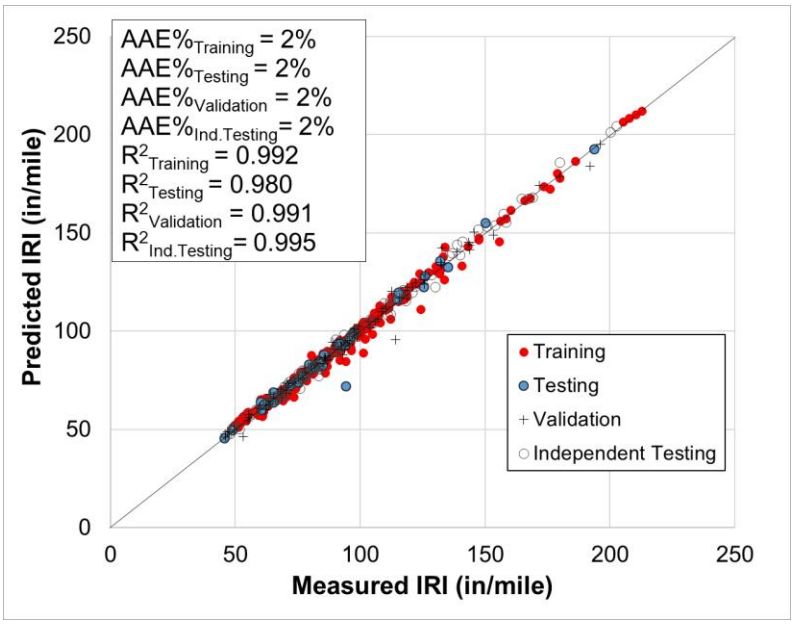

(e)

Figure 5.15 (Continued)

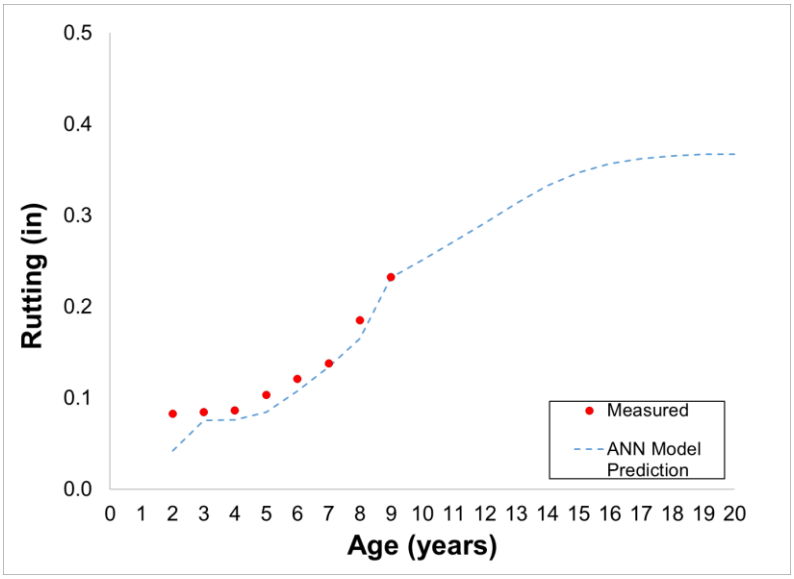

(a)

Figure 5.16 Comparisons between measured pavement condition records and ANN model predictions using a) rutting, b) longitudinal cracking, c) transverse cracking, d) IRI (approach 1) and e) IRI (approach 2) ANN models, respectively, for a composite pavement section as an example (US 20, MP 1.64 to 4.37, E, Traffic (AADTT): 2,848, Restoration year: 2004)

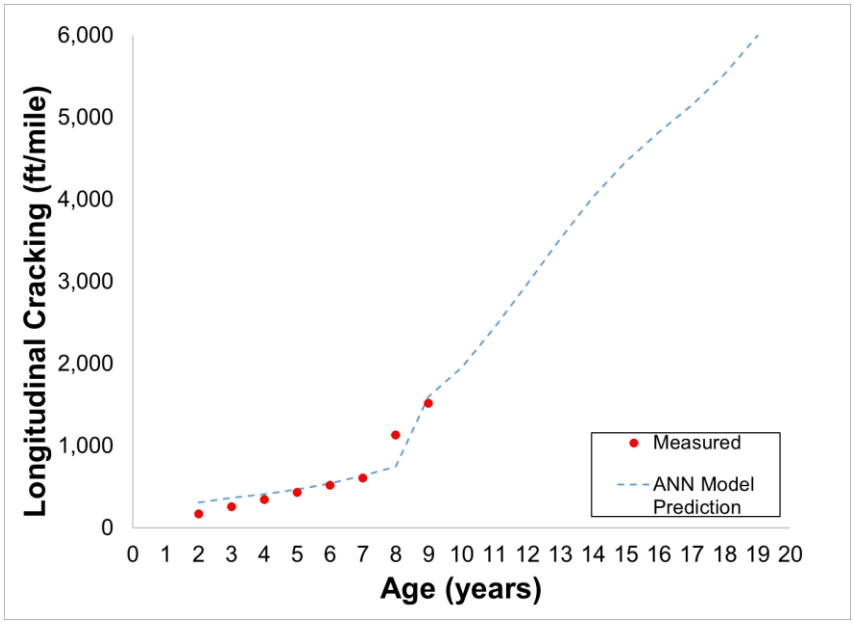

(b)

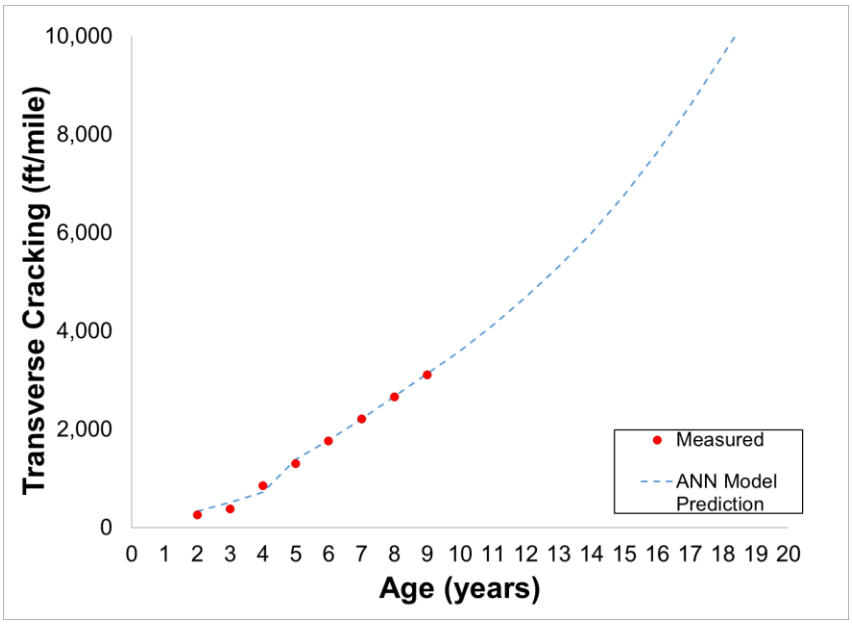

(c)

Figure 5.16 (Continued)

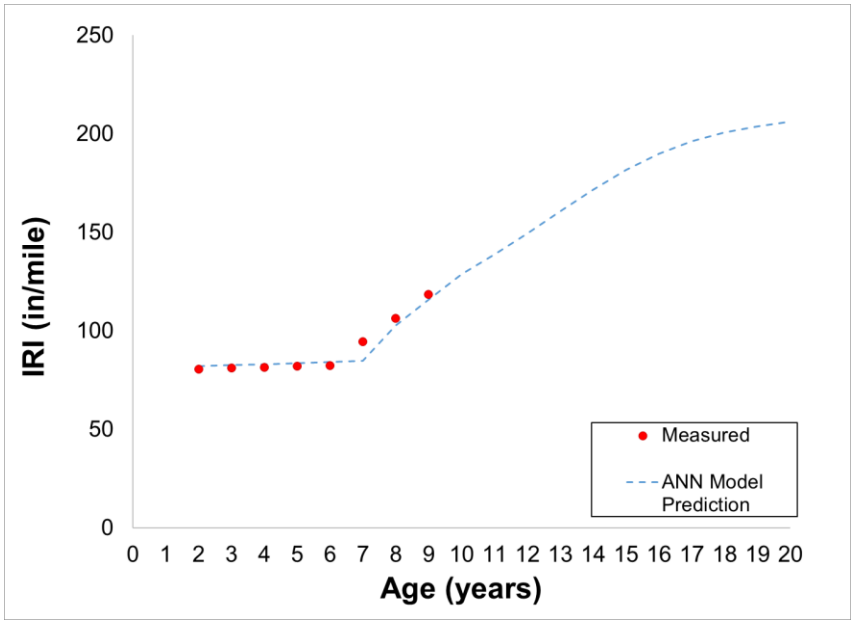

(d)

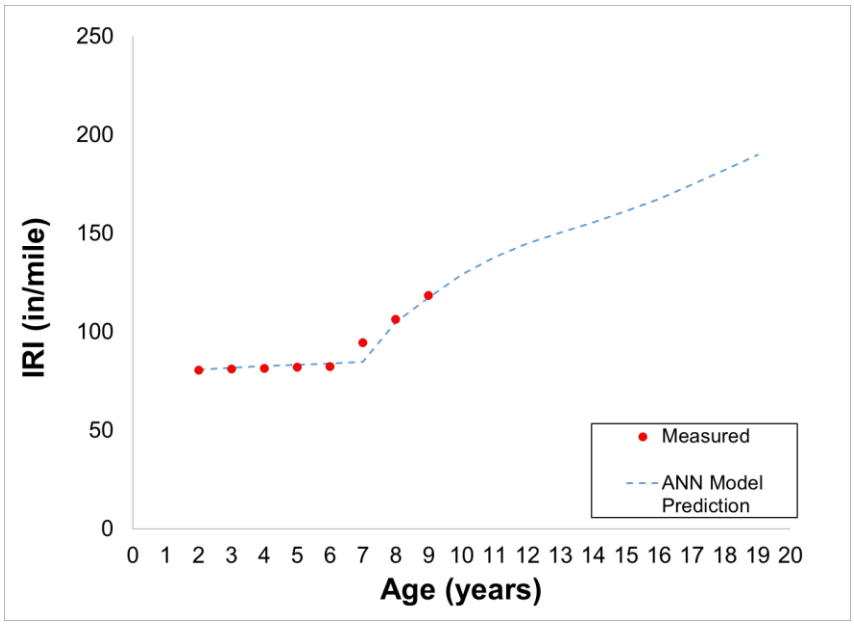

(e)

Figure 5.16 (Continued)

Network-Level Pavement RSL Model Development and Results

Once network level pavement performance models were developed for each pavement performance indicator or condition metric, as explained in the previous section, the remaining service life for each pavement section in a road network could be calculated using these performance models and corresponding threshold limits for the pavement performance indicators. In this study, rutting, percent cracking and IRI were used as performance indicators for network level RSL calculations because, as stated earlier, these condition metrics were determined by FHWA (*1*, *10*). RSL is determined based on the year when future performance predictions reach the poor condition threshold (these thresholds and corresponding condition metrics were highlighted in Table 5.1).

The RSL value for each pavement section in a road network was calculated based on the following steps (Figure 5.17):

1. Using developed AI based pavement performance models, future pavement condition predictions were calculated for each pavement section.
2. Whether future pavement condition predictions reached threshold limits was checked for each corresponding condition metric shown in Table 5.1.
    a. If yes, RSL value for each pavement section was calculated by subtracting the present year from the year when pavement condition predictions first reached the threshold limit.
    b. If no, based on available pavement condition data, this means that future pavement condition predictions do not reach 170 in/mile over a long period of analysis time (i.e. 50 years). In other words, this means that these pavement sections perform very well in terms of the corresponding condition metric,

although adding more data points (i.e., future performance measurements) would increase accuracy of the predictions.

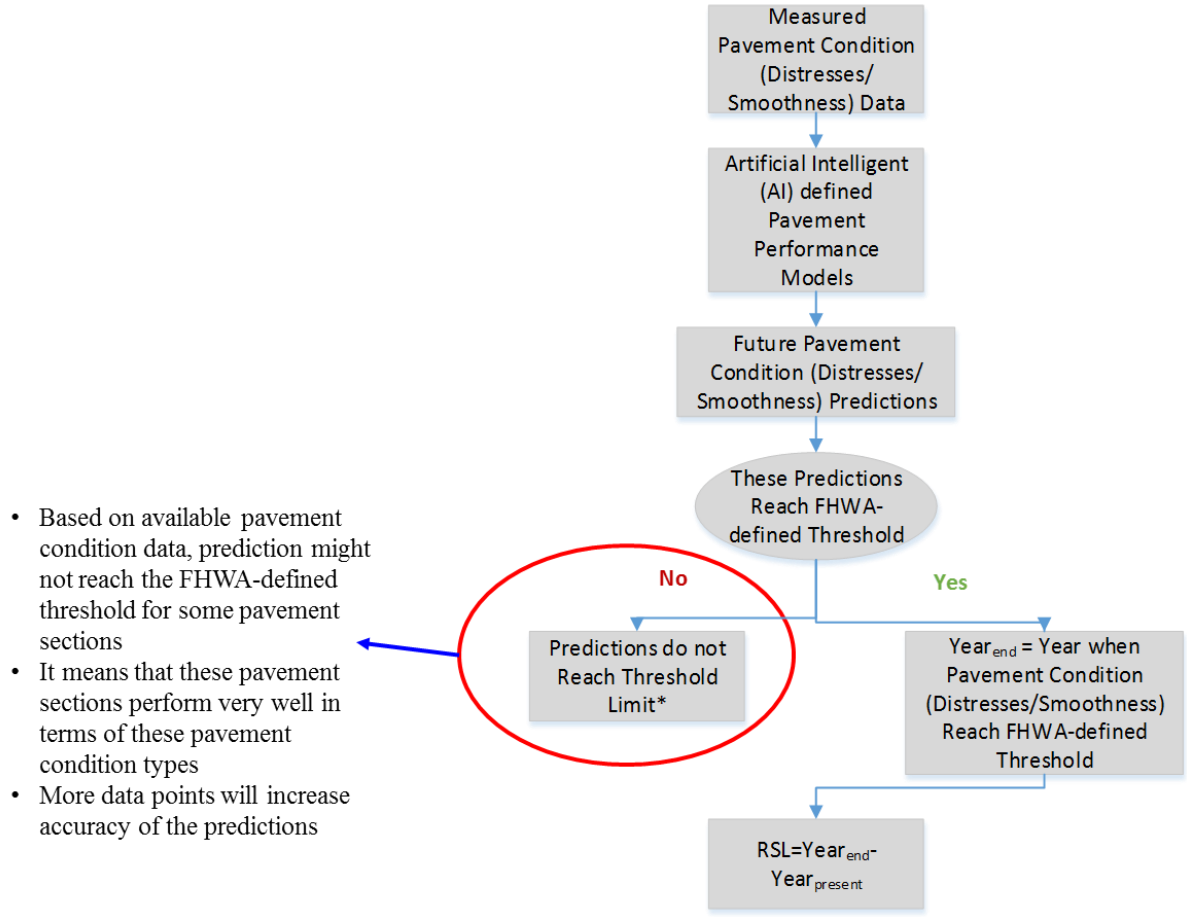

Figure 5.17 Network level RSL calculation steps

JPCP RSL Models for Network Level

Figure 5.18 shows the distribution of RSL for 34 JPCP pavement sections when a percent cracking threshold limit of 15% was used. An ANN-based network level transverse cracking model was used as the pavement performance model in calculation of RSL values, and the average RSL for the JPCP pavement sections was found to be 2.0 years.

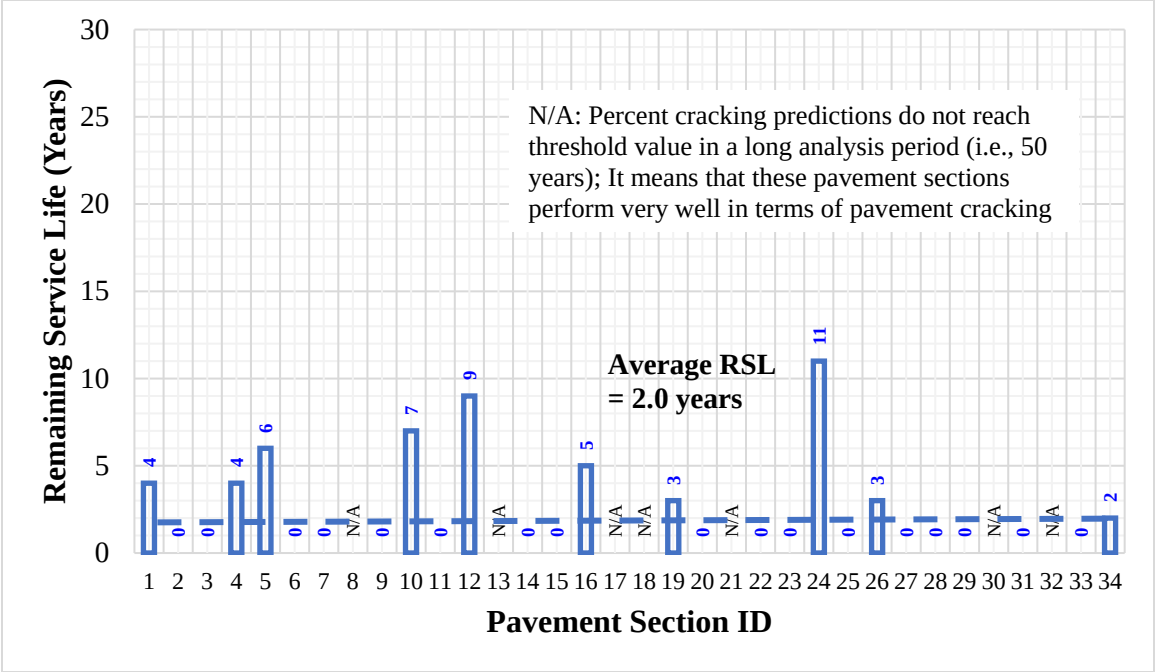

(a)

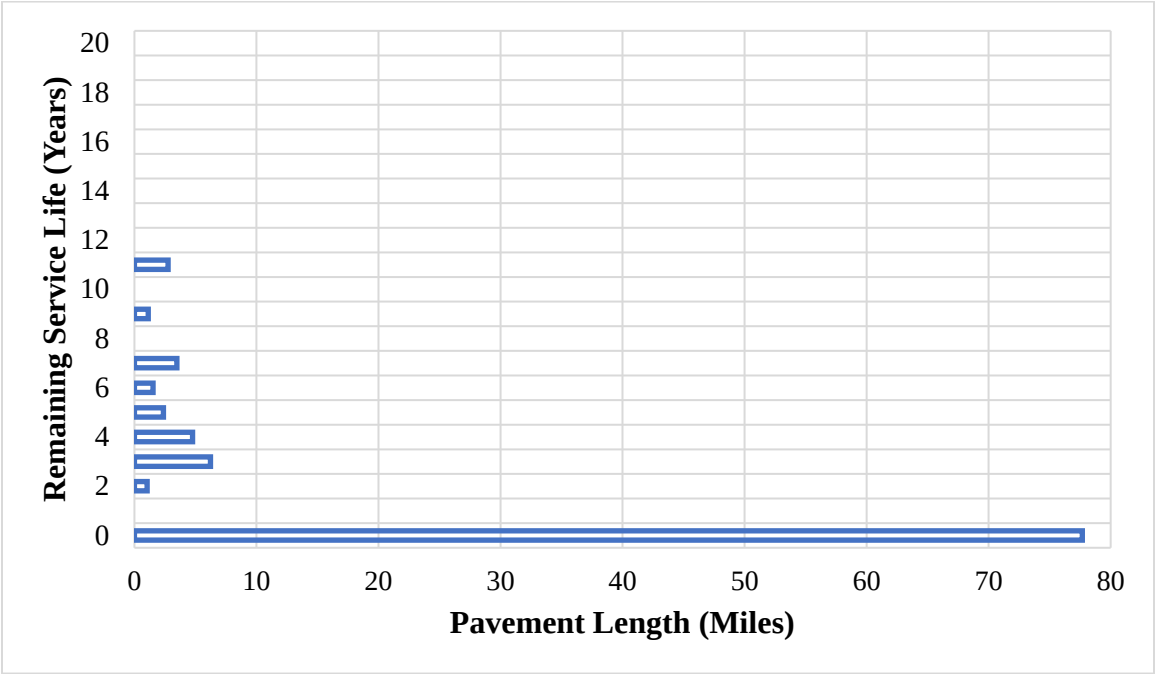

(b)

Figure 5.18 RSL distribution for JPCP pavement sections (a) based on pavement section ID and (b) based on pavement length, when transverse cracking model and percent cracking threshold limit of 15% were used

Figure 5.19 shows the distribution of RSL for 34 JPCP pavement sections when: (1) an IRI threshold limit of 170 in/mile was used as the threshold limit, and (2) the ANN-based network level IRI model (approach 1) was used as the pavement performance model in calculation of RSL values. The average RSL for the JPCP pavement sections was found to be 9.6 years (Figure 5.19).

Figure 5.20 shows the distribution of RSL for 34 JPCP pavement sections when: (1) an IRI threshold limit of 170 in/mile was used as the threshold limit, and (2) an ANN-based network level IRI model (approach 2) was used as the pavement performance model in calculation of RSL values. The average RSL for the JPCP pavement sections was found to be 11.5 years (Figure 5.20).

In summary, different average RSL results (7.2, 9.6, and 11.5 years of RSL) for the JPCP pavement sections were found when project level and network level (approach 1) and (approach 2) pavement performance models, respectively, were used in the calculation of RSL. This difference in average RSL results might be because different pavement performance models were used in the calculation of RSL. Network level pavement performance models were developed for each pavement performance indicator and a single model was used to make future pavement condition predictions for all pavement sections of a given pavement type. Even if they are developed considering various input variables (thickness, traffic, previous years' condition records, etc.) they can't be sufficiently comprehensive to consider all variables determining deterioration of the pavement systems. On the other hand, project-level pavement performance models, valid only for the sections for which they were developed, were developed for each pavement section. For the pavement sections with not many pavement condition records, their accuracies might not be high

enough, and adding more data points (i.e., future performance measurements) would most likely increase the accuracy of these models. Engineers should consider various parameters in determining which pavement performance model (project or network level) should be used in the calculation of RSL. If they have pavement performance records insufficient for developing accurate project level pavement performance models, they might consider using network-level models. Similarly, project-level models developed using many pavement performance records might better reflect the deterioration trend of a pavement section and make more realistic pavement performance predictions compared to network-level models.

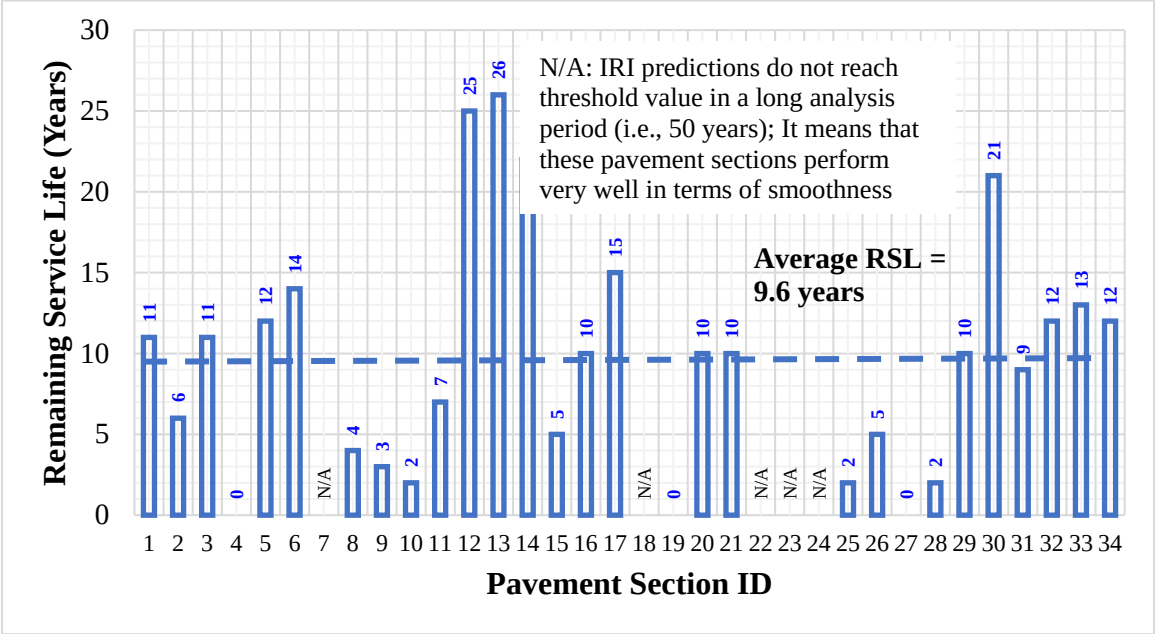

(a)

Figure 5.19 RSL distribution for JPCP pavement sections (a) based on pavement section ID and (b) based on pavement length, when IRI (approach 1) model and threshold limit of 170 in/mile were used

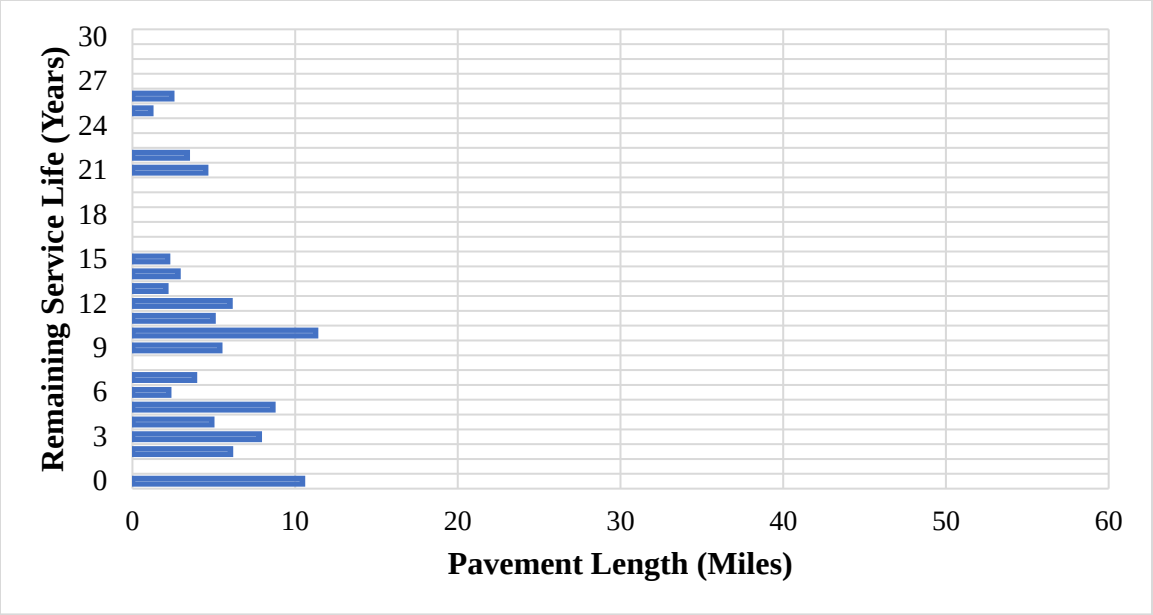

(b)

Figure 5.19 (Continued)

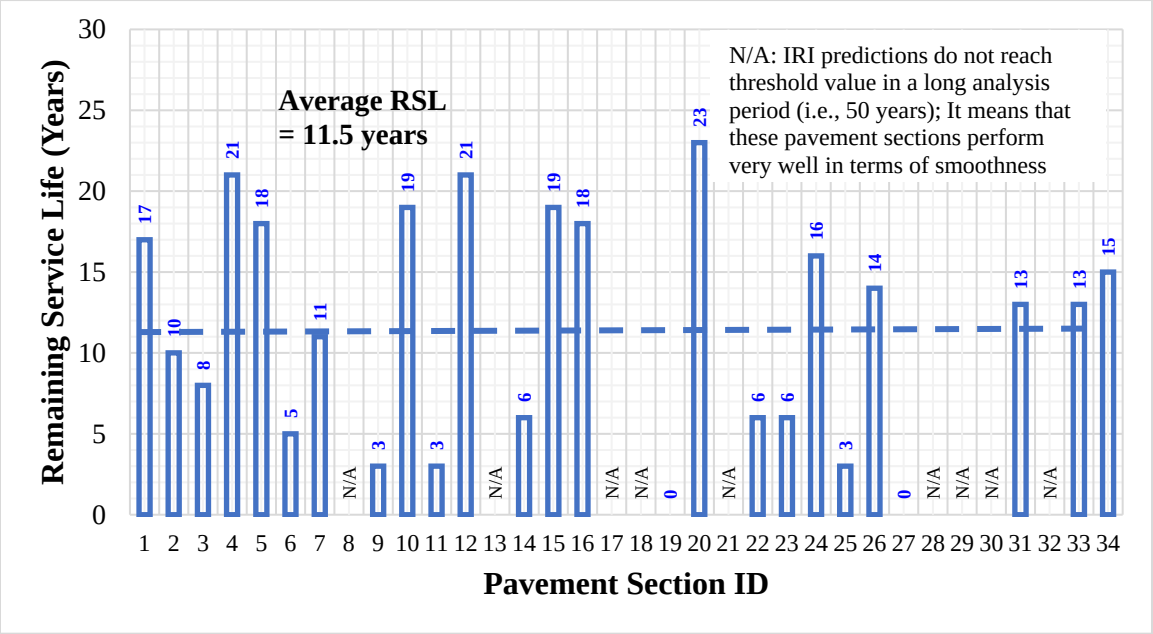

(a)

Figure 5.20 RSL distribution for JPCP pavement sections (a) based on pavement section ID and (b) based on pavement length, when IRI (approach 2) model and threshold limit of 170 in/mile were used

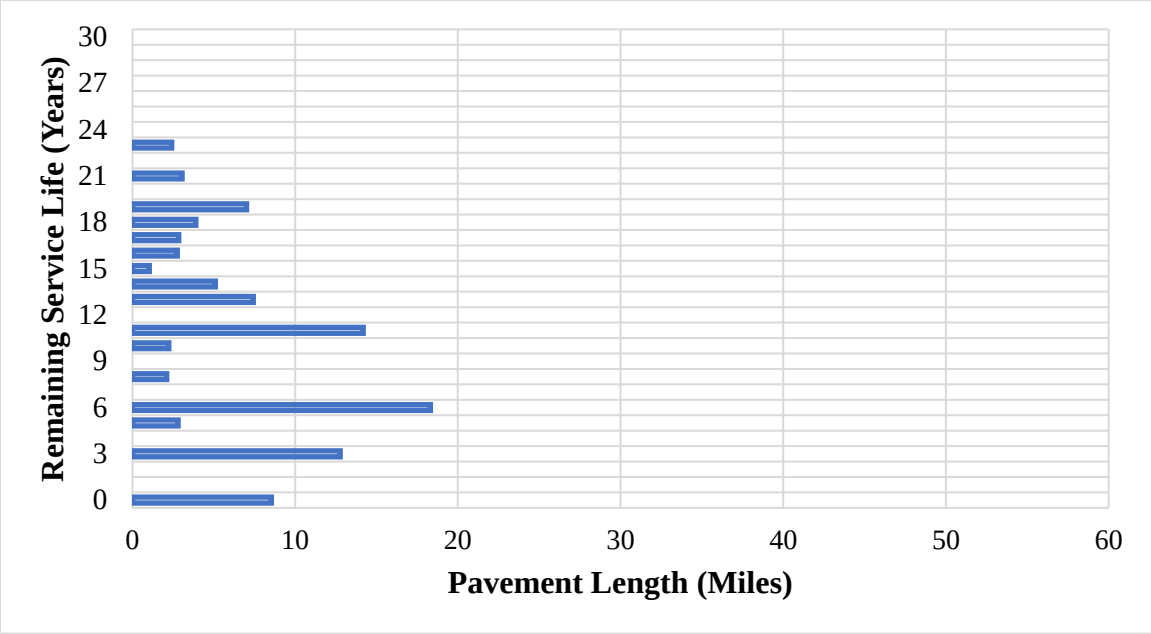

(b)

Figure 5.20 (Continued)

Flexible Pavement RSL Models for Network Level

Figure 5.21 shows the distribution of RSL for 35 flexible pavement sections when rutting threshold limit of 0.4 inch was used. ANN based network level rutting model was used as the pavement performance model in the calculation of RSL values. Average RSL for the flexible pavement sections was found to be 2.3 years.

Figure 5.22 shows the distribution of RSL for 35 flexible pavement sections when: (1) an IRI threshold limit of 170 in/mile was used as the threshold limit and (2) an ANN-based network-level IRI model (approach 1) was used as the pavement performance model in calculation of RSL values. The average RSL value for the flexible pavement sections was found to be 11.8 years (Figure 5.22)

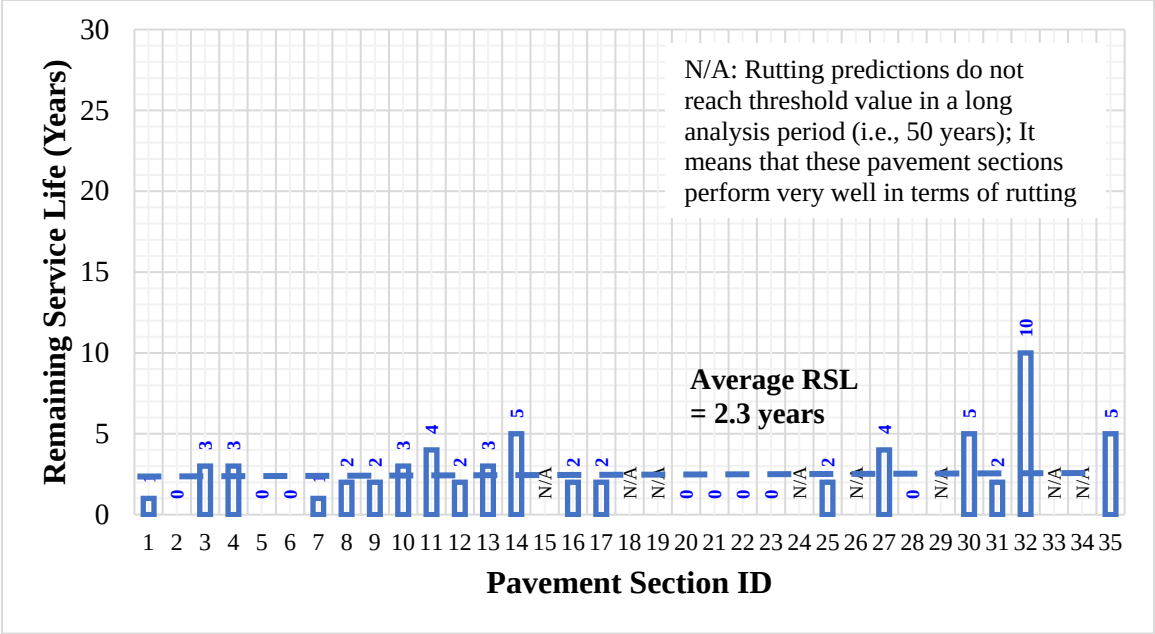

(a)

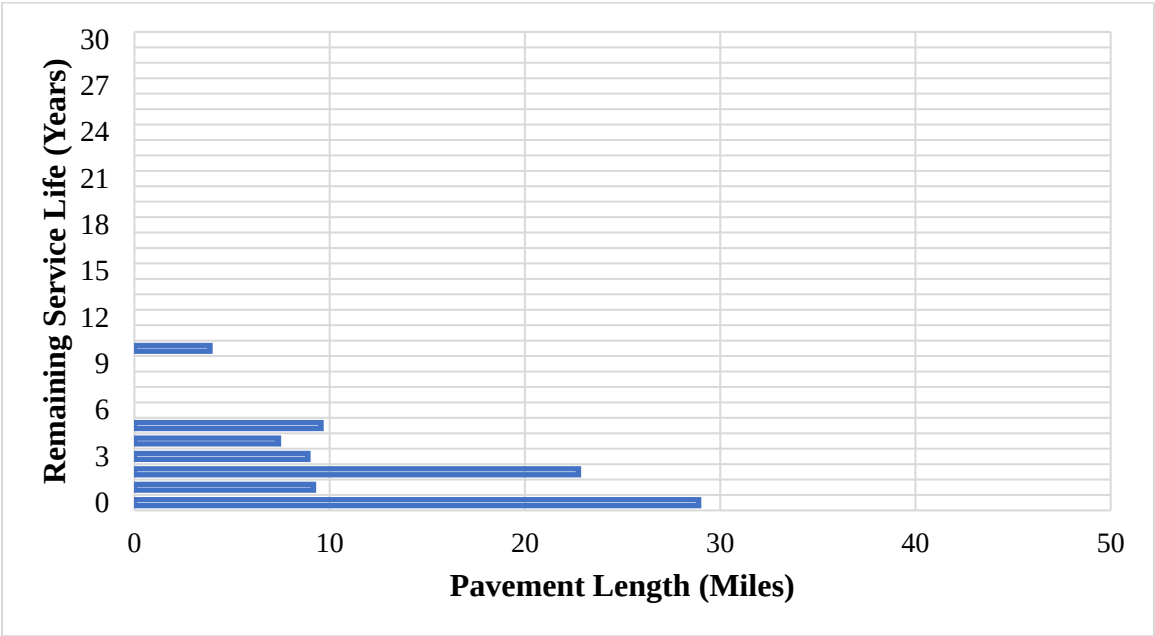

(b)

Figure 5.21 RSL distribution for flexible pavement sections (a) based on pavement section ID and (b) based on pavement length, when rutting model and threshold limit of 0.4 in. were used

Figure 5.23 shows the distribution of RSL for 35 flexible pavement sections when: (1) an IRI threshold limit of 170 in/mile was used as the threshold limit and (2) an ANN-based network-level IRI model (approach 2) was used as the pavement performance model in the calculation of RSL values. The average RSL value for the flexible pavement sections was found to be 11.7 years (Figure 5.23).

While there was not significant difference in average RSL results between cases when ANN-based network level IRI models (approach 1) and (approach 2) were used as pavement performance models in the calculation of RSL, the average RSL result for the flexible pavement sections was slightly lower when a project-level IRI model was used (9.3 years) as the pavement performance model in the calculation of RSL compared to when ANN-based network level IRI models were used (11.8 and 11.7 years).

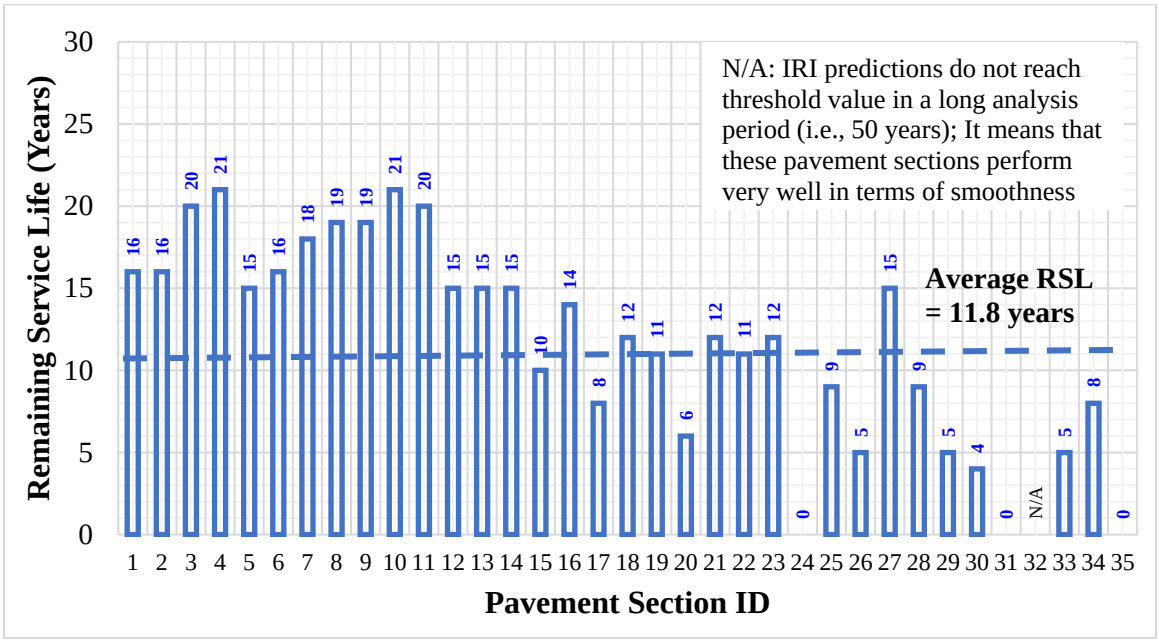

(a)

Figure 5.22 RSL distribution for flexible pavement sections (a) based on pavement section ID and (b) based on pavement length, when IRI (approach 1) model and threshold limit of 170 in/mile were used

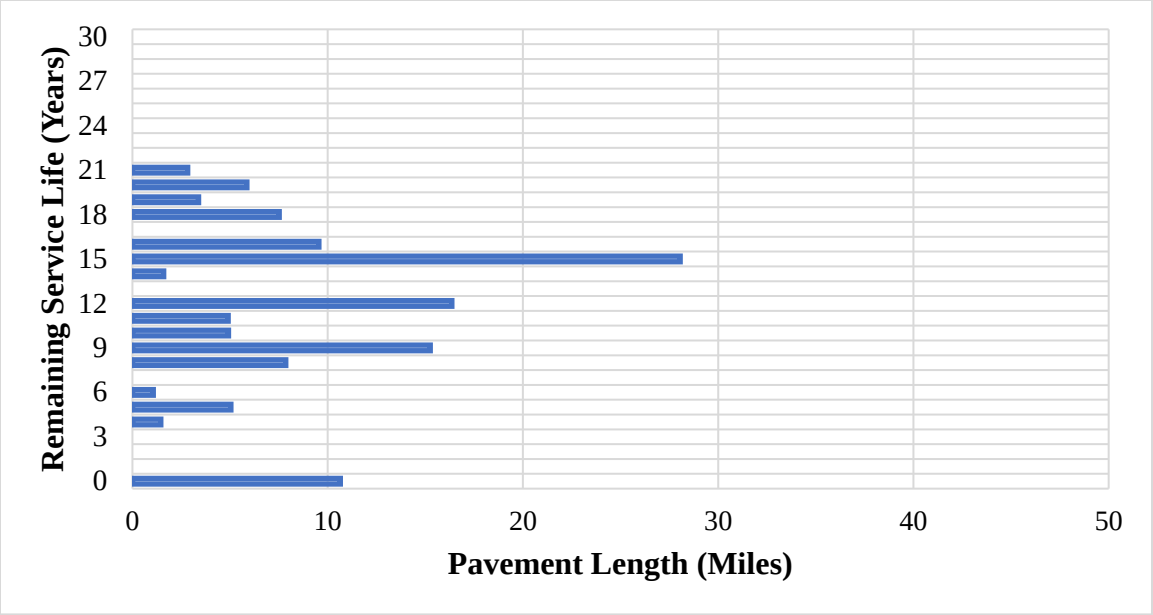

(b)

Figure 5.22 (Continued)

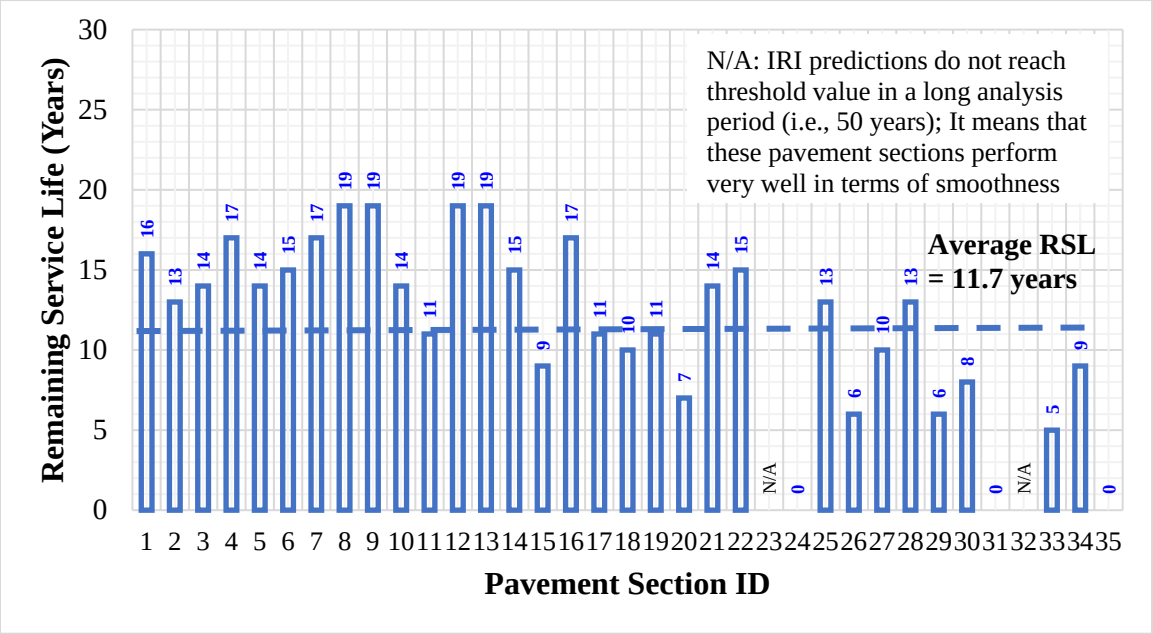

(a)

Figure 5.23 RSL distribution for flexible pavement sections (a) based on pavement section ID and (b) based on pavement length, when IRI (approach 2) model and threshold limit of 170 in/mile were used

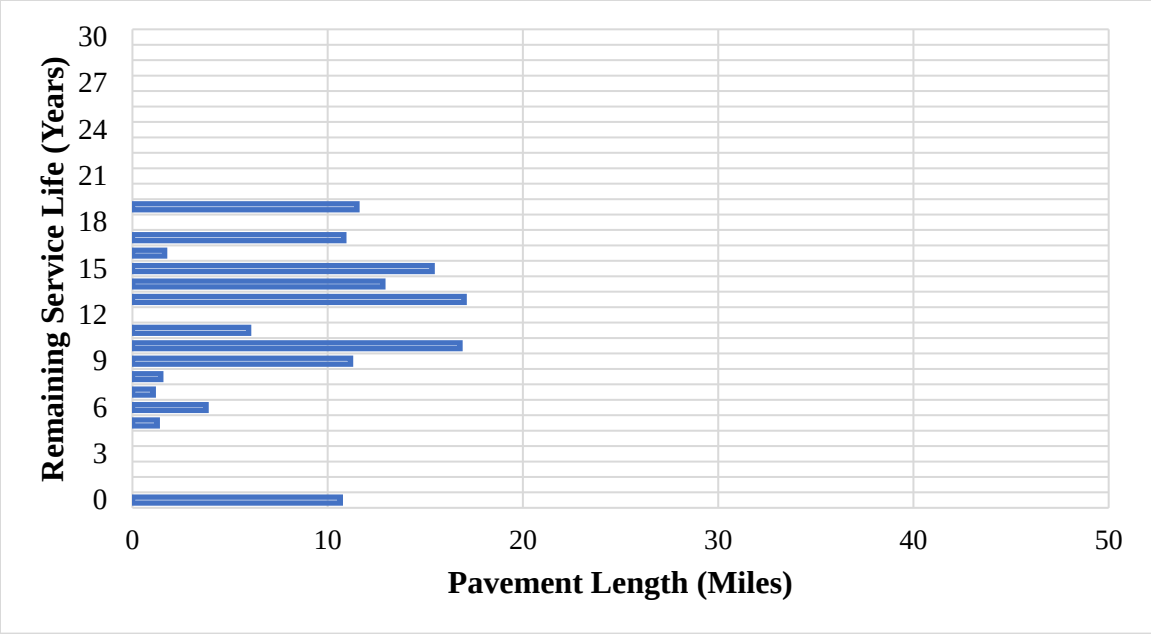

(b)

Figure 5.23 (Continued)

Composite (AC over JPCP) Pavement RSL Models for Network Level

Figure 5.24 shows the distribution of RSL for 60 composite pavement sections when a rutting threshold limit of 0.4 inch was used. An ANN-based network-level rutting model was used as the pavement-performance model in the calculation of RSL values, and the average RSL value for the flexible pavement sections was found to be 14.4 years.

Figure 5.25 shows the distribution of RSL for 60 composite pavement sections when: (1) an IRI threshold limit of 170 in/mile was used as the threshold limit and (2) an ANN-based network level IRI model (approach 1) was used as the pavement performance model in the calculation of RSL values. The average RSL for the composite pavement sections was found to be 9.3 years (Figure 5.25).

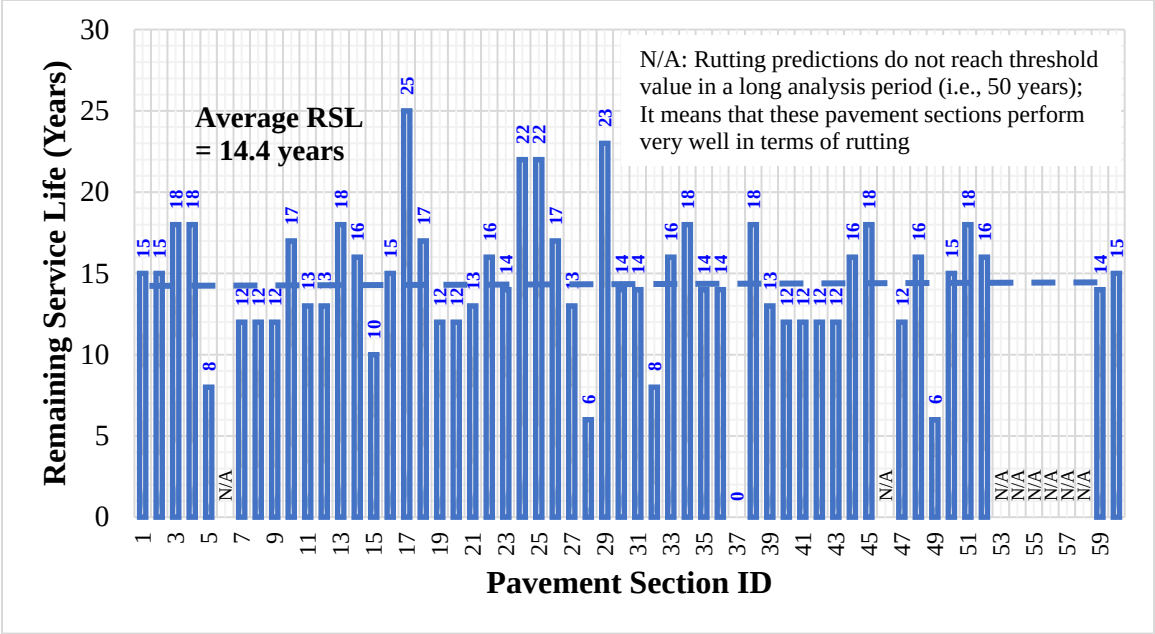

(a)

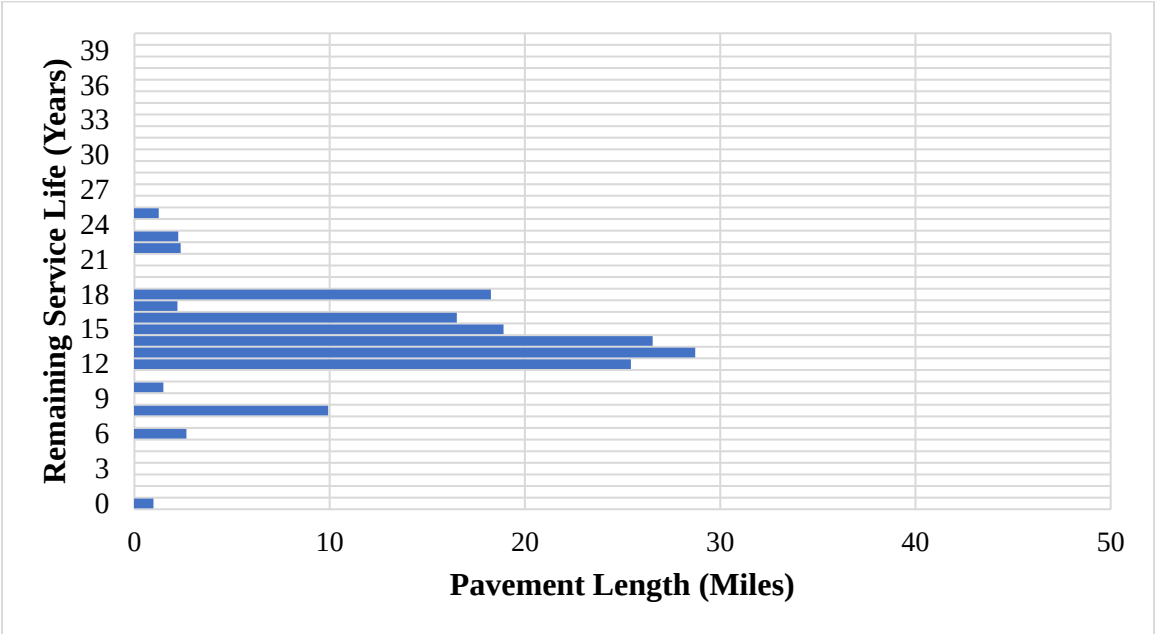

(b)

Figure 5.24 RSL distribution for composite pavement sections (a) based on pavement section ID and (b) based on pavement length, when rutting model and threshold limit of 0.4 in. were used

Figure 5.26 shows the distribution of RSL for 60 composite pavement sections when: (1) an IRI threshold limit of 170 in/mile was used as the threshold limit and (2) an ANN-based network level IRI model (approach 2) was used as the pavement performance model in the calculation of RSL values. The average RSL value for the composite pavement sections was found to be 6.1 years (Figure 5.26).

Average RSL results when project-level and ANN-based network-level performance models, (approach 1) and (approach 2), were used in the calculation of RSL values for the composite pavement sections were found to be 4.4, 9.3 and 6.3 years.

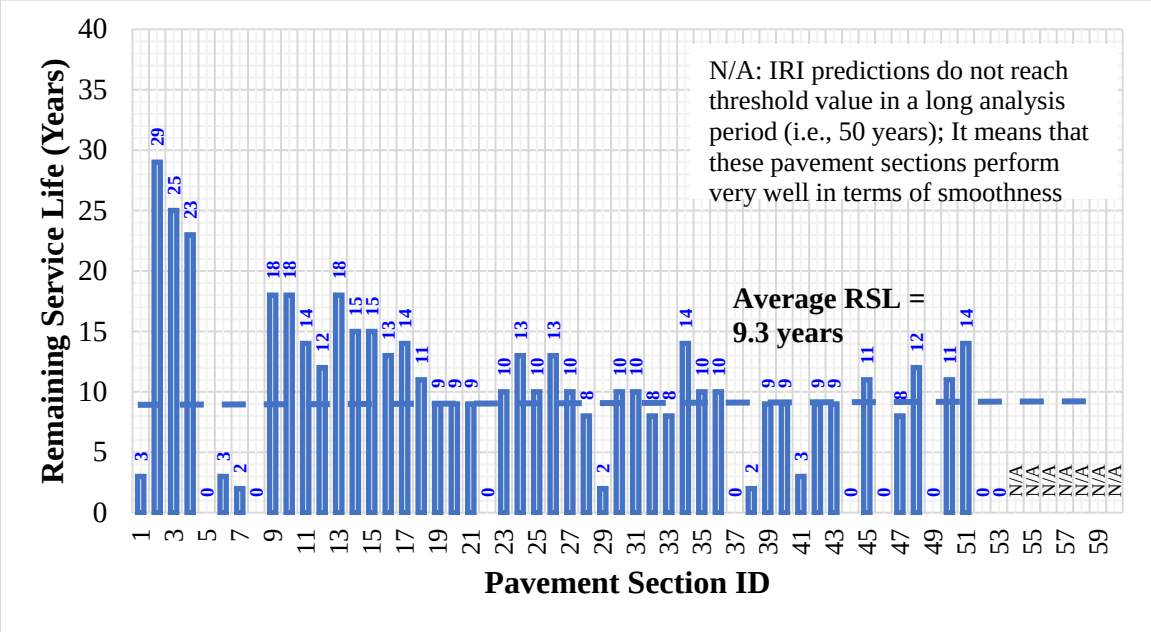

(a)

Figure 5.25 RSL distribution for composite pavement sections (a) based on pavement section ID and (b) based on pavement length, when IRI model (approach 1) and threshold limit of 170 in/mile were used

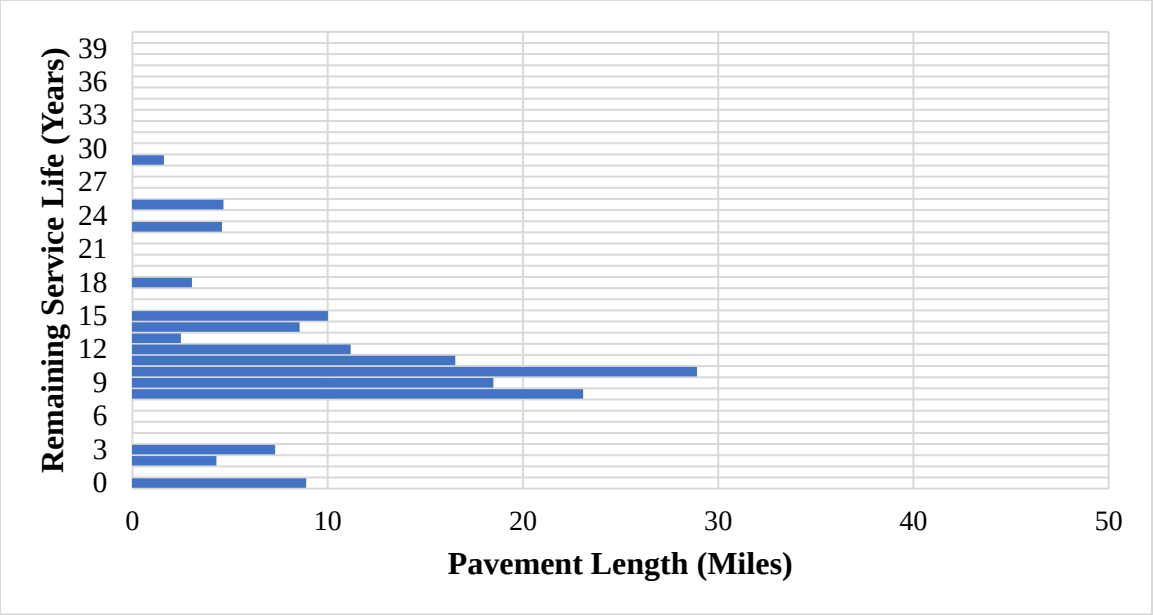

(b)

Figure 5.25 (Continued)

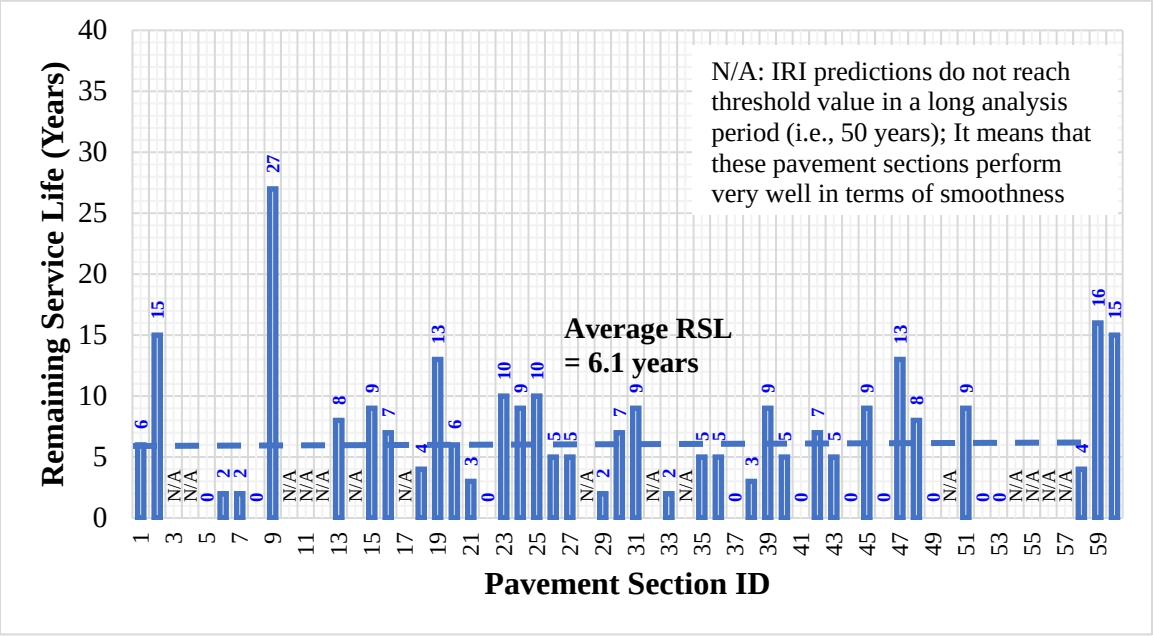

(a)

Figure 5.26 RSL distribution for composite pavement sections (a) based on pavement section ID and (b) based on pavement length, when IRI model (approach 2) and threshold limit of 170 in/mile were used

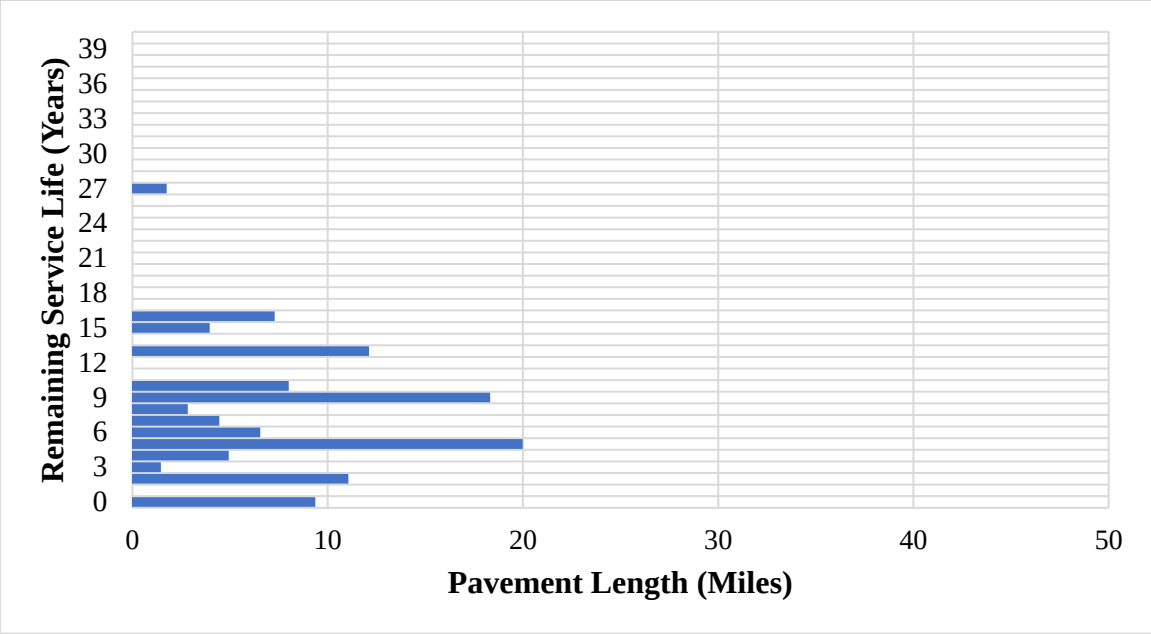

(b)

Figure 5.26 (Continued)

Discussion: Comparisons between Statistical and AI based Network Level Pavement Performance Models

Network-level pavement-performance models were developed using both statistical and ANN-based approaches, with the same input parameters used in both approaches to evaluate the relative success of these two models for network-level pavement-performance modeling. A network-level IRI performance model was developed for each pavement type (JPCP, flexible, and composite (AC over JPCP)) using statistical and ANN models. The same input parameters as for network-level IRI models (approach 1) were also used for the three pavement types:

- Input parameters: Thickness (PCC slab thickness for JPCP and AC thickness for flexible and composite pavements), traffic (accumulated ESALs), age, IRI $_{(i-2)\ year}$, IRI $_{(i-1)\ year}$
- Output parameter: IRI $_{(i)\ year}$

The same generalized sigmoidal equation (Equation 5.3) was also used in the development of network-level statistical models, and the same methodology, error minimization, was used in the optimization of network-level statistical models.

JPCP Pavement Case

A globally-optimized sigmoid equation (Equation 5.4) was developed by correlating the coefficients of sigmoidal equation (C_1, C_2, C_3, and C_4) with the input parameters for the entire dataset of model development (34 JPCP pavement sections (396 data points))

$$IRI = C_1 + \frac{C_2}{1+e^{(17.57+0.93\times age)}} \quad (5.4)$$

Where

- C_1 = - 1.8E-7 × ACC Traffic - 2.06 × Slab Thickness + 0.97 × IRI $_{(i-2)\ year}$ + 0.31 × IRI $_{(i-1)\ year}$
- C_2 = - 0.04 × ACC Traffic - 2.00 × Slab Thickness + 2.94 × IRI $_{(i-2)\ year}$ + 3.90 × IRI $_{(i-1)\ year}$

A model with the model architecture of 5 - 5 - 1 (number of inputs - number of hidden neurons - number of outputs) was used as the network-level ANN model.

Figure 5.27 compares the accuracies of the statistical and ANN based network level IRI models for JPCP pavements. As can be seen in the figure, the ANN model produced greater accuracy with higher R^2 and lower AAE values than the statistical model.

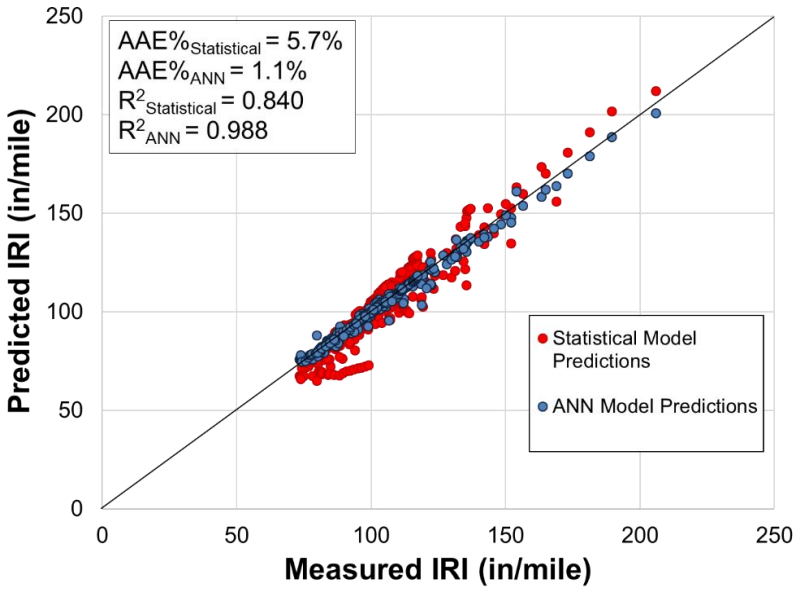

Figure 5.27 Accuracy comparisons between statistical and ANN based network level IRI models for JPCP pavements

Flexible Pavement Case

A globally-optimized sigmoid equation (Equation 5.5) was developed by correlating the coefficients of the sigmoidal equation (C_1, C_2, C_3, and C_4) with the input parameters for the whole dataset of model development (35 flexible pavement sections (360 data points))

$$IRI = C_1 + \frac{C_2}{1+e^{(17.57+0.93\times age)}} \quad (5.5)$$

Where

- C_1 = 7.52E-7 × ACC Traffic - 2.11 × AC Thickness + 1.04 × IRI $_{(i-2)\ year}$ + 0.32 × IRI $_{(i-1)\ year}$
- C_2 = - 0.04 × ACC Traffic - 2.00 × AC Thickness + 2.94 × IRI $_{(i-2)\ year}$ + 3.90 × IRI $_{(i-1)\ year}$

A model with the model architecture of 5 - 5 - 1 was used as the network-level ANN model.

Figure 5.28 compares the accuracies of statistical and ANN-based network-level IRI models for flexible pavements. As can be seen in the figure, the ANN model produced greater accuracy with higher R^2 and lower AAE values than the statistical model.

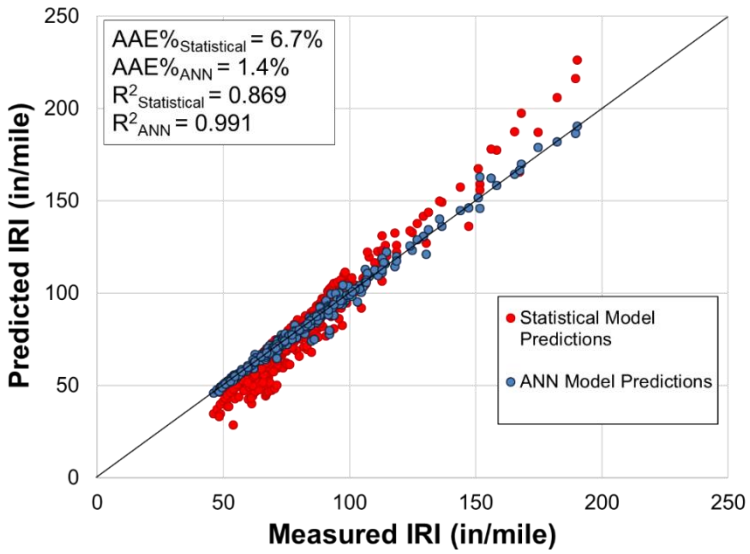

Figure 5.28 Accuracy comparisons between statistical and ANN based network level IRI models for flexible pavements

Composite (AC over JPCP) Pavement Case

A globally-optimized sigmoid equation (Equation 5.6) was developed by correlating the coefficients of the sigmoidal equation (C_1, C_2, C_3, and C_4) with the input parameters for the entire dataset of model development (60 composite pavement sections (524 data points))

$$IRI = C_1 + \frac{C_2}{1+e^{(17.57+0.93\times age)}} \quad (5.6)$$

Where

- C_1 = 1.37E-7 × ACC Traffic - 2.12 × AC Thickness + 0.82 × IRI $_{(i-2)\ year}$ + 0.30 × IRI $_{(i-1)\ year}$
- C_2 = - 0.04 × ACC Traffic - 2.00 × AC Thickness + 2.94 × IRI $_{(i-2)\ year}$ + 3.90 × IRI $_{(i-1)\ year}$

A model with the model architecture of 5 - 5 - 1 was used as the network-level ANN model.

Figure 5.29 compares the accuracies of the statistical and ANN-based network-level IRI models for composite pavements. As can be seen in the figure, the ANN model produced more accuracy with higher R^2 and lower AAE values than the statistical model.

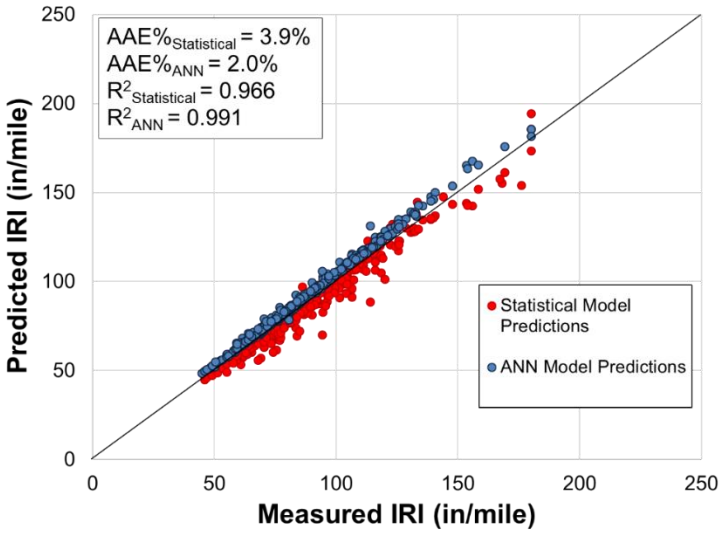

Figure 5.29 Accuracy comparisons between statistical and ANN based network level IRI models for composite pavements

Conclusions and Recommendations

Overall Conclusions

In this study, a detailed step-by-step methodology for development of a framework for pavement performance and RSL prediction models was established and explained using real pavement performance data obtained from the Iowa DOT PMIS database. To develop RSL models, project and network-level pavement performance models were initially developed using two approaches: a statistically (or mathematically) defined approach for project-level model development and an artificial intelligence (AI) based approach for network-level model development. Then, using threshold limits for various pavement-performance indicators (IRI for project-level models, and rutting, percent cracking, and IRI for network-level models) and FHWA-specified threshold limits for pavement performance indicators, RSL models were developed for three pavement types: flexible pavements, jointed plain-concrete pavements (JPCP) and composite (Asphalt concrete (AC) over JPCP) pavements.

A statistically (or mathematically)-defined sigmoid pavement deterioration curve-based approach was used for project-level pavement-performance model development. Sigmoidal equations have been particularly used in the statistical model development because: (1) they have a low initial slope that increases with time, and (2) they follow a trend in which pavement condition always gets worse and damage is irreversible, and both these features make these models mimic the pavement deterioration behavior observed in field studies. Sigmoidal equations were found to successfully model pavement deterioration when there is a single pavement deterioration trend (project-level). One of the benefits of project-level pavement performance models is that they can be developed using very few data. Therefore, they can be extensively used when only a few pavement conditions or structural and traffic data are available for pavement sections.

Artificial intelligence (AI)-based pavement-performance models were used for network-level pavement performance model development in this study. Artificial intelligence (AI) techniques such as artificial neural network (ANN)-based models have been found to be great tools for modeling pavement deterioration when there are many pavement sections with various traffic, thickness, and other various deterioration trends (network-level). They are also very fast tools that can solve thousands of pavement scenarios with various traffic, thickness, and conditions in seconds. Both these features of ANN models make them great tools for use in development of network-level pavement-performance modeling.

As part of this study, network-level pavement performance models were also developed using statistical and ANN-based approaches, with identical input parameters used in both approaches to evaluate their relative success for network-level pavement-performance modeling. It was found that network-level ANN based pavement performance models

produced greater accuracy with higher R^2 and lower AAE values compared to network-level statistical models.

As part of this study, Microsoft Excel based automation tools were developed for both project and network-level pavement performance modeling and analysis:

- The project-level pavement-performance modeling and RSL calculation tool is capable of developing project-based statistical models for predicting future pavement performance as well as calculating RSL values based on user-defined threshold limits. It is also capable of automatically updating and improving pavement-performance prediction models because it allows more data to be added into the model development dataset. The benefit of this tool is that, as engineers add more data into the model development dataset, they will be able to automatically refine performance prediction models and make decisions using more recent and more accurate pavement performance models.
- The network-level pavement performance modeling tool is capable of making pavement-performance predictions based on pre-developed ANN-based pavement-performance models. While having only thickness, traffic, age, and previous two years' pavement performance records for any pavement performance indicator, it can make future pavement-performance calculations in less than a second for any pavement section. It is also capable of producing pavement-performance predictions for thousands of pavement scenarios under various traffic, thickness, and other conditions in seconds. The network-level pavement performance modeling tool is also capable of (1) making future pavement-performance predictions for some distresses (transverse cracking, rutting, and longitudinal cracking), then (2) using these predicted distress values as inputs in making future IRI predictions.

Conclusions for JPCP

- 34 JPCP pavement sections were used in pavement-performance model development in this study.
- Accurate project-level statistically-based IRI performance models and network level transverse cracking, IRI (approach 1) and IRI (approach 2) ANN models were developed for JPCP pavements.
- An IRI threshold limit was used as a pavement-performance indicator in project-level RSL models. An average RSL value of 7.2 years was found for 34 JPCP pavement sections when project-level pavement performance models were used to make future IRI predictions and an IRI threshold limit of 170 in/mile was used in calculation of RSL.
- Threshold limits for percent cracking and IRI were used as pavement performance indicators in network-level RSL models. Average RSL values of 2.0, 9.6, and 11.5 years were found for 34 JPCP pavement sections when network level transverse cracking, IRI (approach 1), and IRI (approach 2) pavement performance models were used to make future pavement-condition predictions and percent cracking threshold limit of 15% and IRI threshold limit of 170 in/mile were used in the calculation of RSL.
- In summary, different average RSL results (7.2, 9.6, and 11.5 years of RSL) for the JPCP pavement sections were found when project level and network level (approach 1) and (approach 2) pavement performance models, respectively, were used in the calculation of RSL. This difference in average RSL results might be because different pavement performance models were used in the calculation of RSL. Network level pavement performance models were developed for each pavement performance indicator and a single model was used to make future pavement condition predictions for all pavement

sections of a given pavement type. Even if they are developed considering various input variables (thickness, traffic, previous years' condition records, etc.) they can't be sufficiently comprehensive to consider all variables determining deterioration of the pavement systems. On the other hand, project-level pavement performance models, valid only for the sections for which they were developed, were developed for each pavement section. For the pavement sections with not many pavement condition records, their accuracies might not be high enough, and adding more data points (i.e., future performance measurements) would most likely increase the accuracy of these models.

Conclusions for Flexible Pavements

- 35 flexible pavement sections were used in pavement performance model development in this study.
- Accurate project-level statistically-based IRI performance models and network-level rutting, longitudinal cracking, transverse cracking, IRI (approach 1), and IRI (approach 2) ANN models were developed for flexible pavements.
- An IRI threshold limit was used as the pavement performance indicator in project-level RSL models. An average RSL value of 9.3 years was found for 35 flexible pavement sections when project level pavement performance models were used to make future IRI predictions and an IRI threshold limit of 170 in/mile was used in the calculation of RSL.
- Threshold limits for rutting and IRI were used as pavement-performance indicators in network-level RSL models, and average RSL values of 2.3, 11.8 and 11.7 years were found for 35 flexible pavement sections when network-level rutting, IRI (approach 1), and IRI (approach 2) pavement-performance models were used to make future pavement

condition predictions and a rutting threshold limit of 0.4 inch and an IRI threshold limit of 170 in/mile were used in the calculation of RSL.

- There was insignificant difference in average RSL results between the cases when ANN-based network-level IRI models (approach 1) and (approach 2) were used as the pavement performance models in the calculation of RSL for 35 flexible pavement sections. On the other hand, the average RSL result was slightly lower (9.3 years) when a project-level IRI model was used as pavement-performance models in the calculation of RSL compared to ANN-based network level IRI models (11.6 and 11.7 years).
- Note that calculated RSL results are based on a limited number of dataset elements, developed pavement performance models and FHWA-specified threshold limits. Adding more data points (i.e., future performance measurements) would change the pavement performance models as well as the calculated RSL results.

Conclusions for Composite (AC over JPCP) Pavements

- 60 composite pavement sections were used in the pavement performance model development in this study.
- Accurate project-level statistically-based IRI performance models and network-level rutting, longitudinal cracking, transverse cracking, IRI (approach 1), and IRI (approach 2) ANN models were developed for composite pavements.
- An IRI threshold limit was used as the pavement performance indicator in project-level RSL models. An average RSL value of 4.4 years was found for 60 composite pavement sections when project level pavement performance models were used to make future IRI predictions and an IRI threshold limit of 170 in/mile was used in the calculation of RSL.

- Threshold limits for rutting and IRI were used as pavement performance indicators in network-level RSL models. Average RSL values of 14.4, 9.3 and 6.1 years were found for 60 composite pavement sections when network-level rutting, IRI (approach 1), and IRI (approach 2) pavement-performance models were used to make future pavement condition predictions and a rutting threshold limit of 0.4 inch and IRI threshold limit of 170 in/mile were used in the calculation of RSL.
- Average RSL results for 60 composite pavement sections when project-level and ANN-based network-level performance models, (approach 1) and (approach 2), were used in the calculation of RSL values were 4.4, 9.3 and 6.3 years.
- Note that calculated RSL results are based on a limited number of dataset, developed pavement-performance models, and FHWA-specified threshold limits. Adding more data points (i.e., future performance measurements) would change the pavement performance models as well as the calculated RSL results.

Recommendations

This study can be further expanded by: (1) including other pavement performance indicators (i.e, faulting, material-related distresses, etc.), (2) defining other agency-specific threshold limits, and (3) prioritizing some pavement performance indicators over others, etc., as part of RSL model development. Some SHAs use decision trees to determine when a major rehabilitation or reconstruction is needed. Multi-objective RSL models can be developed considering various pavement performance indicators with different priorities.

RSL results will allow agencies to distinguish between two pavement sections with the same current condition (i.e., the same current IRI). This can be an ideal approach to

addressing the transportation planning and performance management criteria requirements of the MAP-21 legislation.

Note that RSL models are only to help engineers in their decision-making process. They consider only a limited number of condition metrics (IRI, some distresses, etc.) but may fail to consider other important parameters such as structural capacity and integrity of pavement systems. Engineers should consider various parameters as well as RSL model results, combined with their engineering judgment to determine when a pavement section will fail and need major rehabilitation or reconstruction. Estimated RSL does not necessarily mean that after that date a pavement section cannot be open to public use, and applying preventative or routine maintenance may lead to significantly increased RSL.

Acknowledgements

The authors gratefully acknowledge the Iowa Highway Research Board and Iowa County Engineers Service Bureau for supporting this study. The contents of this paper reflect the views of the authors who are responsible for the facts and accuracy of the data presented within. The contents do not necessarily reflect the official views and policies of the Iowa Highway Research Board, Iowa County Engineers Service Bureau and Iowa State University. This paper does not constitute a standard, specification, or regulation.

References

1. HR 4348, *Moving Ahead for Progress in the 21st Century Act (MAP–21), An Act to authorize funds for Federal-aid highways, highway safety programs, and transit programs, and for other purposes*, 112 Congress, 2nd Session. Enacted October 1, 2012.

2. FHWA. *Pavement Health Track Remaining Service Life (RSL) Forecasting Models, Technical Information,* 2018.

3. G. E. Elkins, T. M. Thompson, J. L. Groeger, B. Visintine, and G. R. Rada. *Reformulated Pavement Remaining Service Life Framework*. FHWA, 2013

4. Mack, J. W. and Sullivan, R. L. 2014. Using Remaining Service Life as the National Performance Measure of Pavement Assets. Proceedings of the 93rd Annual Meeting of the Transportation Research Board (TRB), Washington, DC, January 12–16.

5. Chen, D. and Mastin N. Sigmoidal Models for Predicting Pavement Performance Conditions. *ASCE J. Perform. Constr. Facil*., 2016, 30(4): 04015078

6. Sundin, S., and Braban-Lexdoux, C. Artificial Intelligence-Based Decision Support Technologies in Pavement Management. *Comput. Aided Civ. Infrastruct. Eng*., 2001, 16(2), 143–157.

7. Albuquerque, N. M., and Broten, M. *Local Agency Pavement Management Application Guide*." Project 1-37A, Washington State Dept. of Transportation, Olympia, WA, 1997.

8. AASHTO. *Pavement Management Guide*. Washington, DC, 2001.

9. Wolters, A. S., and Zimmerman, K. A. *Current Practices in Pavement Performance Modeling*, project 08-03 (C07), task 4 report: Final summary of findings. PennDOT, Harrisburg, PA, 2010.

10. FHWA. *Guidelines for Informing Decision making to Affect Pavement Performance Measures: Final Report*. PUBLICATION NO. FHWA-HRT-17-090 February 2018.

11. Kaya, O. *Investigation of AASHTOWare Pavement ME Design/Darwin-ME™ Performance Prediction Models For Iowa Pavement Analysis And Design*. M.Sc. Thesis. Iowa State University. Ames, IA. 2015.

12. Yang, J. Lu, J. J., Gunaratne, M., Xiang, Q. Forecasting Overall Pavement Condition with Neural Networks Application on Florida Highway Network. *Transportation Research Record, Journal of the Transportation Research Board*, 2003.

13. Beckley, M. E. *Pavement Deterioration Modeling Using Historical Roughness Data*. MSc. Thesis, Arizona State University, May 2016.

14. Ercisli, S. *Development of Enhanced Pavement Deterioration Curves*. MSc. Thesis, Virginia Polytechnic Institute and State University, August 2015.

15. Kaya, O., A. Rezaei-Tarahomi, H. Ceylan, K. Gopalakrishnan, S. Kim, and D.R. Brill. Developing Rigid Airport Pavement Multiple-Slab Response Models for Top-Down Cracking Mode using Artificial Neural Networks. Presented at 96th TRB Annual Meeting, Washington D.C., 2017.

16. Federal Highway Administration. *Distress Identification Manual for the Long Term Pavement Performance Program*, No. FHWA-RD-03-031, FHWA, 2003.

17. Kaya, O., A. Rezaei-Tarahomi, H. Ceylan, K. Gopalakrishnan, S. Kim, and D.R. Brill. Neural Network–Based Multiple-Slab Response Models for Top-Down Cracking Mode in Airfield Pavement Design. *Journal of Transportation Engineering, Part B: Pavements*, 2018. 144 (2).

18. Kaya, O., Garg, N., H. Ceylan, and S. Kim. Development of Artificial Neural Networks Based Predictive Models for Dynamic Modulus of Airfield Pavement Asphalt Mixtures. International Conference on Transportation and Development, July 15–18, 2018, Pittsburgh, Pennsylvania.

CHAPTER 6. CONCLUSIONS, RECOMMENDATIONS AND CONTRIBUTIONS OF THIS STUDY TO THE LITERATURE AND TO THE PAVEMENT ENGINEERING FIELD

Conclusions

This study proposes a data-driven and efficient pavement design, analysis, and management concept that considers all aspects of pavement engineering together and could represent a future direction for advanced practice in pavement engineering. In such an approach: (1) mechanisms between various pavement materials and structures are well-understood and well-modeled, (2) for given pavement structures under various traffic and climate conditions, pavement performance is well-evaluated, (3) remaining service lives based on pavement performance model results are well-estimated, and (4) to optimize RSL, various pavement preservation or rehabilitation techniques are considered during the pavement design process. If such a data-driven comprehensive approach could be achieved, pavement structures would be better-optimized and designed during the design stage, potentially avoiding excessive costs because of overdesign or early failure of pavements. As part of this concept, the following methods have been used: soft computing and numerical analysis methods used in the development of pavement structural response models; soft computing and statistical methods used in the development of pavement performance prediction models, and soft computing and statistical methods used in the development of remaining pavement service life models.

As part of this dissertation, ANN based multiple-slab response models were developed for top-down cracking mode in airfield pavement design. ANN was found to be a promising alternative in returning very close estimates of the top-down bending stress computed by NIKE3D in rigid airport pavements. By using the ANN models, very accurate

stress predictions can be produced in a fraction of time compared to the significant amount of time needed to perform a 3D-FE computation. For instance, stress predictions for thousands of cases can be predicted in seconds using ANN models compared to days, if not months, using 3D-FE computation. Dimensional analysis was found to be a promising method to reduce the input feature space in ANN model development. It produced accuracies similar to those produced using individual input parameters in the model development (see Table 2.2). An advantage of using dimensional analysis in the development of ANN models is that it significantly reduces the number of required input parameters. For example, six dimensionless input parameters were found to be enough to successfully predict pavement responses, compared to fourteen individual input parameters needed for mechanical-load-only case. Another advantage of using dimensional analysis in the development of ANN models is that the use of these models can be extended for any types of pavements with the same pavement layer configurations and the next generation aircraft with the same gear configurations, if applicable. As long as the dimensionless parameters for the pavements and the next generation aircraft cases are within the ranges that the ANN models were developed, the models can be directly used for these pavements and aircraft without any modification.

As part of this dissertation, numerical analysis of longitudinal cracking in widened jointed plain concrete pavement systems was carried out. One of the objectives of this study was to understand longitudinal cracking mechanisms and to evaluate longitudinal cracking potential of widened JPCP through numerical analysis. Based on single-axle load simulations, it was found that as negative temperature gradient increases, critical load location moves closer toward the mid-slab from the transverse edge. This might be because: (1) When only mechanical load without any temperature load applied on the transverse

joints, if restriction of the critical slabs by the adjacent slabs through LTE is considered, top tensile stress accumulation is observed around the transverse joints. (2) Slabs try to curl up when temperature load is applied to them (negative temperature gradient), and because they are restricted by adjacent slabs, they develop top-tensile stresses around their mid-slab. When a combined mechanical and temperature load is applied (negative temperature gradient) around the mid-slab, top-tensile accumulation around the mid-slab further increases. A truck with a four-axle configuration with the center of its axle loads placed close to transverse edges was identified as the critical loading scenario, because when axle loads were placed on adjacent slabs, tensile stresses were transferred to the critical slab, resulting in very high tensile stress accumulation around the top surface of the critical slab close to the transverse edge. This is especially true for high negative temperature gradient cases (when slabs curl up) where the center of the axle loads is placed close to the transverse edges of an adjacent slab. In that case, the top tensile stresses on the transverse edges of the adjacent slabs are transferred to the critical slabs and extremely high top tensile stresses are observed around the transverse joints of the critical slabs. This finding satisfactorily explains the longitudinal crack initiation at the transverse joints and top slab surface observed in the field investigations. Another objective of this study was to compare different shoulder types when used adjacent to either a widened (4.3 m. (14 ft.) wide) or a regular size (3.7 m. (12 ft.) wide) slab in terms of their effects in mitigating longitudinal cracking. Initially, widened slabs with a partial-depth tied PCC shoulder alternative were compared with regular slabs with a full-depth tied PCC shoulder alternative, and it was found that higher (1) top-to-bottom tensile stress ratio and (2) top tensile stress were observed when widened slabs with a partial-depth tied PCC shoulder were used, compared to when regular slabs with a full-depth tied PCC

shoulder were used. Higher top-to-bottom tensile stress ratio and top tensile stresses are related to higher longitudinal cracking potential, possibly because even though widened slabs can be used to mitigate transverse cracking, they might increase longitudinal cracking potential. This characteristic of widened slabs does not change much even if when they are used with a partial-depth tied PCC shoulder. In this study, widened slabs (4.3 m. (14 ft.) wide) with an HMA shoulder alternative were also compared to regular slabs (3.7 m. (12 ft.) wide) with an HMA shoulder alternative in terms of their effect on mitigating longitudinal cracking. A higher top-to-bottom tensile stress ratio was observed when regular slabs (3.7 m. (12 ft.) wide) with an HMA shoulder were used compared to the situation of widened slabs (4.3 m. (14 ft.) wide) with an HMA shoulder. The difference between an HMA shoulder alternative and a tied PCC shoulder alternative is that the HMA shoulder is not tied to widened or regular slabs so there is no load transfer between a slab and the HMA shoulder, and a LTE of only 10% is defined between the shoulder and slab bases, explaining why the effect of an HMA shoulder on top tensile stress accumulation in widened or regular slabs is minimal. In short, widened slabs or regular slabs with HMA shoulders demonstrate similar behavior when there is no shoulder used with them in terms of their effect on longitudinal cracking potential.

As part of this dissertation, evaluation of rigid airfield pavement cracking failure models was conducted. The conclusions from this sub-study can be summarized by answering the three fundamental questions raised in the introduction part of this sub-study:

- "*What are the critical mechanical loading and pavement response locations for top-down and bottom-up cracking failure modes?*" In this study, two critical pavement response types were considered: maximum tensile and principal stresses at the bottom and top

surfaces of the slab. In about 35% of all cases, top stresses were higher than bottom stresses, while in about 65% of cases, bottom stresses were higher than top stresses for both tensile and principal stress cases. This result was expected because bottom-up cracking failure mode is the most common failure mode in rigid airfield pavements. Understanding distribution of top-to-bottom stress ratio is important because it reveals the mode of fatigue cracking, top-down or bottom-up, if any. If top-to-bottom stress ratio is greater than 1.0, a possible top-down fatigue crack is likely to occur; if not, it is likely to appear as a bottom-up crack. It was also observed that absolute maximum principal stress values were to some extent higher than absolute maximum tensile stress values for all cases evaluated. For cases where mechanical loading was closer to slab corners, since higher top-to-bottom ratio values were observed, slab corners were found to be critical mechanical load locations for top-down cracking failure mode. Critical response locations mostly accumulated around joints of adjacent slabs rather than within the slabs where mechanical load was applied. This was more pronounced in maximum principal stress cases than maximum tensile stress cases. This finding closely supports field observations where top-down cracks have been found to occur close to joints.

- "*What is the effect of temperature loading in determining which failure mode (top-down or bottom-up cracking) will be dominant in the failure of rigid airfield pavements?*" As negative temperature gradient increased, average top-to-bottom tensile and principal stress ratios also increased. It is clear that input cases with negative temperature gradients were the ones producing higher top-to-bottom stress ratios and resulting higher top-down cracking potential.

- "*How will calculated slab thicknesses be affected and how should the failure model will be revised if top-down and bottom-up cracking failure modes are included in the design?*" There was a general trend in optimum slab thickness results that optimum slab thicknesses were higher when (1) maximum top stresses (as opposed to maximum bottom stresses) and (2) maximum principal stresses (as opposed to maximum tensile stresses) were considered as design stresses. This was because (1) absolute principal stress values were higher than absolute tensile stresses for the same input scenarios, and since a negative temperature gradient [-0.3 ^{o}C/cm (-2 ^{o}F/in)] was applied to all cases investigated, slightly higher top stresses were observed compared to bottom stresses. That the optimum slab thicknesses were higher when maximum top stresses (as opposed to maximum bottom stresses) were considered as design stresses could be explained by the fact that coverage to failure (C_F) values for both cases were calculated using Equation 4.3, which only considers bottom-up cracking mode.

As part of this dissertation, a framework for project and network level pavement performance and remaining service life prediction models for Iowa pavement systems was developed. Sigmoidal equations were found to successfully model pavement deterioration when there is a single pavement deterioration trend (project-level). One of the benefits of project-level pavement performance models is that they can be developed using very few data. Therefore, they can be extensively used when only a few pavement conditions or structural and traffic data are available for pavement sections. Artificial intelligence (AI) techniques such as artificial neural network (ANN)-based models have been found to be great tools for modeling pavement deterioration when there are many pavement sections with various traffic, thickness, and other various deterioration trends (network-level). They are

also very fast tools that can solve thousands of pavement scenarios with various traffic, thickness, and conditions in seconds. Both these features of ANN models make them great tools for use in development of network-level pavement-performance modeling. As part of this study, network-level pavement performance models were also developed using statistical and ANN-based approaches, with identical input parameters used in both approaches to evaluate their relative success for network-level pavement-performance modeling. It was found that network-level ANN based pavement performance models produced greater accuracy with higher R^2 and lower AAE values compared to network-level statistical models. As part of this study, Microsoft Excel based automation tools were developed for both project and network-level pavement performance modeling and analysis:

- The project-level pavement-performance modeling and RSL calculation tool is capable of developing project-based statistical models for predicting future pavement performance as well as calculating RSL values based on user-defined threshold limits. It is also capable of automatically updating and improving pavement-performance prediction models because it allows more data to be added into the model development dataset. The benefit of this tool is that, as engineers add more data into the model development dataset, they will be able to automatically refine performance prediction models and make decisions using more recent and more accurate pavement performance models.
- The network-level pavement performance modeling tool is capable of making pavement-performance predictions based on pre-developed ANN-based pavement-performance models. While having only thickness, traffic, age, and previous two years' pavement performance records for any pavement performance indicator, it can make future pavement-performance calculations in less than a second for any pavement section. It is

also capable of producing pavement-performance predictions for thousands of pavement scenarios under various traffic, thickness, and other conditions in seconds. The network-level pavement performance modeling tool is also capable of (1) making future pavement-performance predictions for some distresses (transverse cracking, rutting, and longitudinal cracking), then (2) using these predicted distress values as inputs in making future IRI predictions.

Recommendations

The following recommendations are drawn from this dissertation:

- Developed ANN based top-down bending stress models are recommended to be used as alternatives to 3D-FE computations. By using the ANN models, very accurate stress predictions can be produced in a fraction of time compared to the significant amount of time needed to perform a 3D-FE computation. For instance, stress predictions for thousands of cases can be predicted in seconds using ANN models compared to days, if not months, using 3D-FE computation.
- Recommendations of this study for mitigating longitudinal cracking in widened JPCP can be summarized follows:
    - Longitudinal cracks are mainly in the traffic lane and about 0.3-0.6 m. (2~4 ft.) away from slab edge
        - Shorter joint spacing can result in lower curling and warping and also can lead to less chance for longitudinal cracking as well
    - Most longitudinal cracks observed start from slab transverse joints
        - Since dowel bars can restrain vertical deflection at joints, so proper dowel bar installation will help mitigate longitudinal cracking

- A tied PCC shoulder design option can perform better than other shoulder design options (HMA and granular) in terms of longitudinal crack potential in widened JPCP.

- Based on the study findings, the following recommendations on potential inclusion of both top-down and bottom-up cracking failure modes in rigid airfield pavement design can be made:
  - This study showed that top and bottom stresses should be considered in rigid airfield pavement design. The coverages-to-failure equation (Equation 4.3) is recommended to be revised and calibrated to accommodate top-down cracking failure mode as well. That way, more realistic slab thicknesses for top-down cracking failure mode can be calculated. Moreover, a set of protocol/framework steps should be established in determining the final slab thickness.
  - Use of maximum principal stress for design stress can be considered as an alternative to maximum tensile stress. In this way, mechanical loading at an angle can be better represented and potential crack propagation direction could be identified. Rather than using pre-determined load locations (as done in the current design methodology) and calculating design stress based on them, a mechanical load can at each time be placed at several load locations and maximum stresses on slab top and bottom of can be automatically calculated. Calculated maximum stresses can then be used as design stresses.
  - In the calculation of design factor (DF), two different tensile strength values can be considered (one for top and the other for bottom of the slab) because the slab top is exposed to the sun and wind so higher evaporation occurs on that surface.

This might reduce slab tensile strength close to the top surface, especially for projects constructed on hot and windy days.

- In this study, while a theoretical temperature gradient [-0.3 ^{o}C/cm (-2 ^{o}F/in)] was used in slab thickness determination cases, each construction site should be individually evaluated so that curling and warping of slabs can be better predicted and more realistic temperature gradients can be used in design.

- "Development of a Framework for Project and Network Level Pavement Performance and Remaining Service Life Prediction Models for Iowa Pavement Systems" sub-study can be further expanded by: (1) including other pavement performance indicators (i.e, faulting, material-related distresses, etc.), (2) defining other agency-specific threshold limits, and (3) prioritizing some pavement performance indicators over others, etc., as part of RSL model development. Some SHAs use decision trees to determine when a major rehabilitation or reconstruction is needed. Multi-objective RSL models can be developed considering various pavement performance indicators with different priorities.
- RSL results will allow agencies to distinguish between two pavement sections with the same current condition (i.e., the same current IRI). This can be an ideal approach to addressing the transportation planning and performance management criteria requirements of the MAP-21 legislation.
- Note that RSL models are only to help engineers in their decision-making process. They consider only a limited number of condition metrics (IRI, some distresses, etc.) but may fail to consider other important parameters such as structural capacity and integrity of pavement systems. Engineers should consider various parameters as well as RSL model results, combined with their engineering judgment to determine when a pavement section

will fail and need major rehabilitation or reconstruction. Estimated RSL does not necessarily mean that after that date a pavement section cannot be open to public use, and applying preventative or routine maintenance may lead to significantly increased RSL.

Contributions of this Study to the Literature and to the Pavement Engineering Field

Some of the contributions of this study to the literature and pavement engineering field can be summarized as follows:

- As a result of this study, soft computing and numerical analysis models for use in pavement design, analysis, and management packages (ANN-FAA, FAARFIELD) have been developed.
- This study established a detailed step-by-step methodology and a framework for pavement performance and RSL prediction models based on real pavement-performance data obtained from Iowa DOT's PMIS database. Microsoft Excel-based automation tools for use at both project and network levels were developed for pavement performance modeling and analysis to help engineers in their decision-making processes. As part of this study, a platform was established using Microsoft Excel-based automation tools that: (1) develop pavement performance models with great accuracy, (2) are "tunable", meaning that they are capable of automatically updating and improving pavement performance prediction models as more data are added into the model development dataset, (3) can calculate RSL for each pavement section based on the various pavement performance indicators. This platform is believed to be one-of-a-kind in terms of its capabilities.
- This study uses numerical analysis to explain underlying mechanisms for longitudinal cracking for both widened JPCP and top-down cracking in rigid airfield pavements.

- This study provides recommendations and guidelines related to how current pavement analysis, design, and management methodologies could be improved.
- This study proposes a data-driven and efficient pavement design, analysis, and management concept that considers all aspects of pavement engineering together; it is believed to represent the future of pavement engineering, and it is known to be the first effort that considers design, analysis and management together for optimizing pavement design during the design stage.
- This study provides real-time solutions to complex pavement-engineering problems.
- It is believed that this study will provide the pavement design community with a better understanding of relationships between pavement design, analysis, and management.